AD-A157 391

DTIC FILE COPY

85 7 31 028

Best Available Copy

UNCLASSIFIED

SECURITY CLASSIFICATION OF THIS PAGE

AD A 157 391

REPORT DOCUMENTATION PAGE

1a. REPORT SECURITY CLASSIFICATION UNCLASSIFIED	1b. RESTRICTIVE MARKINGS
2a. SECURITY CLASSIFICATION AUTHORITY	3. DISTRIBUTION/AVAILABILITY OF REPORT Approved for public release; distribution unlimited.
2b. DECLASSIFICATION/DOWNGRADING SCHEDULE	
4. PERFORMING ORGANIZATION REPORT NUMBER(S) AFRRI SR85-1 through 85-16; AFRRI CR85-1	5. MONITORING ORGANIZATION REPORT NUMBER(S)
6a. NAME OF PERFORMING ORGANIZATION Armed Forces Radiobiology Research Institute 6b. OFFICE SYMBOL (If applicable) AFRRI	7a. NAME OF MONITORING ORGANIZATION
6c. ADDRESS (City, State and ZIP Code) Defense Nuclear Agency Bethesda, Maryland 20814-5145	7b. ADDRESS (City, State and ZIP Code)
8a. NAME OF FUNDING/SPONSORING ORGANIZATION Defense Nuclear Agency 8b. OFFICE SYMBOL (If applicable) DNA	9. PROCUREMENT INSTRUMENT IDENTIFICATION NUMBER
8c. ADDRESS (City, State and ZIP Code) Washington, DC 20305	10. SOURCE OF FUNDING NOS. PROGRAM ELEMENT NO.: NWED QAXM; PROJECT NO.; TASK NO.; WORK UNIT NO.
11. TITLE (Include Security Classification) AFRRI Reports, Jan-Mar 1985	
12. PERSONAL AUTHOR(S)	
13a. TYPE OF REPORT Reprints/Technical 13b. TIME COVERED FROM _____ TO _____	14. DATE OF REPORT (Yr., Mo., Day) 15. PAGE COUNT 209
16. SUPPLEMENTARY NOTATION	
17. COSATI CODES FIELD / GROUP / SUB. GR.	18. SUBJECT TERMS (Continue on reverse if necessary and identify by block number) N/A

19. ABSTRACT (Continue on reverse if necessary and identify by block number)

This volume contains AFRRI Scientific Reports SR85-1 through 85-16, and Contract Report CR85-1, for Jan-Mar, 1985. Scientific reports included in this volume follow.

20. DISTRIBUTION/AVAILABILITY OF ABSTRACT UNCLASSIFIED/UNLIMITED ☒ SAME AS RPT. ☐ DTIC USERS ☐	21. ABSTRACT SECURITY CLASSIFICATION UNCLASSIFIED
22a. NAME OF RESPONSIBLE INDIVIDUAL Junith A. Van Deusen	22b. TELEPHONE NUMBER (Include Area Code) (202)295-3536 22c. OFFICE SYMBOL ADMG

DD FORM 1473, 83 APR EDITION OF 1 JAN 73 IS OBSOLETE.

UNCLASSIFIED

SECURITY CLASSIFICATION OF THIS PAGE

Cont'd PA

CONTENTS

Scientific Reports

SR85-14: Patchen, M. L., DiLuzio, N. R., Jacques, P., and MacVittie, T. J. Soluble polyglycans enhance recovery from cobalt-60-induced hemopoietic injury.

SR85-15: Patchen, M. L., MacVittie, T. J., and Wathen, L. M. Effects of pre- and post-irradiation glucan treatment on pluripotent stem cells, granulocyte, macrophage and erythroid progenitor cells, and hemopoietic stromal cells.

SR85-16: Shea-Donohue, T., Danquechin-Dorval, E., Montcalm, E., El-Bayar, H., Durakovic, A., Conklin, J. J., and Dubois, A. Alterations in gastric mucus secretion in rhesus monkeys after exposure to ionizing radiation.

Contract Report

CR85-1: Goodman, L. J. A practical guide to ionization chamber dosimetry at the AFRRI reactor.

Biochimica et Biophysica Acta 812 (1985) 713–720
Elsevier

BBA 72428

Isolation of cellular membranes from rat mast cells

Lynn M. Amende * and Mildred A. Donlon

Biochemistry Department, Armed Forces Radiobiology Research Institute, Bethesda, MD 20814 (U.S.A.)

(Received May 30th, 1984)
(Revised manuscript received October 3rd, 1984)

Key words: Mast cell; Membrane isolation; Perigranular membrane; Plasma membrane; Sonication; (Rat)

Large amounts of membranes enriched either in perigranular membranes or in plasma membranes have been successfully isolated from rat peritoneal mast cells. A cycle consisting of a single sonication pulse to disrupt the mast cells followed by centrifugation to separate the released granules was repeated until 90% of the mast cells were disrupted. This technique resulted in a high yield of intact granules since the released granules were only exposed to the single sonication pulse. The intact granules were separated from plasma membrane fragments by centrifugation through a Percoll gradient. The perigranular membranes were then obtained by osmotic lysis of the purified intact granules. The plasma membrane fraction was enriched 4.5-fold (range, 4.1–6.1) in 5′-nucleotidase activity, a plasma membrane marker enzyme. No suitable marker enzyme activity was found for the perigranular membrane fraction. An important aspect of this procedure is its potential for obtaining both a plasma and perigranular membrane preparation in high yield and purity from the same mast cell preparation.

Introduction

The secretion of histamine is a membrane-mediated process dependent on the presence of calcium. It has been proposed that a calcium transport mechanism located in mast cell membranes is an integral component of this release process. As an initial step in examining these transport processes, the mast cell plasma and perigranular membranes must be isolated and their purity characterized.

Mast cell granules have been isolated and the perigranular membrane, obtained by variety of techniques [1–6]. We have re-evaluated these techniques with the aim of producing large amounts of purified perigranular and plasma membranes from rat peritoneal mast cells. We here introduce an innovative technique that uses pulsed sonication energy to produce a high yield of purified mast cell perigranular membranes. In addition to high yields of perigranular membranes, this technique also produces an enriched plasma membrane fraction from mast cells. The isolated membranes have been biochemically characterized using membrane marker enzymes. The isolation of these membranes is an important prerequisite for our studies on the biochemical mechanisms controlling histamine release from mast cells.

Materials and Methods

Materials

Aprotinin, leupeptin, ruthenium red, Percoll, Tris-ATP, AMP, DCPIP, EDTA, glucose 6-phosphate, and Hepes were obtained from Sigma Chemical Co. (St. Louis, MO). Bovine serum albumin (fatty acid free, fraction V) was obtained from Miles Laboratories, Inc. (Elkhart, IN) and

* Present address: NIADDK, NIH, Bethesda, MD 20205, U.S.A.

DNAase I from Calbiochem-Behringer (San Diego, CA).

Preparation of rat peritoneal mast cells

Rat peritoneal mast cells were obtained from 300–400 g, male, Sprague-Dawley rats killed by carbon dioxide inhalation. Suspensions of cells were obtained by washing the peritoneal cavity with 20 ml of Ca^{2+}, Mg^{2+}-free Tyrode's buffer containing 10 units/ml heparin and 1 percent bovine serum albumin. These cell suspensions contained 3–7% mast cells and, following centrifugation through a 38% albumin gradient [7], they were purified to greater than 95%. The preparative scale-up for obtaining large amounts of membrane required peritoneal washings from 120 rats.

Mast cell perigranular membrane preparation

All procedures were conducted at 0–4°C. Purified mast cells were resuspended in 10 ml ($1.3 \cdot 10$ cells/ml) of buffer-A (4 mM Na_2HPO_4, 2.7 mM KH_2PO_4, 150 mM NaCl, 2.7 mM KCl, 0.9 mM $CaCl_2$, 0.175% bovine serum albumin (pH 7.2)), prepared as described by Kruger et al. [5] with added leupeptin (0.5 mg/500 ml), aprotinin (56 TIU/500 ml), and DNAase I (5 mg/500 ml), in a 50 ml Sorvall polycarbonate centrifuge tube. The mast cell suspension was sonicated using a Heat Systems (Ultrasonics, Inc.) cell disruptor (Model W-225R) equipped with a microprobe set at 50% duty cycle, pulsed energy, output energy control set initially at '2'. After each single pulse, the cell suspension was vortexed vigorously for 10 s and the mast cell suspension centrifuged at $70 \times g$, 1 min. The supernatant (S1), consisting of released granules, cell debris and membranes, was pooled, and the pellet (P1), consisting of intact mast cells, resuspended to 10 ml with buffer-A composition with gentle vortexing. Pooled S1 were centrifuged at $1000 \times g$, 2 min, following every second pulse to concentrate the granules. The sonicator energy output was incrementally increased to a maximum setting of '6' for a total of 11 pulses.

After the last sonication pulse, the pellet (P1) was washed with 20 ml buffer-A and centrifuged ($70 \times g$, 2 min). The supernatant was added to the pooled S1 supernatants and then centrifuged 1000 $\times g$, 10 min to yield S2 and P2, consisting of granules and cell membranes.

The P2 pellet was gently resuspended in 10 ml buffer A and layered on top of 25 ml Percoll diluted (9 : 1) with 1.5 M NaCl, 27 mM KCl, 9 mM $CaCl_2$, 0.1 M Hepes (pH 7.5) to give final concentrations of 150 mM NaCl, 2.7 mM KCl, 0.9 mM $CaCl_2$ and centrifuged at $27000 \times g$, 20 min, in a Sorvall SS34 rotor. After centrifugation, the material appearing at the interface between the buffer-A and the Percoll, consisting of plasma membranes, and the bottom of the Percoll gradient, consisting of intact granules, were collected and the Percoll removed by washing with buffer-A ($800 \times g$, 10 min) followed by resuspension in 50 mM Hepes (pH 7.5), and centrifugation.

The gradient pellet material was then osmotically lysed by resuspension in 50 ml cold deionized water with vigorous vortexing [8]. After 10 min on ice, the granules were vortexed and centrifuged ($1900 \times g$, 10 min) to pellet the membrane-free granules. The supernatant was centrifuged at 50000 rpm, 60 min using a Spinco Ti 50.2 rotor ($200000 \times g$) to sediment the perigranular membranes. The perigranular membranes were resuspended in 50 mM Hepes (pH 7.5), rapidly frozen in liquid nitrogen, and stored at −180°C. Total preparation time including mast cell preparation was less than 8 h.

Perigranular membranes were also prepared from granules isolated as described by Raphael et al. [4]. The perigranular membranes were obtained by osmotic lysis [8]. The membrane fractions were then compared using membrane marker enzymes.

Enzyme assays

Membrane marker enzymes and DNA content were assayed as described by Evans [9]. Two enzyme activities generally accepted as plasma membrane markers are the $(Na^+ + K^+)$-ATPase and the 5'-nucleotidase. However, in the mast cell, the $(Na^+ + K^+)$-ATPase, whether measured as the ouabain-sensitive or sodium-dependent activity [9], could not be detected in the whole mast cell sonicate or the final plasma membrane fraction. Therefore, the enzyme used for the plasma membrane marker was 5'-nucleotidase. The distribution of intracellular membranes (Golgi and endoplasmic reticulum) was assayed using glucose-6-phosphatase, while the mitochondrial membrane marker enzyme was succinate dehydrogenase.

The 5′-nucleotidase activity was measured using a reaction medium which contained, in 100 μl, 100 mM KCl, 10 mM $MgCl_2$, 50 mM Hepes (pH 7.4), 10 mM potassium sodium tartrate, 5 mM AMP, and the membrane protein (3–30 μg). After 1–2 h at 37°C, the reaction was stopped by the addition of 50 μl 10% SDS. The phosphate released from both experimental and control assay tubes was determined by an automated assay [10].

Glucose-6-phosphatase activity was measured in 100 μl final volume containing 10 mM glucose 6-phosphate, 50 mM Hepes (pH 6.5), 4 mM EDTA, 1 mM KF, and the membrane protein (3–30 μg protein). Appropriate blanks were also assayed. After 1–2 h at 37°C, the reaction was stopped and the phosphate released was determined as described above.

Succinate dehydrogenase was assayed in a reaction mixture (640 μl) which contained 50 mM sodium phosphate buffer (pH 7.6), 1 mM KCN, 0.04 mM 2,6-dichlorophenolindophenol (DCPiP), 20 mM sodium succinate, and membrane protein (30–150 μg). After 2–3 h at 37°C, the reaction was stopped by transfer to an ice bath and quantified by the decrease in absorbance (*A* 600 nm) due to the reduction of DCPIP.

Chemical assays

Protein was estimated using a modification of the Lowry et al. method [11], with bovine serum albumin as standard. Histamine was assayed by an automated fluorometric assay [12,13]. Ruthenium red, which binds to the granule matrix, was used to quantitatively assay granule integrity. Since ruthenium red does not bind to granules with intact perigranule membranes, the decrease in the absorbance of ruthenium red-granule suspensions is quantitatively related to the number of disrupted granules. The percent intact granules was determined by ruthenium red binding in the absence and presence of Triton X-100, as described by Kruger et al. [5].

Results

Table 1 shows the results of the membrane marker enzyme analysis of various fractions prepared using the technique of Raphael et al. [4]. The final fraction, the supernatant from osmotic lysis of the granules (sucrose gradient pellet), contains the perigranular membrane. The yield of perigranular membrane fraction was significant (7% of the starting protein), as a result of contamination with other membrane fractions. The 5′-nucleotidase specific activity of the perigranular membrane fraction remained at 60% of the initial homogenate activity, indicating substantial plasma membrane contamination. No reduction in the glucose-6-phosphatase specific activity was observed in the perigranular membrane fraction and a 60% decrease in the specific activity of succinate dehydrogenase was found. Clearly the large amount of protein in the perigranular fraction was due to contamination by plasma membranes, intracellular organelle membranes, and mitochondrial membranes. This contamination may be the result of inefficient separation of intact granules from the broken cells and granules, as shown by the high specific activity of the membrane marker enzymes in the sucrose gradient pellet fractions.

To optimize the separation of intact granules, we studied the effect of varying two parameters of the isolation technique, the sonication energy and buffer. First the sonication treatment conditions were varied. A microprobe sonicator was used to disrupt the mast cells and the granule preparation technique of Kruger et al. [5] was then followed. The microprobe allows the application of either pulsed or continuous treatments of sonication energy. Initially, the effect of varying the number of pulses per sonication treatment was determined by measuring the percent intact cells and percent intact granules. As shown in Fig. 1, disruption of the cells is not proportional to the number of sonication pulses. Sonication has only an initial disruptive effect, that is, there appears to be a population of mast cells easily disrupted with only a few pulses. The remaining mast cells require increased sonication energy for disruption. The results in Fig. 1 show that the mast cell is more sensitive to sonication with 4–6 pulses per sonication treatment than 2–4 pulses per sonication treatment. However, the proportion of intact granules to intact cells decreases with more pulses per treatment. We therefore reduced the number of pulses to one pulse per treatment in subsequent experiments.

The methods of Kruger et al. [5] and Raphael et al. [4] rely on sonication but use different buffers. Raphael et al. [4] specify a Ca^{2+}, Mg^{2+}-free buffer

TABLE I

ANALYSIS OF MEMBRANE FRACTIONS ISOLATED BY THE TECHNIQUE OF RAPHAEL et al. [4]

Values are means (S.E., $n = 3$. S.A., specific activity; T.A., total activity; n.d., no activity detected.

Fraction	Protein (mg)	Histamine (mg)	5'-Nucleotidase		Glucose-6-phosphatase		Succinate dehydrogenase	
			S.A. (nmol P_i·mg^{-1}·min^{-1})	T.A. (nmol P_i·mg^{-1})	S.A. (nmol P_i·mg^{-1}·min^{-1})	T.A. (nmol P_i·mg^{-1})	S.A. (nmol indophenol reduced/mg per min)	T.A. (nmol indophenol reduced/min)
Sonicate	37.0 (8.0)	3.4 (0.5)	11.1 (0.9)	411 (30)	1.0 (0.1)	36 (2.3)	0.40 (0.12)	14.9 (4.6)
Sucrose gradient								
Pellet	5.0 (0.3)	0.6 (0.1)	11.3 (2.4)	56 (12)	0.5 (0.2)	2.4 (0.4)	0.37 (0.03)	1.9 (0.2)
Supernatant	10.9 (0.3)	2.8 (0.1)	24.4 (4.0)	244 (40)	n.d.	–	n.d.	–
Osmotic lysis								
Pellet	4.3 (0.5)	0.12 (0.02)	0.5 (0.1)	2 (0.4)	0.2 (0.05)	1.0 (0.2)	n.d.	–
Supernatant	2.7 (0.2)	0.08 (0.02)	6.6 (0.8)	18 (2.4)	1.3 (0.1)	3.6 (0.3)	0.16 (0.04)	0.4 (0.1)

TABLE II

ANALYSIS OF MEMBRANE FRACTIONS ISOLATED ACCORDING TO THE METHOD OUTLINED IN Fig. 1

Values are means (S.E.), $n = 3$. S.A., specific activity; T.A., total activity; n.d., no activity detected.

Fraction	Protein (mg)	Histamine (mg)	5'-Nucleotidase		Glucose-6-phosphatase		Succinate dehydrogenase	
			S.A. (nmol P_i·mg^{-1}·min^{-1})	T.A. (nmol P_i·mg^{-1})	S.A. (nmol P_i·mg^{-1}·min^{-1})	T.A. (nmol P_i·mg^{-1})	S.A. (nmol indophenol reduced/mg per min)	T.A. (nmol indophenol reduced/min)
Sonicate	38.0 (1.3)	3.26 (0.25)	7.9 (1.0)	300 (36)	1.3 (0.2)	49.0 (7.6)	0.34 (0.03)	13.0 (1.2)
P_1	6.8 (0.8)	0.18 (0.04)	6.0 (1.0)	41 (7)	1.9 (0.1)	13.5 (0.7)	0.02 (0.01)	0.2 (0.04)
S_1	25.2 (1.4)	1.69 (0.11)	12.3 (1.6)	310 (40)	2.2 (0.2)	50.0 (5.0)	0.34 (0.03)	8.4 (0.8)
P_2	17.7 (1.0)	1.47 (0.20)	17.2 (1.4)	304 (25)	1.4 (0.2)	24.8 (3.6)	0.22 (0.03)	3.7 (0.6)
S_2	6.0 (1.0)	0.11 (0.03)	n.d.	–	2.8 (0.1)	17.0 (0.6)	n.d.	–
Percoll								
Interface	4.9 (0.5)	0.20 (0.03)	35.6 (2.3)	174 (11)	1.3 (0.5)	6.4 (2.4)	0.47 (0.09)	1.9 (0.5)
Pellet	9.4 (1.2)	1.11 (0.13)	n.d.	–	0.9 (0.2)	8.2 (1.9)	0.25 (0.03)	2.1 (0.3)
Osmotic lysis								
Pellet	6.0 (0.4)	0.65 (0.09)	0.02 (0.01)	0.12 (0.04)	0.2 (0.05)	1.2 (0.3)	0.31 (0.06)	1.9 (0.3)
Supernatant	1.7 (0.3)	0.008 (0.001)	0.80 (0.17)	1.36 (0.30)	0.2 (0.04)	0.4 (0.1)	0.9 (0.03)	0.2 (0.05)

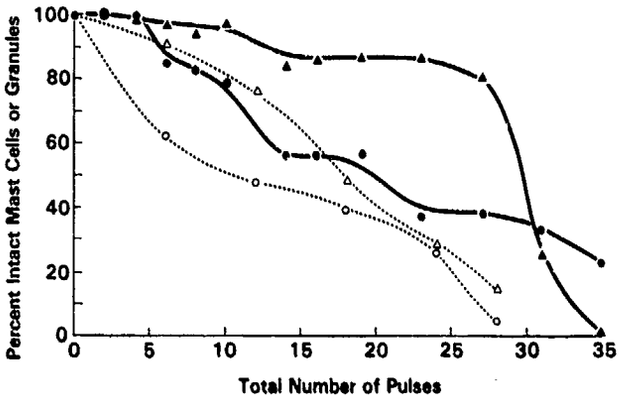

Fig. 1. Effect of varying the number of pulses per sonication treatment on the disruption of mast cells and granules. The preparation sonicated with 2–4 pulses per treatment is indicated by filled symbols, the open symbols indicate the preparation with 4–6 pulses per treatment. The percent intact granules (△, ▲) were meausured by ruthenium red binding. The percent intact mast cells were determined by cell counts (○, ●).

with the addition of EDTA, while Kruger et al. [5] added 0.9 mM $CaCl_2$ and 0.175% bovine serum albumin. The effect of these two buffers on sonication efficiency was compared using only 1 pulse/sonication treatment. For these experiments, the percent intact granules was measured by histamine release and ruthenium red binding. As shown in Fig. 2, these two methods of determining intact granules yield similar results. More of the granules released by sonication in buffer with added calcium remain intact than the granules in buffer without calcium. Thus, the calcium containing buffer was used for our granule preparation technique.

These new sonication conditions and the calcium containing buffer were incorporated into the perigranular membrane preparation described in Methods. After each cycle of sonication/centrifugation/resuspension, the percent intact cells was determined from the decreased cell number. These results are shown in Fig. 3. The level of sonication energy was kept constant with each pulse until, as indicated by the arrow, the energy level was increased. This results in a stairstep effect whereby continued sonication at the same energy level yields no further decrease in cell number, until the energy level per pulse is increased. Sonication was terminated following 12 or 13 pulses, where less than 10% intact mast cells remained.

The results of the characterization of the different membrane fractions isolated using this procedure are shown in Table II. The plasma membrane fraction (the fraction at the Percoll interface) contained 13% of the total cellular protein while the Percoll pellet contained 25% of the total cellular

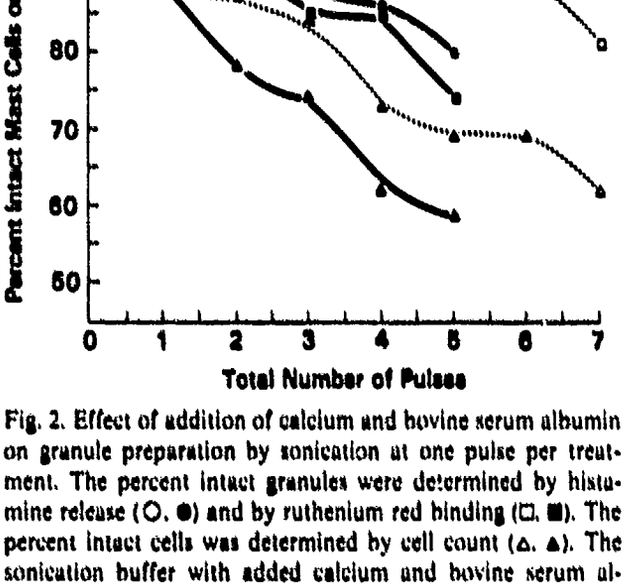

Fig. 2. Effect of addition of calcium and bovine serum albumin on granule preparation by sonication at one pulse per treatment. The percent intact granules were determined by histamine release (○, ●) and by ruthenium red binding (□, ■). The percent intact cells was determined by cell count (△, ▲). The sonication buffer with added calcium and bovine serum albumin (open symbols) increased the yield of intact granules compared to buffer without addition (solid symbols).

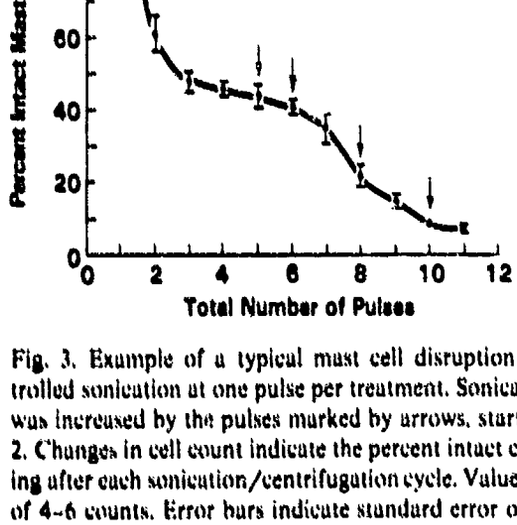

Fig. 3. Example of a typical mast cell disruption using controlled sonication at one pulse per treatment. Sonication energy was increased by the pulses marked by arrows, starting at level 2. Changes in cell count indicate the percent intact cells remaining after each sonication/centrifugation cycle. Values are means of 4–6 counts. Error bars indicate standard error of the mean. For the point without error bars, the standard error is smaller than the symbol.

protein. Only 45% of the initial total protein was associated with the perigranular membranes (osmotic lysis supernatant).

Total histamine content averaged 3 mg for $1.2 \cdot 10^8$ cells. Our values for histamine content (22 $\mu g/10^6$ cells) are similar to published values (15–30 $\mu g/10^6$ cells, reviewed in Ref. 2). Nearly all of the histamine in the S1 fraction was associated with the P2 pellet, indicating that the granules were 90% intact after sonication. Following the deionized water lysis of the intact granules, and separation of the membrane-free granules, very little histamine (0.2% of initial total histamine) was associated with the perigranular membranes. This remaining histamine may be removed by additional washing of the perigranular membranes.

The cycle of repeated sonication steps may have disrupted mast cell intracellular organelles such as nuclei. The released DNA may adhere to membranes and be co-purified along with them to contaminate the final membrane preparation. The extent of DNA contamination was determined to be minimal since the DNA content of the intact mast cell was 30 μg/mg protein. The perigranular membrane pellet contained very little DNA (less than 2 μg/mg protein).

Also shown in Table II are the results of the membrane marker enzyme assays. The membranes at the Percoll interface (plasma membranes) were enriched 4.1–6.1-fold in 5'-nucleotidase with no detectable activity remaining in the Percoll pellet (intact granules). 60% of the total 5'-nucleotidase activity was recovered in the top Percoll fraction. The enzyme activity of the other membrane marker enzymes was minimal in all fractions assayed. No enrichment of any of these enzymes was found in the membrane fractions. Examination of the glucose-6-phosphatase activity, a marker enzyme for Golgi and endoplasmic reticulum membranes [9], showed that the plasma membrane fraction retained the same initial activity of the whole mast cell homogenate while the perigranular membranes contained 19% of the inital specific activity. Glucose-6-phosphatase activity was increased in the S2 fraction, the soluble cytoplasmic protein fraction. 50% of the mitochondrial membranes, as indicated by the succinate dehydrogenase total activity, were also lost in the S2 fraction. Fifteen percent of the total succinate dehydrogenase activity remained with the plasma membranes, with only 1% of the total activity in the perigranular membranes. We could not detect monoamine oxidase activity in any of the fractions.

The perigranular membranes were removed from the granules following osmotic lysis with deionized water. This was verified by electron microscopy which demonstrated that the granules were depleted of their membranes and were less electron dense than intact granules. These results were similar to the electron micrographs of granules isolated from their perigranular membranes described by Raphael et al. (Ref. 4, Fig. 1b). While membrane marker enzyme activities could not be evaluated as specifically characterizing the perigranular membrane, this membrane could be recovered by high speed centrifugation. Electron microscopic examination of the perigranular membrane pellet ($200000 \times g$ pellet) showed membranous material contaminated with fragments of granule matrix (micrographs not shown).

In the several preparations we examined, contamination of this membrane fraction with granule matrix was a consistent finding. This may reflect an intimate association of the granule membrane with specific components of the granule matrix so that highly purified perigranular membrane may not be technically attainable at this time.

Discussion

High yields of intact granules are easily obtained using the method proposed here. The most important aspect of this technique is the removal of released granules immediately after a single pulse of sonication by centrifugation. The granules are not exposed to potential damage by released protease enzymes, and do not clump together or adhere to membranes. They remain intact since they are not subjected to repeated damage by prolonged sonication exposure. The second key step in this method, separation of the intact granules from broken granules and plasma membranes, is rapidly obtained with a Percoll gradient. The Percoll gradient is self-generating at $15000 \times g$. The use of Percoll has the additional advantage of easy removal since the granules sediment at low speeds and the plasma membrane fraction does not penetrate the gradient. The advantages of Per-

coll have also been utilized for the isolation of adrenal chromaffin granules [14]. Finally, use of this procedure allows the simultaneous isolation of both plasma membranes and perigranular membranes in high yield and purity from the same mast cell preparation.

This procedure produces a significant yield of mast cell plasma membranes, using a simple and rapid technique. Until now, the only published report of mast cell plasma membrane purification [15] used a laborious and time-consuming technique requiring a sucrose gradient, which was potentially damaging to the isolated membranes. Mast cell plasma membranes purified by Ishizaka et al. [15], using flotation through a discontinuous sucrose gradient [16], were 2.8-fold increased in specific activity compared to the initial homogenate, using 5'-nucleotidase activity to determine plasma membrane purity and yielded 5 μg protein/10^6 cells. Our preparations of plasma membranes averaged 4.5-fold enrichment (some preparations yielded 6.1-fold enrichment) in 5'-nucleotidase activity with 40 μg protein/10^6 cells. These results were obtained using a single Percoll gradient centrifugation step. Further improvement in the plasma membrane purity should be easily accomplished by using an additional Percoll or sucrose gradient. Furthermore, the rapidity of this technique reduces the amount of time the membranes are exposed to the harsh isolation conditions.

Previous investigators reported that gentle sonication provides a higher percentage of intact dense granules, but with a lower percent yield [5,6]. However, these studies used continuous sonication with either a bath sonicator or a probe sonicator. The use of pulsed sonication has not been previously reported. Pulsed sonication is easily controlled since the pulse duration is repeatable within milliseconds and the energy level can be varied. By using pulsed sonication with the microprobe set at one pulse per sonication treatment, in the presence of calcium, and by following the procedure described in Methods (modified from Ref. 5), we were able to routinely achieve 90% disruption of mast cells with minimal damage to the granule membrane, as determined by histamine release. Our finding that the use of fewer pulses per treatment yields a larger number of intact granules is in agreement with reports using the continuous sonication technique.

Raphael et al. [4] employed a Ca^{2+}, Mg^{2+}-free sonication buffer. Use of other sonication buffers yields decreased granule recovery. The deletion of calcium and magnesium may increase the granule yield by preventing the adherence of the released granules to each other and to membranes. The sonication protocol reported here is designed to disrupt a high percentage of mast cells while leaving the perigranular membrane intact. The results demonstrate that sonication buffer containing added calcium and bovine serum albumin increased the percent disrupted cells without adversely affecting granule integrity. The added calcium may increase membrane stability, while the added albumin may prevent granules from adhering to other cellular membranes.

Perigranular membrane yields may be compared to the similar membranes isolated from adrenal chromaffin granules. Two different techniques [17,18] yielded chromaffin granules that contained 7 and 12% of the total original protein. Osmotic lysis of these granules gave vesicles or ghosts with yields of 0.6–0.8% of total protein. Thus, the yield of mast cell granules (25%) is twice that of the chromaffin granules and the resulting yield of perigranular membranes (4.5%) is also higher.

These membranes have been characterized using established membrane marker enzymes. This is the first biochemical assessment of the mast cell plasma membrane or the perigranular membrane. The membrane marker enzymes used for these studies are commonly found in specific membranes of other cell types. It is not known, however, if these are valid indicators of the same membranes in the mast cell. For example, glucose-6-phosphatase is considered as an endoplasmic reticulum membrane marker enzyme, but it has also been reported in nuclear membranes and Golgi membranes [9]. The ($Na^+ + K^+$)-ATPase is identified as a plasma membrane marker in most cells. However, it is not a useful indicator here since no ($Na^+ + K^+$)-ATPase activity could be detected in the mast cell. Therefore, we used the 5'-nucleotidase as the plasma membrane marker. Although widely accepted as a plasma membrane bound enzyme [9] and previously used as such for mast

cells [15], 5'-nucleotidase has been detected in intracellular membranes [19]. The mitochondrial membrane enzyme markers (monoamine oxidase and succinate dehydrogenase) displayed low activity in mast cell homogenates, which may be related to the fact that rat peritoneal mast cells contain low numbers of mitochondria. Helander and Bloom [20], using stereological methods, estimate that mitochondria comprise only 2% of the mast cell volume.

Acknowledgements

We would like to thank John P. Christopher for his critical advice, William W. Wolfe for his excellent technical assistance, June Poplack for her assistance with the phosphate analyzer and Elsa Chock for her assistance with the electron microscopy. L.M.A. was supported by a National Research Council Associateship.

References

1 Lagunoff, D. and Benditt, E.P. (1963) Ann. N.Y. Acad. Sci. 103, 185–198
2 Uvnas, B. (1982) in The Secretory Granule (Posner, A.M. and Trifaro, J.M., ed.), pp 357–384, Elsevier Biomedical Press, New York
3 Uvnas, B. (1974) Methods Enzymol. 31, 395–403
4 Raphael, G.D., Henderson, W.R. and Kaliner, M. (1978) Expt. Cell Res. 115, 428–431
5 Kruger, P.G., Lagunoff, D. and Wan, H. (1980) Expt. Cell Res. 129, 83–93
6 Anderson, P., Rohlich, P., Slorach, S.A. and Uvnas, B. (1974) Acta Physiol. Scand. 91, 145–153
7 Sullivan, T.J., Parker, K.L., Stenson, W. and Parker, C. (1975) J. Immunol. 14, 1473–1478
8 Uvnas, B., Aborg, C.H. and Bergendorff, A. (1970) Acta Physiol. Scand. 78. Suppl. 336, 3–26
9 Evans, W.H. (1978) Preparation and Characterization of Mammalian Plasma Membranes, pp. 104–127, North Holland, New York
10 Raess, B.K. and Vincenzi, F.F. (1980) J. Pharmacol. Methods 4, 273–283
11 Peterson, G.L. (1977) Anal. Biochem. 8, 346–356
12 Siraganian, R.P. (1974) Anal. Biochem. 57, 383–394
13 Siraganian, R.P. (1975) J. Immunol. Methods 7, 283–290
14 Carty, S.E., Johnson, R.G. and Scarpa, A. (1980) Anal. Biochem. 106, 438–445
15 Ishizaka, T. Hirata, F., Sterk, A.R., Ishizaka, K. and Axelrod, J.A. (1981) Proc. Natl. Acad. Sci. USA 7, 6812–6816
16 Emmelot, P., Bos, C.J., Van Hoeven, R.P. and Van Blitterswijk, W.J. (1974) Methods Enzymol. 31, 75–90
17 Phillips, J.H. (1974) Biochem. J. 144, 311–318
18 Muller, T.W. and Kirshner, N. (1975) J. Neurochem. 24, 1155–1161
19 Stanley, K.K., Edwards, M.R. and Luzio, J.P. (1980) Biochem. J. 186, 59–69
20 Helander, H.F. and Bloom, G.D. (1973) J. Microsc. 100, 315–321

Life Sciences, Vol. 36, pp. 525-531
Printed in the U.S.A.

EFFECT OF PROTEASES ON THE β-THROMBOGLOBULIN RADIOIMMUNOASSAY

Jerome A. Donlon*, Elinora A. Helgeson†, and Mildred A. Donlon†

*Hematology Service- Clinical Pathology Department, Clinical Center,
National Institutes of Health, Bethesda, Maryland 20205
†Biochemistry Department, Armed Forces Radiobiology Research Institute
Bethesda, Maryland 20814-5145

(Received in final form November 19, 1984)

Summary

Rat peritoneal mast cells and mast cell granules were evaluated by radioimmunoassay for the presence of β-thromboglobulin and platelet factor 4. The initial assays indicated that a β-thromboglobulin cross reacting material was released from mast cells by compound 48/80 in a similar dose-dependent manner as histamine release. The material was also found to be associated with purified granules. However, the use of protease inhibitors in the buffers completely abolished the positive assays. Further evaluation of the effects of various proteases on the β-thromboglobulin assay indicated that elastase would also generate a false positive assay which could then be neutralized by the use of α_1-antitrypsin as a protease inhibitor. There was no protease effect on the platelet factor 4 radioimmunoassay which always showed no detectable amounts with mast cells, granules or proteases. These results clearly indicate the artifactual positive assays which can arise when using certain radioimmunoassay tests in the presence of cell proteases. The use of protease inhibitors is a necessary control when applying a radioimmunoassay to a system with potentially active proteases.

β-Thromboglobulin (βTG) and platelet factor 4 (PF4) are small cationic proteins located in the α granules of platelets and released upon activation of platelets. Both βTG and PF4 have been localized almost exclusively to the α granules of platelets (1). Although their specific physiological functions are unclear, they have been shown to have a heparin binding capacity and may act as endogenous antiheparins (2). There is a report of βTG inhibiting the production of prostaglandin I_2 from endothelial cells (3), and reports of PF4 inhibiting the enzyme collagenase (4) and stimulating leukocyte elastase (5). Platelet factor 4 has also been shown to be a chemoattractant for monocytes, neutrophils, and fibroblasts (6, 7). One study using peroxidase - antiperoxidase immunochemistry on fixed tissue sections demonstrated PF4 in human skin mast cells, but could not demonstrate βTG (8, 9). This finding is of interest since mast cells are known to contain heparin (10). The PF4 may be acting like a binding protein in association with the heparin in the mast cell granules. Human mast cells are difficult to obtain in sufficient quantity or purity to evaluate their granule contents. However, pure preparations of rat peritoneal mast cells (RPMC) are readily available and purified granules can be obtained (11, 12). This study was initially begun to evaluate the possibility of βTG and PF4 association with RPMC and their granules. However, it quickly became apparent that a positive result in the β-thromboglobulin radioimmunoassay was due to the presence of active mast cell granule proteases. The study then sought to clarify the basis of the false positive results associated with the βTG radioimmunoassay of mast cells.

0024-3205/85 $3.00 + .00

Methods

Mast cells were obtained by peritoneal lavage from Sprague-Dawley rats. The cells were purified to > 95% following centrifugation through a 38% albumin gradient (11). Thereafter, the cells were washed twice in a Hepes buffered Hanks balanced salt solution containing calcium and resuspended in the same buffer to about 10^6 cells per milliliter. Granules were prepared from the purified mast cells by the sonication and differential centrifugation technique as previously described (12). Granules prepared in this way retain all histamine and specific enzymes. Histamine was measured fluorometrically using the o-pthalaldehyde (OPT) reaction (13, 14).

The radioimmunoassay for β-thromboglobulin was performed in general as indicated in the commercial kit package insert. Briefly, 50 µl of a standard or an unknown was placed in a 12 mm x 75 mm plastic tube. Antiserum to βTG (200 µl) and ^{125}I tracer βTG (200 µl) were added to all tubes, mixed and incubated at room temperature for 1 hour. The antigen-antibody complexes were precipitated by the addition of 500 µl of saturated ammonium sulfate, mixing and standing for 15 min. The tubes were centrifuged at 2000 x g for 20 min and the supernatant decanted. The tubes were placed in a gamma counter to determine the bound radioactivity in the precipitate.

The radioimmunoassay for platelet factor 4 was performed in general as indicated in the commercial kit package insert. Briefly, 50 µl of a standard or an unknown was placed in a 12 mm x 75 mm plastic tube. Antiserum to platelet factor 4 (250 µl) and ^{125}I tracer platelet factor 4 (250 µl) was added to each tube, mixed and incubated at room temperature for 2 hr. The antigen-antibody complexes were precipitated by adding 1 ml of saturated ammonium sulfate, mixing and standing for 15 min. The tubes wee centrifuged at 2000 x g for 20 min and the supernatants decanted. The tubes were placed in a gamma counter to determine the bound radioactivity in the precipitates. The β-thromboglobulin radioimmunoassay kit was obtained from Amersham (Arlington Heights, IL), and the platelet factor 4 kit from Abbott (Chicago, IL).

Polyacrylamide gel electrophoresis was performed on a disc gel apparatus using 10% polyacrylamide, 1% SDS 60 mm gels (15). β-Thromboglobulin ^{125}I tracer (50,000 cpm) was added to each of three gels after mixture in buffer or elastase or elastase and α_1 antitrypsin. Gels were run for 2 hr at 48 mA and then sliced.

A quantitative method with benzoyl tyrosine ethyl ester (BTEE) as a synthetic substrate was used for the protease determination (16). Compound 48/80, elastase (porcine pancreas), thrombin (human), activated factor X (Xa, Russel viper venom activated, bovine), plasmin (human), lysozyme (chicken egg white), aprotinin (Trasylol), leupeptin, and α_1 antitrypsin (human) were obtained from Sigma Chemical Co. (St. Louis, MO).

Results

Rat peritoneal mast cells were lysed by freeze-thaw x 3 and the cell debris pelleted at 10,000 x g for 10 min in a microfuge. The supernatant was assayed for histamine, βTG and PF4. Similarly a mast cell granule preparation was assayed for histamine, βTG and PF4. The PF4 assay gave no detectable reaction. The results of the βTG and histamine assays shown in Table 1 seem to indicate the presence of βTG in mast cells, possibly localized to the granules.

Assuming a rat mast cell cytoplasmic volume of 0.7 ul per 10^6 cells (17), the calculated intracellular concentration of "β-thromboglobulin" would be about 2.5 mg/ml.

Rat mast cells release histamine in a dose-dependent response to compound 48/80. Figure 1 illustrates a similar dose-dependent release of the apparent βTG.

TABLE I

Apparent β-Thromboglobulin Content of Rat Mast Cells

	"β-Thromboglobulin" (ng)
Rat Mast Cells	1.75 ± 0.82 ng/10^3 cells
	0.060 ± 0.025 ng/ng histamine
Mast Cell Granules	4.32 ± 1.73 ng/µg protein
	0.085 ± 0.037 ng/ng histamine

Mean ± 2 S.D. of three determinations.

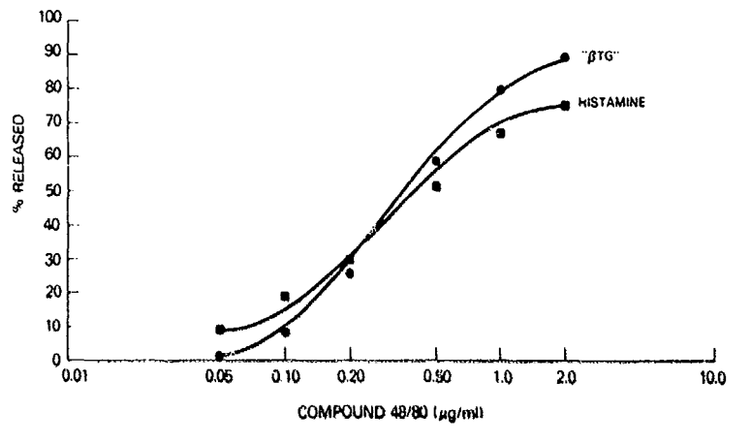

FIG. 1

Dose response curve for histamine and "β-thromboglobulin" release from rat mast cells by compound 48/80. Rat mast cells were suspended in Hepes-HBSS to 10^6 cells/ml. Results are expressed in percent of total cell content. Total content determined by assay of lysed specimens (freeze thaw x 3).

When protease inhibitors, aprotinin (Trasylol) or leupeptin were added to the cell suspension buffer prior to lysis, the βTG assay gave no reactions as shown in Table II. These results suggested a protease artifact in the determination of βTG by radioimmunoassay.

Various proteases that are likely to be present in plasma were tested to determine if they would generate a false positive βTG result. The data of Table III clearly indicate that only elastase at greater than 2.8 u/ml gave a significant false positive βTG result. Although the other enzymes were tested at significant levels they had little or no effect on the radioimmunoassay. Results are the average of two determinations.

The effect of elastase on the β-thromboglobulin tracer was dose-dependent and was abolished in the presence of the protease inhibitor α_1 antitrypsin. These results are presented in Table IV.

TABLE II

Effect of Protease Inhibitors on β-Thromboglobulin Radioimmunoassay of Rat Mast Cells

	"β-Thromboglobulin" ng/10^3 cells
Buffer A	2.10 ± 0.75
Buffer B	0.03 ± 0.02
Buffer C	0.06 ± 0.03

Buffer A: 50 mM Hepes, Hanks Balanced Salt Solution, pH 7.4.

Buffer B: 50 mM Hepes-HBSS pH 7.4, 0.1% v/v Aprotinin.

Buffer C: 50 mM Hepes-HBSS pH 7.4, 0.4% v/v Aprotinin, 1 µg/ml leupeptin, 0.1% w/v bovine serum albumin.

Mean ± S.D. of three determinations.

TABLE III

Effects of Proteases on β-Thromboglobulin Tracer

Enzyme			"βThromboglobulin" (ng/ml)
Thrombin	10.0	U/ml	3.1
Thrombin	1.0	U/ml	< 2.0
Elastase	28.0	U/ml	> 220
Elastase	2.8	U/ml	8.9
Elastase	0.28	U/ml	< 2.0
Plasmin	1.0	U/ml	5.7
Plasmin	0.1	U/ml	< 2.0
Factor Xa	2.0	U/ml	2.5
Factor Xa	0.2	U/ml	< 2.0
Lysozyme	20000	U/ml	< 2.0
Lysozyme	2000	U/ml	< 2.0
Hepes-HBSS buffer			< 2.0

TABLE IV

Effect of α_1 Antitrypsin on the Elastase Interaction With β-Thromboglobulin Tracer

	"β-Thromboglobulin" ng/ml		
Elastase	Elastase + Buffer	Elastase + α_1 antitrypsin	Elastase + BSA
50 U/ml	> 220 ng/ml	5.5 ng/ml	>220 ng/ml
20 U/ml	34.1	2.6	31.5
10 U/ml	5.2	2.0	4.5
5 U/ml	3.4	1.2	3.0

Elastase in 0.1 M Tris pH 7.4 buffer
α_1 Antitrypsin (2.5 mg/ml)
Bovine Serum Albumin (BSA) (2.5 mg/ml)

Results are average of two determinations

Figure 2 illustrates the results of the SDS-PAGE of the βTG tracer after preincubation with buffer or elastase or elastase plus α_1 antitrypsin. It is clear in Figure 2B that the elastase breaks down the tracer but that the presence of α_1 antitrypsin will prevent the tracer breakdown (Fig. 2C).

A specimen of purified human lung mast cells was provided by Dr. Henry Meier and Dr. Edward Schulman. These cells gave minimally detectable levels of βTG and PF4 by radioimmunoassay in the absence of protease inhibitors.

Discussion

This study clearly indicates that certain proteases can produce a false positive result in the βTG radioimmunoassay. Mast cells are known to contain a small molecular weight chymase which is associated with the granules (16, 18, 19). Apparently the enzymes degrade the tracer protein thereby releasing a radiolabeled fragment which is not immunoreactive. A similar artifact was observed for corticotropin/β endorphin immunoreactivity of rat mast cells (20, 21). The effect may be relatively enzyme and substrate specific since the PF4 tracer, which is similar in many structural sequences to βTG, although not immuno cross reactive, did not generate false positive results by the enzymes tested.

The addition to the cell suspension buffer of a standard amount of a general protease inhibitor (aprotinin) was sufficient to abolish the false positive results. The practice of using protease inhibitors in cell suspension buffer where radioimmunoassays will be applied is encouraged.

Some of the plasma proteases likely to be active in plasma were tested and shown not to give a significant false positive result. Therefore they would be very unlikely to contribute to plasma βTG levels when a radioimmunoassay is used. Although elastase did generate a significant false positive result, it is unlikely that a plasma specimen would have elastase levels in the range necessary to generate a false positive result. The mast cell enzymes are concentrated in the granules and thereby can cause a significant effect. Rat mast cell chymase may represent 15% of the total granule protein (10, 19).

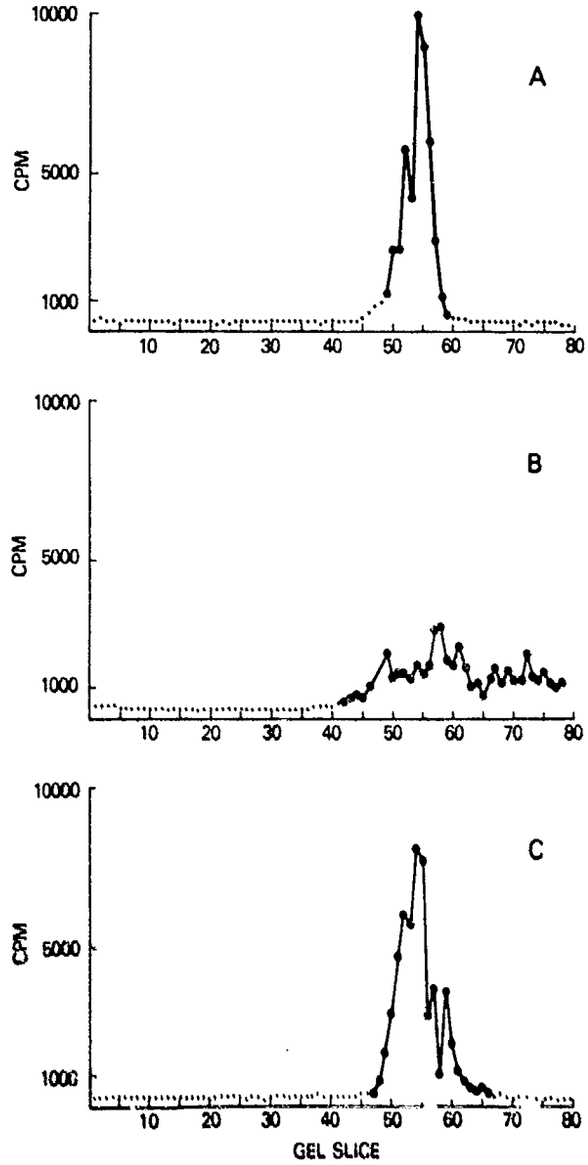

FIG. 2

SDS-PAGE of β-thromboglobulin tracer. 50000 cpm of ^{125}I tracer premixed with Hepes-HBSS buffer (A) or elastase (30 U/ml) (B) or elastase (30 U/ml) and $_1$ antitrypsin (2.5 mg/ml) (C). After a 10 min preincubation at room temperature, the mixtures were made 1% SDS and loaded on the gels. Gels were sliced and each slice counted in a gamma counter.

Reports of localization of PF4 in human tissue (skin) mast cells have relied on immunochemical (peroxidase-antiperoxidase) assays in gluteraldehyde fixed tissue (8, 9). Proteases may be active in the fixed tissue and therefore their results may not be subject to a protease artifact. In addition, we did not show any protease effect on the PF4 tracer. Our assay of the human lung mast cells did not demonstrate any βTG or PF4. Human lung mast cells contain about 10% of the heparin and histamine content of rat mast cells. Lung mast cells may lack detectable levels of these proteins and/or the protease enzymes or enzyme levels may be different from rat mast cells such that no tracer degradation occurred. Knauer et al. observed an increase in plasma platelet factor 4 levels in asthmatic patients exposed to ragweed antigen (22). However,

stimulation of human lung mast cells (85% pure) with antibody to IgE caused histamine release but no detectable release of PF4 (23). Platelet factor 4 has been reported to cause human basophils to release histamine (24). The specific functions of the platelet proteins βTG and PF4 remain unclear.

In conclusion, caution should be used in applying radioimmunoassays in specimens in which proteases are likely to be present. Protease inhibitors should be used to avoid false positive results.

Acknowledgments

The authors gratefully acknowledge the suggestions and advice given by Dr. H. Gralnick and Dr. M. Rick. The typing expertise of M. Owens is greatly appreciated.

References

1. K. L. KAPLAN, Platelets in Biology and Pathobiology - 2 (J. L. Gordon, ed.) Chap 4, pp. 77-90, Elsevier/North Holand Press, Amsterdam (1981).
2. S. NIEWIAROWSKI and D. PAUL, Platelets in Biology and Pathobiology - 2 (J. L. Gordon, ed.) Chap 5, pp. 91-106, Elsevier/North Holland Press, Amsterdam (1981).
3. W. HOPE, T. J. MARTIN, C. N. CHESTERMAN and F. J. MORGAN, Nature 282 210-212 (1979).
4. J. HITI-HARPER, H. WOHL and E. HARPER, Science 199 991-992 (1978).
5. S. A. LONKY and H. WOHL, J. Clin. Invest. 67 817-826 (1981).
6. T. F. DUEL, R. M. SENIOR, D. CHANG, G. L. GRIFFIN, R. L. HEINRICKSON and E. T. KAISER, Proc. Natl. Acad. Sci. 78 4584-4587 (1981).
7. R. M. SENIOR, G. L. GRIFFIN, J. S. HUANG, D. A. WALZ and T. F. DEUEL, J. Cell Biol. 96 382-385 (1983).
8. K. M. MCLAREN, L. HOLLOWAY and D. S. PEPPER, Throm. Res. 19 293-297 (1980).
9. K. M. MCLAREN and D. S. PEPPER, Histochem. J. 15 795-800 (1983).
10. D. D. METCALFE, M. KALINER and M. A. DONLON, Critical Reviews in Immunology (M. Z. Atassi, ed.) Vol. 3, pp. 23-74, CRC Press Inc., Boca Ratan, Florida (1981).
11. T. J. SULLIVAN, K. L. PARKER, W. STENSON and C. PARKER, J. Immunol. 114 1473-1479 (1975).
12. G. D. RAPHAEL, W. R. HENDERSON and M. KALINER, Exp. Cell Res. 115 428-431 (1978).
13. R. P. SIRIGANIAN, Anal. Biochem. 57 383-394 (1974).
14. R. P. SIRIGANIAN and W. A. HOOK, Manual of Clinical Immunology (N. E. Rose and H. Friedman, eds.) pp. 808-821, American Society for Microbiology, Washington, DC (1980).
15. K. WEBER and M. OSBOURNE, J. Biol. Chem. 244 4406-4415 (1969).
16. R. G. WOODBURY, M. T. EVERITT and H. NEURATH, Methods in Enzymology (L. Lorand, ed.) Vol. 80, pp. 588-609, Academic Press, Inc., New York, New York (1981).
17. H. F. HELANDER and G. D. BLOOM, J. Microscopy 100 315-321 (1974).
18. L. B. SCHWARTZ and K. F. AUSTEN, J. Invest. Dermat. 74 349-353 (1980).
19. D. LAGUNOFF and E. P. BENDITT, Ann. N.Y. Acad. Sci. 103 185-198 (1963).
20. R. P. DIAUGUSTINE, L. H. LAZARUS, G. JAHNKE, M. N. KAHN, M. D. ERISMAN and R. I. LINNOILA, Life Sci. 27 2663-2668 (1980).
21. G. D. JAHNKE, L. H. LAZARUS, R. P. DIAUGUSTINE, C. M. SOLDATO and D. D. ERISMAN, Life Sci. 29 397-403 (1981).
22. K. A. KNAUER, L. M. LICHTENSTEIN, N. F. ADKINSON and J. E. FISH, N. Engl. J. Med. 304 1404-1407 (1981).
23. K. A. KNAUER, J. E. FISH, N. F. ADKINSON, L. M. LICHTENSTEIN, S. P. PETERS and H. H. NEWBALL, N. Engl. J. Med. 305 893 (1982).
24. L. L. BRINDLEY, J. M. SWEET and E. J. GOETZL, J. Clin. Invest. 22 1218-1223 (1983).

Effect of γ-Irradiation on the Healing of Gastric Biopsy Sites in Monkeys

An Experimental Model for Peptic Ulcer Disease and Gastric Protection

ANDRE DUBOIS, ETIENNE DANQUECHIN DORVAL, LAWRENCE R. WOOD, JAMES E. ROGERS, LINDA O'CONNELL, ASAF DURAKOVIC, and JAMES J. CONKLIN

Reprinted with permission from the American Gastroenterological Association

GASTROENTEROLOGY 1985;88:375–81

Effect of γ-Irradiation on the Healing of Gastric Biopsy Sites in Monkeys

An Experimental Model for Peptic Ulcer Disease and Gastric Protection

ANDRE DUBOIS, ETIENNE DANQUECHIN DORVAL, LAWRENCE R. WOOD, JAMES E. ROGERS, LINDA O'CONNELL, ASAF DURAKOVIC, and JAMES J. CONKLIN

Department of Medicine, Uniformed Services University of the Health Sciences; and Radiation Sciences Department, Armed Forces Radiobiology Research Institute, Bethesda, Maryland

The acute effects of γ-irradiation on the gastric mucosa have been studied in a primate model. Fiberoptic gastroscopies were performed in 6 rhesus monkeys in the basal state as well as 3 h and 3, 7, and 9 days after total body irradiation (800 rads). Gastric biopsy specimens (diameter 1 mm) obtained during each session were examined using light microscopy and scanning electron microscopy; in addition, subsequent healing of the biopsy sites was assessed visually. Gastric biopsy sites were completely healed in 3 days in the basal state; in contrast, ulcer craters (diameter 1 mm) were still present at the site of the biopsies 3, 7, and 9 days after the biopsies were performed in irradiated animals. Light microscopic examination of the biopsy specimens demonstrated only lymphocytic infiltration of the lamina propria. In contrast, scanning electron microscopic examination revealed that the size and number of microvilli of the gastric surface epithelial cells were increased on the day of irradiation compared to basal; 3–9 days later, numerous gastric surface epithelial cells were damaged or had dissappeared so that bare areas of the lamina propria were visible in the specimens taken outside of the ulcer craters. These changes may reflect inadequate protection or insufficient regeneration of gastric mucosal cells which, in turn, would explain the persistence of ulcers after gastric biopsies were performed in irradiated monkeys.

Many experimental models have been developed in an attempt to clarify the pathophysiology and the treatment of gastric and duodenal ulcer disease. Most models have used rats, which have the advantage of permitting the study of a large number of animals. However, the rodent stomach differs markedly from that of the human in its anatomic and physiologic features. Furthermore, drug dosage required for experimental production, prevention, and healing of gastroduodenal ulcer is much larger than the dosage recommended in humans.

Thus, there is a need for an animal model closer to humans that would permit the experimental study of peptic ulcer disease. In the past 7 yr, we have used rhesus monkeys to evaluate basal and stimulated gastric secretion and gastric emptying (1) as well as the effect of various prostaglandins (2–4) and opioid peptides (5). These studies demonstrated marked similarities of monkey and human gastric functions (6), and the drug dosage was close to that used in clinical medicine. In this same model, psychologic contingencies coupled with delivery of electric shocks consistently produced superficial gastroduodenal erosions (7), although most lesions disappeared in several days despite the continuation of stress; this effect is consistent with the habituation of gastric function suppression found in the same animal model (8).

Received April 2, 1984. Accepted July 6, 1984.

Address requests for reprints to: Andre Dubois, M.D., Ph.D., Department of Medicine, Uniformed Services University, 4301 Jones Bridge Road, Bethesda, Maryland.

This work was supported, in part, by the Uniformed Services University of the Health Sciences Protocol No. R08342.

The opinions and assertions contained herein are the private ones of the authors and are not to be construed as official or reflecting the views of the Department of Defense or the Uniformed Services University of the Health Sciences.

The authors thank L. Iwanyck and J. Barchers for editorial assistance and M. Flynn, J. Stewart, J. Warrenfeltz, and N. Fleming for support in animal handling.

Abbreviations used in this paper: SEC, surface epithelial cells.

The purpose of the present studies was to investigate whether rhesus monkeys exposed to ionizing radiation would develop chronic gastric ulcerations either spontaneously or after endoscopic biopsies were performed. In addition, we used light microscopy and scanning electron microscopy to evaluate possible underlying changes of the gastric surface epithelial cells.

Materials and Methods

Endoscopies

Six male rhesus monkeys were subjected to fiberoptic endoscopy performed under ketamine anesthesia using an Olympus GIF-P3 gastrointestinal fiberscope with an outer diameter of 9 mm (Olympus Corporation of America, New Hyde Park, N.Y.). The experiments reported herein were conducted according to the principles set forth in the "Guide for the Care and Use of Laboratory Animals," Institute of Animal Resources, National Research Council, Department of Health, Education, and Welfare Publication No. (NIH)78-23. The gross appearance of the gastric mucosa was assessed in the basal state, 3h after irradiation, and 3, 7, and 9 days later. On the day of irradiation, the animals were exposed to 800 rads (800 cGy) delivered bilaterally to the whole body using a large 10^5 Ci ^{60}Co irradiator at 500 rads/min. In addition, pinch biopsy specimens 1 mm in diameter were obtained from the gastric antrum at the time of each endoscopy and were prepared for light and scanning electron microscopy. Finally, the presence or absence of healing at the site of each previously performed biopsy was assessed visually.

Light Microscopy

Biopsy specimens were fixed in 10% buffered formalin for at least 6 h, dehydrated in ethanol and xylene, and embedded in paraffin; 4-μm sections were stained with hematoxylin and eosin and observed by a blinded investigator (J.E.R.) using a Zeiss microscope (Carl Zeiss, Thornwood, N.Y.).

Scanning Electron Microscopy

Biopsy specimens were immediately placed in 2% glutaraldehyde in 0.1 N sodium cacodylate and stored for 24 h at 4°C. To eliminate the layer of material coating the gastric surface epithelial cells, each biopsy specimen was then washed with phosphate-buffered saline and a glycosidase enzyme solution (mixed glycosidase, T. cornutus, Miles Laboratories, Elkhart, Ind.) as previously described (9). Biopsy specimens were then postfixed separately for 1 h in 1% OsO_4 in 0.1 N sodium cacodylate at 4°C, and dehydrated using an ethanol series of 50%, 70%, 95%, and 100% with three changes of absolute ethanol. Biopsy specimens were dried in a critical-point drying apparatus from liquid CO_2 (Samdri, pvt-3, Tousimis Research, Rockville, Md.), mounted on aluminum stubs, and sputter-coated with gold palladium (Samsputter 2A, Tousimis Research) for examination on a JSM-35 scanning electron microscope (JEOL, Peabody, Mass.) operated at 25 kV. Scanning electron microscope pictures were taken by a blinded investigator (L.W.) using a locally developed computer-assisted random number sequence program. This program allows the random photographing of eight pictures at ×1000 per biopsy, thus avoiding the bias presented by taking one type of image rather than another. A few cells in each area were then photographed at ×5000 to obtain a greater magnification. Finally, each picture was analyzed blindly in writing by another investigator (A.D.). These notes were subsequently reconciled with the type of treatment.

Results

Gross Endoscopic Appearance

Endoscopies performed before and for up to 9 days after irradiation failed to demonstrate any spontaneous lesion of the gastric antrum. Immediately after biopsies were performed, a small amount of bleeding was observed; although no attempt was made to quantitate precisely the hemorrhage, no important difference was noted after irradiation compared with the basal state.

Biopsies performed 10 to 7 days before irradiation completely healed in 3 days and no scarring was observed. In contrast, the site of biopsies performed on the day of the irradiation appeared 3 days later as a reddish ulceration, depressed in its center and surrounded by a raised margin (Figure 1, *left panel*). Seven days after the initial biopsy, the center of the erosion appeared white with a pink raised margin (Figure 1, *right panel*). Nine days after irradiation, the ulcer created at the site of the initial biopsy was unchanged and a biopsy performed on day 7 had produced an ulcer similar to that seen 3 days after irradiation. These observations were consistent in all 6 monkeys.

Light Microscopy

Biopsy specimens usually comprised the full mucosa including the muscularis mucosae. In the basal state, the surface of the gastric mucosa was composed of cylindrical cells with a basally positioned nucleus and containing mucus in their apical pole. Pits and glands were well delineated and the lamina propria contained only a few plasma cells and lymphocytes. After irradiation, the general architecture of the mucosa was normal and the epithelial cells were not significantly changed. However, the diffuse lymphocytic infiltration of the lamina propria was more pronounced in 4 of 6 animals, 3, 7, and 9 days after irradiation (Figure 2). In addition, biopsy specimens obtained from 3 of these 4 mon-

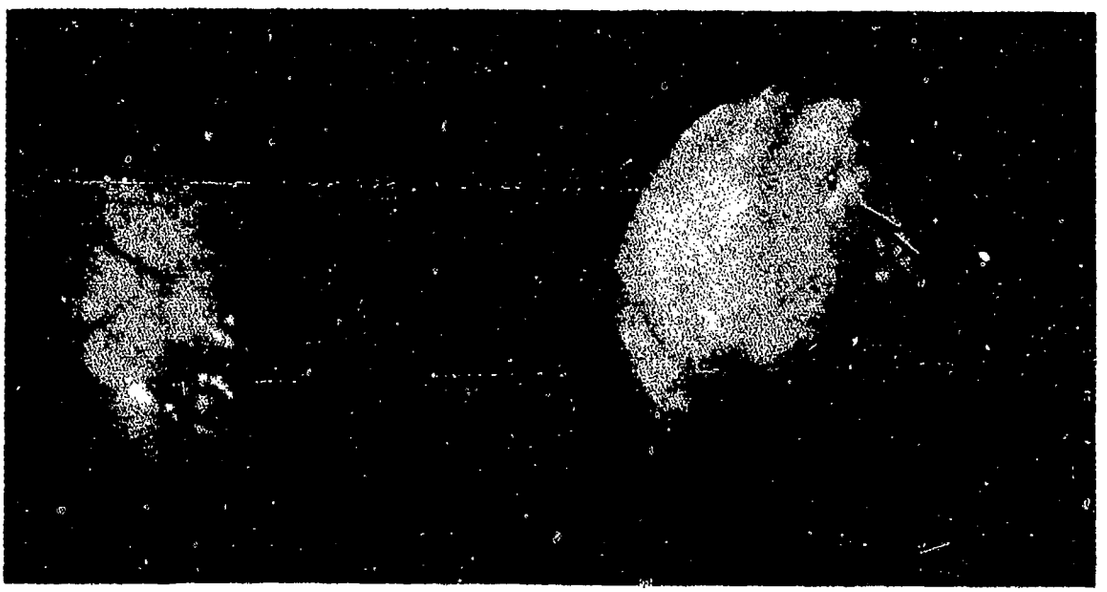

Figure 1. Endoscopic appearance of the antral mucosa after irradiation. *Left panel*: ulcer observed at the site of the biopsy 3 days after it was taken on the day of irradiation. Central depression is covered with a fibrinous necrosis and raised margins show discrete inflammation. *Right panel*: 7 days after irradiation in a different animal, the center of the ulceration is covered with white fibrin whereas the margins are less prominent than 4 days earlier (arrow); in the left lower area, the site of a biopsy performed 4 days earlier has given way to a small ulceration, which is intermediate between the two other ulcers shown on this figure.

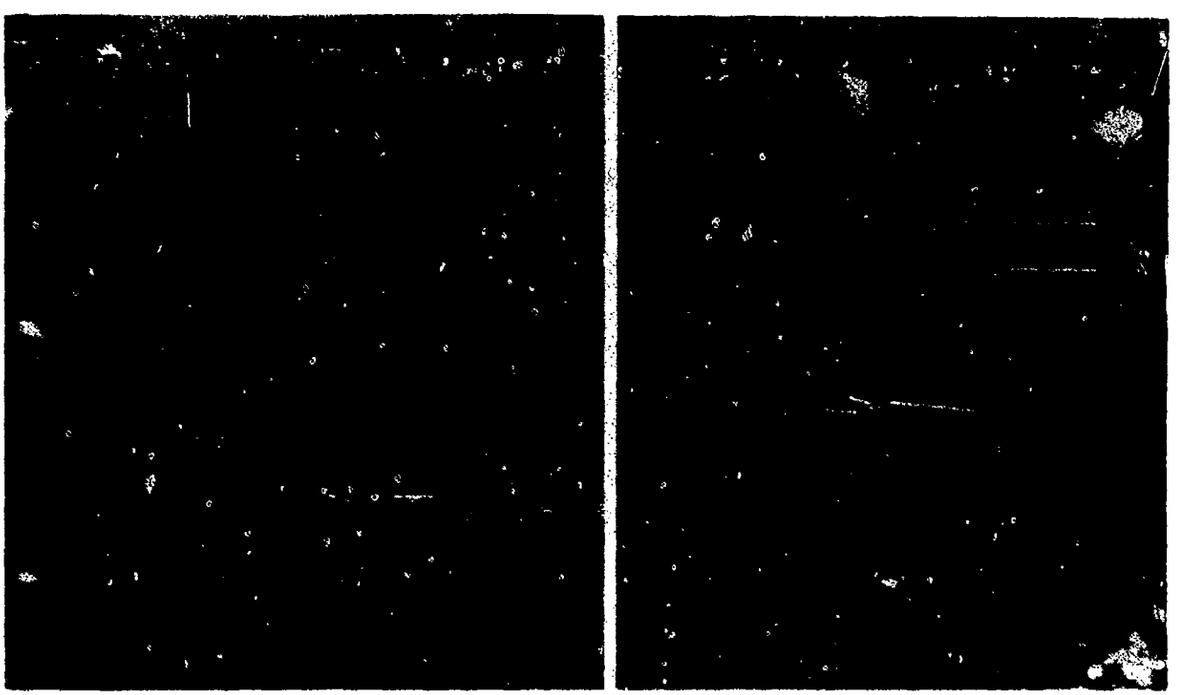

Figure 2. Light microscopic appearance of a gastric biopsy specimen taken 7 days after irradiation. *Left panel* (×400) demonstrates diffuse lymphocytic infiltration of the lamina propria (arrow); *right panel* (×400) illustrates a nodular infiltrate (double arrows) located at the level of the muscularis mucosae (single arrow).

keys contained focal infiltration of the lamina propria (Figure 2). Biopsies of the ulcers showed a center covered with a homogeneous layer of fibrinoid necrosis covering the muscularis mucosae; the margins of the ulcers demonstrated inflammation and moderate granulation.

Scanning Electron Microscopy

In the basal state, gastric surface epithelial cells (SEC) were clearly separated from each other and arranged circularly around the openings of the gastric pits (Figure 3); parts of the luminal membranes of SEC were covered with microvilli sending out short projections into the gastric lumen (Figure 3, *inset*). Three hours after irradiation, the microvilli of many SEC were more closely packed and larger than in the basal state (Figure 4); in addition, the valleys separating SEC from each other were less prominent or even sometimes disappeared (Figure 5). In some areas, cavities entering the cytoplasm were formed in the membranes of some SEC (Figure 5). Seven and 9 days after irradiation, many SEC appeared damaged or had been shed (Figure 6); in addition, some areas were devoid of SEC, leaving the lamina propria exposed except inside the gastric pits (Figure 6, *inset*). These different changes were seen in at least one of the coded pictures obtained for each animal.

Discussion

The present studies demonstrate that, in monkeys, endoscopic gastric biopsies performed immediately after total body irradiation with 800 rads lead to the formation of gastric ulcers. As these small ulcers do not heal spontaneously in up to 9 days, this experimental model could be used in order to study some of the factors involved in the pathophysiology and treatment of peptic ulcer disease. However, this dose causes the death of all animals within 2–4 wk; therefore, such a model would require the use of autologous bone marrow transplantation or of local gastric irradiation if long-term studies were planned.

The mechanism of this absence of healing is unclear. Human gastric mucosa is known to be more resistant to acute damage caused by γ-irradiation than the small intestine. In humans, doses of 800 rads administered in 5 days do not modify the upper part of gastric glands, although the base of some glands display discrete abnormalities such as eosinophilia of parietal and chief cells, pyknotic nuclei, and cell flattening (10). In addition, polymorphonuclear infiltration of the lamina propria is often present (11). These latter changes are similar to those observed by light microscopic examination of the biopsy specimens taken from the stomach of our monkeys.

However, light microscopic examination of gastric biopsy specimens is not a sensitive method to detect

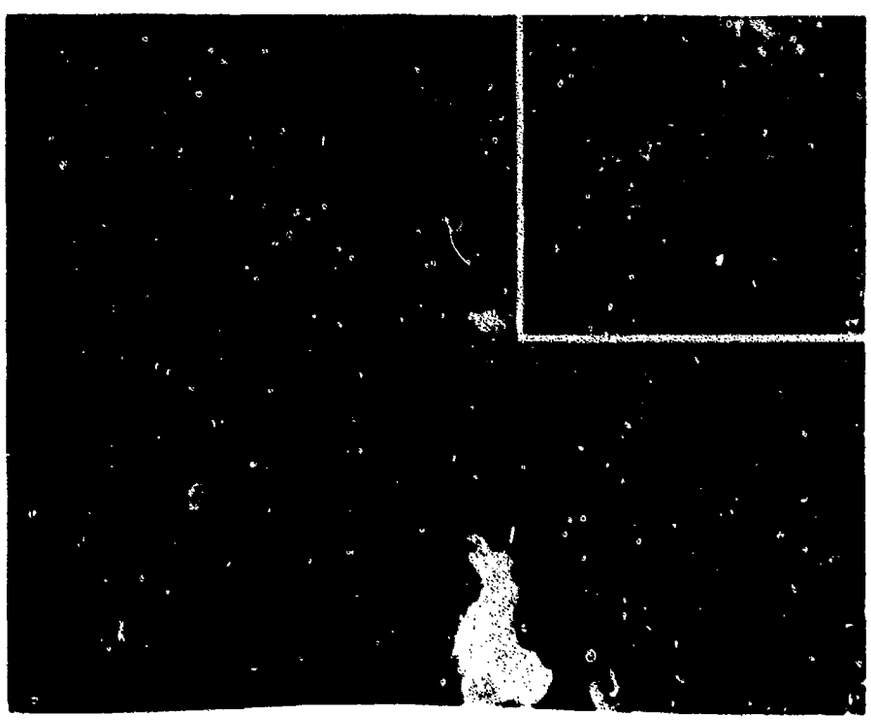

Figure 3. Scanning electron microscopic appearance of gastric biopsy specimen taken before irradiation (×1000). *Inset*: detail of one of the mucosal cells seen in the ×1000 portion (×5000).

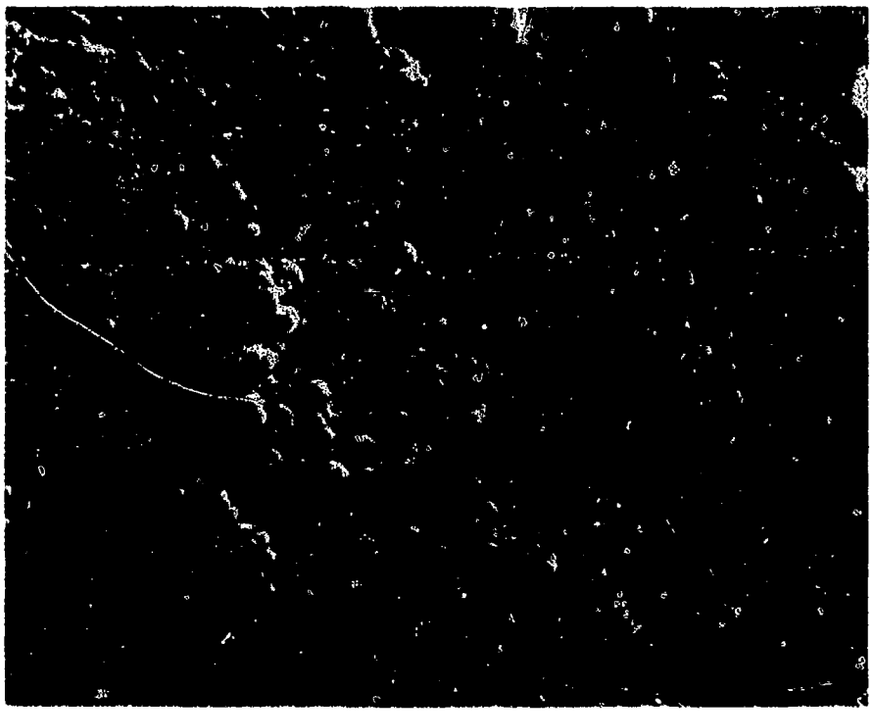

Figure 4. Scanning electron microscopic appearance of gastric biopsy specimen taken 3 h after irradiation (×5000); note that the microvilli of many surface epithelial cells appear more closely packed and larger than on the inset of Figure 3.

patchy changes of the gastric mucosa. First, fixation and section for light microscopy is not always perfect and gaps between epithelial cells are often interpreted as technical defects; second, a maximum of six sections are usually performed for light microscopy, which is far from covering an area comparable to the one examined with scanning electron microscopy. In contrast, our use of scanning electron

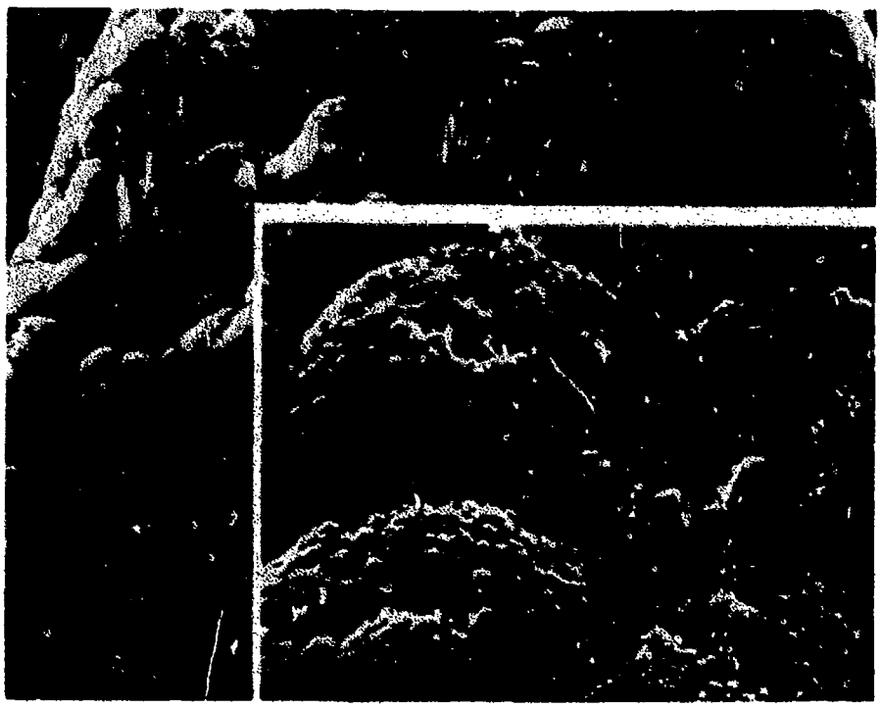

Figure 5. Scanning electron microscopic appearance of another area of the biopsy specimen shown in Figure 4; note that the valleys separating surface epithelial cells from each other are less prominent than on Figure 3 (×1000). Inset: detail of one mucosal cell seen in the ×1000 portion (×5000); observe the cavities entering the cytoplasm and formed in the membranes of some surface epithelial cells.

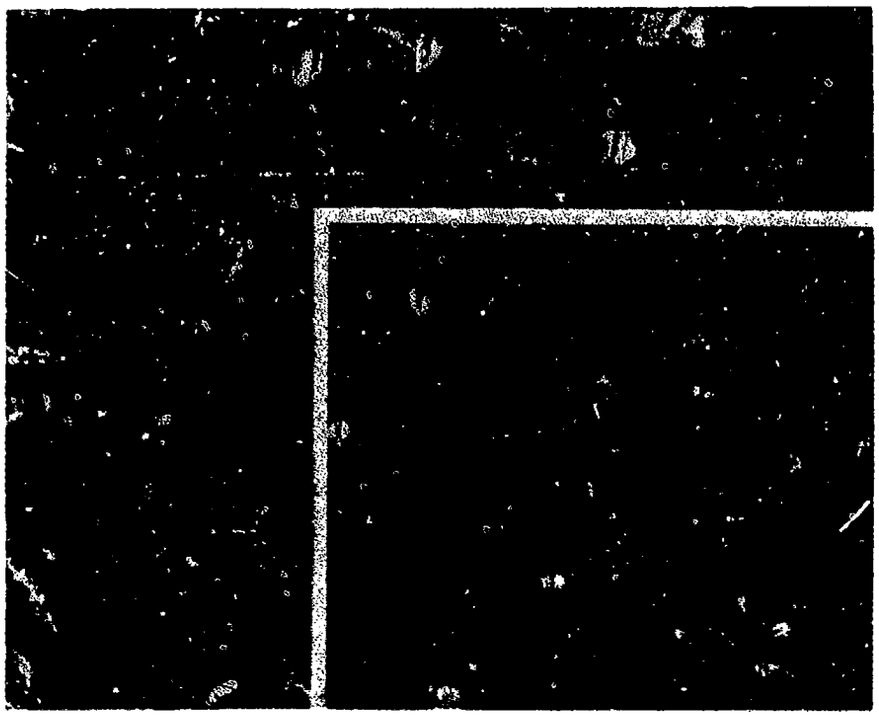

Figure 6. Scanning electron microscopic appearance of gastric biopsy specimen taken 7 days after irradiation (×1000); note that many surface epithelial cells appear damaged. *Inset* shows an area devoid of surface epithelial cells, leaving the lamina propria exposed except inside gastric pits (×5000).

microscopy permits the observation of acute changes of the gastric SEC within 3 h of total body exposure (Figure 4). These changes are observed in coded specimens examined blindly and are compatible with the release of mucus by SEC immediately following irradiation (12). Seven and 9 days after irradiation, SEC display evidence of damage and exfoliation, which may explain why bare areas of the lamina propria are visible. These late changes occur concurrently with a complete abolition of gastric mucus output (12). Thus, scanning electron microscopy permits the demonstration of two successive effects of γ-irradiation on the gastric mucosa which are not detectable with light microscopy. The initial hypertrophic response of the gastric surface epithelial cells is followed rapidly by destruction and desquamation of numerous epithelial cells. These secondary changes may reflect inadequate protection or insufficient regeneration of gastric mucosal cells which, in turn, would explain the persistence of ulcers after gastric biopsies in irradiated monkeys. To our knowledge, scanning electron microscopy had not been previously used to assess gastric mucosal damage after irradiation. Using transmission electron microscopy, however, Helander (13) has reported similar ultrastructural changes in the rat gastric mucosa after total body irradiation.

Gastric ulcers occur spontaneously after exposure to doses of radiation much greater than the ones we used. In dogs, Brecher et al. (14) found marked alterations of gastric epithelial cells in the mid-third of the stomach 6 days after total body exposure to 1200 rads; numerous cells were "hyperchromatic with centrally located, occasionally swollen nuclei and prominent nucleoli reminiscent of the early changes in the small intestine." In rabbits, a solitary total body exposure to 1500 rads consistently produced gastric ulcerations in 2–4 wk (15,16). In humans, radiation ulcer is observed in only 7% of patients receiving fractionated doses up to a total of 2500–3500 rads, this frequency increasing to only 15% with exposure to 4500–5400 rads (17,18). Overall, 50% of patients exposed to doses >5000 rads can be expected to develop significant gastric injury (19). These acute changes of gastric mucosal histology are temporary and can be followed by complete recovery for low doses of irradiation. With doses between 1500 and 2500 rads, the mucosa becomes atrophic and acid secretion is suppressed (19,20). This acid-suppressant effect of gastric irradiation was used for more than 20 yr in the treatment of peptic ulcer disease; interestingly, no acute perforation was observed in these patients. In contrast, symptomatic radiation gastritis characterized by fibroatrophy of the mucosa and accompanied by dyspepsia developed in 32% of patients exposed to 5500–6400 rads (18). The exact cause of these alterations is unknown but could be related to lack of cell renewal or vascular endothelial damage.

Thus, major changes are observed in the gastric

mucosa both acutely and chronically after exposure to high levels of ionizing radiations. With the doses used in the present experiments, however, a traumatic intervention such as biopsy is necessary to make apparent a defect in the normal gastric healing process. Although the pathophysiology of these ulcerations may be different from that of human peptic ulcer disease, the present model appears to provide an excellent opportunity to evaluate the efficacy of the various therapies of this condition.

References

1. Dubois A, Natelson B, Van Eerdewegh P, Gardner JD. Gastric emptying and secretion in the rhesus monkey. Am J Physiol 1977;232:E186–92.
2. Nompleggi D, Myers L, Castell DO, Dubois A. Effect of a prostaglandin E_2 analog on gastric emptying and secretion in rhesus monkeys. J Pharmacol Exp Ther 1980;212:491–5.
3. Shea-Donohue PT, Myers L, Castell DO, Dubois A. Effect of prostacyclin on gastric emptying and secretion in rhesus monkeys. Gastroenterology 1980;78:1476–9.
4. Shea-Donohue PT, Nompleggi D, Myers L, Dubois A. A prostaglandin endoperoxide analog increases gastric emptying and suppresses gastric secretion in rhesus monkeys. J Pharmacol Exp Ther 1982;222:379–82.
5. Shea-Donohue PT, Adams N, Arnold J, Dubois A. Effects of Met-enkephalin and naloxone on gastric emptying and secretion in rhesus monkeys. Am J Physiol 1983;245:G196–200.
6. Dubois A, Van Eerdewegh P, Gardner J. Gastric emptying and secretion in Zollinger–Ellison syndrome. J Clin Invest 1977; 59:255–63.
7. Natelson BH, Dubois A, Sodetz FJ. Effect of multiple-stress procedures on monkey gastroduodenal mucosa, serum gastrin, and hydrogen ion kinetics. Am J Dig Dis 1977;22:888–97.
8. Dubois A, Natelson BH. Habituation of gastric function suppression in monkeys after repeated free-operant avoidance session. Physiol Psych 1978;6:524–8.
9. Wood L, Dubois A. Scanning electron microscopy of the stomach during modifications of acid secretion. Am J Physiol 1983;244:G475–9.
10. Goldgraber MB, Rubin CE, Palmer WL, Dodson RL, Massey BW. The early gastric response to irradiation: a serial biopsy study. Gastroenterology 1954;27:1–20.
11. Doig RK, Fender JF, Vaiden S. Serial gastric biopsy studies in a case of duodenal ulcer treated by deep x-ray therapy. Med J Australia 1951;38:828–30.
12. Shea-Donohue PT, Desquechin-Dorval E, Montcalm E, et al. Alterations in gastric mucus secretion in rhesus monkeys following exposure to ionizing irradiation. Gastroenterology 1985 (in press).
13. Helander HF. Early effects of x-irradiation on the ultrastructure of gastric fundus glands. Radiat Res 1965;26:244–62.
14. Brecher B, Cronkite EP, Conard RA, Smith WW. Gastric lesions in experimental animals following single exposures to ionizing radiation. Am J Pathol 1958;34:105–19.
15. Engelstad RB. The effect of roentgen rays on the stomach in rabbits. Am J Roentgenol 1938;40:243–63.
16. Haot J. Radiologically induced ulcers of the stomach. Rev Belge Pathol 1965;31:203–25.
17. Bowers RF, Brick IB. Surgery in radiation injury of the stomach. Surgery 1974;22:20–38.
18. Friedman M. Calculated risks of radiation injury of normal tissue in the treatment of cancer of the testis. Proceedings of the Second National Cancer Conference. Vol. I. Philadelphia: Lippincott, 1952;390–400.
19. Palmer WL, Templeton F. The effect of radiation therapy on gastric secretion. JAMA 1939;112:1429–34.
20. Ricketts WE, Kirsner JB, Humphrey SEM, Palmer WL. Effect of roentgen irradiation on gastric mucosa. Gastroenterology 1948;11:818–31.

BRIEF COMMUNICATION

CALCIUM- AND VOLTAGE-ACTIVATED POTASSIUM CHANNELS IN HUMAN MACROPHAGES

ELAINE K. GALLIN
Physiology Department, Armed Forces Radiobiology Research Institute, Bethesda, Maryland 20814

ABSTRACT Single calcium-activated potassium channel currents were recorded in intact and excised membrane patches from cultured human macrophages. Channel conductance was 240 pS in symmetrical 145 mM K^+ and 130 pS in 5 mM external K^+. Lower conductance current fluctuations (40% of the larger channels) with the same reversal potential as the higher conductance channels were noted in some patches. Ion substitution experiments indicated that the channel is permeable to potassium and relatively impermeable to sodium. The frequency of channel opening increased with depolarization and intracellular calcium concentration. At 10^{-7} M $(Ca^{++})_i$, channel activity was evident only at potentials of +40 mV or more depolarized, while at 10^{-5} M, channels were open at all voltages tested (−40 to +60 mV). In intact patches, channels were seen at depolarized patch potentials of +50 mV or greater, indicating that the ionized calcium concentration in the macrophage is probably $<10^{-7}$ M.

INTRODUCTION

Calcium-activated potassium conductances have been described in a wide variety of cells (1, 11). Several observations indicate that macrophages also exhibit a calcium-activated potassium conductance. First, macrophages exhibit spontaneous membrane hyperpolarizations associated with an increase in conductance, which can be blocked by the addition of EGTA, verapamil, and cobalt (2, 6). Second, injection of intracellular calcium or exposure to the calcium ionophore, A23187, produces hyperpolarizations similar to the spontaneously occurring ones (6, 10). However, because stable intracellular recordings using standard microelectrodes have been difficult to obtain in macrophages, the conductance underlying these events has not been well characterized. In this study, patch clamp techniques were used to demonstrate the presence in human macrophages of voltage- and calcium-activated potassium channels with a conductance of 130 pS in 5 mM external potassium, and 240 pS in symmetrical KCl. The frequency of channel opening increased with depolarization and increasing intracellular ionized calcium in the range of 10^{-7}–10^{-5} M. These channels are very similar to the large-conductance calcium-activated potassium channels described in other cells (1, 7, 13).

MATERIALS AND METHODS

Human peripheral blood monocytes were isolated by density centrifugation on Ficoll-Hypaque gradients (5) and cultured at 37°C in RPMI-1640 containing 5% fetal bovine serum (heat inactivated at 56°C for 30 min), 10,000 μ/ml penicillin-streptomycin, and 5% glutamine. RPMI-1640, a synthetic tissue culture medium originally designed for growing leukemia cells, was developed at Roswell Park Memorial Institute. After various periods of cultivation (up to 3 wk), cells were placed in recording solutions and patch clamp experiments were performed at room temperature (21–23°C).

Recordings were obtained using a patch clamp with 1 kHz low-pass filtering (EPC-5; List Industries, Inc. Matteson, IL). Patch electrodes had resistances of 3–6 MΩ. Seals resistances ranged from 10 to 100 GΩ. The resting membrane potential of the cells was measured following the destruction of the patch membrane by increased suction. Channel activity was recorded on a chart recorder (Gould, Inc., Instrum. Div., Santa Clara, CA) and an FM tape recorder (frequency response DC to 5 kHz). Channel data were analyzed by hand after playing back at ⅛ speed into a Gould chart recorder.

The ionic composition of the medium in the patch electrode and the bath varied in different experiments. NaCl-Hanks' contained 145 mM NaCl, 4.6 mM KCl, 1.13 mM $MgCl_2$, 1.6 mM $CaCl_2$, and 10 mM HEPES-NaOH pH 7.3. KCl-Hanks' contained 145 mM KCl, 10 mM NaCl, 1.13 mM $MgCl_2$, 10 mM HEPES-KOH, pH 7.3, and various concentrations of EGTA and calcium. K-aspartate-Hanks' contained 145 mM K-aspartate instead of KCl. For free calcium levels $<10^{-5}$ M, 1.1 mM EGTA and various amounts of calcium were added to the medium to obtain the desired levels of free calcium (1.08 mM calcium for a final concentration of 4×10^{-6} M Ca^{++}; 1.06 mM for 3×10^{-6} M Ca^{++}; 0.92 mM for 5×10^{-7} M Ca^{++}; 0.55 mM for 1×10^{-7} M Ca^{++}). The free calcium concentration was calculated using 10^{-7} M as the apparent dissociation constant for the Ca-EGTA complex (8). The free calcium concentration in each solution was checked using a calcium-sensitive electrode calibrated with calcium buffers obtained from W-P Instruments, Inc. (New Haven, CT). The calculated and measured calcium levels were in good agreement. The calcium concentration of recording medium containing no calcium or EGTA was $\sim 10^{-9}$ M, as determined by a calcium-sensitive electrode.

RESULTS

Cell-attached patches from cells bathed in KCl-Hanks' exhibited large, brief (30 ms or less) outward currents at

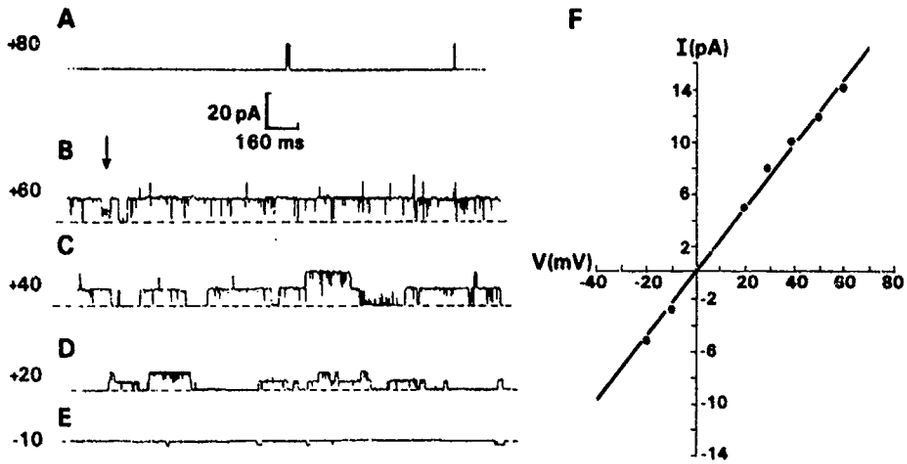

FIGURE 1 (*A–E*) Single-channel current traces. Both electrode and bath contained KCl-Hanks' (4×10^{-6} M Ca^{++}). (*A*) Current trace obtained in the cell-attached mode at a holding potential of +80 mV. (*B–E*) Current traces from the same patch as in *A* following excision. Patch is inside-out. Potentials for each tracing and zero current level (dashed line) are indicated. Traces are typical exerpts of longer records. Upward deflections represent outward current in this and other figures. (*F*) Current-voltage relationship of the same patch. Channel amplitudes were read from the chart records.

depolarized patch potentials of +50 mV or greater. Channel activity increased with increasing depolarization. These channels were rarely seen in cells bathed in NaCl-Hanks' at voltages ranging from −80 to +80 mV. However, channels were often recorded at potentials of +100 mV or more depolarized. Fig. 1 *A* shows an in situ current-tracing at a patch holding potential of +80 mV in a cell bathed in KCl-Hanks' (4×10^{-6} M Ca^{++}). No channel activity was noted at less depolarized holding potentials. Upon detachment of the patch in the inside-out configuration, channels were absent at voltages negative to −20 mV. Fig. 1, *B–E*, depicts channel activity recorded at various voltages. The frequency of opening and open-time increased as the patch was depolarized. As shown in Fig. 1 *D*, channel conductance (225 pS) was constant in the voltage range tested, and reversed at 0 mV. The channel conductance of 13 patches in symmetrical potassium solutions ranged from 200 to 275 pS and averaged 240 pS.

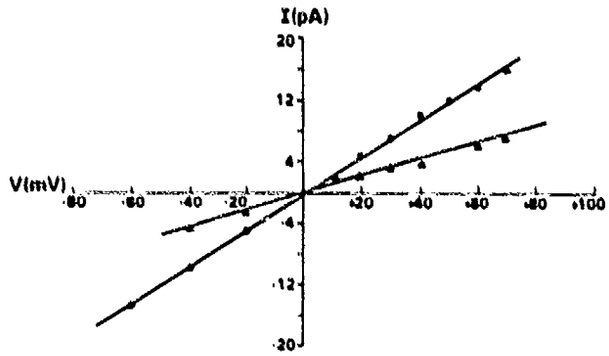

FIGURE 2 Single-channel current amplitude for large (●) and small (▲) conductance fluctuations as a function of voltage. Excised inside-out patch. Electrode contained K-aspartate-Hanks' and bath contained KCl-Hanks' (10^{-5} M Ca^{++}).

Ninety percent of the patches from which recordings were taken exhibited these channels, and patches often contained three or more channels, as judged by the number of conductance states. Smaller current fluctuations, with a conductance of ~40% of the higher conductance state, were noted in a number of experiments. The arrow in Fig. 1 *B* points to one of these events. These fluctuations were only seen in patches exhibiting the 240-pS channels, and they always had the same reversal potential as the larger conductance channels. The current-voltage relationship of both the high (240 pS) and low (100 pS) conductance state from an excised inside-out patch is shown in Fig. 2. In some studies, small outward currents with a much lower conductance (<20 pS) were also evident (Fig. 4 *D*). These currents have not been characterized, but they occurred in isolation and were often noted at lower calcium concentrations, conditions under which the higher conductance channels were not active.

A series of experiments to determine which ion(s) was responsible for this conductance indicated that the channel was permeable predominantly to potassium. The data from one of these studies are shown in Fig. 3 *A*, in which an excised outside-out patch with K-aspartate-Hanks' in the electrode was exposed to extracellular solutions containing different concentrations of potassium. The voltages are given with respect to the intracellular surface. Large channels with a conductance of 200 pS, that inverted at zero holding potential, were noted in 145 mM KCl outside, indicating that the channel was relatively impermeable to chloride, which had a negative equilibrium potential under these conditions. Replacing half the KCl in the bath with NaCl decreased the conductance of the channel from 200 to 160 pS, and shifted the reversal potential by 15 mV. Subsequent replacement of all the KCl with NaCl further reduced the channel conductance, produced a nonlinear

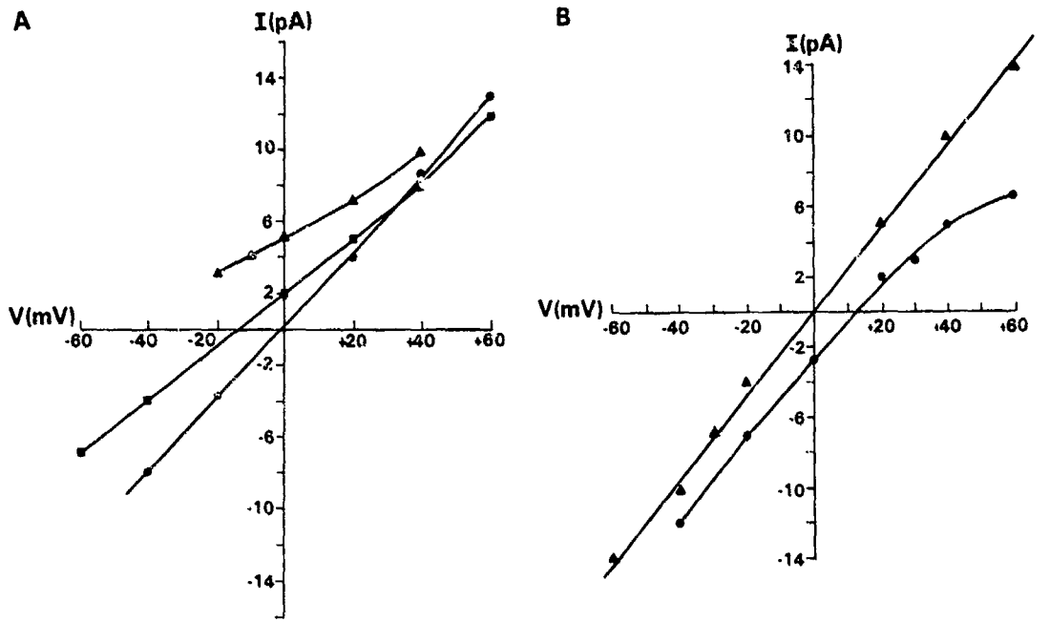

FIGURE 3 Single-channel current amplitude as a function of voltage. (*A*) Excised outside-out patch. The electrode contained K-aspartate-Hanks' (3×10^{-6} M Ca^{++}). (●) Channel current amplitudes obtained with bathing solution same as electrode solution except K-aspartate was replaced with 145 mM KCl. Bath KCl was subsequently reduced initially to 76 mM KCl by increasing NaCl to 79 mM (■), and finally to 10 mM KCl by increasing NaCl to 145 mM (▲). (*B*) Excised inside-out patch. Electrode contained the same solution as in *A*. (▲) indicates channel amplitudes with bath containing KCl-Hanks' (4×10^{-6} M Ca^{++}). (●) Bath potassium reduced to 73 and Na to 83 mM.

I-V relationship, and shifted the reversal potential to a more negative level, indicating that the channel was relatively impermeable to sodium. The null potential could not be obtained under these conditions, since channels did not open at levels more negative than −20 mV current. This experiment was repeated six times with similar results. The average conductance of seven different excised patches when NaCl bathed the outside of the membrane and KCl the inside, was 130 pS. These results indicate that (*a*) the channel behaves as if it is permeable to potassium and relatively impermeable to sodium or chloride, (*b*) increasing the sodium concentration decreases the channel's conductance, and (*c*) in the presence of 145 mM extracellular Na, the conductance is nonlinear, decreasing with hyperpolarization.

Similar experiments were performed on inside-out patches. That is, the concentration of potassium in the bath was decreased, while that of sodium was increased. The current-voltage relationship from one of these studies is shown in Fig. 3 *B*. Replacing 75 mM potassium with sodium shifted the reversal potential from 0 to +12 mV. In addition, the conductance decreased, as would be expected with the reduction of the permeant ion (potassium).

Changing the level of ionized calcium at the intracellular surface altered channel activity (the number of openings per second and the open-time) without affecting channel conductance or reversal potential. Changing the ionized calcium in the extracellular medium had no effect on the channels. Fig. 4 depicts single channel currents from an inside-out patch at a holding potential of +40 mV with various concentrations of ionized calcium in the bath. In 3×10^{-6} M Ca^{++} (Fig. 4 *A*) channels opened frequently. Decreasing the free calcium to 5×10^{-7} M reduced

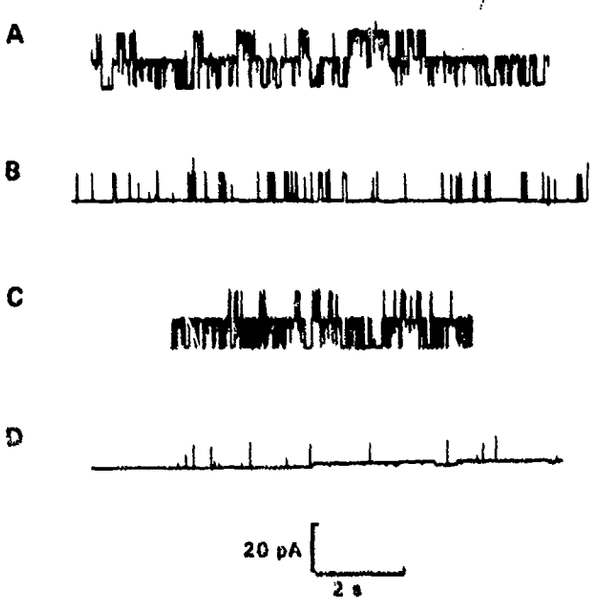

FIGURE 4 Single channel current traces from an excised inside-out patch at +40 mV holding potential. Tracings obtained in KCl-Hanks' (3×10^{-6} M Ca^{++}) in the electrode. Bath contained same medium as electrode except ionized calcium concentration was 3×10^{-6} M in *A* and *C*, 5×10^{-7} M in *B*, and 1×10^{-7} M in *D*.

channel activity (Fig. 4 *B*), which returned to the original level when the medium was changed back to one containing 3×10^{-6} M calcium (Fig. 4 *C*). Subsequent reduction of ionized calcium to 1×10^{-7} M (Fig. 4 *D*) further reduced channel activity. Similar records were obtained with eight other patches. At a calcium concentration of 10^{-5} M (calcium-free-EGTA-free Hanks'), channels were open at all holding potentials studied (+60 to −40 mV). In Fig. 5, the percent channel open-time at different holding potentials is plotted for the patch shown in Fig. 4.

In a number of studies, the patch membrane was destroyed following recordings in the cell-attached patch configuration. Cells in NaCl-Hanks' (recording electrodes contained KCl-Hanks' and 10^{-6} M Ca^{++} or less) had resting membrane potentials averaging −43 mV (range −25 to −60 mV). Cells bathed in KCl-Hanks' predictably had potentials near zero (range +5 to −3 mV).

DISCUSSION

The calcium- and voltage-activated potassium channel described in this paper has a similar conductance and voltage dependence to the calcium-activated potassium channel described in a variety of cells (1, 11, 13). The calcium sensitivity of these channels in the macrophage is similar to that of skeletal muscle (1). Two other channels have been described in macrophages. The first is a large conductance (>100 pS) cation-nonselective and calcium-independent channel (7), and the second is an inward-rectifying channel with a conductance in the range of 16–30 pS (4). Both of these channels have properties different from the channels described in this paper.

Membrane potential measurements of macrophages following destruction of the patch membrane yielded resting potentials similar to those reported by McCann et al. (9). From measurements of both resting membrane potential and the electrode potential at which channel activity was first evident in the cell-attached patch mode, the membrane potential at which the calcium- and voltage-activated potassium channels are activated in the intact cell can be determined. Cells bathed in either KCl-Hanks' or NaCl-Hanks' exhibited these channels at potentials of +50 mV or more depolarized. Assuming that the properties of the channel, i.e., calcium sensitivity, are the same in situ as they are in the excised patch, the intracellular concentration of calcium must be 10^{-7} M or less in the intact macrophage.

The presence of calcium- and voltage-activated potassium channels in macrophages is consistent with previous observations that the injection of calcium induces hyperpolarizations, and that EGTA, cobalt, and D-600 (methoxyverapamil) block spontaneously occurring hyperpolarizations in macrophages (6, 10). It is likely that the channels described in this paper represent the individual events that produce these spontaneous and induced membrane hyperpolarizations.

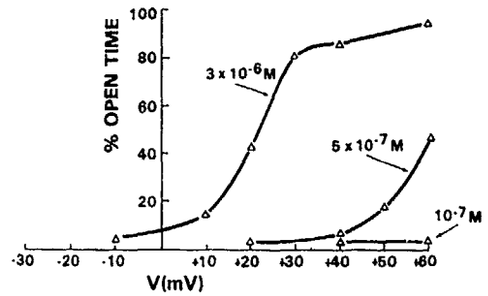

FIGURE 5 Plot of percentage of time channels were open against holding potential for the indicated $(Ca)^{++}_i$. Channel open time was determined by playing back 30–40 s of channel data at 1/8 speed into a Brush chart recorder and analyzing the data by hand. Data were obtained from same patch as in Fig. 4.

The relationship of the calcium-activated potassium conductance to macrophage function is unclear. Macrophages are well known for their secretory, phagocytic, and motile properties. Changes in membrane potential and intracellular calcium levels have been implicated in some of these functions (5, 14). Both the calcium ionophore A23187 and endotoxin-activated serum stimulate secretion in macrophages and produce membrane hyperpolarizations, presumably by activating a calcium-activated potassium conductance (5, 6). However, it is not known whether or not these changes in conductance play an important role in the secretory response to these stimuli. The calcium-activated potassium conductance, once triggered, might modulate other voltage-dependent conductances in much the same way it does in neuronal cells. In addition, potassium released from macrophages following activation of this conductance may influence cells, such as T lymphocytes, that are often found in close physical contact with the macrophage (12).

In summary, this paper demonstrates that both intracellular calcium and voltage activate a potassium channel in human macrophages that is similar to the large-conductance calcium-activated potassium channel in other cells (1, 11).

I thank S. Green for valuable technical assistance, J. Metcalf for providing human monocytes, and J. Freschi for advice on patch clamp techniques and critical review of the manuscript.

This work was supported by the Armed Forces Radiobiology Research Institute, Defense Nuclear Agency, under Research Work Unit MJ 00020. The views presented in this paper are those of the author. No endorsement by the Defense Nuclear Agency has been given or should be inferred.

Received for publication 3 April 1984 and in final form 6 August 1984.

REFERENCES

1. Barrett, J. N., K. L. Magleby, and B. S. Pallotta. 1982. Properties of single calcium-activated potassium channels in cultured rat muscle. *J. Physiol. (Lond.).* 331:211–230.
2. Dos Reis, G. A., and G. M. Oliveiro-Castro. 1977. Electrophysiology of phagocytic membranes. I. Potassium-dependent slow membrane

hyperpolarizations in mice macrophages. *Biochim. Biophys. Acta.* 469:257–263.

3. Gallin, E. K. 1981. Voltage clamp studies on macrophages from mouse spleen cultures. *Science* (*Wash. DC*). 214:458–460.
4. Gallin, E. K. 1984. Electrophysiological properties of macrophages. *Fed. Proc.* 43:2385–2389.
5. Gallin, E. K., and J. J. Gallin. 1977. Interaction of chemotactic factors with human macrophages. Induction of transmembrane potential changes. *J. Cell Biol.* 75:160–166.
6. Gallin, E. K., M. Wiederhold, P. Lipsky, and A. Rosenthal. 1975. Spontaneous and induced membrane hyperpolarizations in macrophages. *J. Cell. Physiol.* 86:653–662.
7. Kolb, H. A., and W. Schwarze. 1984. Properties of a cation channel of large unit conductance in lymphocytes, macrophages, and cultured muscle cells. *Biophys. J.* 45:136–138.
8. Marty, A. 1981. Ca-dependent K channel with large unitary conductance in chromaffin cell membranes. *Nature* (*Lond.*). 291:497–500.
9. McCann, F. V., J. J. Cole, P. M. Guyre, and J. A. Russell. 1983. Action potentials in macrophages derived from human monocytes. *Science* (*Wash. DC*). 219:991–993.
10. Persechini, P. M., E. G. Araiyo, and G. M. J. Oliveiro-Castro. 1981. Electrophysiology of phagocytic membranes: induction of slow membrane hyperpolarizations in macrophages and macrophage polykaryons by intracellular calcium injection. *J. Membr. Biol.* 61:81–90.
11. Peterson, O. H., and Y. Maruyama. 1984. Calcium-activated potassium channels and their role in secretion. *Nature* (*Lond.*). 307:693–696.
12. Rosenstreich, D. L., J. J. Farrah, and S. Dougherty. 1976. Absolute macrophage dependency of T lymphocyte activation by mitogens. *J. Immunol.* 116:131–140.
13. Singer, J., and J. Walsh. 1984. Large conductance Ca^{++}-activated potassium channels in smooth muscle membranes. Reduction in unitary currents due to internal Na^{+} ions. *Biophys. J.* 45:68–69.
14. Yin, H., and T. P. Stossel. 1982. Mechanism of phagocytosis. *In* Phagocytosis—Past and Future. M. Karnovsky and L. Bolis, editors. Academic Press, Inc., New York. 13–24.

Thymus 7, 3–11 (1985)

Radiation abrogation of myelopoietic inhibitors found in thymus-conditioned medium

DALE F. GRUBER

Experimental Hematology Department, Armed Forces Radiobiology Research Institute, Bethesda, MD 20814, U.S.A.

Key words: adherent; nonadherent; granulocyte-macrophage colony-forming cell (GM-CFC); monocyte-macrophage colony-forming cell (M-CFC); radiation; inhibition

Summary. We have previously reported conditioned medium from cultures of murine 'nonlymphoid' adherent thymus cells to be a source of myelopoietic inhibitor substance(s). The inhibitor has a molecular weight of less than 1000 daltons. It is dialyzable. and its effects are reversible with washing, but it is not significantly cytotoxic. The inhibitor(s) abrogate both the 10-day granulocyte-macrophage colony-forming cell (GM–CFC) and the 25–day monocyte-macrophage colony-forming cell (M–CFC). Morphologically, cultures appear to be lymphocyte-free after 10–12 days, and consist primarily (80%) of nonspecific esterase positive cells and epitheloid appearing (20%), nonspecific esterase negative cells. Radiation of thymic cultures at 12 days reduces levels of inhibitor(s) found in the medium. Inhibitor levels from pooled samples collected over 4 days demonstrate reductions of 10% at 100 rads 15% at 200 rads, 25% at 300 rads, and 85% at 400 rads. The steepest area of radiation reduction occurs between 300 and 400 rads, with the interpolated 50% radiation reduction level at 342 rads. Analysis of once-harvested radiated culture supernates showed no significant inhibitors present when medium was examined 5–10 days postradiation.

Introduction

The radiosensitivity of thymic tissue is a known phenomenon [1]. This may be due to the fact that ontogenetically most thymic tissue is lymphoidal. Lymphomyelopoeisis [2, 3] has been shown to be responsive to homeostatic perturbations, and the thymus is suspected as participating in the routine maintenance of homeostatic hemopoiesis. Lymphoidal tumor involvement has been evident in many instances of hemopoietic dyscrasias.[4]. Generally, thymic epithelial cells have been considered to be the cellular source of thymic humoral factors [5], although lymphocytes also have been implicated. Reduction of the Thy 1.2 lymphocyte subpopulation resulted in a decrease of both erythroid and granuloid splenic colonies [6]. Supernatants from thymic epithelial cell cultures have been found to be capable of inducing theta antigen expression on splenocytes from athymic mice [7]. E-rosette formation on fractionated bone marrow cells [8], and an increase in the mitogenic responsiveness of rat thymocytes [9].

Media conditioned by thymus (with or without radiation) were examined for granulopoietic (GM–CFC and M–CFC) inhibition because (a) thymus tissue is uniquely susceptible to radiation, (b) its metabolites affect or regulate hemopoiesis, and (c) the thymus has an obvious role in immunoregulation.

Materials and methods

Animals. Male (C57BL/6 X CBA)F1 Cum BR hybrid (B6CBF1) mice (Cumberland View Farms, Clinton, Tennessee) were used throughout the study. Thymic cultures were prepared from mice 8 to 10 weeks old. All animals were maintained on a 6 a.m. (light) to 6 p.m. (dark) cycle in filtercovered cages. Wayne Lab-Blox and acidified water (pH 2.5) were available *ad libitum.* All mice were housed for 2 weeks in quarantine until certified free of histologic lesions and *Pseudomonas* sp.

Thymic epithelial and control cultures. In each experiment, thymuses from six mice were aseptically removed, pooled in 4°C RPMI-1640 (Flow Laboraties, Rockville, Maryland), and minced with scissors into small fragments. The organ fragments (15–20) were explanted into 75-cm^2 tissue culture flasks (Corning #25110, Corning Glass Company, Corning, New York) with 5 ml of starter medium. The medium components were RPMI–1640 tissue culture medium (Flow Labs) supplemented with 10% (v/v) heat-inactivated (56°C, 30 min) fetal calf serum (Grand Island Biological Company, Grand Island, New York), 2 mM l-glutamine (GIBCO), penicillin (100 IU/ml) streptomycin (100 ug/ml,) and fungizone (0.25 ug/ml, GIBCO). All cultures were kept at 37°C in a humidified incubator and were gassed with 5% CO_2 –95% air. After 24 h, 3 ml of fresh medium was added to each flask. Attempts were made not to disturb explants during early medium changes. On day 4, 4 ml of fresh medium was added (final culture volume 12 ml). Subsequent medium changes were collected, pooled, and replaced volume for volume with fresh medium. A maximum of 8 ml/flask was replaced as needed. Changing frequency generally increased as the monolayer moved toward confluency. Under these conditions, monolayer confluency was generally established by day 21.

Monolayer histology. All cultures were regularly observed with an inverted-phase microscope (Opton Model, Zeiss, West Germany). Representative flasks and cytocentrifuge preparations were fixed with 0.2 M phoshphate-buffered glutaraldehyde (pH 7.3) and stained with Wrights-Giemsa or α-napthyl acetate to determine the presence and frequency of nonspecific esterase-positive cells.

Ultrafiltration. The TCM after collection was centrifuged at 250 X g for 10 min. The supernatant was filtered through a 0.45-micron filter unit (Nalge Company, Rochester, New York) to remove cells or cellular debris. The filtrate was fractionated by molecular ultrafiltration by subjecting it to an Immersible–CX Molecular Separator-type PTGC (Millipore Corporation, Bedford, Massachusetts) with nominal cutoff at 10000 daltons. The ultrafiltrate was then passed though an Amicon Molecular Ultrafiltration Membrane UM-2 (Amicon Corporation, Lexington, Massachusetts) with nominal cutoff at 1000 daltons. The ultrafiltrate was adjusted to a pH of 7.3, and had an osmolarity of 300 m Osm/kg.

GM–CFC and M–CFC assays. The soft-agar clonogenic assay was used to assess the stimulating acitivites of TCM and L-cell-conditioned medium (LCM) alone or in conjuction with each other on the granulocyte-macrophage and moncyte-macrophage progenitor cell populations. The bottom of the two-layered system was 0.5% nutrient supplemented agar (Bacto-agar, Difco Laboratories, Detroit, Michigan) containing known aliquots of CSF and/or TCM. The top layer was nutrient-supplemented 0.33% agar containing 2.2×10^4 bone marrow cells. All plates were incubated in a humidified incubator (Model 3016, Forma Scientific, Marietta, Ohio) at 37°C and were gassed with a 5% CO_2–95% air mixture. Plates were counted for GM–CFC colonies (>50 cells) at 10 days and M–CFC colonies (>50 cells) at 25 days, using an inverted-phase microscope (Opton Model, Carl Zeiss Incorporated, Oberkochen, West Germany) at a magnification of 25 X.

Reversibility of inhibitor. Bone marrow cells were incubated (37°C) with the RPMI-1640 and 10% inactivated fetal calf serum previously described, and divided into four aliquots. One aliquot received no additonal treatment for 90 min. The other three aliquots received 100 μl each (5% volume) TCM. One of these three treated aliquots received no further treatment; one was washed once with medium after 90 min and centrifuged at 250 X g for 10 min, and the third aliquot was washed twice after incubation and treatment. The cells from all four aliquots were resuspended in culture medium, counted, and plated in the usual manner in soft agar to determine proliferative competency.

Culture radiation and collection. Cultures were bilaterally irradiated by a ^{60}Co source at a rate of 40 rads/min. Media from irradiated cultures were pooled (days 1–4 and 5–10), aspirated, centrifuged at 1500 rpm for 10 min at 4°C, passed through a 0.45-micron filter, and frozen at 0°C until assayed.

Results

Monolayer growth. Outgrowths from thymus explants were visible on day 2 of culture and were confluent by 21 days. The monolayers exhibited heterogeneous morphology composed mainly of what appeared to be epitheloid polygonal cells and dendritic-type cells with cytoplasmic extensions. Microscopic examinations of cytocentrifuge preparations of aspirated cells showed the cultures to be lymphocyte-free after approximately 12 days.

The monolayer constituents appeared to consist mainly (80%) of nonspecific esterase positive cells resembling macrophages. The other cell type is nonspecific esterase negative epitheloid-type, which exists within the monolayer in small aggregates or colonies.

Reversibility of TCM inhibition. Table 1 demonstrates the reversibility of the TCM inhibitor as shown by the soft-agar clonogenic assay for GM–CFC and M–CFC. Baseline control values were obtained for GM-CFC and M–CFC in the presence of LCM. Addition of 5% by volume of TCM inhibits almost all GM–CFC and M–CFC growth. Washing the TCM-treated bone marrow cells once resulted in clonogenic mean values that were 77% (GM–CFC) and 78% (M–CFC) of control values. A second washing resulted in further improvement, giving 93% (GM–CFC) and 95% (M–CFC) of baseline control values.

TCM inhibition. Table 2 shows TCM inhibition, the results of which have been seen in three successive replications. TCM appears to be a potent inhibitor of both GM–CFC and M–CFC when present initially in the bottom layer. Volumes as small as 1 part to 39 parts CSF are capable of significant inhibiton. In an attempt to ascertain whether there was colony stunting, TCM was added in varying amounts at 6 days after initiation. Results (Table 3) show a direct relationship between the volume of TCM added and the degree of GM–CFC and M–CFC inhibition. There was no noticeable morpho-

Table 1. TCM inhibition and reversibility demonstrated by GM–CFC[a] and M–CFC[b]

Treatment	GM-CFC (x ± SEM)	% of control	M–CFC (x ± SEM)	% of control
L-cell medium[e]	18.8 ± 0.9	100	19.2 ± 0.8	100
L-cell medium, TCM[c]	0	0	0	0
L-cell medium, TCM, 1 wash[d]	14.5 ± 0.6	77	15.2 ± 0.9	78
L-cell medium, TCM, 2 washes	17.4 ± 0.5	93	18.2 ± 0.9	95

[a] 10-day granulocyte-macrophage colony (> 50 cells) count per 2.2×10^4 live nucleated cells plated
[b] 25-day monocyte-macrophage colony (> 50 cells) count per 2.2×10^4 live nucleated cells plated
[c] Thymus-conditioned medium – 5% of final volume
[d] Washed in medium and centrifuged at 250 × g for 10 min
[e] L-cell medium, 200 µl per plate

Table 2. Graded dose inhibiton of GM–CFC[a] and M–CFC[b] by TCM

Treatment	GM–CFC (x ± SEM)	M–CFC (x ± SEM)
L-cell medium[c]	17.8 ± 1.4	18.2 ± 0.9
L-cell medium + 2.5 vol % TCM	1.0 ± 0	1.0 ± 0
L-cell medium + 5.0 vol % TCM	0	0
L-cell medium + 10.0 vol % TCM	0	0
L-cell medium + 25.0 vol % TCM	0	0

[a] See footnote a in Table 1
[b] See footnote b in Table 1
[c] L-cell-conditioned medium, 200 µl/plate

metric difference between colonies, normal colonies, and those receiving TCM on day 6.

Radiation. Figure 1 demonstrates the reduction of inhibitor by ^{60}Co irradiation. When compared to GM–CFC control values, radiation levels of 100 rads decreased inhibitor levels by approximately 10%, 200 rads by 15%, and 300 rads by 25%. Between 300 and 400 rads, a steep reduction (60%) of control values is demonstrated. It is in this range of 300–400 rads that the 50% reduction level is interpolated (≃342 rads). The highest level of radiation (500 rads) in this experiment still contains 6% of control inhibitor levels. Cultures radiated with 300 rads of ^{60}Co radiation (40 rads/minute) were found to possess 16X more inhibitor in samples pooled between days 1 and 4 than that found in samples pooled between days 5 and 10 (Figure 2). At 400 rads and at 500 rads, 7 X and 15 X, respectively, more are found in the earlier pooled sample, days 1–4. Preliminary data on the effects of irradiated TCM on M–CFC have presented curves similar to the GM–CFC

Table 3. GM–CFC[a] and M–CFC[b] response to graded doses of TCM added six days after initiation by L-cell medium[c]

Volume % TCM added	GM–CFC (x ± SEM)	% of control	M–CFC (x ± SEM)	% of control
0	17.8 ± 1.4	100	18.2 ± 0.9	100
2.50	12.8 ± 1.7	72	13.5 ± 0.6	74
5.0	10.8 ± 1.5	60	4.3 ± 0.5	23
12.5	4.8 ± 0.6	27	4.5 ± 0.5	25
25.0	4.7 ± 0.9	26	4.2 ± 0.3	23

[a] See footnote a in Table 1
[b] See footnote b in Table 1
[c] L-cell-conditioned medium, 200 µl

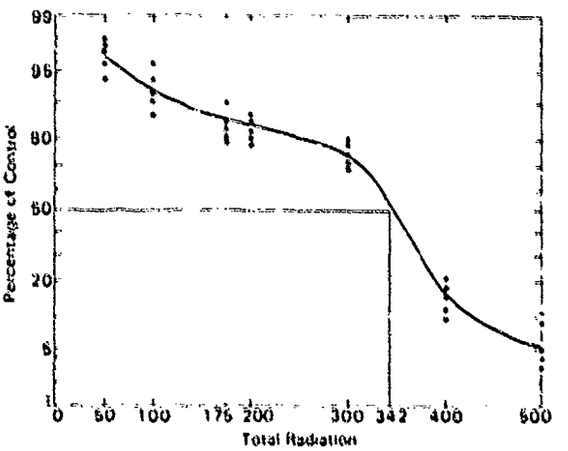

Figure 1. Reduction of TCM inhibitor levels in quadruplicate cultures irradiated by a ^{60}Co source. Results are presented as a curve, generated over five assays, of the percent presence of TCM inhibitor based on the presence, or lack of, GM–CFC inhibition.

curves. Protein levels were equilibrated using heat-inactivated (57°C, 40 min) fetal calf serum.

Cytotoxicity. The cytotoxic effects of TCM on murine bone marrow cells was followed through 48 h (see Table 4). Counts were established using standard hemocytometer and trypan blue exclusion techniques. Over the full range of amounts (2%–25% TCM by volume) and times tested, TCM reduced bone marrow viability by 10%–17% (mean 14.4%).

Discussion

Hematopoietic homeostasis is dynamic equilibrium reached when proliferative and inhibitor substances have exacted their influences on target cell

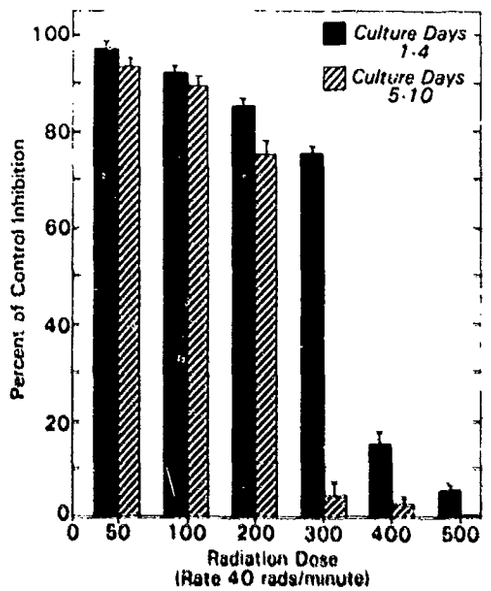

Figure 2

Table 4. Percent viability of murine bone marrow grown in graded quantities of thymus-conditioned medium.

Volume % TCM[a] added to control medium	Percent Viability[b] Tested at:			
	6 h	24 h	30 h	48 h
0	99	97	95	95
2	87	86	85	83
5	83	82	80	80
10	82	82	80	79
25	83	81	81	79

[a] TCM, thymus-conditioned medium.
[b] Determined by hemocytometer and trypan blue exclusion

polulations. Both thymic tissue and thymocytic derived factors have been reported to play significant roles in the regulation of hemopoiesis. At the augmentation portion of regulation, the presence of thymocytes and/or factors have been reported to augment bone marrow and stem cell/progenitor cell growth [10–12]. Inhibitory type regulation has also been reported.

Lebowitz and Lawrence [13] reported that tissue culture medium conditioned by PPD-stimulated lymphocytes possess a cytostatic property that inhibits HeLa cell clonogenic formations. The term applied to that particular cytostatic property was 'cloning inhibitory factor – CIF' [14]. Further, it was found that medium conditioned by phytohemagglutinin (PHA)-stimulated lymphocytes contained factors that inhibited DNA synthesis in HeLa cells. This capacity was teremed 'proliferative inhibitory factor – PIF' [15].

It is reported here that adherent thymus cells produce substances of low molecular weight (1000 daltons) that are capable of abrogating the formation of myeloid progenitor cell colonies. Application of ^{60}Co radiation (300–400 rads at 40 rads/min) resulted in an 85% reduction in the levels of elaborated inhibitor(s). The majority of inhibitor(s) produced are elaborated into the culture medium within the first 4 days of culture. Medium that was collected 5–10 days after 300 rads and one medium harvest had no significant levels of inhibitor present. The abrogation of inhibitor levels may indicate radiation-induced cellular injury occurring at around 300 rads.

A number of investigators have implied that thymic humoral factors are elaborated by epithelial-type cells [8]. On the basis of histologic and morphologic criteria, it appears that epitheloid cells represent only a small fraction (20%) of the adherent cell culture population. The majority (80%) of the cells appear to be of macrophagic lineage, based on their demonstration of positive esterase staining and their ingestion of IgG-coated bovine red blood cells. Quantitatively, these observations agree with the morphological descriptions of thymic microenvironmental cells reported by Jordan and Crouse [16] and Jordan et al. [17].

Data presented here is in accord with observations of Maschler and Maurer [17], who reported that ultrafiltrate fractions obtained from calf thymus inhibited the formation of lymphocytes and of granulocyte soft-agar colonies in capillary tubes. Physiochemical characterization of the inhibitor shows it to be different from CIF and PIF. It does not possess the thermolability shown by CIF [19]; in contrast to PIF [20], the inhibitor is dialyzable and the inhibitor(s) are released in vitro in the absence of either antigenic/mitogenic stimulation.

It is anticipated that further work will be conducted to determine (a) whether this factor is of monokine origin and (b) to what extent this regulation may participate in trauma-related energy.

Acknowledgements

This work was supported by the Armed Forces Radiobiology Research Institute, Defense Nuclear Agency, under Research Work Unit MJ 00041. Views presented in this paper are those of the authors; no endorsement by the Defense Nuclear Agency has been given or should be inferred.

Research was conducted according to the principles enunciated in the 'Guide for the Care and Use of Laboratory Animals,' prepared by the Institute of Laboratory Animal Resources, National Research Council.

References.

1. Rieger CHL, Kraft SC, Rothberg RM: T-cell function in patients with early thymic irradiation. J Allergy Clin Immunol 53:76, 1974.
2. Craddock CG: Production, distrubution and fate of granulocytes. In: WJ Williams, E Beutler, AJ Erslev, RW Rundles (eds) Hematology. McCraw-Hill, New York, 1972, p. 607.
3. Bentwich Z, Kunkel HG: Specific properties of human B and T lymphocytes and alterations in disease. Transplant Rev 16:29, 1973.
4. Fisher ER: Pathology of the thymus and its relation to human disease. In: RA Good, AE Gabrielsen (eds) The Thymus in Immunobiology. Hoeber-Harper, New York, 1964, p. 676.
5. Bach J, Carnaud C: Thymic factors. In: P Kallos, BH Waksman, A Weck (eds) Progress in Allergy. S. Karger AG, Basel, Switzerland, 1976, p 342.
6. Goodman JW, Basford NL, Shinpock SG: On the role of thymus in hemopoietic differentiation. Blood Cells 4:53, 1978.
7. Papernik M, Nabarra B, Bach J: In vitro culture of functional human thymic epithelium. Clin Exp Immunol 19:281, 1975.
8. Pyke KW, Gelfand EW: Morphological and functional maturation of human thymic epithelium in culture. Nature 251:421, 1974.
9. Kruisbeck AM, Krose TC, Zylstra JJ: Increase in T-cell mitogen responsiveness in rat thymocytes by thymic epithelial culture supernatant. Eur J Immunol 7: 375, 1977.
10. Goodman JW, Basford NL, Shinpock SG, Chamber ZE: An amplifier cell in hemopoiesis. Exp Hemat 6:151, 1978.
11. Pritchard LL, Goodman JW: Dose-dependence of the augmentation of hemopoiesis by thymocytes. Exp Hemat 6:161, 1978.
12. Metcalf D, Russell S, Burgess AW: Production of hemopoietic stimulating factors by pokeweed-mitogen-stimulated spleen cells. Transplant Proc 10:91, 1978.
13. Lebowitz A, Lawrence HS: Target cell destruction by antigen stimulated lymphocytes. Fed Proc 28:630, 1969.
14. Lebowitz AS, Lawrence HS: The technique of clonal inhibition: A quantitative assay for human lymphotoxin activity. In: BR Bloom, PR Glade (eds) In Vitro Methods in Cell Mediated Immunity. Academic Press, New York, 1971, p. 375.
15. Cooperband SR, Green JA: Production and assay of a lymphocyte derived 'proliferation inhibitory factor - PIF.' In: BR Bloom, PR Glade (eds) In Vitro Methods in Cell Mediation Immunity. Academic Press, New York, 1971, p 381.
16. Jordan RK, Crouse DA: Studies on the thymic microenvironment: Morphologic and functional characterization of thymic nonlymphoid cells grown in tissue culture. J Reticuloendothel Soc 26:385, 1979.
17. Jordan RK, Crouse DA, Owen JJT: Studies on the thymic microenvironment: Nonlymphoid cells responsible for transferring the microenvironment. J Reticuloendothel Soc 26:373, 1979.
18. Maschler R, Maurer HR: Screening for specific cell thymus inhibitors (chalones) of T-hymphocyte proliferation. Hoppe Seylers Z Physiol Chem 360:735, 1979.

19. Holzman RS, Lebowitz AS, Valentine FT, Lawrence HS: Preparation and properties of cloning inhibitory factor. Cell Immunol 8:240, 1973.
20. Yoshida T: Purification and characterization of lymphokines. In: S Cohen, E Pick, JJ Oppenheim (eds) Biology of the Lymphokines. Academic Press, New York, 1979, p. 278.

Biblthca haemat., No. 48, pp. 384–402 (Karger, Basel 1984)

C. Cell Proliferation Kinetics Analyzed with BrdU and Near-UV Light Treatment[1]

M.P. Hagan

Experimental Hematology Department, Armed Forces Radiobiology Research Institute, Bethesda, Md., USA

Introduction

Since its discovery by *Greer and Zamenhof* [11] in 1957, the sensitization to ultraviolet (UV) light of cells containing bromodeoxyuridine (BrdU)-substituted DNA has proven to be a powerful tool for the molecular biologist. The photolysis of DNA substituted with BrdU has provided techniques for such diverse applications as mutant selection [1], gene mapping [2], and DNA repair 'patch-length' analysis [20]. Also, the increased mass of the BrdU-substituted DNA has formed the basis for studies of semiconservative replication [9] and DNA repair replication [24, 30]. A third property of BrdU, its interaction with various fluorescent dyes, has yielded increased sensitivity for the analysis of sister chromatid exchange [15, 18]. The latter technique has also provided considerable information concerning in vitro cell cycle kinetics [4, 8].

Although BrdU has shown merit for these in vitro assays, its use in vivo has shown only limited success. The primary reason for this lack of success in vivo is the rapid breakdown of BrdU in the host [16, 17].

[1] Supported by Armed Forces Radiobiology Research Institute, Defense Nuclear Agency, under Research Work Unit MJ 00052. Views presented in this paper are those of the authors; no endorsement by the Defense Nuclear Agency has been given or should be inferred.

As an example, the half-life of a 5-mg dose of BrdU injected intravenously into B6D2F1 female mice is less than 12 min (data not shown). As a result, only those experimental techniques involving a BrdU infusion have met with success [13, 15, 28]. For this reason, the invention of the osmotically active 'minipump', permitting the routine use of BrdU infusion, now permits a wide realm of possible experiments [33]. The material below draws upon previous in vitro studies to describe a method for the observation and analysis of in vivo cell cycle kinetic parameters.

BrdU Labeling

The replacement of thymidine (dT) residues by BrdU is accomplished with a constant subcutaneous infusion via an osmotically active Alzet 2000 minipump (Alza Corp., Palo Alto, Calif.). The infusate consists of an aqueous solution of either bromodeoxycytidine (BrdC) or BrdU. For a 75 m*M* BrdU infusate, the infusion results in only a 2% substitution of BrdU for dT. In the infusate, however, the BrdU solution is near the solubility limit. Switching to BrdC, a direct precursor of BrdU in vivo [7], allows the level of replacement to remain approximately the same while the solubility limit is increased to approximately 0.65 *M*. For example, using the techniques of 313-nm-light photolysis and alkaline sucrose gradient sedimentation [32] of DNA from mice infused with a 150 m*M* solution of BrdC, the percent substitution of BrdU for dT was determined to be 4.2% (data not shown). This level of replacement produces an easily detectable sensitivity to 313-nm light, and is well below the replacement level that has been associated with developmental effects [19].

By incorporating radioactively labeled BrdU or BrdC in the infusate, one may observe the 'start-up' time for the pump. This time routinely lies between 6 and 8 h after the implantation. For these observations, the nucleoside labeled at the 6 position provides a longer plasma lifetime for the label, facilitating the measurement. On the other hand, catabolism of the BrdU or BrdC can be more easily observed when the molecule is labeled at the C-2 position, this portion of the molecule being rapidly lost from the plasma [14]. In mice, the rate of catabolism for BrdU is strain dependent, and must be measured to assure that no BrdU build-up occurs. The BrdU plasma half-life for B6D2F1 female mice is under 12 min.

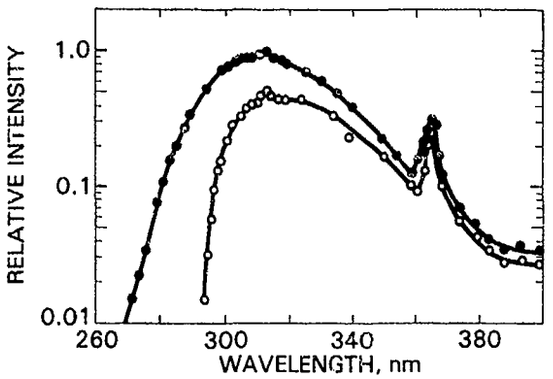

Fig. 1. Spectra from FS20 sunlamp (Westinghouse). Spectra were determined with a γ spectroradiometer. ● = Unattenuated; ○ = filtered through cover of 100-mm Falcon plastic Petri dish (0.98 mm polystyrene).

313-nm Light Irradiation

DNA-containing BrdU is more sensitive to light at all wavelengths of absorption. However, as the wavelength increases from 260 nm, the BrdU specificity increases until the drop in absorption beyond 320 nm forces the use of extremely high fluences of light to achieve the same level of DNA damage [27]. Because the action spectrum for cell killing falls more rapidly for unsubstituted DNA above 300 nm [5], the band of wavelengths between 300 and 320 nm is particularly useful for cell-killing experiments incorporating BrdU.

Fortunately, one of the emission lines from Hg-arc sources lies at ~313 nm. This fact permits the construction of a 313-nm light source in one of several ways. Three of the more practical sources are described below. The most economical system consists of 2–4 Westinghouse FS 'Sun Lamps' either of the 20- or the 40-watt variety. When these lamps are set on 1–¾ in centers at a distance of 44 cm above the sample, they produce a fairly uniform beam (i.e., 10% variation in intensity across the field) and an average intensity of ~2 J/m² when properly filtered. The filtration should absorb the infra red (IR) component and wavelengths below ~300 nm. A 1-in depth of water will effectively remove the heat. If the water is held in a polystyrene dish (1 mm polystyrene), then that portion of the spectrum below 295 nm will be reduced by more than two orders of magnitude. An example of this spectrum is shown in figure 1. The disadvantages of this system are the low flux, which requires long

exposure times, and the inability to exclude more of the spectrum below 313 nm. The exposure times can be significantly shortened by the construction of a source moderately more expensive. A Philips 500-watt Hg-arc lamp can be focused through water and mylar film onto a standard quartz cuvette. Here the intensity can reach 100 J/m²/s. This simple arrangement has the added advantage of raising the high-energy end of the spectrum to ~305 nm. Finally, the most sophisticated of these three sources consists of a high-pressure Hg-arc lamp spectrum filtered through a 1×10^{-4} *M* solution of deoxyadenosine (dA). This removes both the IR component and wavelengths below 285 nm. The resulting light load can then be handled easily by a variety of monochromators. With a Hanovia 1,000-watt Hg-Xe-arc lamp, 2-in optics, and an Oriel f/3.7, 1,200 1/mm grating monochromator, a flux of 90 J/m²/s can be obtained over a bandwidth of 10 nm centered on 313.7 nm. For this source, the sample should be held on an optical bench. The addition of a water-jacket to the quartz cuvette permits better control of the conditions of the irradiation.

Irradiation and Culture of Cells

For irradiation, cells are suspended in Dulbecco's phosphate-buffered saline free of Mg^{2+} and Ca^{2+}. To reduce the likelihood of cell loss due to adherence to vessel walls, 0.02% EDTA is also included in the suspending medium. Cell culture conditions for mouse bone marrow cells require that cells be irradiated at concentrations greater than 1×10^6 nucleated cells/ml. At these high cell concentrations, the suspension is turbid, a condition that requires vigorous stirring of the sample during the exposure. The absorption of 313-nm light by mammalian cells is so low that transmission losses may be attributed to light scatter. To compute the average fluence at the center of the cuvette, Morowitz's correction is applied [23]. Table 1 shows the correction values for cell concentrations of interest.

Before irradiation, the cuvette is sterilized by a 'pen-light' germicidal low-pressure lamp placed into the cuvette. At this time, the location of the beam may be checked in subdued lighting by placing a sheet of fluorescent bond paper behind the cuvette. The cell suspension is then added to the cuvette and an electronically timed shutter is used to control exposures.

Table I. Intensity correction factor for turbid suspensions[a]

OD_{313}	Normal marrow cells[b]	V79 Cells[b]	Correction factor
0.01			0.99
0.05		$\sim 1.0 \times 10^5$	0.94
0.10		$\sim 2.0 \times 10^5$	0.89
0.20	$\sim 1.0 \times 10^6$	$\sim 4.0 \times 10^5$	0.80
0.40	$\sim 2.0 \times 10^6$		0.65
0.60	$\sim 3.0 \times 10^6$		0.54
0.80	$\sim 4.0 \times 10^6$		0.46
1.00	$\sim 5.0 \times 10^6$		0.39

[a] This correction is applicable for stirred solutions. The correction factor is appropriate for transmission losses due to scattered light only when scattered light is lost from the sample.
[b] Cell concentrations are shown for serum-free Dulbecco's phosphate-buffered saline. Cell concentrations are approximate values only.

Cell suspensions used for the *Till and McCulloch* [34] CFU-S determination may be directly diluted for injection. For GM-CFU-C [25] determination, 20- to 500-μl samples of the suspension are pipetted into tubes containing 8 ml of 'top layer' material. (Top layer: 2 ml 0.66% agar; 2 ml double-strength medium. Bottom layer: 2 ml 1.0% agar; 2 ml double-strength medium; 150 μl mouse L-cell-conditioned medium [31]; 100 μl of pregnant mouse uterus extract [6]. Double-strength medium: Connaught Medical Research Laboratory 1066 medium containing 10%, V/V, fetal calf serum, 5%, V/V, horse serum, 5%, V/V, trypticase soy broth, 30μg/ml *L*-asparagine, and antibiotics.) The top layer material, now containing the cells, is vortexed and layered in 2-ml aliquots onto 4-ml bottom layers in 60-mm plastic Petri dishes. The concentration of irradiated cells is chosen to produce 100 colonies per dish. This size dish allows the determination of GM-CFU-C survival below the second decade of survival. At these low levels of survival, the use of smaller dishes produces poor growth and causes a loss of linearity between the size of the inoculum and the number of colonies obtained. For the data described herein, GM-CFU-C were routinely determined on the 10th day after inoculation; CFU-S were determined on the 8th day after tail vein injection.

Kinetics of a Cell Population with Simple Properties

The interpretation of the results of the BrdU/313-nm light treatment can be best understood using a simple cell system. With the V79 Chinese hamster cell line as an example, the kinetics of the BrdU-labeling period are straightforward. That is, after two separate experimental procedures, three plots of the data obtained complete the kinetics analysis available through the BrdU/313-nm-light technique. What follows is a short description of each protocol.

In the first procedure, one observes the cellular uptake of BrdU in the cell cycle observed immediately after the addition of the drug. Since the BrdU-labeled cells are inactivated by 313-nm-light irradiation immediately after they take up the drug, no effect of the BrdU incorporation on cell progression is observed. This allows the use of higher concentrations of BrdU.The upper limit for the BrdU concentration in this case is that of feedback inhibition produced by the BrdU, much the same as for dT. Feedback inhibition occurs at BrdU levels in the medium greater than 100 μM [21].

For this experiment, V79 cells are seeded onto dishes at 300 cells per dish and allowed to grow overnight. BrdU is then added to a final concentration of 10 μM, and the cells are exposed to 1 kJ/m^2 of 313-nm light. After the exposure, the cells are trypsinized and respread for colony formation. It was previously determined that this level of treatment would reduce survival below 1% in the first cycle. As can be seen in figure 2b, approximately 4 h of BrdU exposure is required to completely sensitize the cell population. The data in figure 2a, show no change in the proliferation rate during the BrdU exposure. The shape of the curve in figure 2b results from the initial sensitization of the S-phase compartment followed by the sensitization of those cells initially not in the S-phase as they progress into the S-phase. One minus the Y-intercept of the slower-component curve in figure 2b yields the S-phase cell fraction ($F_{s,cell}$; $F_{s,cell}$ = fraction of cells in the S-phase; $F_{s,t\ cells}$ = fraction of the cell cycle occupied by the S-phase). This point is verified by a 2 mM-hydroxyurea treatment of a nonirradiated cell culture; see open symbol in figure 2b; the hydroxyurea treatment also inactivates cells in S-phase [29]). Also in figure 2b, a second parameter, indentified as the combined time for the $G_1 + G_2 + M$ phases (T_c^-), is given by the X intercept of the same component curve. Through the use of the simple expression shown below, the generation time (GT) may be determined from these two values (the

S-phase cell fraction and the S-phase time fraction are not precisely equivalent; however, the use of one as an approximation of the other is acceptable when no significant proportion of the cell population is lost from the assay; for the V79 cells, $F_{s,t} \div F_{s,cell} = 1.07$ [29]).

$$GT = T_s^- \div (1-F_{s,t}) \quad (1)$$

Thus this first procedure yields the S-phase cell fraction and an estimate for the GT.

The second type of experiment is laborious and yields little new information for an in vitro cell line. This procedure, primarily designed for the analysis of cell proliferation in vivo, requires the determination of complete survival curves after several increasing times of BrdU exposure. This procedure requires further that the 313-nm-light fluence and the BrdU concentration be rigorously controlled. In principle, the data provided by this technique can show the generation times of the four cell cycles occurring before the time of the irradiation. In practice, the demonstration of two cell cycle times is reasonable. For the V79 cell line, the GT is a constant so that the interpretation of the data is simple. This will not be the case for the in vivo measurements discussed below.

The theoretical basis for this methodology relies on two observations. The first is that beyond ~1% substitution of BrdU for dT, the sensitivity to near-UV light of cells labeled for two generations increases linearly with dT replacement [3]. The second observation is that the near-UV light sensitivity of BrdU-substituted cells increases in the first generation over a much wider range than during the generations that follow [12]. The application of these observations in the determination of cell-cycle kinetics is shown below.

A plot of a set of survival curves for V79 Chinese hamster cells is shown in figure 3. In this figure the sensitivity changes in the first 12 h of BrdU exposure can easily be seen to dominate the range of the total sensitivity change. For example, for survival at the 0.1 level, the extrapolated fluences are 1,760 J/m² at 4 h, 120 J/m² at 12 h, and 75 J/m² at 120 h. These changes in fluence of 313-nm light required to reach a specified level of survival are plotted in figure 4. These *isosurvival* curves are shown here for survival values of 0.5, 0.1 and 0.05. Because the increase in sensitivity after the first cell cycle is linearly dependent on the level of BrdU replacement [3], one observes an exponential increase in the near-UV light sensitivity from the first generation through subsequent genera-

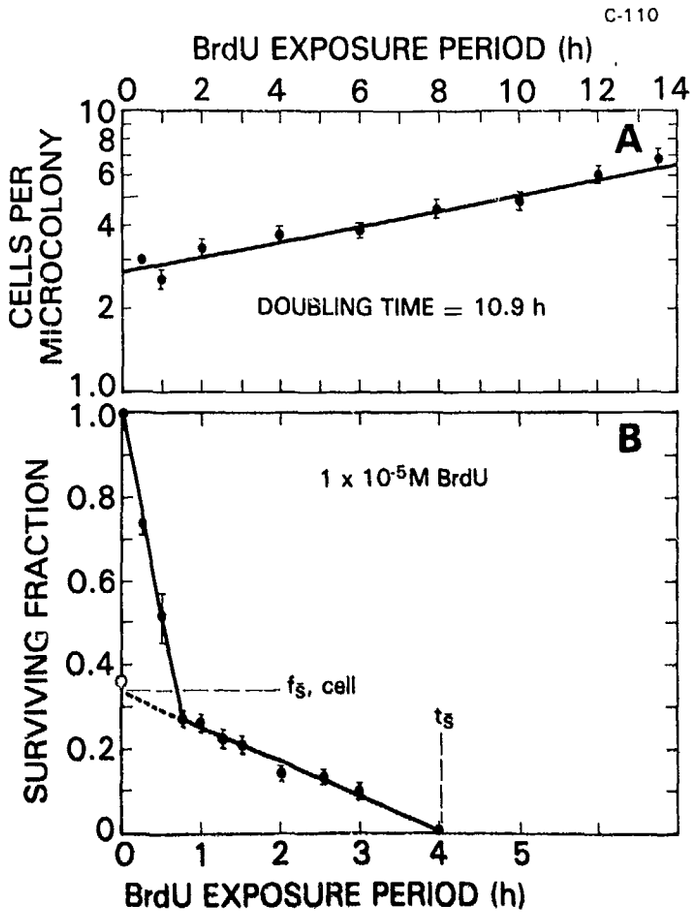

Fig. 2. Increase in sensitivity to 313-nm light is shown for V79 Chinese hamster cells in the first cell cycle after addition of 10 μ*M* BrdU. *A* Average number of cells per microcolony for 50 microcolonies. *B* ● = Fraction of cells surviving a 1 kJ/m² fluence of 313-nm light administered at time indicated; ○-fraction of cells surviving hydroxyurea exposure (2 m*M*, 3 h at 37 °C in growth medium); F_s, cell-fraction of cell in G_1+G_2+M phases; T_s = combined time of the G_1+G_2+M phases. Error bars representing ± 1 SE are shown when they are larger than the datum symbol.

tions as the amount of unsubstituted DNA decreases by 50% at each sucessive generation. After four generations, ~94% of the cell's DNA should be substituted. If the BrdU concentration has remained constant throughout the exposure, then the fraction of dT residues replaced by BrdU will reflect the halving of the unsubstituted DNA during each generation.

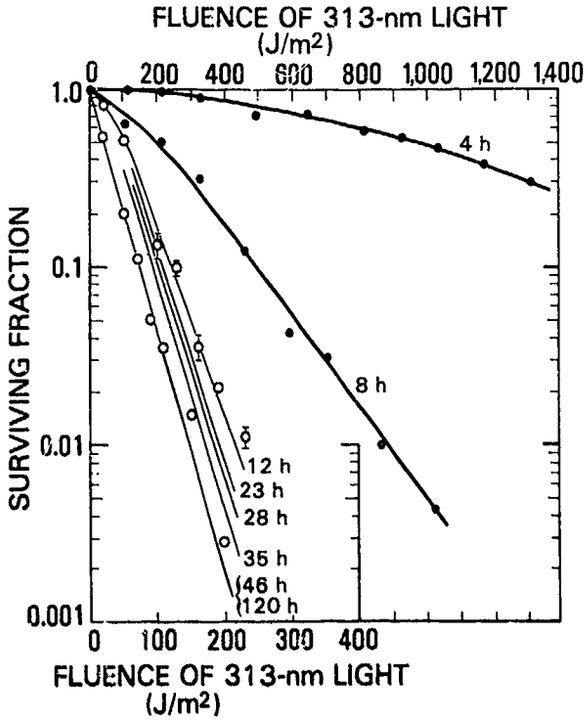

Fig. 3. Single cell survival curves for V79 Chinese hamster cells exposed to 313 nm light at a flux of 5.1 J/m²/s. Cells were irradiated in suspension at 1×10^4 cell · ml^{-1}. Time of BrdU exposure before irradiation is shown in figure. Individual data are not shown for 23, 28, 35 and 120 h time points. Data shown for 46 h are plotted on curve representing 120-hour survival data. Error bars representing ± 1 SE are shown when they are larger than datum symbol.

In principle, this pattern for the increase in BrdU substitution should result in a predictable increase in the cell's sensitivity to 313-nm light. During the first generation of exposure, the light sensitivity should rapidly increase to a level of 50% of its maximum value. After the first generation, the rate of sensitivity change should slow to an exponential rate with a half-time equivalent to the generation time. After 4 generation times, assuming the variance of the survival determination to be ≥ 0.01, there should be no detectable further increase in sensitivity to 313-nm light. As shown in figure 4a for the V79 cells, the time for which the 313-nm-light fluence just equals 2.0 times, the fluence value at 120 h (~10 generations) is between 11 and 12 h (the average value is 11.2 h). This value agrees well with the generation time values determined by direct cell count (10.9 h) and BrdU/313-nm-light suicide (11.9 h).

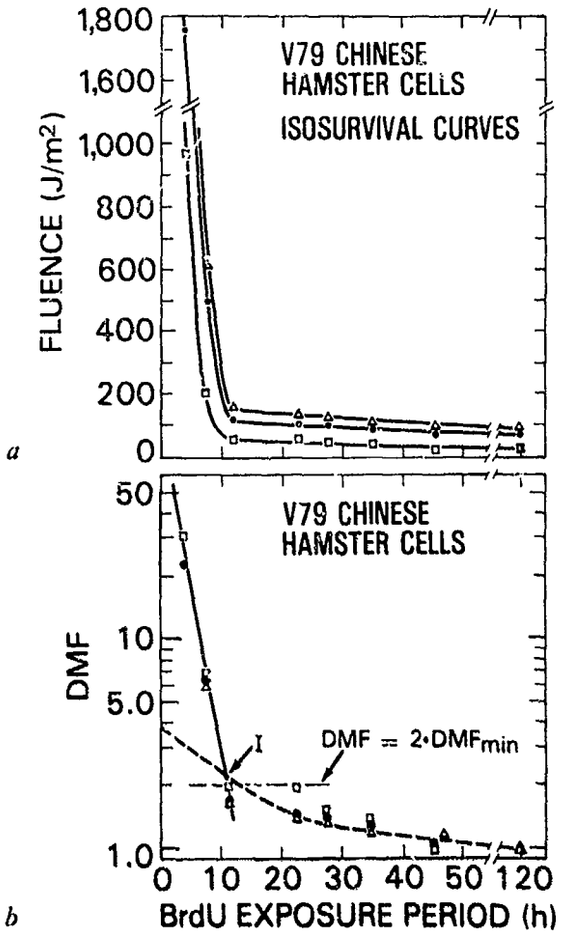

Fig. 4. Isosurvival curves for BrdU/313-nm-light inactivation of V79 Chinese hamster cells. Survival values are taken from figure 3. *a* Uncorrected fluence values for survival values of 0.5 (□), 0.1 (●) and 0.05 (△). *b* Data in *a* have been replotted as ratio of fluence value at time shown to fluence value at 120 h (DMF). I = Intercept value of the two component curves. Dashed line represents an exponential curve fit to equation given in the text. Symbols are the same as for *a*.

If the time rate of change in the fluence required to produce a given level of survival is independent of the particular survival value chosen, then one may say that this change reflects a dose modification factor (DMF). A plot of the DMFs (i.e., the ratio of the fluence at the time of interest to the limiting fluence value) for various survival levels should then yield a single curve. To demonstrate this point, the data in figure 4a have been replotted in figure 4b as DMF values. For this case, the fluence

value measured at 120 h has been taken to be the limiting fluence. (The lack of a shoulder on the measured survival curves for 46 and 120 h may indicate an actual departure from rigorous adherence of dose modification). This replot of the data has two advantages. First, the intercept of the two component curves should be more easily determined. For reasons stated above, this intercept should occur at a DMF value of 2.0 and should equal the GT value. Further, the data observed for times greater than that associated with the intercept (figure 4b; 'I') can be analyzed for goodness of fit with equation (2):

$$\mathrm{DMF} = 1 + e^{-\lambda t}, \tag{2}$$

where

$$\lambda = \ln 2/\mathrm{GT}. \tag{3}$$

If the population of cells is homogeneous, each level of survival chosen will yield a similar plot for the DMF. What is more, the GT will correspond to other measurements for the GT, including the time associated with DMF = 2. When fitted to the equation above, the data in figure 4b fit best the dashed line drawn through the data points. This curve is associated with a GT of 9.0 h and a correlation coefficient of $r = 0.86$. Although the correlation is not remarkable and the estimate for GT hardly impressive when compared with the other estimates shown above, there is significant information here. The cell cycles that gave rise to the estimate are those occurring 2–4 generations before the 313-nm light exposure.

For an in vivo cell population, ancestral cells of 2–4 previous generations may have been quite removed, by way of both kinetics and function, from the cell present at the time of the assay. An example of this disparity is shown later for the GM-CFU-C. We will now turn our attention to the use of these methods in the analysis of cell kinetics of the murine bone marrow.

Kinetic Analysis of the CFU-S Population

The same types of curves described for the V79 Chinese hamster cell line can be plotted for the murine CFU-S. The BrdU/313-nm-light suicide determination analogous to the curve shown in figure 2b shows an ~6% S-phase kill. This level of killing reflects an S-phase population

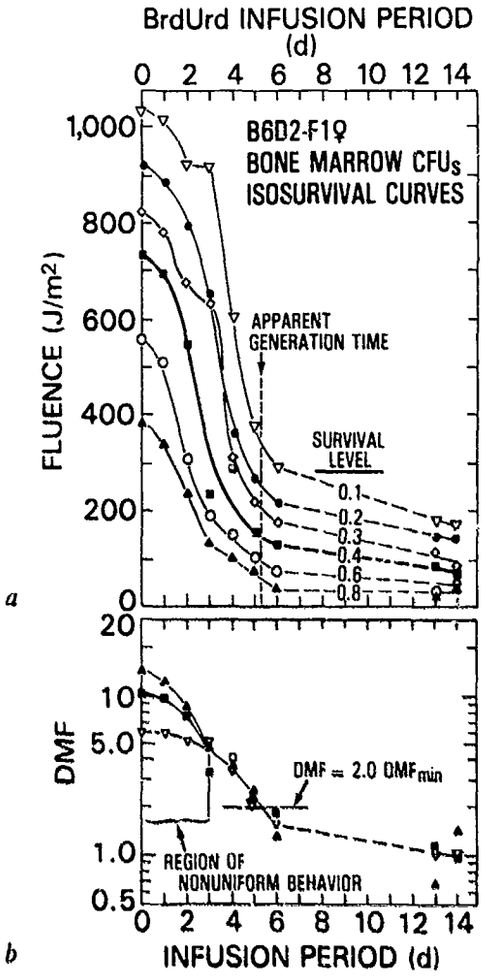

Fig. 5. Isosurvival curves for BrdU/313-nm-light inactivation of B6D2F1 female femur-derived CFU-S. Survival values are taken from mice infused with a 75 m*M* aqueous solution of BrdU. *a* Uncorrected fluence values for the following survival levels: 0.8 (▲); 0.6 (○); 0.4 (■); 0.3 (◇); 0.2 (●); 0.1 (▽). *b* Data in a are replotted as the DMF.

between 6 and 12% [22] for B6D2F1 female mice (CFU-S in the S-phase have been shown to seed less efficiently in the spleen of irradiated mice; the decrease is approximately 50% [22]). The assumption of an ~6-h S-phase [35] for this cell gives rise to two possible interpretations of the 6% survival level. The CFU-S could live in an extended cell cycle, 6–12% of which corresponds to the approximate 6 h of S-phase. For this case, the GT would be between 50 and 100 h in duration. This being the case, the DMF plot should cross the DMF = 2 value at a value between 50

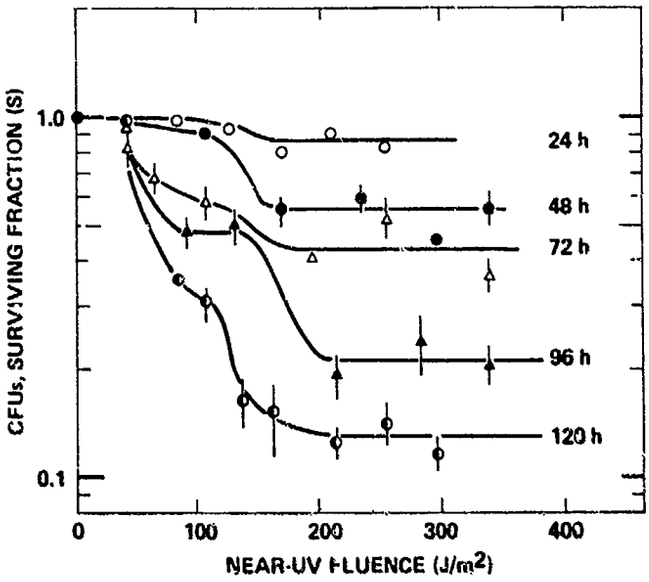

Fig. 6. Survival curves for normal femoral marrow-derived CFU-S after BrdU/313-nm-light treatment. B6D2F1 female mice were infused with 75 n*M* BrdU at 2 μl · h^{-1} for period shown in figure. Reprinted with permission from Exp. Hematol. [13].

and 100 h. Figure 5a shows the fluence values for CFU-S as a function of time for up to 2 weeks of BrdU infusion. These data, replotted in figure 5b to show DMF values, depict an apparent GT of at least 130 h. If the length of the S-phase has not been seriously underestimated, then this first interpretation appears to be wrong.

A second indication of the inappropriateness of the first interpretation can be seen in the divergence of the three DMF curves in figure 5b for infusion periods of less than 3 days. Recall that a plot of the DMF should be idependent of the survival level.

The second possible interpretation, and the one that is apropos for the murine CFU-S, involves a parameter of the BrdU/313-nm-light survival data not yet discussed. As can be seen in figure 6, each of the CFU-S survival curves eventually forms a plateau at fluence values above 250 J/m^2. At still higher fluences, these survival curves follow the same shape as those for BrdU-free cells. Therefore, the plateau reflects the unlabeled fraction of the CFU-S [12]. If this plateau in survival reflects a nonproliferative fraction (i.e., a G_0 phase), then the 6–12% S-phase kill for a 6-hour S-phase could reflect a 1–2%/h commitment to cycle of the non-

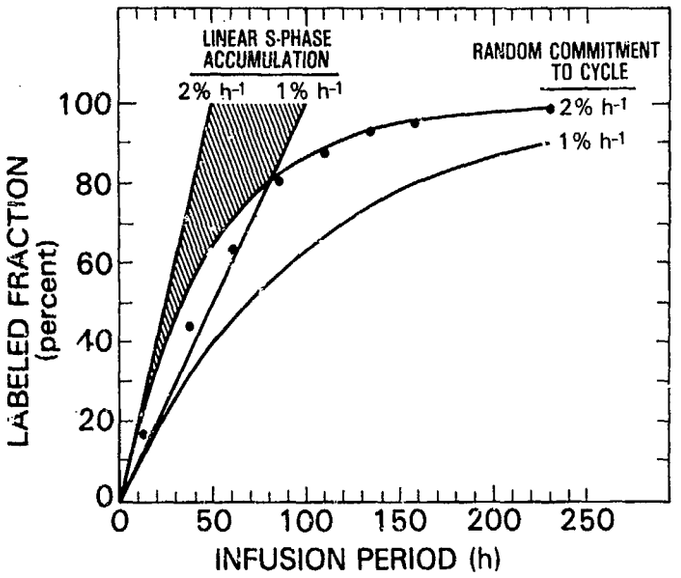

Fig. 7. Kinetics for changes in labeled cell fraction as a function of infusion period. Solid lines represent theoretical behavior discussed in text. Plateau survival values shown were taken from data presented in figure 6.

cycling subpopulation. This interpretation and that of the 50- to 100-hour GT actually form extremes of a continuum of possibilities. If the actual kinetic behavior falls close enough to one of these extremes, then a plot of the plateau survival value versus time will demonstrate the correct choice. On one hand, if the cell population exists in a long cell cycle, every hour 1–2% of the population will enter the S-phase, become sensitized to 313-nm light, and eventually be killed. For this case, the plateau value for survival will decrease linearly with a slope of 1–2%/h. However, if the CFU-S randomly exit a G_0 phase, cycle, incorporate BrdU, and then return to the G_0 state, a plot of the plateau values will be exponential with a time constant of 1–2%/h. As can be seen in figure 7, the plot is exponential in nature and the slope is 1.9%/h.

The rate of decrease for the unlabeled fraction represents the third kinetic parameter that can be determined for a cell population after BrdU/313-nm-light treatment. Having examined both a simple cell population and a cell population with a G_0 phase, we will now examine a cell population containing separate kinetic subpopulations.

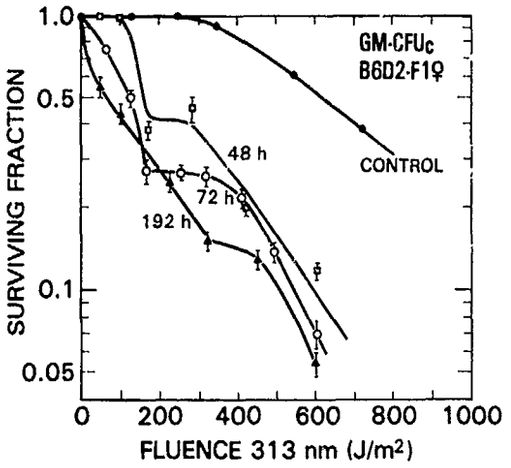

Fig. 8. Survival curves for normal femoral marrow-derived GM-CFU-S after BrdC/313 nm-light treatment. B6D2F1 female mice were infused with 150 m*M* BrdC at 1 $\mu l \cdot h^{-1}$ for period of time indicated on figure. Control mice were implanted with pumps lacking BrdC.

Kinetic Analysis of the GM-CFU-C Population

Survival curves for GM-CFU-C are shown in figure 8. From these curves, a large decrease in survival is seen between the first and third days of the BrdU infusion. From the 3rd to the 8th day, changes in the shape of the curve involve (a) the development of a subpopulation with an increased slope for survival values greater than 0.7 and (b) a decrease in the size of the population most resistant to 313-nm light. The decrease in survival after the 1st day of infusion is analogous to the data for the first cell cycle obtained with the V79 Chinese hamster cells. However, the existence of subpopulations of GM-CFU-C with differing sensitivities to 313-nm light complicates the figure, making a solution by inspection impossible.

The now familiar DMF replot of the data (figure 9), demonstrates that although the isosurvival curves were complex, the curves are composed of but two separate kinetic components. The first component is observed as the DMF drops quickly to a value of ~3.0. This value is maintained until the 8th day, when the DMF again decreases. The GM-CFU-C then are a composite, of which approximately 60% cycles quickly. In fact, this population cycles quickly enough that at the one data point per day level of resolution used here, the DMF curve appears to have been completely developed by the 3rd day of infusion. From

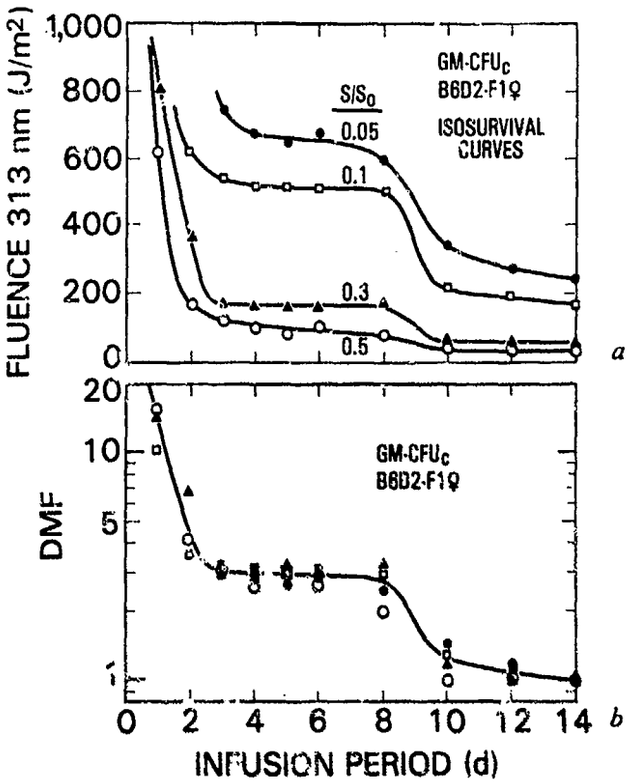

Fig. 9. Isosurvival curves, for GM-CFU-C derived from femoral marrow. were plotted from data obtained as described for figure 8. These data are shown both as a function of the fluence (*a*) and as a function of the DMF (*b*). For DMF curve, survival at 14 days of infusion was taken as estimate of minimum survival level.

these data, observe that determination of the kinetics for this subpopulation requires that a series of survival curves be measured at closer intervals over the first 72-hour period. The remaining 40% of the GM-CFU-C appear to cycle slowly, having completed the first cycle only by the first week of infusion. This cell population, observed as those cells resistant to the 313-nm-light exposure, decreases in size throughout the 14 days of the assay. The rate of decrease can thus be analyzed in a fashion analogous to the one used for the CFU-S-G_0 population.

There are obviously many more questions to be answered for both the CFU-S and GM-CFU-C kinetics. It has not been the intent here to solve these complicated kinetics. Rather, the above material serves to describe a technique that, upon the correct choice of parameters, can add considerably to the solution process.

References

1 Aebersold, P.M.: Mutagenic mechanism of 5-bromodeoxyuridine in Chinese hamster cells. Mutation Res. *36:* 357–362 (1976).

2 Aebersold, P.M.; Burki, H.J.: 5-Bromodeoxyuridine mutagenesis in synchronous hamster cells. Mutation Res. *40:* 63–66 (1976).

3 Ben-Hur, E.; Elkind, M.M.: Survival response of asynchronous and synchronous Chinese hamster cells exposed to fluorescent light following 5-bromodeoxyuridine incorporation. Mutation Res. *14:* 237–295 (1972).

4 Bohmer, R.M.: Flow cytometric cell cycle analysis using the quenching of 33258 Hoechst fluorescence by bromodeoxyuridine incorporation. Cell Tissue Kinet. *12:* 101–110 (1979).

5 Boyce, R,; Setlow, R.: The action spectra for ultra-violet light inactivation of systems containing 5-bromouracil-substituted deoxyribonucleic acid. I. *Escherichia coli* 15 $T^-A^-U^-$. Biochim. biophys. Acta *68:* 446–454 (1963).

6 Bradley, T.R.; Stanley, E.P.; Sumner, M.A.: Factors from mouse tissues stimulating colony growth of mouse bone marrow cells in vitro. Aust. J. exp. Biol. med. Sci. *49:* 595–603 (1971).

7 Camiener, G.W.; Smith, C.G.: Studies of the enzymatic deamination of cytosine arabinoside. I. Enzyme distribution and species specificity. Biochem. Pharmac. *14:* 1405–1416 (1965).

8 Craig-Holmes, A.P.; Shaw, M.W.: Cell cycle analysis in asynchronous cultures using the BrdU-Hoechst technique. Expl. Cell Res. *99:* 79–87 (1976).

9 Djordjevic, B.; Szybalski, W.: Genetics of human cell lines. III. Incorporation of 5-bromo- and 5-iododeoxyuridine into the deoxyribonucleic acid of human cells and its effect on radiation sensitivity. J. exp. Med. *112:* 509–531 (1960).

10 Goffinet, D.R.; Kaplan H.S.; Donaldson, S.S.; Bagshaw, M.A.; Wilbar, J.R.: Combined radiosensitizer infusion and irradiation of osteogenic sarcomas. Radiology *117:* 211–214 (1975).

11 Greer, S.; Tamenhof, S.: Effect of 5-bromouracil in deoxyribonucleic acid of *E. coli* on sensitivity to ultraviolet irradiation. Abstr. 131st Meet. Am. Chem. Soc., 1957, p. 3C.

12 Hagan, M.P.; Elkind, M.M.: Changes in repair competency after 5-bromodeoxyuridine pulse labeling and near-ultraviolet light. Biophys. J. *27:* 75–85 (1975).

13 Hagan, M.P.; MacVittie, T.J.: CFUs kinetics observed in vivo by bromodeoxyuridine and near-UV light treatment. Exp. Hematol., Copenh. *9:* 123–128 (1981).

14 Henderson, J.F.; Paterson, A.R.P.: Nucleotide metabolism: an introduction, p. 202, (Academic Press, New York 1973).

15 Kato, H.: Possible role of DNA synthesis in formation of sister chromatid exchanges. Nature, Lond. *252:* 739–741 (1974).

16 Kriss, J.P.; Maruyama, Y.; Tung, L.A.; Bond, S.B.; Revesz, L.: The fate of 5-bromodeoxyuridine, 5-bromodeoxycytidine and 5-iododeoxycytidine in man. Cancer Res. *23:* 260–268 (1963).

17 Kriss, J.P.; Revesz L.: The distribution and fate of bromodeoxyuridine and bromodeoxycytidine in the mouse and rat. Cancer Res. *22:* 254–265 (1965).

18 Latt, S.A.: Microfluorometric detection of deoxyribonucleic acid replication in human metaphase chromosomes. Proc. natn. Acad. Sci. USA *70:* 3395–3393 (1973).

19 Lett, J.T.: Measurement of single-strand breaks by sedimentation in alkaline sucrose gradient; in Friedberg, Hanawalt, DNA repair; a laboratory manual of research procedures, B, p. 363 (Marcel Dekker, New York 1981).
20 Ley, R.D.: Measurement of gap filling by bromouracil photolysis; in Friedberg, Hanawalt, DNA repair; a laboratory manual of research procedures, B, p. 493 (Marcel Dekker, New York 1981).
21 Meuth, M.; Green, H.: Induction of a deoxycytidineless state in cultured mammalian cells by bromodeoxyuridine. Cell *2:* 109–112 (1974).
22 Monette, F.C.; DeMello J.R.: The relationship between stem cell seeding efficiency and position in cell cycle. Cell Tiss. Kinet. *12:* 161–175 (1979).
23 Morowitz, H.J.: Absorption effects in volume irradiation of microorganisms. Science *111:* 229–230 (1950).
24 Pettijohn, D.E.; Hanawalt, P.C.: Evidence for repair-replication of ultraviolet damaged DNA in bacteria. J. Mol. Biol. *9:* 395–410 (1964).
25 Pluznik, P.H.; Sachs, L.: The cloning of normal 'mast' cells in tissue culture. J. cell. Physiol. *66:* 319–324 (1965).
26 Puck, T.T.; Kao, F.T.: Genetics of somatic mammalian cells. V. Treatment with 5-bromodeoxyuridine and visible light for isolation of nutritionally deficient mutants. Proc. natn. Acad. Sci. USA *58:* 1227–1234 (1967).
27 Rothstein, B.S.: The action spectrum (313–435 nm) for killing Hoechst 33258 treated Chinese hamster ovary cells containing bromodeoxyuridine substituted DNA. Photochem. Photobiol. *35:* 163–166 (1982).
28 Schneider, E.L.; Sternberg, H.; Tice, R.R.: In vivo analysis of cellular replication. Proc. natn. Acad. Sci. USA *74:* 2041–2044 (1977).
29 Sinclair, W.K.: Hydroxyurea: effects on Chinese hamster cells grown in culture. Cancer Res. *27:* 297–308 (1967).
30 Smith, C.A.; Hanawalt, P.C.: Phage T4 endonuclease V stimulates DNA repair replication in isolated nuclei from ultraviolet-irradiated human cells, including xeroderma pigmentosum fibroblasts. Proc. natn. Acad. Sci. USA *75:* 2598–2602 (1978).
31 Stanley, E.R.; Heard, P.M.: Factors regulating macrophage production and growth. J. biol. Chem. *252:* 4305–4312 (1977).
32 Stellwogen, R.H.: Tomkins, G.: Preferential inhibition of tyrosine aminotransferase by 5-bromodeoxyuridine in hepatoma cell cultures. J. molec. Biol. *56:* 167–182 (1971).
33 Theeuwes, F.; Yum, S.I.: Principles of the design and operation of generic osmotic pumps for the delivery of semisolid or liquid drug formulations. Ann. biomed. Eng. *4:* 343–353 (1976).
34 Till, J.E.; McCulloch, E.A.: A direct measurement of the radiation sensitivity of normal mouse bone marrow cells. Radiat. Res. *14:* 213–222 (1961).
35 Vassort, F.; Winterholer, E.; Frindell, E.; Tubiana, M.: Kinetic parameters of bone marrow stem cells using in vivo suicide by tritiated thymidine or by hydroxyurea. Blood *41:* 789–796 (1973).

M.P. Hagan, PhD, Experimental Hematology Department,
Armed Forces Radiobiology Research Institute, Bethesda, MD 20814 (USA)

Subject Index

2. Special Techniques for the Separation of Hemopoietic Cells

Biblthca haemat., No. 48, pp. 12–41 (Karger, Basel 1984)

A. Elutriation

John F. Jemionek, Rodney L. Monroy[1]

Experimental Hematology Department, Armed Forces Radiobiology Research Institute, Bethesda, Md., USA

Introduction

Several basic methods of cell separation have been developed for the isolation of a purified or enriched cell population from peripheral blood or bone marrow. The basic techniques use variations of three fundamental separation procedures. The first is cell sedimentation at unit gravity with or without prior sedimenting agents (such as dextran) to cause rouleau formation of the erythrocytes (RBCs), to increase the removal of RBC from suspension. The second technique is the adherence or adhesion of cells to fibers, plastic surfaces, or glass surfaces and their subsequent removal by selective elution with solutions of salts or chelating agents. The third technique involves density gradient centrifugation using continuous or discontinuous gradients composed of salts, albumins, or starch.

Other recent techniques of cell separation have evolved over the last decade. One procedure uses bound monoclonal antibodies directed to specific receptors so that either a positive (adhesion of the particular cell of interest onto a bound antibody matrix) or negative (binding to the bound antibody matrix of all other cells other than the cell of interest) cell selection is achieved. A second technique is light-activated cell sorting [*Van den Eng and Visser*, this volume]. The third procedure is counterflow centrifugation-elutriation (CCE; centrifugal elutriation or

[1] The authors wish to acknowledge the assistance of *Mark Behme* for the preparation of graphs and figures and *Junith Van Deusen* and *Helen Speight* for the editing and typing of manuscript.

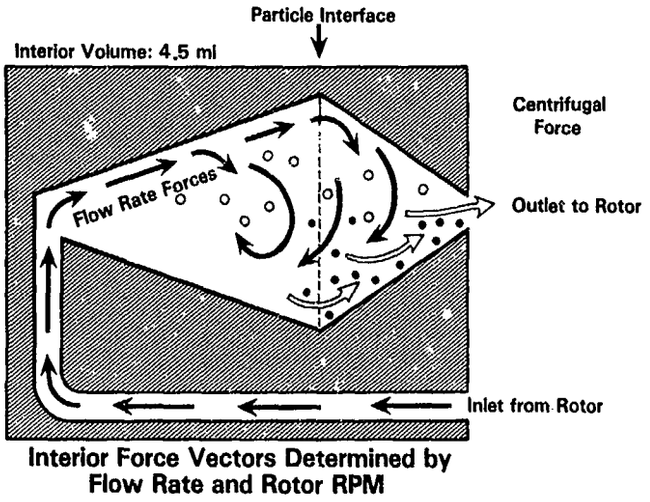

Fig. 1. Principle of CCE. Cells enter bottom of chamber with fluid flow in opposition to centrifugal force of rotor. Based primarily on cell size, cells of a small diameter exit from chamber with fluid flow, while larger cells remain in suspension in chamber. By adjusting either fluid flow rate or rotor speed, cells of various sizes can be recovered from chamber.

counter-streaming centrifugation). In this technique, cells are entered into a chamber with a fluid-flow field in opposition to a centrifugal force field (fig. 1). Based on cell size and density, the cells either exit the chamber with the fluid flow or remain in suspension within the chamber under the influence of the centrifugal force field. By either increasing the flow rate or decreasing the centrifugal force field, various cell populations can be selectively eluted from the chamber. This chapter discusses the use of CCE in cell separation, along with recent advancements and limitations of the technique.

History and Theory of CCE

While the method of centrifugal elutriation to cell separation was not widely used until the early 1970s, the basic process has been applied by industry for particle size separation. The industrial procedure is diagrammed schematically in figure 2. A mixed particle suspension is entered into a separatory funnel to which a fluid pump is connected. By slowly increasing the flow rate, various particles of various sizes and densities can be recovered.

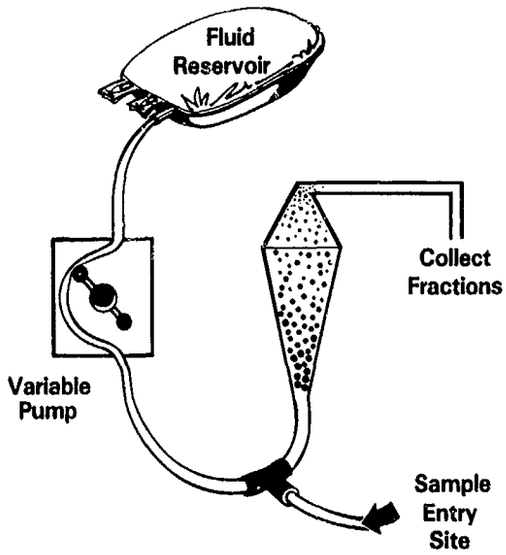

Fig. 2. Basic use of counterflow sedimentation for separation of particles based on cell size and density.

The application of CCE to the separation of biological cells was first described by *Lindahl* [12] in 1948. The term 'counterstreaming centrifugation' was coined by *Lindahl* to describe an instrument he constructed and used for the fractionation of yeast, eosinophils, sea urchin embryo, and ascities tumor cells [12–14] into various cellular fractions. The Lindahl cell separator operated with the centrifuge rotor mounted in a vertical plane, to negate gravitational effects when operating at low rotational speeds. The chamber was complex in design to overcome fluid flow and wall effects during cell separation.

Beckman Instruments, Inc., Spinco Division, began work in the mid-1960s to develop a simplified version of the Lindahl instrument that could be adapted to the research laboratory. After several research modifications [4], a standard Beckman rotor (JE6 rotor) was first described in 1968 by *McEwen* et al. [18] and used in initial experiments for separation of yeast cells. The basic Beckman separation chamber has a total volume of approximately 4.3 ml. The cells enter at the base of the chamber and rapidly fill it, approaching the level of the gasket. By increasing either the flow rate or decreasing the rotor speed, cells are selectively eluted from the top of the chamber.

A second separation chamber (available from Beckman Instruments) was developed by *Sanderson* et al. [27], working at the Webb

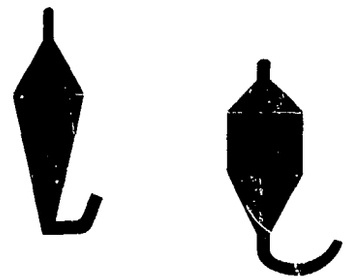

Fig. 3. Differences in chamber configurations for standard Beckman chamber and Sanderson chamber. Both chambers have significant differences that favor one chamber over the other in terms of cell collection or cell fractionation.

Waring Lung Institute of the University of Colorado School of Medicine. The Sanderson chamber has several design modifications and differs significantly from the Beckman chamber (fig. 3). First, the bottom third portion of the Sanderson chamber has a sharply tapered side where the cells tend to collect after entry into the chamber. In contrast, the Beckman chamber has gently tapered sides so that the cells tend to fill the entire volume of the chamber below the level of the gasket. Second, the nearly parallel walls in the middle third of the Sanderson chamber permit a greater resolution of cell separation than the Beckman chamber in the same region of the chamber. Third, in the Sanderson chamber, the cells enter from the bottom of the chamber in direct line with the exit channel at the top of the chamber. The entry port in the bottom of the Beckman chamber is placed on the side of the chamber. The Sanderson chamber in this respect appears to have two advantages over the Beckman chamber. First, there is a less likely chance for cells to form a clump, which would fall to the bottom of the chamber and cause clogging of a side entry port. Second, the cells that enter the Sanderson chamber appear to establish a stable cell interface more rapidly than those entering the Beckman chamber. In the latter case, the cells enter the chamber and appear to 'sweep up' the opposite wall toward the top of the chamber before looping back down into the chamber to establish a stable cell interface. The benefit of the Beckman chamber is the larger number of cells that can be entered into the chamber for separation or concentration. Since the older RBCs appear to be distinguishable by density, smaller size, and change in shape and membrane flexibility, *Sanderson* et

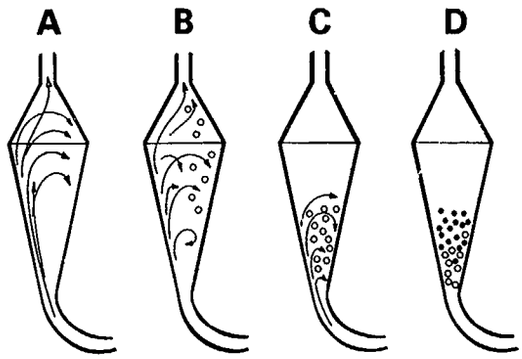

Fig. 4. Fluid flow pattern during cell entry into chamber. Minimum number of cells in the chamber are required to disrupt fluid flow and to establish a stable cell interface in chamber.

al. [27] used his chamber to separate RBCs into various age-groups. The chamber was also used for the isolation and characterization of blood monocytes with a 40–50% recovery of monocytes of 90% purity from the initial blood sample [28].

The behavior of cells in an area of opposing field forces (gravitational and fluid flow) exerts a strong influence on the separation that is achieved by CCE. When cells enter the Beckman chamber in opposition to the centrifugal force field, no discernable cell front initially appears (fig. 4). There is a fair amount of turbulence within the chamber due to the initial unrestricted fluid flow during cell entry. As more cells enter and fall back toward the base of the chamber (due to the gravitational forces and reduced fluid flow force as measured by unit flow per cross-sectional area), the unrestricted fluid flow becomes modulated due to the presence of cells near the base of the chamber. Eventually, a sufficient number of cells enter the chamber to disrupt the unrestricted flow and to set up a stable interface of cells in the chamber during subsequent cell entry. During the course of a fractionation procedure, in which an increase in flow rate or decrease in rotor speed will generate turbulence in the chamber, conditions may arise where an insufficient number of cells are in the chamber to maintain the stable cell interface. Therefore, the elutriation system requires some minimal numbers of cells for entry into the system to establish a stable cell interface.

The RBCs in the peripheral blood (for leukocyte isolation) act as ideal cells for establishing the stable cell interface during subsequent chamber loading with the leukocytes. It has been suggested by several

investigators using CCE that incorporation of latex beads into a mixed cell suspension of low total cell number may permit the latex beads to establish a stable front during entry of cells into the chamber. This would lessen the loss of cells during chamber filling and establishment of the stable cell front, thereby enhancing cell resolution. The number of cells required for establishment of a stable front appears to be relatively small; it is estimated by the authors to be in the range of 10^5 cells. The cell number required will depend on the visibility of cells in the chamber to distinguish a cell interface, the medium viscosity, and the operating temperature in the centrifuge well.

Variations in CCE Protocol for Cell Isolation

CCE can be used in either of two modes: (a) for the fractionation of a mixed cell suspension based on cell size and density, or (b) for the isolation or purification of a single cell type from a mixed cell suspension by selective elution or retention in the chamber.

In the first instance of fractionation of a mixed cell suspension, the cell separation may be obtained by (a) increasing the fluid flow rate while holding the rotor speed constant, (b) decreasing the rotor speed while maintaining a constant flow rate, or (c) using media of varying densities as a continuous or discontinuous gradient while maintaining a constant flow rate and rotor speed.

Precaution must be taken to avoid large variations in either the flow rate or rotor speed if the fractionation of a mixed cell suspension is to occur by variation in rotor speed or flow rate. This may necessitate the use of a rheostat connected to the peristaltic pump to permit small discrete changes in flow rate. If the change in rotor speed is used as a controlling mechanism of fractionation, then changes in the speed regulation circuit may be required [19, 29]. *Van Es and Bont* [29] and *Meistrich and Hunter* [19] indicated that changes in the speed circuit are required to eliminate 'overshoot' in attaining the desired rotor speed and to negate any effect on the rotor speed due to electrical interference from the refrigeration system. Perhaps the easiest variable to control is the flow rate while maintaining a constant rotor speed. Cell fractionation may also be obtained by maintaining a constant rotor speed and flow rate and using solutions of various densities either as a continuous or discontinuous gradient [5, 11]. Figure 5 is a diagram of the assembly for cell

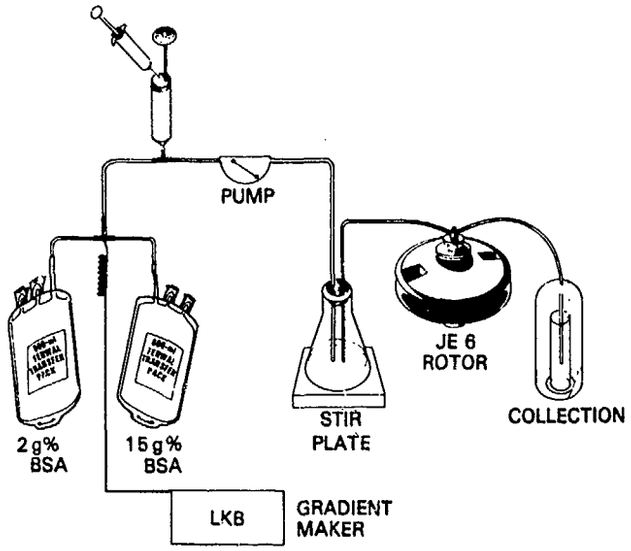

Fig. 5. System used for cell fractionation based on continuous density gradient formation controlled by an LKB Ultragrad gradient maker. This system precludes need to alter either flow rate or rotor speed to achieve cell fractionation. Cell separation occurs as factor of medium viscosity at constant rotor speed and flow rate.

fractionation using a continuous or discontinuous gradient controlled by an LKB Ultragrad gradient maker. This arrangement permits cell fractionation at a reproducible mode without disturbing a constant flow rate or rotor speed. The introduction of a continuous gradient is perhaps better than a discontinuous gradient since there is less disruption of the cell interface due to 'jet streaming' when introducing a discontinuous gradient.

In the second mode for the isolation of a single cell type from a mixed cell suspension by selective elution or retention of cells within the chamber, the degree of cell purification will depend on the size/density relationship of cells in the mixed cell population. Purification or isolation of a particular cell type occurs when the cells in the population of interest are of greater or lesser density than the other cells in the mixed cell suspension. An example of this situation is the isolation of granulocytes from peripheral blood. Granulocytes and monocytes have the greatest volume/density value relative to the other cells present in peripheral blood, and therefore are easily retained within the chamber. At a constant rotor speed, platelets, RBCs, and lymphocytes exit the chamber in the initial stages of elutriation. As the flow rate gradually increases, residual RBCs and lymphocytes are eluted from the chamber,

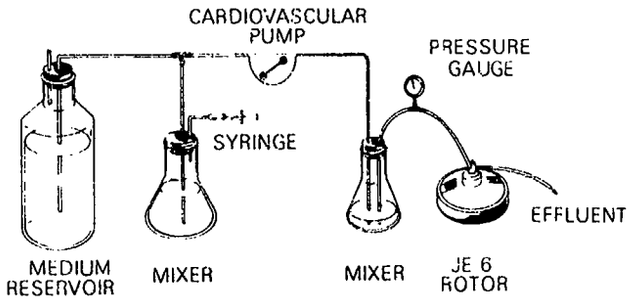

Fig. 6. System used for recovery of cells (granulocytes, monocytes) from a peripheral blood sample. System describes various parts of elutriation system used for cell isolation.

followed by monocytes, thereby leaving a pure granulocyte suspension in the chamber. Likewise, a particular cell type that is of the smallest volume/density present in a mixed cell suspension would be the first cell population to be eluted from the chamber, if chamber overloading does not occur.

If the cell population of interest is not the cell of heaviest or lightest volume/density in the mixed cell suspension, then prior treatment of the sample with agents or techniques (e.g. Ficoll, differential centrifugation) is required to remove cells that have a heavier or lighter volume/density than the cell population of interest. An example is the isolation of monocytes from peripheral blood, where the granulocytes must be eliminated from the sample by Ficoll-Hypaque, before elutriation of the mononuclear cell fraction to recover a pure monocyte fraction in the chamber.

The Elutriation System

The basic components (fig. 6) of the elutriation system are: (a) the centrifuge (J21B or J21C) and the JE6 rotor; (b) a peristaltic pump; (c) a sample entry site; (d) an elutriation medium site; (e) a pulse suppressor and/or bubble trap.

In order to enter cells into the chamber and to maintain a constant flow rate, various pumps have been used at various sites to propel fluids through the system. The ability or inability to pass cells directly through the pump dictates the selection of a pump and the position of the pump relative to the rotor and sample entry site. Figure 7 illustrates some of the pump sites commonly used for elutriation.

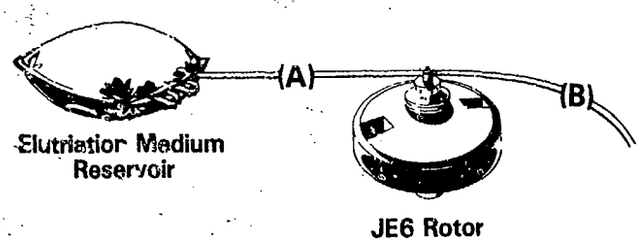

Fig. 7. Location of pump to deliver medium and cells to rotor can be located in either of two positions, depending on ability of cells to pass through pump. Position A presupposes ability of cells to pass through pump, which in essence pushes cells through the system. If cells to be recovered remain in chamber and cannot pass through pump, then pump can be positioned after rotor, which pulls cells through the system.

Selection of a particular pump should be based on three factors: (a) The ability to pass cells through the pump with no cell disruption (e.g., cardiovascular pump). (b) A low peristaltic action in the fluid to ensure an even, continuous flow of medium through the system, especially the rotor chamber. (c) The ability to adjust small incremental changes in flow rate over the flow rate range required for a particular cell separation. Some separation techniques may require flow rate ranges of 4–12 ml/min versus 18–35 ml/min.

The elutriation rotor system is extremely sensitive to the introduction of air into the system. The entry of an air bubble as small as 20 µl into the rotor is capable of causing an air occlusion. The air bubble will stop the fluid flow (resulting in pelleting of cells to the bottom of the chamber) until a sufficient fluid back pressure develops to dislodge the air bubble. This normally results in a pulsing of the pelleted cells out of the chamber. To eliminate the accidental entry of air to the rotor, a bubble trap is usually used just before the rotor (fig. 8). The bubble trap may take two forms. In the first, a vertical 'T' is inserted in the line and is filled with elutriation medium through a bleed valve at the top of the 'T'. Therefore, any air entering the system would be caught in the 'T', displacing an equal volume of medium. In the second form, the bubble trap is incorporated with a pulse suppressor chamber. A 50-ml closed flask containing approximately 10–15 ml of medium is connected in line between the pump and rotor, and serves as a bubble trap or as a pulse suppressor for those pumps with a high peristaltic action (e.g., a two-roller cardiovascular pump).

The last component of the elutriation system to be discussed is the sample entry site. The position of the sample entry site relative to the

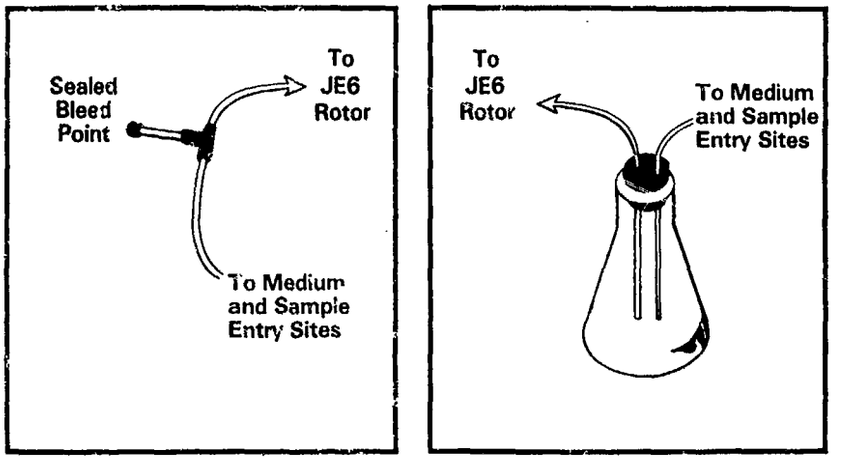

Fig. 8. Two methods for elimination of bubbles entering rotor system. Use of either an inverted 'T' or a flask filled with 10–15 ml of medium acts as bubble trap and mixing chamber for density gradients or cell entry site.

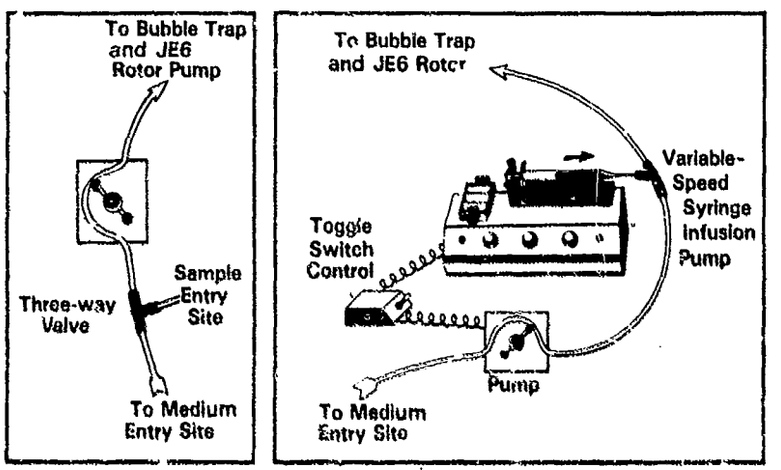

Fig. 9. Various modes of cell entry, depending on volume of sample to be entered and ability to pass cells through peristaltic pump. System A can be used for small or large cell sample sizes, and presupposes ability to pass cells through pump. System B uses a syringe infusion pump for various cell sample volumes when cells are not able to be passed through peristaltic pump.

pump depends on two factors: the volume of sample to be entered, and the ability of the cells to pass through the pump without inducing cell disruption.

If sample volumes of 20 ml to 2 liters are to be entered and the cells are capable of passing through the pump, the diagram in figure 9a can be

used. However, if a large sample volume of 10–150 ml is to be introduced and the cells cannot be passed through the pump, a variable-speed syringe infusion pump can be used (fig. 9b). Both pumps must be adjusted to the same initial flow rate and a toggle switch must be used to control the activation of both pumps in order to obtain a continuous fluid flow when switching between pumps. For smaller volumes (less than 10 ml), the sample can be injected directly into the pulse suppressor/bubble trap. For volumes less than 2 ml, the sample can be entered directly in a line through a self-sealing port or three-way valve.

Techniques of Cell Isolation

Granulocyte Isolation from Peripheral Blood

The isolation of granulocytes from human [1, 9], canine [7, 8], guinea pig [17], and baboon [16] donors has been reported in the literature. Granulocyte purity averaged 96% independent of the donor species and independent of sample volume, which ranged from 5 ml of peripheral blood to 150 ml of leukapheresis concentrates. In all cases, the average cell recovery was 84% (range 80–100%). The absolute number of cells isolated ranged from 1.4×10^7 granulocytes recovered from 5 ml of peripheral blood [25] to 1.4×10^9 granulocytes recovered from 150 ml canine leukapheresis concentrates [8]. As determined by various in vitro assay procedures for physiological activity, the isolated granulocytes appeared to retain excellent morphological and physiological parameters.

As noted in the numerous reports, in addition to variations in the selection of a rotor speed and flow rate, the individual investigator may have personal preferences for anticoagulant and sample pretreatment. The most commonly used anticoagulants are heparin (50–100 units/ml), 7.5% (v/v) of acid-citrate-dextrose or citrate-phosphate-dextrose, or a rapid tenfold dilution of the blood sample with the elutriation medium of choice.

The need for sample pretreatment (to reduce the number of RBCs) is generally dictated by the sample size of peripheral blood and therefore the time required for entry of the diluted cell suspension. We have found that entry of peripheral blood with too high an RBC concentration reduces the PMN recovery and that a sample RBC concentration not exceeding 4.5×10^8 RBC/ml permits at least an 80% granulocyte yield.

Therefore, sample introduction into the CCE system may take several forms:

(a) No prior sample treatment except for dilution with elutriation medium to an RBC concentration of $3.0–4.5 \times 10^8$ RBC/ml.

(b) Centrifugation of the sample at 450 *g* for 15 min to recover a leukocyte-rich buffy coat layer, which is then diluted to the desired RBC cell concentration.

(c) Sedimenting the RBC using 6% dextran (dissolved in normal saline) T-100 at 1/15 ratio of 6% dextran to whole blood. After 30–60 min, the leukocyte-rich supernatant can be decanted from the sedimented RBCs. Following a one- or two-cycle wash of the leukocytes to remove the dextran, the leukocytes may be resuspended in elutriation medium for cell entry.

Our preference for elutriation medium is a 0.05 *M* phosphate-buffered saline (PBS) containing 1–2 g% Cohn fraction V bovine serum albumin (BSA) adjusted to a pH 7.2 and 325 mosm/kg.

For granulocyte isolation from canine [7] or human [1] donors, the following protocol may be followed. Adjust centrifuge temperature and rotor speed to 15 °C and 2,010 ± 10 rpm, respectively. Set the initial entry flow rate for cells at 9–10 ml/min. After completion of cell entry, allow elutriation medium to continue through the system at the same initial flow rate for 10–15 min until the RBC interface in the chamber drops to the level of the chamber gasket. Slowly increase the flow rate by 0.5 ml per 3-min interval until a flow rate of 12–15 ml/min is achieved. The final flow rate is affected by the number of granulocytes entered into the chamber. The greater the number of granulocytes, the lower the final flow rate required to clear RBCs and monocytes from the chamber. Once the RBCs have been eliminated from the chamber, the granulocytes can be collected from the chamber effluent by decreasing the rotor speed while increasing the fluid flow rate (cell collected in 100–150 ml of effluent), or by hemostating the entry line to the rotor and turning off the pump while shutting off the rotor speed. In the latter case, the cells will pellet to the bottom of the chamber, and the cells can then be recovered from the chamber in a volume of approximately 4.3 ml.

Hemopoietic Cell Isolation

CCE has been used for the purification and study of progenitor cells responsible for megakaryopoiesis in the mouse [21–23], for murine splenic CFU-E [24], and murine bone marrow CFU-S activity [6]. *Meys-*

kens et al. [20] conducted a morphological examination of human bone marrow fractionated by CCE, and showed a significant separation of mononuclear cells from more mature granulocytic cells. *Jemionek* et al. [11] compared the granulocyte-macrophage colony-forming cell (GM-CFC) activity in CCE-fractionated bone marrow aspirates obtained from murine, canine, monkey, and human donors.

Murine CFU-S Isolation

The procedure by *Inoue* et al. [6] for murine CFU-S concentration involved a preliminary erythrocytolysis using Gey's salt solution, in which ammonium chloride was substituted for sodium chloride. The nucleated cell suspension was washed in medium 199 containing 10% fetal calf serum and layered over a discontinuous Percoll gradient, followed by a 20-min centrifugation at 400 *g*. The highest CFU-S activity relative to control was in association with densities between 1.058 and 1.066. The average enrichment of CFU-S in the Percoll fraction was 1.34 ± 0.13 times that of the control. The CCE purification step was conducted at a rotor speed of 2,500 rpm with an entry flow rate of 2.5 ml/min using the Beckman separation chamber. Fraction 1 was collected at a flow rate of 3–5 ml/min, and it contained RBC and cellular debris. Fraction 2, recovered at a flow rate of 12.5 ml/min, contained primarily lymphocytes. Fraction 3, collected at a flow rate of 13.5 ml/min, contained a mixture of lymphocytes and granulocytes, and showed the highest enrichment of CFU-S between 2.28 and 7.60 times that of the control, depending on experimental protocol. Fraction 4, collected at a flow rate of 14.0 ml/min, contained primarily mature granulocytes.

Following the isolation procedures, there appeared to be no difference in the proportion of spleen colony type or in the size of the erythrocytic colonies for the cell isolated by CCE. The size and sedimentation velocity for the cell population isolated at a flow rate of 13.5 ml/min and having the highest CFU-S activity were calculated to be for a cell sedimenting at 4.056 ± 0.124 mm/h/unit gravity with a diameter of 6.21 ± 0.096 μm and a cell volume of 125 ± 6 μm³.

Megakaryocyte Isolation from Rat Femoral Marrow

Nakeff and Worthington [23] reported a procedure for a rapid CCE separation of monodispersed rat femoral marrow cells into a megakaryocyte-rich fraction. Within 30 min, 2.3×10^9 marrow cells could be

fractionated to yield a concentrate containing 10^6 megakaryocyte (80% efficiency of recovery) of 7% purity for a 150-fold concentration of megakaryocytes relative to the starting marrow suspension.

The rat femoral marrow was collected, dispersed, and nylon-mesh-filtered (70 μ) into 15 m*M* Tris-HCl saline (pH 6.5) chelated with 3 m*M* EDTA and supplemented with 7.5 m*M* glucose, 5 m*M* KCl, and 1 m*M* Na_2SO_4 adjusted to a 300 mosm maintained at 12 °C. The CCE procedure required attention to several detailed preparatory steps in the CCE system as outlined below:

(a) Between isolation attempts, the chamber was soaked for several hours in KOH and adequately rinsed to remove all cellular and particle debris.

(b) The loading or mixing chamber, medium reservoirs, and all tubing lines were immersed in a water bath at the same temperature as the rotor and chamber (12 °C).

(c) The Sanderson chamber was used rather than the Beckman chamber.

(d) The cells were drawn rather than pushed through the system. This eliminated the mechanical damage of cells when passed through the pump.

The cell suspension was entered into the system at a flow rate of 20 ml/min and rotor speed of 2,130 rpm so that cells with a sedimentation velocity of approximately less than 10 mm/h/unit gravity exited the chamber. Cells of a greater sedimentation velocity were retained within the chamber. The enriched megakaryocyte concentrate was obtained from the fraction retained in the chamber, and it averaged 150-fold the concentration in the initial sample.

BFU-E and CFU-E Enrichment from Murine Spleen

Nijhof et al. [24] reported a three-step procedure for the isolation of a CFU-E-enriched and BFU-E-enriched population. The three steps were:

(a) Treatment of the mice with thiamphenicol for 4 days with concurrent bleeding of 0.5 ml/day/animal. 4 days after removal from thiamphenicol, the spleen tissue was removed and dispersed through 100-mesh stainless steel to form a cell suspension. The cells were resuspended in α-medium plus 10 m*M* Hepes (pH 7.2.).

(b) Elutriation using an ethanol-sterilized Beckman chamber. All tubing lines and rotor were sterilized using 70% ethanol followed by ster-

ile water and α-medium supplemented with 5% fetal calf serum. The rotor speed was adjusted to 2,000 rpm with an initial flow rate of 20 ml/min and rotor temperature set at 25 °C. Approximately 10^9 nucleated cells in 4 ml of medium was injected into a 25-ml bypass chamber. The flow rate was slowly increased to 30 and 40 ml/min. At each flow rate, five fractions of 35 ml each were collected, pooled, and concentrated to yield four individual fractions. Fraction 1, collected at 20 ml/min, contained approximately 60% of the total recovered nucleated cells and the bulk of the BFU-E and CFU-E activity. Fraction 2, collected at 30 ml/min, contained approximately 20% of the total recovered nucleated cells and most of the CFU-E activity for an average three- to fourfold concentration of the CFU-E activity in this fraction. Fraction 3, collected at 40 ml/min, contained approximately 5% of the total recovered nucleated cells and approximately 18% of the recovered CFU-E activity. Fraction 4 consisted of aggregate formed at the bottom of the chamber during the fractionation procedure. The pellet accounted for approximately 10% of the total recovered nucleated cell count, and contained approximately 24% of the total recovered CFU-E activity.

(c) The fraction 2 cells were mixed with 35 ml of Percoll medium (54% Percoll) in α-medium supplemented with 15% fetal calf serum and 10 m*M* Hepes (pH 7.2). The density of the medium was 1.072 g/ml. The suspension was centrifuged at 20 °C at 18,000 *g* for 40 min in a Ti60 rotor using a Beckman L5–65 centrifuge. After the Percoll gradient centrifugation, 2-ml fractions were collected and concentrated by centrifugation to 0.5-ml aliquots. The maximal CFU-E activity was recovered in the Percoll gradient corresponding to a density of 1.068–1.072 g/ml. In these fractions, the CFU-E and CFU-C activity was less than 0.02 and 0.15%, respectively, of the total cell number.

Nijhof et al [24] indicated that, from thiamphenicol-treated animals, a spleen cell suspension containing an average of 7.78×10^6 nucleated cells was separated by a two-step procedure (CCE and Percoll gradient) to yield a cell population containing an average 23×10^4 CFU-E. The time required for CFU-E isolation was approximately 2 h.

Separation of Mammalian Bone Marrow

Meyskens et al. [20] reported the use of CCE for the separation of human bone marrow cells. Using morphological analysis, he indicated not only that CCE separated mononuclear cells from polymorphonuclear leukocytes but also that subfractionation of the neutrophilic gran-

ulocytes occurred. The method of cell fractionation was to increase the flow rate from 4 to 28 ml/min in 1.5 ml/min increments while maintaining a constant rotor speed of 1,740 rpm. A total of 17 fractions of 50 ml each were collected for analysis.

Jemionek et al. [11] have used CCE in conjunction with a continuous albumin gradient to examine the nucleated cell recovery profile and associated GM-CFC activity for bone marrow aspirates from murine, canine, monkey and human donors. During the CCE fractionation procedure, the rotor speed and flow rate were held constant. The cell fractionation was achieved by using a continuous albumin gradient so that cell separation occurred by density equilibrium. The arrangement used is diagrammed in figure 5. All tubing lines, glassware and connections were sterilized by steam autoclave. The media used for the gradient (2 and 15 g% [w/v] BSA in 0.05 *M* PBS, pH 7.2, and 325 mosm/kg) were both sterilized by filtration through 0.2-μm Nalgene filter units before use. The common tubing lines through the pump, mixing chamber, and rotor were sterilized using 50% (v/v)$NaClO_2$ and H_2O (pH 7.5), followed by copious amounts of sterile water and the 2-g% BSA-PBS medium. The bone marrow samples from each species were diluted with sufficient 2 g% BSA-PBS medium to achieve an RBC concentration of 4×10^8 RBC/ml. The diluted bone marrow sample was filtered through nylon mesh to remove cell debris and aggregates before sample entry into the CCE system.

For all fractionation studies, a rotor speed of 2,010 rpm was used with a centrifuge well temperature of 15 °C. For murine bone marrow, the flow rate used was 7.0 ml/min, for canine bone marrow the flow rate was 8.0 ml/min, and monkey and human bone marrow were entered at a flow rate of 8.5 ml/min. Sample collection every 5 min of approximately 35–45 ml (depending on species) was initiated once cells began to enter the Beckman rotor. When the sample had entered the system, fluid flow was returned to the 2 g% BSA-PBS medium via a three-way valve. When cell clearing in the mixing chamber/bubble trap occurred, formation of the continuous albumin gradient was initiated. Therefore, the gradient was initiated at different fraction numbers for each species, depending on sample volume and degree of RBC dilution required. In general, for mouse and monkey marrow, the gradient was initiated at the start of sample collection in tubes No. 2 and 5, respectively; for human and canine marrow, the gradient was initiated at the start of sample collection of tube No. 4.

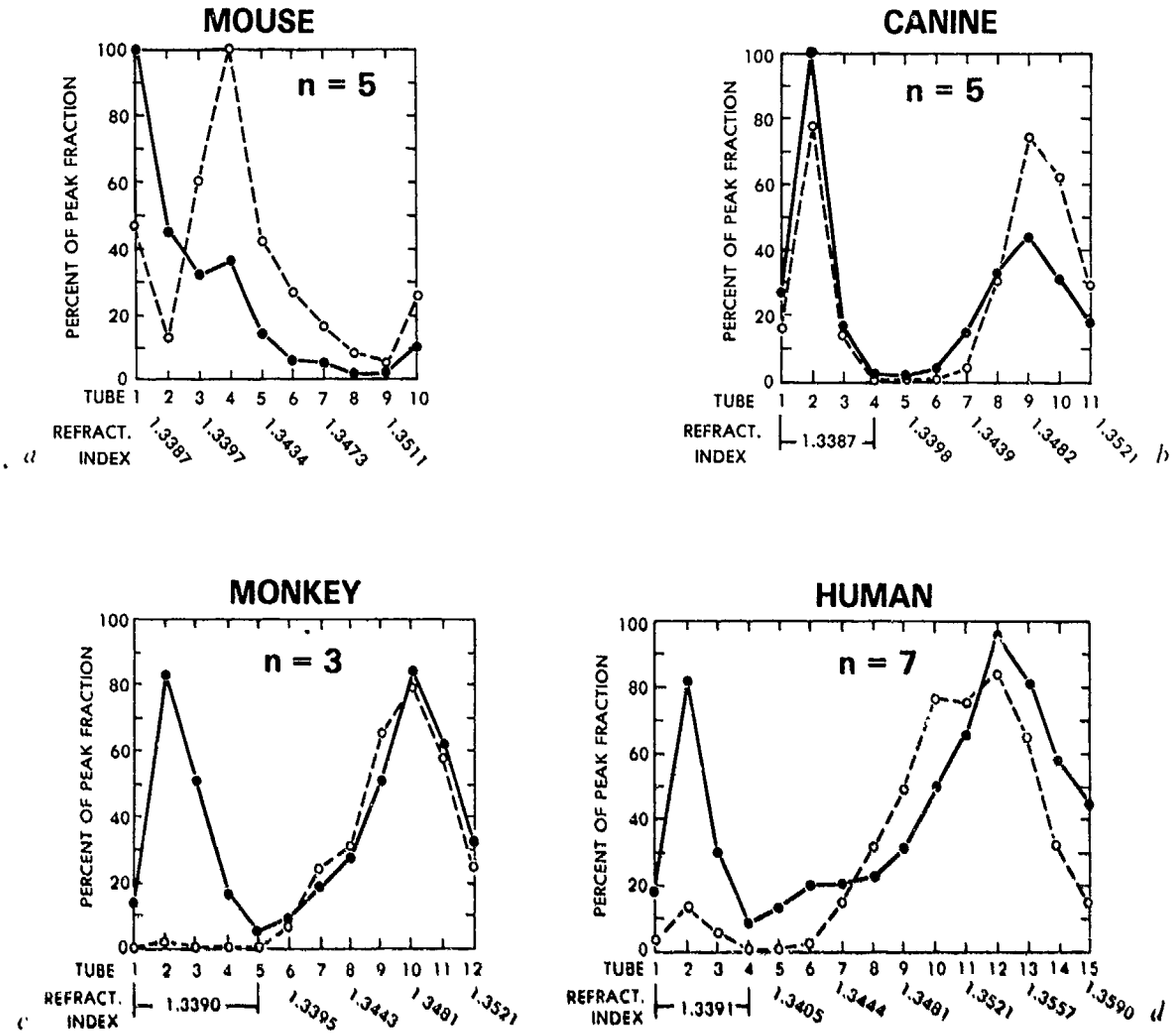

Fig. 10. Profile of various mammalian bone marrow aspirates fractionated by CCE using a continuous albumin gradient at constant rotor speed and flow rate to achieve cell separation. Profile indicates nucleated cell recovery (●) and levels of (GM-CFC) activity (○) in each of various fractions as function of medium density. *a* Mouse. *b* Dog. *c* Monkey. *d* Man.

As indicated in figure 10, each species has a unique representative profile of nucleated cell recovery and associated GM-CFC activity. The percent nucleated cell recovery following fractionation averaged 52 and 85% for murine and canine marrow, respectively; recovery for human and monkey marrow averaged 89 and 92%, respectively.

Table I represents the various cell populations recovered in the various tube fractions for human bone marrow. In agreement with the

Table I. Morphological characterization of representative human iliac crest aspirate separated by CCE

	Initial sample	Tube No.														
		1	2	3	4	5	6	7	8	9	10	11	12	13	14	15
Erythroid series																
Rubriblasts	–	1	–	–	–	–	–	–	–	1	2	1	–	–	–	–
Prorubricytes	–	–	–	–	–	2	–	–	2	1	1	–	–	–	–	–
Normochromatic rubricytes	8	3	4	5	2	9	5	6	22	13	6	–	–	–	–	10
Polychromatic rubricytes	–	–	–	–	–	–	–	–	–	–	–	–	4	–	–	–
Metarubricytes	9	10	3	3	9	2	9	11	21	14	3	–	1	–	–	5
Total	17	14	7	8	11	13	14	17	45	29	12	1	5	–	–	15
Mononuclear series																
Lymphocytes	6	69	60	53	71	62	66	46	18	11	1	–	–	–	–	–
Monocytes	1	4	23	34	16	24	20	35	14	12	1	–	–	–	–	–
Total	7	73	83	87	86	86	81	32	23	2	–	–	–	–	–	–
Granulocytic series																
Myeloblasts	3	–	–	–	–	–	–	–	–	1	2	3	6	6	7	5
Progranulocytes	3	–	2	–	–	–	–	–	6	3	2	3	7	4	2	1
Neutrophil myelocytes	10	8	3	1	–	–	–	–	13	13	22	13	12	3	14	20
Eosinophil myelocytes	5	–	–	–	–	–	–	–	–	–	–	–	1	15	–	–
Neutrophil metamyelocytes	6	2	2	3	–	–	–	1	2	7	18	20	21	5	13	2
Eosinophil metamyelocytes	–	–	–	–	–	–	–	–	–	–	–	–	–	16	4	3
Neutrophil bands	13	–	1	–	–	–	–	–	–	7	17	29	21	2	19	11
Eosinophil bands	–	–	–	–	–	–	–	–	–	–	–	–	–	21	–	–
Neutrophil segmented	34	3	2	1	1	–	–	–	–	15	24	31	28	8	36	28
Eosinophil segmented	–	–	–	–	–	–	–	–	–	–	–	–	–	20	4	14
Total	74	13	10	5	1	–	–	1	21	46	85	99	96	100	99	84

Data presented as percent of total cells counted. Average of 250 cells counted per fraction.

results of *Meyskens* et al. [20], the RBC and mononuclear leukocytes (primarily lymphocytes) are recovered in the early tube fractions. In the later tube fractions, the myelocytes + myeloblasts are predominant, followed by the mature cells of the granulocytic series. Among the last cells to be recovered from the chamber are eosinophils.

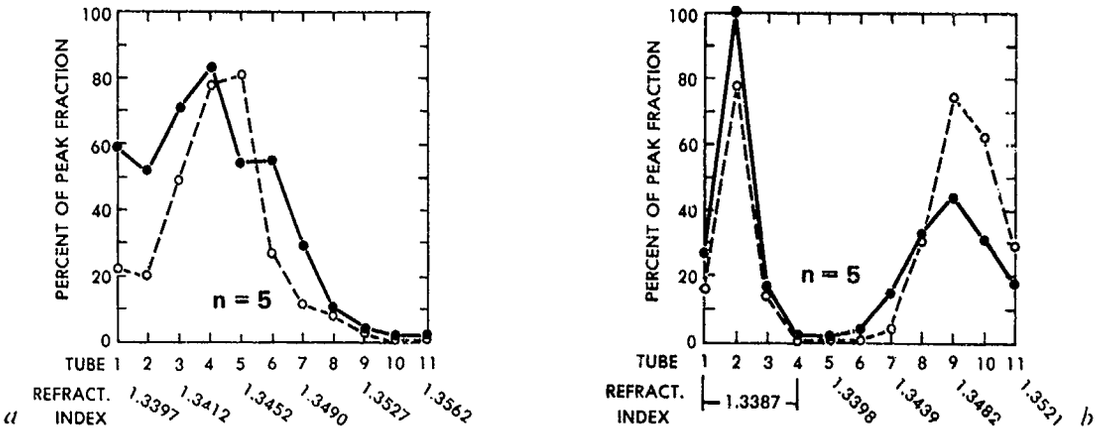

Fig. 11. Profile of canine bone marrow aspirates fractionated by CCE using a continuous albumin gradient. ● = Nucleated cell count/fraction; ○ = GM-CFC/fraction. *a* Cells were pretreated with Ficoll-Hypaque to remove RBCs before cell entry into system. *b* Marrow cells diluted with medium to an RBC concentration of 4×10^8 RBC/ml (no other cell pretreatment) and entered into system.

The average run time for a normal 5- to 10-ml bone marrow aspirate sample is approximately 1 h. A maximum of 9×10^8 nucleated human bone marrow cells in dilute suspension can be entered into the CCE system for cell fractionation. However, a major point should be noted. The bone marrow sample was fractionated without any prior attempt to remove the RBCs by dextran or Ficoll-Hypaque. Table I presents those data and figure 11 shows the fractionation profiles for canine bone marrow samples with and without prior RBC removal using Ficoll-Hypaque. As can be seen, pretreatment of the bone marrow with Ficoll-Hypaque produced a marked shift in the recovery profile for both nucleated cell count and associated GM-CFC activity. We therefore suggest that any attempt to further purify nucleated cells from a mixed cell suspension should occur after the CCE fractionation step.

Mononuclear Cells

Monocytes and Lymphocytes

CCE has been successfully used as a second step in the purification of lymphocytes and monocytes. Since this technique separates the lymphocytes from the monocytes of an original enriched mononuclear cell fraction, the methods for purification of each cell type are combined in

Table II. Physical parameters of elutriation system for isolation of mononuclear cells

Reference	Rotor chamber	Centrifuge speed rpm	Temperature °C	Flow rate ml/min	Medium
Contreras et al. [2]	Beckman	2,020	18	10–12	PBS (pH 7.4); 2% BSA
Sanderson et al. [28]	Sanderson	2,500	23	10-28	Hanks' balanced salt solution minus Ca^{2+} and Mg^{2+}; EDTA (100 mg/o); 0.2 BSA
Weiner and Shah [30]	Sanderson	2,500	(a) 10 (b) 22–24	(a) 17 (b) 22 (c) 28	Hanks' balanced salt solution minus Ca^{2+} and Mg^{2+}; EDTA (100 mg/o)
Fogelman et al. [3]	Beckman	2,000	15	(a) 10–12.5 (b) 14–17.5 (c) 19.0	Kreb's-Ringer phosphate buffer (pH 7.4); 0.15 m*M* glucose; 1% BSA

this discussion. In the following paragraphs, the various methods of mononuclear cell purification using CCE will be compared, and an example of a methodology will be described in detail.

The physical parameters of the various CCE procedures used for either lymphocyte or monocyte purification are summarized in table II. As previously discussed, two characteristic rotor chambers (Sanderson and Beckman) are used for the purification of other cell types. When the Sanderson chamber is used, the centrifuge is run at the higher speed of 2,500 rpm, as compared with 2,000 rpm when using the Beckman rotor chamber. The higher centrifuge speed requires a higher elutriation medium flow rate in order to successfully elutriate the cells. The Sanderson chamber and the Beckman chamber require a final flow rate of 28 and 19 ml/min, respectively, to elutriate the cells. The higher flow rate and rotor speeds used in conjunction with the Sanderson chamber did not appear to damage cell viability.

Results of the various investigators suggest that the rotor temperature for the most efficient purification of either lymphocytes or monocytes should be slightly less than room temperature, in the range of 15–18 °C. *Weiner and Shah* [30] compared two rotor temperatures (10 °C vs. 22–24 °C and showed that the purification of monocytes from lym-

phocytes was significantly influenced by temperature. They reported a 5.9% lymphocyte contamination in the monocyte fraction when the rotor temperature was at 22–24 °C, in contrast to a 1.3% lymphocyte contamination at 10 °C. The authors did not indicate that the entering temperature should be maintained at the rotor temperature.

The elutriation medium with respect to its actual composition is a variable that depends on the investigator. However, there are some common requirements for these media. The elutriation medium should be devoid of both CA^{2+} and Mg^{2+}, it should be at physiological pH, and it should have a distinct protein content. Several of the investigators further supplemented their media with EDTA (100 mg/l) to preclude any chance of cellular aggregation.

The key physical parameter used in purification of the different mononuclear cells is the flow rate of the elutriation medium. The control of flow rate to bring about purification is not totally precise. As shown in table II, each laboratory uses a different range of flow rates, and the rate of increase is not specified. The rate at which the flow rate is increased is variable between investigators. For example, *Contreras* et al. [2] and *Sanderson* et al. [28] made increases in the flow rate dependent on the eluted cell type, where the eluted cell type was continually monitored using a Coulter Channelyzer. *Contreras* et al. [2] collected the first four fractions (50 ml each) at a flow rate of 10 ml/min, after which the flow rate was slowly increased until the eluted cell types were 50% lymphocytes and 50% monocytes in the eluate. At this point, the flow rate was not increased further, and only one additional fraction was collected. The final flow rate at this point was 12 ± 0.4 ml/min. The total number of fractions collected ranged from 9 to 14. In comparison, *Sanderson* et al. [28] increased the flow rate increments based on the monitored fall-off of a specific cell population from the eluted cells. At a starting flow rate of 10 ml/min, platelets were eluted; at 15 ml/min, small lymphocytes were recovered. A lymphocyte-monocyte mixture was eluted at a flow rate of 20 ml/min, and at 28 ml/min, the most concentrated monocyte fraction was collected. The eluted medium volume using this method was not reported. Thus, the elutriation methods of *Contreras* et al. [2] and *Sanderson* et al. [28] appear to adapt to sample variability by allowing a given cell type to be eluted before the medium flow rate is further increased.

Weiner and Shah [30] and *Fogelman* et al. [3] preferred to use a set flow rate schedule based on the volume of medium eluted. However, each investigator accomplished this with different procedures. *Weiner*

and Shah [30] eluted three fractions (400 ml each) at three defined flow rates. The first fraction, eluted at 17 ml/min, was shown to contain 85% lymphocytes with a 5% monocyte contamination. The second fraction, eluted at a flow rate of 20 ml/min, contained 94% monocytes with only a 1.3% lymphocyte contamination. The last fraction was eluted at 28 ml/min and contained an insignificant number of cells.

Fogelman et al. [3] also collected three fractions but of different volumes and at different flow rates. Their first fraction (120 ml) was eluted at a flow rate that was increased from 10 to 12.5 ml/min during its collection. This fraction contained 98.9% lymphocytes. The second fraction (100 ml) was eluted as the flow rate was increased from 14 to 17.5 ml/min, and it contained 33.4% monocytes, which were predominantly contaminated with granulocytes. The final fraction was eluted at a flow rate of 19 ml/min, and contained the cells remaining in the rotor chamber. These cells were found to be mainly granulocytes. Hence, each laboratory was able to obtain a high level of purity of a specific mononuclear cell as long as due regard was given to flow rate and speed. Initial preparation of the sample is important for successful elutriation. An enriched mononuclear cell is obtained from peripheral blood or leukapheresis concentrates by isopyknic centrifugation with Ficoll-Hypaque. This technique allows the investigator to enter an enriched cell population that is generally free of RBC, platelets and granulocytes. *Fogelman* et al. [3] used Plasmagel instead of Ficoll-Hypaque. This change resulted in heavy granulocyte contamination of their monocyte fraction. Thus, the efficiency of the initial preparation to obtain a pure mononuclear cell fraction is critical in the purification of either lymphocytes or monocytes.

As shown in table III, a wide range of mononuclear cells (4.5×10^6 to 7.2×10^9 can be loaded into the rotor chambers and successfully elutriated. The various investigators report that approximately 90% of the cells entered are recovered and are greater than 95% viable. No difference is apparent between the viability and recovery of cells isolated using the Sanderson chamber versus those isolated using that of Beckman.

The isolated lymphocyte populations were between 85.0 and 98.9% pure with monocytes and granulocytes as the major contaminants. The highest level of purity was reported by *Fogelman* et al. [3], who used Plasmagel as an initial preparatory step before elutriation. This procedure required the washout of RBCs before starting collection, which was not

Table III. Comparative results of purified mononuclear cells

Reference	Origin of cells	Initial preparation	Number of nuclear cells entered	Recovery %	Viability %	Purity	
						lymphocyte fraction	monocyte fraction
Contreras et al. [2]	peripheral blood leukapheresis concentrate	Ficoll-Hypaque	4.5×10^8 to 2.2×10^9	96.5	96.6	93.0% lymph (granulocyte)	92.0% mono (granulocyte)
Sanderson et al. [28]	peripheral blood	Ficoll-Hypaque	$4.0–8.3 \times 10^6$	90.0	>99	92.9% (monocyte)	90.0% (lymphocytes)
Weiner and Shah [30]	leukapheresis concentrate	Ficoll-Hypaque	$1–1.5 \times 10^9$	87.0	>95.0	85.0% lymph (monocyte)	95.0% mono (lymphocyte)
Fogelman et al. [3]	peripheral blood	Plasmagel	n.r.	n.r.	95.0	98.9% lymph (monocyte)	33.4% mono (granulocyte)

Primary contaminating cell type indicated in parentheses; n.r. = not reported.

completely accomplished. This suggests that the remaining RBCs will be a contaminant in the lymphocyte fraction. Thus, their reported purity was possibly based only on the nucleated cells. This possibility was mentioned by *Pretlow and Pretlow* [26].

In comparison to the recovered monocyte fractions, all the investigators, with the exception of *Fogelman* et al. [3], had 90 and 95% purity. The monocytes had only a minor contamination of lymphocytes and granulocytes. *Fogelman* et al. [3] had a 33.4% monocyte purity with granulocytes as the contaminant. As previously discussed, this contamination can be attributed to the initial preparation in which Plasmagel was used instead of Ficoll-Hypaque.

The protocol for lymphocyte and monocyte isolation from canine or human donors is as follows. Initial preparation of an enriched mononuclear cell suspension using standard Ficoll-Hypaque density centrifugation is necessary. The isolated cells are washed in Hanks' balanced salt solution without calcium and magnesium, and resuspended in elutriation medium to a volume of 10–20 ml. Centrifuge temperature and rotor speed are adjusted to 15 °C and 2,010 ± 10 rpm, respectively. Initial entry flow rate for cells is set to 10 ml/min. After completion of cell entry, the elutriation medium is allowed to continue through the system at the same initial flow rate for 10–15 min. The flow rate is then increased at a rate of 0.5 ml per 3-min interval until a flow rate of 12–13 ml/min is achieved. When the emerging cell population has an equal number of lymphocytes and monocytes, as determined by the Coulter Channelyzer, then that fraction becomes the next-to-last fraction. The final fraction is collected by stopping the rotor while maintaining a constant flow rate. This last fraction contains the purified monocytes. In comparison, after the first 50 ml of eluate is obtained from the initiation of the elutriation process, primarily purified lymphocytes are obtained. The volume of medium collected in each run depends on the number of cells to be processed.

Advances in CCE

While CCE has the recognized advantage over other cell-isolating techniques such as unit gravity sedimentation, cell sorter, and gradients for isolating relatively large numbers of cells (1×10^9), these cell numbers are still inadequate for conducting in vivo studies in large-animal models

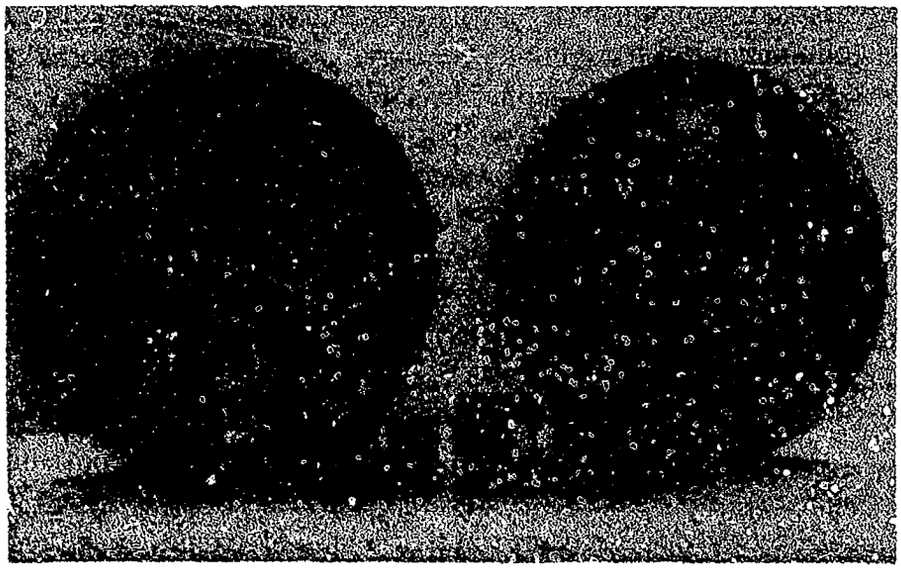

Fig. 12. Comparison of Beckman rotor and standard 4.3-ml chamber on left, and AFRRI rotor and 13.3-ml chamber on right.

such as the dog or monkey. The authors decided to attempt an enlargement of the Beckman chamber for cell isolation with several interests in mind: (a) increasing the absolute number of cells that can be isolated; (b) retaining the same level of purification and percent cell recovery from the initial sample as was possible with the standard Beckman chamber, and (c) decreasing the time required for cell isolation by increasing the flow rate used for cell recovery.

Our initial attempt was a threefold increase in the granulocyte recovery from canine [10] or human [20] leukapheresis concentrates, using a 13.3-ml chamber. The Armed Forces Radiobiology Research Institute (AFRRI) rotor and enlarged 13.3-ml chamber are compared in figure 12 to the standard Beckman rotor and 4.3-ml chamber. The AFRRI rotor has the same physical dimensions as the Beckman rotor, can be used in conjunction with the Beckman elutriation spindle, and fits into the standard Beckman J21B and J21C centrifuges. The AFRRI rotor system is therefore completely interchangeable with the standard Beckman system. Although the Beckman chamber can isolate 0.9×10^9 and 1.2×10^9 human and canine granulocytes, respectively, the AFRRI 13.3-ml chamber can isolate 3.0×10^9 and 4.4×10^9 human and canine granulocytes, respectively. The degree of granulocyte purity (97%) is the same

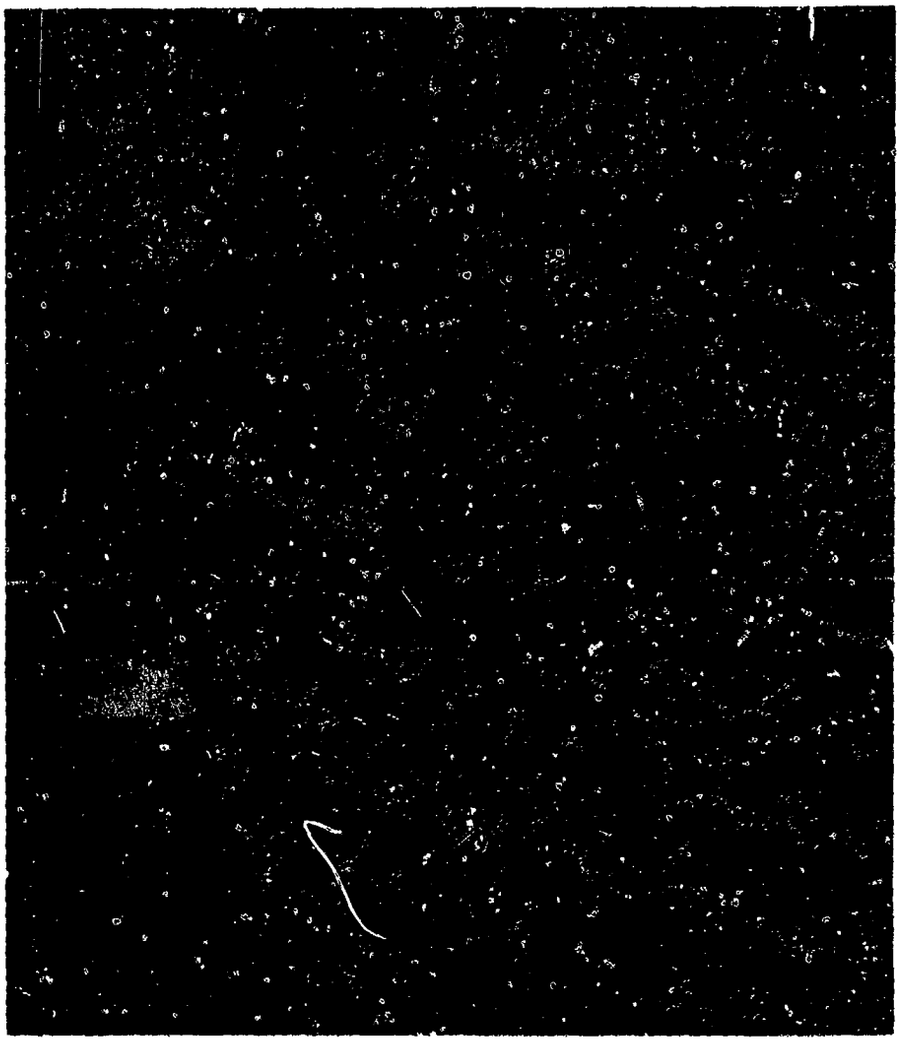

a

b

Fig. 13. Comparison of Beckman 4.3-ml chamber *(a)* and AFRRI 13.3-ml and 28.3-ml chambers *(b)*.

for both the Beckman and AFRRI chamber. However, the AFRRI chamber permits the same absolute number of cells to be purified in one third the amount of time of the Beckman chamber [9,10]. Using the AFRRI rotor, 4.0×10^9 canine granulocytes can be isolated in approximately 3 h, in comparison to 4.5 h of multiple runs on the Beckman rotor and chamber.

A second, larger chamber of 28.8 ml capacity (fig. 13) was fabricated. This second chamber permitted the isolation of 5×10^9 and 6.5×10^9 human and canine granulocytes, respectively. The degrees of

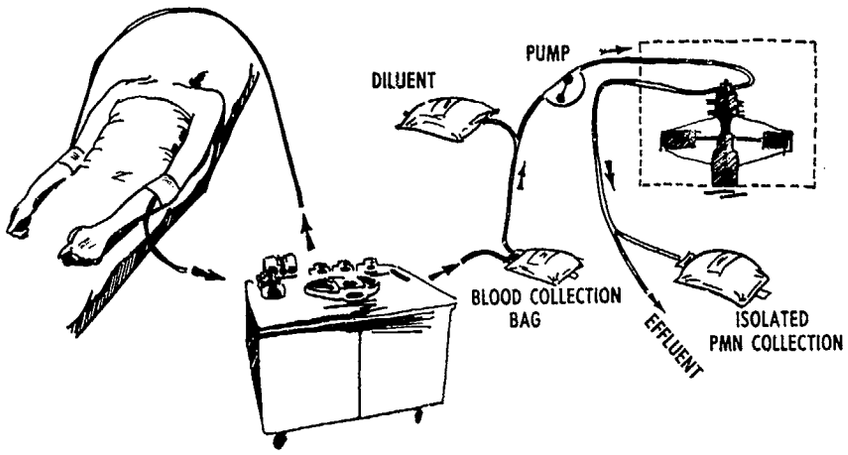

Fig. 14. Possible system for simultaneous collection of purified human granulocytes from a leukapheresis concentration during cell pheresis. Flow-rated tubing delivered blood concentrate from collection pheresis bag and medium to dilute blood before entry into enlarged CCE rotor system.

granulocyte purity (97%) and percent recovery (84%) were similar to those expected with the Beckman chamber. However, in terms of absolute numbers of cells recovered, the 28.8-ml AFRRI chamber permitted a 50% reduction in isolation time compared to the Beckman chamber. The AFRRI chamber permitted the recovery of $5–6 \times 10^9$ granulocytes from leukapheresis concentrates in 2–3 h compared to 6 h of multiple runs on the Beckman rotor and chamber. Both in vitro analyses [7] and in vivo analyses [10] of canine granulocytes isolated by a combined leukapheresis and CCE procedure indicated no loss of physiological activity.

The advantage of purified granulocytes in research can be centered around biochemical, physiological and clinical studies. The ability to isolate sufficient quantities of granulocytes for both in vitro and in vivo analyses is no longer limited by a time consideration. Sufficient quantities of human or canine granulocytes can be recovered from leukapheresis concentrates for cryopreservation analyses or even clinical studies using radiolabeled granulocytes. The efficiency of granulocyte collection in human blood banking might also be augmented by a dual tandem pheresis-CCE granulocyte collection, if suitable methods of granulocyte storage or cryopreservation were developed.

Although we do not espouse the existing Beckman system as appropriate for the collection of human granulocytes for transfusion purposes with sterility considerations, we do believe that the principles of CCE

should be considered in the next generation of leukapheresis instrumentation. If such instrumentation were not feasible, then the possibility of adapting CCE instrumentation in tandem with existing leukapheresis equipment may be another viable alternative for the collection of human granulocytes for transfusion purposes. As indicated in figure 14, while a leukapheresis was being conducted on current state-of-the-art instrumentation, flow rated tubing from the leukapheresis collection bag through a peristaltic pump could dilute the leukapheresis concentrate with medium and deliver it directly to CCE equipment for immediate granulocyte isolation. In this manner, a tandem isolation would permit both leukapheresis and CCE to be conducted simultaneously and efficiently for cell isolation. Therefore, the applicability of CCE for the isolation of large quantities of various cell types (bone marrow, granulocytes, monocytes, etc.) for both basic research and clinical studies is limited only by the current restraints of chamber size and not by the basic principle of CCE. The basic field of investigation by *Lindahl* [12] in 1948 is just beginning to be recognized in the clinical field.

References

1 Contreras, T.J.; Jemionek, J.F.; French, J.E.; Shields, L.J.: Human granulocyte isolation by continuous flow centrifugation leukapheresis and counterflow centrifugation elutriation. Transfusion *19:* 695–703 (1979).

2 Contreras, T.J.; Jemionek, J.F.; Stevenson, H.C.; Hartwig, V.M.; Fauci, A.S.: An improved technique for the negative selection of large numbers of human lymphocytes and monocytes by counterflow centrifugation-elutriation. Cell. Immunol. *54:* 215–229 (1980).

3 Fogelman, A.M.; Seager, J.; Edwards, P.A.; Hokom, M.; Popjak, G.: Cholesterol biosynthesis in human lymphocytes, monocytes and granulocytes. Biochem. biophys. Res. Commun. *76:* 167–173 (1977).

4 Grabske, R.J.: Separating cell populations by elutriation. Fractions *1:* 1–8 (1978).

5 Griffith, O.M.: Separation of T and B cells from human peripheral blood by centrifugal elutriation. Analyt. Biochem. *87:* 97–107 (1978).

6 Inoue, T.; Carsten, A.L.; Cronkite, E.P.; Kelly, J.E.: Separation and concentration of murine hematopoietic stem cells (CFU_s) using a combination of density gradient sedimentation and counterflow centrifugation elutriation. Exp. Hematol., Copenh. *9:* 563–572 (1981).

7 Jemionek, J.F.; Contreras, T.J.; French, J.E.; Hartwig, V.M.: Improved technique for increased granulocyte recovery from canine whole blood samples by counterflow centrifugation-elutriation. I. In vitro analysis. Exp. Hematol., Copenh. *6:* 558–567 (1978).

8 Jemionek, J.F.; Contreras, T.J.; French, J.F.; Shields, L.J.: Granulocyte isolation by counterflow centrifugation elutriation of canine blood obtained by countinuous-flow centrifugation leukapheresis. Exp. Hematol., Copenh. *6:* 801–808 (1978).
9 Jemionek, J.F.; Stevens, D.N.; Bernhards, F.W.; Walden, D.A.: The use of counterflow centrifugation-elutriation for the isolation of human granulocytes from leukapheresis concentrates. Transfusion *20:* 637 (1980).
10 Jemionek, J.F.; Contreras, T.J.; Baker, W.H.; Stevens, D.N.; Bernhards, F.W.; Walden, D.A.: Neutrophil migration in leukopenic dogs: in vivo comparison of granulocyte function after transfusion of leukapheresis concentrates or purified granulocytes isolated by counterflow centrifugation-elutriation. Transfusion *21:* 268–276 (1981).
11 Jemionek, J.F.; MacVittie, T.J.; Byrne, P.J.; Schein, P.S.; Walden, D.A.: Fractionation of mammalian bone marrow by counterflow centrifugation elutriation using a continuous albumin gradient: analysis of granulocyte-macrophage colony forming units. Br. J. Haemat. (in press, 1982).
12 Lindahl, P.E.: Principle of counter-streaming centrifuge for the separation of particles of different sizes. Nature, Lond. *161:* 648–649 (1948).
13 Lindahl, P.E.; Lindahl, K.M.: On the concentration of eosinophile leukocytes. Experientia *11:* 310 (1955).
14 Lindahl, P.E.: On counter streaming centrifugation in the separation of cells and cell fragments. Biochim. biophys. Acta *21:* 411–415 (1956).
15 Lionetti, F.J.; Hunt, S.M.; Lin, P.S.; Kurtz, S.R.; Valeri, C.R.: Preservation of human granulocytes. II. Characteristics of granulocytes obtained by counterflow centrifugation. Transfusion *17:* 465–472 (1977).
16 Lionetti, F.J.; Hunt, S.M.; Mattaliano, R.J.; Valeri, C.R.: In vitro studies of cryopreserved baboon granulocytes. Transfusion *18:* 685–692 (1978).
17 Lionetti, F.J.; Hunt, S.M.; Schepis, J.P.; Roy, A.J.; Liss, R.H.; Valeri, C.R.: In vivo distribution of cryogenically preserved guinea pig granulocytes. Cryobiology *17:* 1–11 (1980).
18 McEwen, R.R.; Stallard, R.W.; Juhos, E.T.: Separation of biological particles by centrifugation elutriation. Analyt. Biochem. *23:* 369–377 (1968).
19 Meistrich, M.L.; Hunter, N.M.: Temperature regulation during centrifugal elutriation and its effect on cell separation. Cell Biophys. *3:* 127–140 (1981).
20 Meyskens, F.L.; Kiefer, C.A.; Holmes, D.K.; Gerner, E.W.: Separation of normal human bone marrow cells by counterflow centrifugation elutriation. I. Morphological analysis and subfractionation of neutrophilic granulocytes. Exp. Hematol. Copenh. *7,* 401–410 (1979).
21 Nakeff, A.; Valeriote, F.; Gray, J.W.; Grabske, R.J.: Application of flow cytometry and cell sorting to megakaryocytopoiesis. Blood *53:* 732–745 (1979).
22 Nakeff, A.: Flow cytometric analysis of megakaryocytopoiesis: strategy for defining mitotic and endoreduplicative events in the committed progenitor compartment. Blood Cells *6:* 665–678 (1980).
23 Nakeff, A.; Worthington, R.E.: Thromboxane synthesis in megakaryocytes isolated by centrifugal elutriation. Blood *58:* 175–178 (1981).
24 Nijhof, W.; Wierenga, P.K.; Goldwasser, E.: A regenerating stem cell system and its use for isolating stem cells by centrifugal elutriation and percoll gradient centrifugation. I. The isolation of CFU-E. Exp. Hemat. Today (in press, 1981).

25 Persidsky, M.D.; Olson, L.S.: Granulocyte separation by modified centrifugal elutriation system. Proc. Soc. exp. Biol. Med. *157:* 599–604 (1978).
26 Pretlow, T.G.; Pretlow, T.P.: Centrifugal elutriation (counter-streaming centrifugation) of cells. Cell Biophys. *1:* 195–210 (1979).
27 Sanderson, R.J.; Bird, E.E.; Palmer, N.F.; Brenman, J.: Design principles for a counterflow centrifugation cell separation chamber. Analyt. Biochem. *71:* 615–622 (1976).
28 Sanderson, P.J.; Shepperdson, F.T.; Vatter, A.E.; Talmage, D.W.: Isolation and enumeration of peripheral blood monocytes. J. Immun. *118:* 1409–1414 (1977).
29 van Es, W.L.; Bont, W.S.: An improved method for the fractionation of human blood cells by centrifugal elutriation. Analyt. Biochem. *103:* 295–301 (1980).
30 Weiner, R.S.; Shah, V.O.: Purification of human monocytes: isolation and collection of large numbers of peripheral blood monocytes. J. immunol. Methods *36:* 89–97 (1980).

J.F. Jemionek, PhD, Experimental Hematology Department,
Armed Forces Radiobiology Research Institute, Bethesda, MD 20814 (USA)

JOURNAL OF SURGICAL RESEARCH 38, 55–65 (1985)

Hematopoietic Colony-Forming Cells from Mice after Wound Trauma[1,2]

G. D. LEDNEY, D. A. STEWART, D. F. GRUBER, H. M. GELSTON, JR., E. D. EXUM, AND P. A. SHEEHY

Immunology Division, Experimental Hematology Department, Armed Forces Radiobiology Research Institute, Bethesda, Maryland 20814

Submitted for publication March 11, 1983

The changes produced in the pluripotential and progenitor cell compartments of the hind leg bone marrow and spleen of skin-wounded mice were examined over a 2-week post-trauma period. Pluripotent cells (colony-forming unit–spleen, CFU–s) were significantly increased in the spleen and slightly reduced in the leg marrow the first week after trauma. Granulocyte macrophage colony-forming cells (GM–CFC) were significantly increased in the spleen throughout the 2-week period and were increased in the leg marrow during the first post-trauma week. Macrophage colony-forming cells (M–CFC) were significantly decreased in the spleen during the 2-week period and were slightly elevated in the leg marrow during that time. The peripheral blood contained significantly increased concentrations of CFU–s and GM–CFC but not M–CFC. Serum of wounded mice supported growth of GM–CFC but not M–CFC. The growth-promoting factor was extractable by $CHCl_3$ treatment. Serum C-reactive protein concentrations were significantly increased for a 5-day period after wound trauma.

INTRODUCTION

Surgical trauma and wounding result in he loss of mature cells from the blood at the ite of injury and in their utilization in the wound-healing process. For example, mac-ophages and granulocytes migrate to the traumatized area and assist in wound debridement and neutralization of bacteria [7, 16]. Erythrocytes are lost through the injured tissue, and platelets act to maintain homeostasis by their adhesion and aggregation capacity [12].

In addition to the effects of surgical trauma upon mature cells, it was recently reported that the circulating granulocyte progenitor cell compartment was significantly altered after abdominal hysterectomy [14]. In mice, wound trauma provoked changes in both the myeloid progenitor cell compartments and the proliferative potential of mature lymphocytes obtained from hematopoietic organs 24 hr after injury [5, 6]. In this study, we examined the changes in the pluripotential and progenitor cell compartments in the hematopoietic organs of mice during the 2-week healing period after a standard wound trauma. Additionally, data are presented on some serum-borne factors that may be implicated in the pathophysiologic changes found in the hematopoietic tissues of mice after wound trauma.

MATERIALS AND METHODS

Animals. Female (C57BL/6 × CBA)F1 Cum BR mice were obtained from Cumberland View Farms, Clinton, Tennessee. All mice were acclimated to laboratory conditions in the following way. First, for a period of 1 week, the animals were housed in groups of 20 mice each in a quarantined facility until a random sample was found to be free of histologic lesions of common murine diseases and until sterile water bottle cultures of all animals were found to be free of *Pseudomonas* spp. Second, the animals were housed

[1] Supported by the Armed Forces Radiobiology Research Institute, Defense Nuclear Agency, under Work Unit 8322-00018. Views presented in this paper are those of the authors. No endorsement by the Defense Nuclear Agency has been given or should be inferred.

[2] Research was conducted according to the principles enunciated in the "Guide for the Care and Use of Laboratory Animals," prepared by the Institute of Laboratory Animal Resources, National Research Council.

0022-4804/85 $1.50

in groups of five mice each for 2 weeks prior to experimentation. The mice were 10–20 weeks old when used. At all times, the mice were kept on a 6 AM (light) to 6 PM (dark) cycle in filter-covered cages. Wayne Lab-Blox diet was provided throughout the quarantine and experimental time periods. Chlorinated (10 ppm) water was provided after the quarantine period.

Wounded mice. Groups of mice were wounded under light Metafane (methoxyflurane, Pittman-Moore, Inc., Washington Crossing, N. J.) anesthesia between the hours of 10 AM and 2 PM. A 2.0- to 2.5-cm^2 circular wound was cut in the anterior-dorsal skin fold and underlying panniculus carnosus muscle (between the shoulder blades) with a steel punch. The punch was cleaned after the wounding of each animal by immersion in 70% ethanol. Such a wound constitutes about 4% of the total skin surface area and is not lethal to the mouse. The wounds were left open to the environment and were not treated in any way. However, subsequent to the wounding procedure, all mice were placed in sanitized cages that contained an autoclaved, commercially available, hardwood chip bedding (Ab-Sorb-Dri, Maywood, N. J.)

Control mice. Age-related mice housed in a similar manner as the wounded animals were used in all experimental replicates. Control mice were subjected to anesthetic and handling stress in the same manner as the wounded animals except for the wounding procedure.

Bacteriologic culture of wound sites. The wound sites of mice were monitored for bacteria 3, 7, 10, and 14 days after injury. A sterile swab was moistened with sterile saline and applied to the wound area. The swab was aseptically transferred to thioglycolate broth tubes and incubated for 18–24 hr at 37°C. Subcultures were made and bacterial identification to the genera level was made by standard microbiologic techniques.

Cell preparations. The spleen, both femurs, and both tibia–fibular processes were removed aseptically from cervically dislocated mice and placed in Roswell Park Memorial Institute (RPMI)-1640 medium (Flow Labs, Rockville, MD) on ice (±4°C). Bone-marrow cells were expulsed with a syringe and a 25-gauge needle. The spleens were minced with scissors in a glass vessel. All cell preparations were passed through six to eight layers of nylon mesh and then washed three times in RPMI-1640 at 250*g* for 10 min and resuspended in RPMI-1640. Viability estimates and nucleated cell counts were performed in a hemocytometer with 0.2% trypan blue dye and Turk's solution. The total nucleated cellularity (TNC) was determined for each tissue. Cell dilutions for the assays were done with RPMI-1640.

Colony-forming unit–spleen (CFU–s) assay. The CFU–s assay [19] was used to determine the pluripotent cell concentration and quantity in the spleen and in the paired long bones of the hind legs. Experimental groups consisted of six to eight B6CBF1 mice. Within 4 hr of irradiation, each mouse was injected iv with either 25×10^4 spleen cells or 25×10^3 marrow cells. The spleens were removed 8 days later and fixed in Bouin's solution for 2–4 hr. The surface colonies were counted independently by three persons, and the average number of CFU–s per spleen was determined from the three counts. The number of CFU–s per 10^6 nucleated spleen and marrow cells was determined by multiplying the average number of nodules per spleen by the appropriate factor and then preparing a grand mean from the adjusted values for each group. The total tissue quantity of CFU–s was determined by taking into account the number of CFU–s per 10^6 nucleated cells and the total number of nucleated cells. Endogenous CFU formation was obviated by 1000 rad ^{60}Co radiation given at 40 rad/min.

Seeding efficiencies. The seeding efficiency [16] percentages were determined for femoral marrow and spleen cells of mice 3 days after wounding in accordance with the procedures suggested by Lord [8]. Endogenous CFU formation was obviated in all assay mice by 1000 rad ^{60}Co radiation. The concentration and quantity of CFU–s in the injured and

control-treated animals (primary donor) was estimated by injecting groups of irradiated mice with either 2×10^5 spleen cells or 2.5×10^4 femoral bone-marrow cells. The seeding factor was determined by injecting additional groups of irradiated mice (secondary donor) with either 5×10^6 spleen or 2.5×10^6 femoral marrow cells. Twenty-four hours later these "secondary donor" mice were killed, their spleens removed, and cell suspensions prepared. Other groups of irradiated mice were engrafted with 10^6 spleen cells derived from the "secondary donor." Eight days after engraftment with cells, all assay mice were killed, the colonies formed on the spleen were counted, and the number of CFU-s received per mouse was determined. The percentage seeding efficiency was calculated by dividing the number of CFU-s recovered from each "secondary donor" by the number injected. The number of CFU-s injected into each "secondary donor" was determined from the groups of irradiated mice engrafted with cells from the "primary donors."

Colony-forming cell in vitro assays. Soft agar *in vitro* assays [11] were used to determine the committed progenitor cell concentrations and quantities of granulocyte macrophage colony-forming cells (GM-CFC) and monocyte macrophage colony-forming cells (M-CFC). In culture, GM-CFC have a growth lag period of 2-3 days and reach maximal levels at 10 days of *in vitro* growth. GM-CFC are found in cells derived from adult mouse marrow, spleen, and peripheral blood. M-CFC have a growth lag period of 10-15 days and reach maximal numbers at 25 days of culture growth. M-CFC are detectable in cells obtained from all lymphomyelopoietic tissues.

GM-CFC and M-CFC were grown in a double-layer agar culture with an optimum concentration of 5% (v/v) pregnant mouse uterine extract (PMUE), used as a growth stimulator to culture medium plus agar. A single preparation of PMUE was used throughout this investigation. Triplicate cultures of 1×10^6 spleen and 25×10^4 bone-marrow cells were performed for each cell preparation. Colonies containing more than 50 cells were counted at 10 days (GM-CFC) and 25 days (M-CFC) after culturing. The number of each colony type per 10^6 and the total tissue quantity were determined in the manner described in the section on CFU-s.

Mobilization of clonogenic cells into peripheral blood. The CFU-s and CFC assays were used to determine if cells with clonogenic potential had migrated from the central lymphomyelopoietic tissues to the peripheral blood after wound trauma. Peripheral blood was obtained by exsanguination from the axillary vessels while the mice were under metaphane anesthesia. The blood was collected in preservative-free heparin and mixed with an equal amount of RPMI-1640. The red blood cells were sedimented by layering over Ficoll-Paque and centrifuging at 800*g* at room temperature for 30 min. The nucleated cell layers between the plasma and the erythrocytes were collected and washed three times for 10 min at 250*g* in RPMI-1640. These cells were counted and diluted and the concentration was adjusted as follows. In CFU-s assays, groups of irradiated mice received 1, 2, and 5×10^5 cells each. In soft-agar assays, 2 and 4×10^5 cells were cultured from control mice, and 0.5, 1, and 2×10^5 cells from wounded mice were cultured. The assays were done as presented previously and the data expressed as clonogenic cells per 10^6 nucleated blood cells.

Colony-stimulating factor (CSF). Groups of mice were exsanguinated via the axillary vessels 2 or 3 days after either wounding or control treatment. The blood was permitted to clot at 4°C for 24 hr, centrifuged at 2000*g* for 20 min, and the serum removed. The serum samples were frozen at −20°C until used. When tested for CSA activity, one half of the serum was used in its native state subsequent to centrifugation of 2000*g* and passage through a 0.45-u filter. The other half of the serum was treated with four volumes of analytical grade chloroform in glass tubes for 1 hr to remove colony-inhibiting factors (CIF) as described by Granstrom [3]. The extracted serum was removed by

Pasteur pipette, centrifuged at 2000*g*, and passed through a 0.45-u filter. All the sera were tested for CSA without further freezing. Analyses for CSA used the *in vitro* colony-forming assays previously described in this section.

C-Reactive protein (C-RP). Mouse sera were reacted with anti-human C-RP (Dako-Accurate Corp., Westbury, N. Y.). The turbidity of the mixture was measured with a laser nephelometer (Calbiochem-Behring Corp., La Jolla, Calif.) after a 1-hr incubation period. Each serum C-RP concentration was determined by using a standard curve developed by reacting several dilutions of a known human C-RP standard (Cal Biochem-Behring Corp., La Jolla, Calif.) with the anti-human C-RP. This procedure is a modification of a technique which will be detailed in a forthcoming paper.[3]

Experimental design and statistical testing. Four replicate experiments were done over a 4-month period with the tissues of wounded and nonwounded mice for the clonogenic cell data presented in Figs. 1–3. Each replicate consisted of the pooled tissues from each of three mice. The animals selected for each month's study were housed as indicated under *Animals;* the unused cagemates were not reentered into other experimental replicates.

In the clonogenic cell assays (Figs. 1–3), spleen and bone-marrow cells were obtained for analyses on Days 3, 7, 10, and 14 after wound trauma. These intervals were chosen for convenience and for times when wound closure was completed (Day 10) and nearly all evidence of tissue damage had disappeared (Day 14).

Additional special studies were done as indicated in Tables 1–3 and Fig. 4. The protocols for each of these experiments are presented in each instance. Data expressed as a response per 10^6 nucleated cells were used to identify selective alterations in subpopulations of cells from tissues. Data that take into account the total organ or tissue cellularity were used to determine if the responses were a manifestation of a general change in cellularity. Differences between the responses of cells from wounded and control-treated mice were established by Student's *t* test.

[3] H. M. Gelston, Jr., W. H. Baker, and G. D. Ledney, entitled "Canine C-Reactive Protein Determinations by End-Point Laser Nephelometry."

RESULTS

Wound Healing and Wound Surface Bacteriology

The wound increased 10–20% in size 1–2 days after trauma. Granulation tissue formation was noted at this time. Wound contraction occurred thereafter with wound closure completed about 10–12 days after injury. Hair growth encompassed the area about 14 days after wounding. The skin wounds from four experimental series of mice, each totaling 60 animals, were cultured for bacteria. A total of 286 positive bacterial cultures were obtained from 240 mice. Single bacterial isolates were obtained from 80% of the wound surfaces while 20% of the wound sites had two to three organisms. Six genera were identified, and their distribution percentages were similar in all experiments. These included α-Streptococcus (65%), Proteus (13%), Staphylococcus (8%), Lactobacillus (6%), Acinetobacter (5%), and Bacillus (3%). No detectable shift in bacteria genera were noted over the time period examined. In all mice, wound sepsis, identified either as the formation and drainage of pus or overt lymph node involvement (swelling) in the anterior body area, was never found.

Cellularity

The cellularities of the spleens and the long bones of the hind legs in mice were not significantly altered by the wound trauma and subsequent healing processes. In wounded mice, the splenic and long-bone-marrow cellularities ranged between 70 and 90×10^6 and 45 and 55×10^6, respectively. In anesthetized control mice, the splenic and long-bone-marrow cellularities ranged be-

tween 65 and 90 $\times$ 10^6 and 40 and 55 $\times$ 10^6, respectively.

Colony-Forming Unit-Spleen (CFU-s).

Depicted in Fig. 1 are the CFU-s concentrations in the nucleated cells from the spleens and the long bones of wounded and control mice. A near twofold, statistically significant ($P < 0.01$) increase in splenic CFU-s was noted on the third day after wounding. There was a slight elevation in splenic CFU-s above control-treated values (51 $\pm$ 2 per 10^6 TNC, $N = 8$) at 14 days after wound trauma.

The CFU-s concentration of the bone marrow was decreased over the first week after wound trauma, but this was not statistically significant. The control bone marrow CFU-s concentration per 10^6 TNC was 601 $\pm$ 20.

The 24-hr seeding efficiencies of splenic and bone-marrow CFU-s were determined for mice 3 days after wounding. The seeding factors and observed and calculated CFU-s quantities are presented in Table 1. In these experiments a three- to fourfold increase in splenic concentrations of CFU-s was observed. This supported our findings for Day 3 as presented in Fig. 1. While the seeding factor for spleen cells from wounded mice appeared elevated, this was not statistically significant from the control-treated animals (3.9 $\pm$ 0.5 versus 2.4 $\pm$ 0.8). The high variability in seeding factors for both wounded and control mice resulted in the corrected CFU-s concentration determinations for wounded (2675 $\pm$ 402) and control (1832 $\pm$ 435) to be statistically indistinct.

The seeding factors for bone-marrow cells were determined with the same mice used to estimate the seeding factors for spleen cells. The bone-marrow cell-seeding percentages were 1.8 $\pm$ 0.5 for wounded mice and 2.4 $\pm$ 0.3 for control-treated mice. In this experimental series, the marrow cellularity of wounded mice was lower ($P < 0.05$) than that for control-treated mice. This was not in agreement with our findings on marrow cellularity mentioned previously under Results. The explanation for this may be (1) the different ages of the animals used in the test experiments and (2) the limitation of the harvesting technique regarding absolute cell quantifications. The observed CFU-s/10^6 TNC and the splenic seeding factors for marrow cells were variable and this resulted in differences in calculated values to be more apparent than real.

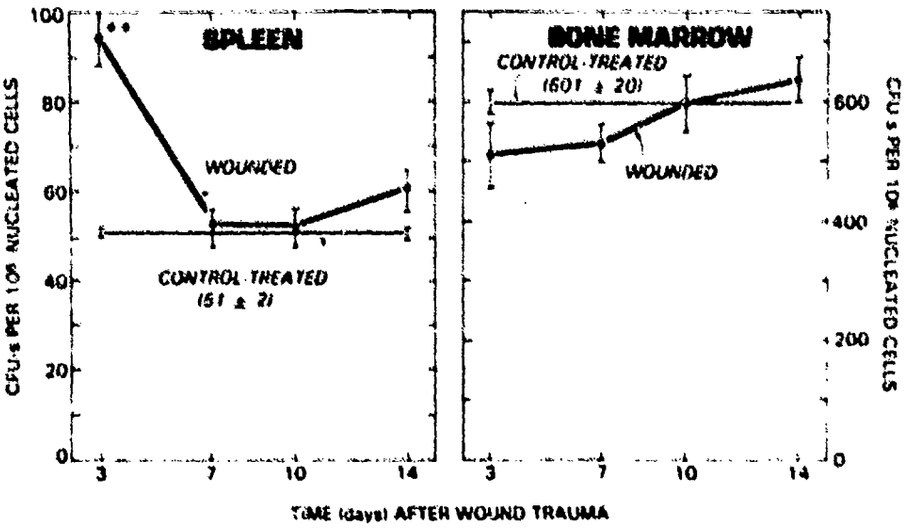

FIG. 1. Colony-forming units-spleen (CFU-s) concentrations per 10^6 nucleated hind leg bone-marrow and spleen cells in mice after wound trauma. Each point is the mean $\pm$ 1 standard error. The relative (concentration) and absolute (total organ population) CFU-s changes mirrored each other. Thus, only the concentration values are depicted.

TABLE 1

SPLENIC SEEDING FACTORS (f) AND COLONY-FORMING UNITS–SPLEEN (CFU–S) OF SPLEEN AND FEMORAL BONE-MARROW CELLS FROM MICE 3 DAYS AFTER WOUND TRAUMA

	Spleen		Marrow	
	Wounded	Control	Wounded	Control
Total nucleated cellularity (TNC) $\times 10^{-3}$ [a]	136 ± 9[b]	131 ± 11	24 ± 1[c,*]	29 ± 1
Observed CFU-s/10^6 NC	93 ± 5[c,**]	26 ± 2	509 ± 33	420 ± 53
24-hr splenic seeding factor (f)[d]	3.9 ± 0.5	2.4 ± 0.8	1.8 ± 0.5	2.4 ± 0.3
Calculated CFU-s/10^6 NC ($\times 10^{-3}$)[d]	2.68 ± 0.4	1.83 ± 0.44	34 ± 7	21 ± 5
Observed CFU-s per tissue ($\times 10^{-3}$)	12.510 ± 0.62[c,**]	3.37 ± 0.44	12.38 ± 1.0	11.81 ± 1.4
Calculated CFU-s per tissue ($\times 10^{-3}$)[d,e]	360 ± 54	254 ± 70	803 ± 212	619 ± 175

[a] The cellularities listed here differ from those described under the Results section on cellularity. In the experiments reported here, the femurs of 20-week-old mice were used to compile the data. In the data reported under Results, marrow cells were obtained from both tibiae and femora of 10- to 12-week-old mice.

[b] Means ± 1 standard deviation from seven experiments. Tissues from three mice were used in each experiment.

[c] *Statistically significantly different ($P < 0.05$) from control value. **Statistically highly significantly different ($P < 0.01$) from control value.

[d] Determined by dividing the observed number of CFU-s by the seeding factor (f).

[e] All values indicated rounded to next highest number.

In Vitro Colony-Forming Cells

A. Granulocyte macrophage colony-forming cells (GM-CFC). Presented in Fig. 2 are the GM-CFC concentrations in splenic cells and marrow cells from the long bones of wounded and control-treated mice. A statistically significant ($P < 0.01$) fivefold increase

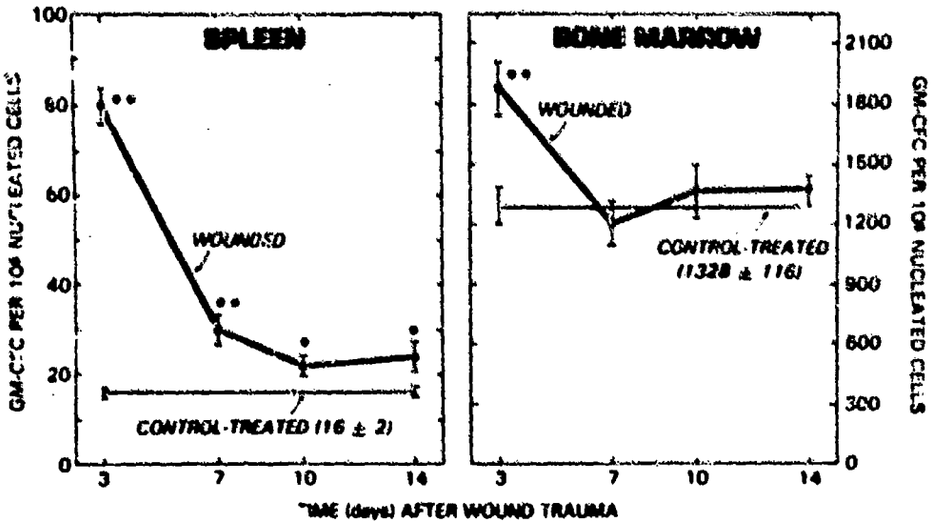

FIG. 2. Granulocyte macrophage colony-forming cell (GM-CFC) concentrations per 10^6 nucleated hind leg bone-marrow and spleen cells in mice after wound trauma. Each point is the mean ± 1 standard error. The relative (concentration) and absolute (total organ population) GM-CFC changes mirrored each other. Thus, only the concentration values are depicted.

was found for splenic GM–CFC from wounded mice versus control-treated mice the third day after wound trauma (80 ± 4 versus 16 ± 2). Thereafter, a 50–100% increase in splenic GM–CFC was observed in mice during the wound-healing period. On Day 3, the GM–CFC concentration in the marrow of the long bones of wounded mice was significantly increased ($P < 0.01$) over that of control-treated animals (1870 ± 139 versus 1328 ± 116). On Days 7, 10, and 14 all marrow GM–CFC values from wounded mice were within the control-treated range of 1328 ± 116/10^6 nucleated cells.

B. Macrophage colony-forming cells (M–CFC). The M–CFC concentrations in the spleen and bone marrow cells of wounded and control-treated mice are seen in Fig. 3. Statistically significant ($P < 0.01$) reductions of 30–70% in splenic M–CFC were observed for wounded mice at every time tested. The control-treated splenic M–CFC value was 152 ± 9/10^6 TNC. Contrary to the splenic M–CFC values, the marrow concentration of M–CFC tended to be increased during the entire 2-week wound-healing period. Specifically, 14 days after trauma, a 50% increase ($P < 0.01$) was found for marrow M–CFC from wounded mice compared to that detected for control-treated mice (3224 ± 403 versus 2136 ± 157).

C. Clonogenic cell mobilization into peripheral blood. Day 3 after wound trauma was a time point when either maximum or minimum clonogenic cell quantities were detected in the spleen and bone marrow. We used that time period to determine the concentration of clonogenic cells in the peripheral blood of wounded and control-treated mice. The concentrations per 10^6 nucleated blood cells of CFU-s, GM–CFC, and M–CFC are reported in Fig. 4. Wounding resulted in statistically significant ($P < 0.01$) increases for CFU-s (71 ± 4 versus 16 ± 4) and GM–CFC 48 ± 11 versus 6 ± 2 in the peripheral blood. However, the M–CFC content of the blood of wounded mice was similar to that of control-treated mice.

Colony-Stimulating Activity (CSA)

Unextracted sera from mice, taken 2–3 days after wounding, supported the growth of normal mouse bone-marrow-derived GM–CFC as is seen in three replicate experiments presented in Table 2. Different wounded mouse sera and normal mouse

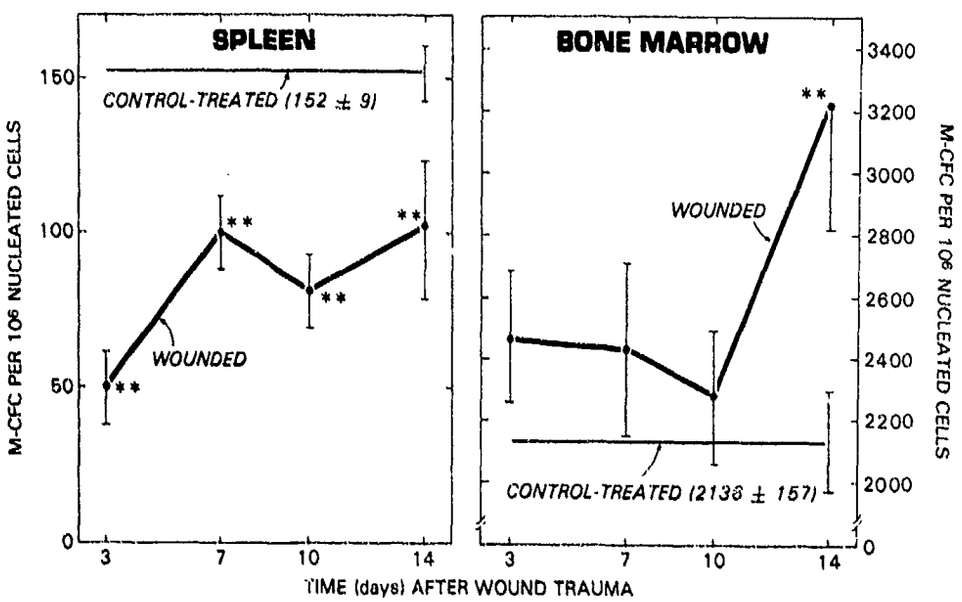

FIG. 3. Macrophage colony-forming cell (M–CFC) concentrations per 10^6 nucleated hind leg bone-marrow and spleen cells in mice after wound trauma. Each point is the mean ± 1 standard error. The relative (concentration) and absolute (total organ population) M–CFC changes mirrored each other. Thus, only the concentration values are depicted.

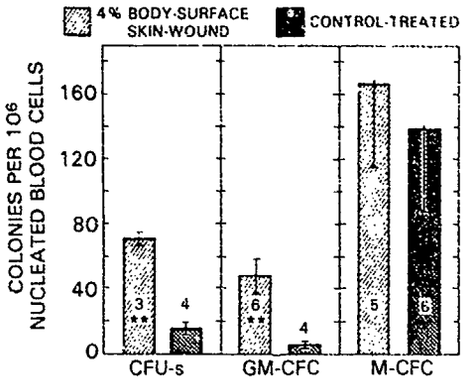

FIG. 4. Clonogenic cells in the peripheral blood of mice 3 days after wound trauma. CFU–s = colony-forming units spleen; GM–CFC = granulocyte macrophage colony-forming cell; M–CFC = macrophage colony-forming cell. Number within or near each bar is the number of replicate experiments. In each replicate, blood was pooled from three to five mice.** Statistically very significantly different ($P < 0.01$) from control values.

marrow were used for each replicate experiment. $CHCl_3$ extraction of the serum appeared either to reduce or remove the factor(s) responsible for supporting GM–CFC growth. M–CFC growth in either the whole or extracted serum was minimal. While the serum from wounded mice supported the growth of GM–CFC from normal marrow, this growth was not as good as that for cells grown in pregnant mouse uterus extract (PMUE). The growth of normal marrow cells in PMUE resulted in 1250 ± 200 GM–CFC and 2025 ± 200 M–CFC per 10^6 nucleated cells. Normal mouse sera did not support the growth of either GM–CFC or M–CFC.

C-Reactive Protein (C-RP)

The C-RP concentration (micrograms/milliliter) in the sera of wounded and control-treated anesthetized mice are shown in Table 3. The C-RP level depended on both the size of the wound and the time after wounding when sera were assayed. Generally, however, there was a significant increase ($P < 0.01$) (50–300%) in C-RP concentrations 2–4 days after wound trauma. On Day 7 after wounding, C-RP concentrations returned to normal values (4.0 ± 0.1 μg/ml) and remained there throughout the rest of the 2-week wound-healing period.

DISCUSSION

In this paper, we report for the first time that alterations occur in the myeloid clonogenic cell populations of the spleen and hind leg bone-marrow cells of mice during the post-trauma wound-healing period. These proliferative cell changes include both relative increases in concentration per 10^6 cells and absolute changes (data not presented) in the cell populations examined.

Three explanations may be used in interpreting our data. These include (1) the mobilization or migration of clonogenic cells from one hematopoietic compartment to another, (2) the differentiation of clonogenic cells to meet the mature cell demands of the wound site, and (3) the *in situ* proliferation of clonogenic cells.

Regarding mobilization, the CFU–s data may be interpreted as follows. The two- to fourfold increase in splenic CFU–s concentration (Fig. 1 and Table 1) seen in two

TABLE 2

MOUSE CLONAL CELLS GROWN WITH SERUM FROM WOUNDED MICE

	Unextracted serum[a]		$CHCL_3$ extracted serum	
Replicate[b]	GM–CFC	M–CFC	GM–CFC	M–CFC
1	38 ± 4	0	10 ± 1	3 ± 1
2	07 ± 1	0	0	0
3	20 ± 3	7 ± 2	ND[c]	ND

[a] Test sera were obtained from either 10–20 B6CF1 mice or C57BL/6 mice 2–3 days after wound trauma. Control sera were obtained from B6CBF1 mice 2–3 days after anesthesia. The PMUE used in the *in vitro* clonal growth studies shown in Figs. 2–4 was used as a CSF source with positive growth potential. All *in vitro* cultures used 25×10^3 femoral bone-marrow cells and 100 μl of serum or PMUE. No clonal cell growth was seen when normal B6CBF1 or C57B1/6 marrow cells were cultured with the control sera. With the PMUE, 1250 ± 200 GM–CFC and 2025 ± 200 M–CFC -10^6 nucleated normal marrow cells were cultured.

[b] In replicates 1 and 2 cells and serum products were from B6CBF1 mice. In replicate 3 the cells and serum were from C57B1/6 mice.

[c] ND = Not done.

TABLE 3

CONCENTRATIONS OF C-REACTIVE PROTEIN IN MOUSE SERA AFTER SKIN-WOUND TRAUMA[a]

Time (days) after wounding	Size of wound area[b] (Percentage of total skin surface)		Anesthetized untreated controls
	4	6	
1	4.6 ± 0.2	6.4 ± 0.8**	3.6 ± 0.1[c]
2	7.6 ± 1.0**	13.0 ± 3.1**	3.7 ± 0.2
3	8.0 ± 1.0**	12.0 ± 2.8**	4.2 ± 0
4	6.2 ± 0.7**	12.0 ± 2.7**	4.6 ± 0.1
5	4.9 ± 0.4*	4.8 ± 0.3*	3.9 ± 0.4
7	4.2 ± 0.4	5.0 ± 0.6	3.7 ± 0.3
10	3.8 ± 0.2	4.9 ± 0.2**	4.5 ± 0.3
14	3.6 ± 0.2	3.3 ± 0.1	4.6 ± 0.5

[a] C-Reactive protein (C-RP) concentrations (μg/ml) are based on standard curves obtained by reacting human C-RP with rabbit anti-human C-RP. Since polyethylene glycol, a polymer enhancer, was used in the assay to facilitate the cross reaction between mouse C-RP and anti-human C-RP, the values shown are probably elevated. However, the pattern demonstrated is indicative of the mouse C-RP response to wound trauma.

[b] *Statistically significantly different ($P < 0.05$) from control values. **Statistically very significantly different ($P < 0.01$) from control value. Indicated significance levels are a result of *t*-test comparisons with pooled controls. The *t*-test comparisons were made only if significance was indicated by a one-way ANOVA (for each day) with the α-level set at 1.25%. Values shown are means ± 1 standard error for five mice per group.

[c] Means ± standard error for four mice tested at each time point. Normal range is 3.4–4.7 μg/ml ($n = 32$), which encompasses ±1 standard deviation from the mean of all control values. Pooled mean values ±1 standard error for all controls = 4.0 ± 0.1 μg/ml.

independent sets of experiments may be the consequence of mobilization of these cells out of the marrow cell centers into the spleen. This idea is supported by the four- to fivefold increase in CFU-s concentration found in the peripheral blood 3 days after wound trauma (Fig. 4) and the small decrease in hind leg bone-marrow CFU-s concentration at the same time. Regarding the leg marrow decreases in CFU-s concentration, it is noted that the decrease was not statistically significantly reduced. It is not known if similar reductions in CFU-s concentrations occurred in other bone-marrow cell compartments such as the rib cage, skull, and humerous. Nonetheless, the actual 15% reduction from approximately 600 CFU-s/10^6 TNC for control-treated mice to 510 CFU-s/10^6 for mice 3 days after wounding could help explain the near 100% increase in splenic CFU-s from about 50 in control-treated to 95 in wounded mice.

Another explanation of our data is that the requirement for granulocytes [17] and macrophages [7] at the wound site increases the demand for differentiated progeny. In the leg bone marrow, the early reduction in CFU-s and early increase in GM-CFC followed by the late increases in M-CFC may be interpreted as a demand for differentiation at the levels of the pluripotent and progenitor cell compartments to provide mature cells. Indirect stimulation resulting from the differentiation of cell progeny may also explain our findings.

Regarding the differentiation demand after wound trauma, it is difficult to interpret clearly the splenic contribution to the observed clonogenic cell responses. While mobilization of clonogenic cells from the marrow to the spleen can account for some of our findings, it is important to note that the spleen is capable of significant proliferation, particularly after undergoing hematopoietic stress. Thus, a component of the increased concentrations of splenic CFU-s and GM-CFC could have derived from within that tissue itself. Support for this comes from studies of treatment of mice with lipid A which increased the proliferative activity of both splenic CFU-s and GM-CFC [10]. In addition, our data on GM-CFC growth *in vitro* in the presence of serum from wounded mice (Table 2) point to a GM-CSF which could promote growth of such cells within the spleen and the bone marrow. However, *in vitro* demonstration of a CSA does not imply that such a material is effective *in vivo*. The data from other laboratories are equivocal as to an *in vivo* effect for CSA which has a known capacity to stimulate clonal growth *in vitro* (see Ref. [1] for review).

The M-CFC response patterns (Fig. 3) of

splenic and marrow cells from wounded mice were distinctly different from each other. It is known that mature macrophages are required for repair of tissue damage at the wound site(s). Thus, one plausible explanation for our findings could be that the recruitment of macrophages at the wound site would result in the production of M-CFC progenitor cells in the bone marrow to meet the demand. The significant reduction in splenic M-CFC might be the result of the demand at the site of injury being greater than the pooling of such cells in the extramedullary site.

In addition to the mobilization and differentiation, the *in situ* proliferation of cells in mice after wound trauma may explain the increased concentrations of clonogenic elements depicted in Figs. 1–4. We previously reported that hydroxyurea (HU) treatment of mice, at a specific time after wound trauma and before irradiation, (1) ablated the endogenous colony-forming unit (E-CFU) response seen in subiethally irradiated mice and (2) obviated survival seen in mice wounded prior to a lethal radiation dose [5]. Since (1) proliferating cells are sensitive to HU and (2) survival from radiation is dependent upon pluripotential cell proliferation, it may be that wound trauma results in *in situ* clonogenic cell proliferation. It should be stated that the proliferating cells measured by the E-CFU assay [5] and the cells measured by the CFU-s assay in this report may or may not be estimates of a similar clonogenic cell population. Lastly, it is not known if GM-CFC and M-CFC generation occurred *in situ* after wound trauma.

Our findings of increased serum concentrations of C-RP in mice up to 5 days after wound trauma (Table 3) may be of significance in interpreting our M-CFC data. There is *in vitro* evidence that C-RP inhibits macrophage colony growth [9]. It is interesting to consider that the increased C-RP levels noted after wound trauma might inhibit the *in vivo* expression of M-CFC. However, it is difficult to conceive how increased levels of C-RP *in vivo* could simultaneously inhibit splenic M-CFC while marrow M-CFC tended to be increased.

The myeloid proliferation recorded in this paper may be the result of host responses to infection. While bacteria were isolated from the surfaces of the wounds, several lines of evidence mitigate against the direct involvement of bacteria in these responses. These are as follows: (a) Abscesses and pus formation at the injury site were never found. (b) Cell cultures for *in vitro* testing (as described under Methods) and for microbial monitoring never resulted in bacterial growth. (c) Histopathologic examination of the livers and spleens in two animal series never revealed microbial growth. (d) Plasma C-RP levels in three series of mice always returned to normal levels between 5 and 7 days after injury. After the primary C-RP response subsided, there were no secondary increases indicative of delayed infection. Along these lines, the C-RP response is severely increased after infection compared to that noted here after trauma [13]. (e) We reported that the appropriately timed wounding relative to lethal radiation exposure results in survival [5]. Survival from radiation is not possible if the animals are infected. Lastly, there is no difference in the rate of wound contraction between conventional and germ-free rats even though the intensity of the inflammatory reaction is greater in animals with a "normal" bacterial flora [2]. Along these lines, in the rat, skin wounds infected with various bacterial species prior to closure had a greater tensile strength than uninfected wounds [15]. While our observations seem to limit any direct effect of bacteria upon host clonogenic myeloid responses, indirect effects may be mediated by bacterial endotoxin. Bacterial endotoxin is a known stimulator of myeloid proliferative cells [11] and may cross disrupted intestinal cell-tight junction barriers into the circulation after trauma [20]. Also, endotoxin released by bacteria at the wound site into the circulation could contribute to myeloproliferation. Experiments to detect wound-related bacteria and their endotoxins and their effects on myeloproliferation in trauma situations remain to be done.

The pathophysiologic stimulus of wound trauma may result in the release of other

substance besides CSA and C-RP that can modulate hematopoiesis. Among the most physiologically important are adrenalcorticosteroids and prostaglandins.

Adrenalcorticosteroids have been implicated in host adaptation to the stress of wound trauma [18]. Corticosterone released after trauma may control CFU-s populations *in vivo* in mice since adrenalectomy prior to wounding resulted in two- to threefold increases in CFU-s over that for intact animals [18].

Prostaglandins of the E series (PGE) were recently implicated in the modulation of hematopoiesis [4] and they have been implicated in the cellular events occurring after wound trauma [21]. Along these lines M-CFC are more sensitive to PGE *in vitro* than are GM-CFC [22]. Thus, it may be that in our study reported here that the M-CFC responses were influenced by the endogenous release of PGE after wound trauma. Further testing along these lines is currently being done to support this point.

ACKNOWLEDGMENTS

The editorial skill of Ms. J. Van Deusen, the typing assistance of Ms. H. Speight and Ms. T. Hunt, and the graphic reproduction of Mr. M. Behme and Mr. J. Pitts are gratefully acknowledged. Statistical analyses were done by Mr. W. E. Jackson.

REFERENCES

1. Burgess, A. W., and Metcalf, D. The nature and action of granulocyte-macrophage colony stimulating factors. *Blood* **56**: 947, 1980.
2. Dorati, R. M., Frank, D. W., Stromberg, L. W. R., and McLaughlin, M. M. The effect of the germ-free state on wound healing. *J. Surg. Res.* **11**: 163, 1971.
3. Granstrom, M. Studies on inhibitors of bone marrow colony formation in normal human sera and during a viral infection. *Exp. Cell Res.* **82**: 426, 1973.
4. Kurland, J., and Moore, M. A. Modulation of hemopoiesis by prostaglandins. *Exp. Hematol.* **5**: 357, 1977.
5. Ledney, G. D., Gelson, H. M., Jr., Weinberg, S. R., and Exum, E. D. Survival and endogenous spleen colonies of irradiated mice after skin wounding and hydroxyurea treatment. *Experientia* **38**: 1228, 1982.
6. Ledney, G. D., Stewart, D. A., and Exum, E. D. Proliferative responses of lymphomyelopoietic cells of mice after wound trauma. *J. Trauma* **20**: 141, 1980.
7. Leibovich, S. J., and Ross, R. The role of the macrophage in wound repair. A study with hydrocortisone and antimacrophage serum. *Amer. J. Pathol.* **78**: 71, 1980.
8. Lord, B. I. The relationship between spleen colony production and spleen cellularity. *Cell Tissue Kinet.* **4**: 211, 1971.
9. Marcelletti, J. F., Johnson, C. S., Mortensen, R. F., and Furmanski, P. Effect of C-reactive protein on granulocyte-macrophage progenitor cells. *J. Lab. Clin. Med.* **100**: 70, 1982.
10. Mergenthaler, H. G., Staber, F. G., Hultner, L., and Doimer, P. The response of murine splenic granulocyte-macrophage colony-forming cells to lipid A in vivo. *Exp. Hematol.* **10**: 637, 1982.
11. Metcalf, D. *Hematopoietic Colonies: In Vitro Cloning of Normal and Leukemic Cells.* New York: Springer-Verlag, 1977. P. 277.
12. Moreno, H. Platelet function. *In* L. Menaker (Ed.) *Biologic Basis of Wound Healing.* Hagerstown, Md.: Harper & Row, 1975.
13. Morley, J. J., and Kushner, I. Serum C-reactive protein levels in disease. *Ann. N. Y. Acad. Sci.* **389**: 406, 1982.
14. Philip, M. A., Standen, G., and Fletcher, J. The effects of surgical trauma on human granulopoiesis. *Brit. J. Haematol.* **44**: 263, 1980.
15. Raju, D. R., Jindrak, K., Weiner, M., and Enquist, I. F. A study of the critical bacterial inoculum to cause a stimulus to wound healing. *Surg. Gynecol. Obstet.* **144**: 347, 1977.
16. Siminovitch, L., McCulloch, E. A., and Till, J. E. The distribution of colony-forming cells among spleen colonies. *J. Cell. Comp. Physiol.* **62**: 327, 1963.
17. Simpson, D. M., and Ross, R. The neutrophilic leukocyte in wound repair. A study with antineutrophil serum. *J. Clin. Invest.* **51**: 2009, 1972.
18. Stevenson, A. F. G. Haemopoietic recovery during radiation disease: Comments on combined-injuries. *Radiat. Environ. Biophys.* **20**: 29, 1981.
19. Till, J. E., and McCulloch, E. A. A direct measurement of the radiation sensitivity of normal mouse bone marrow cells. *Radiat. Res.* **14**: 213, 1961.
20. Walker, R. I., and Porvaznik, M. Association of bacteria and endotoxin with post-trauma events. In J. L. Ninneman (Ed.), *Traumatic Injury, Infection and Other Immunologic Sequelae.* Baltimore, Md.: U. Park Press, 1983. Pp. 1–15.
21. Wang, B. S., Heacock, E. H., and Mannick, J. A. Characterization of suppressor cells generated in mice after surgical trauma. *Clin. Immunol. Immunopathol.* **24**: 161, 1982.
22. Williams, N. Preferential inhibition of murine macrophage colony formation by prostaglandin E. *Blood* **53**: 1089, 1979.

Biblthca haemat., No. 48, pp. 112–130 (Karger, Basel 1984)

C. The Macrophage Colony-Forming Cell

T.J. MacVittie

Armed Forces Radiobiology Research Institute,
Experimental Hematology Department, Bethesda, Md., USA

Introduction

Virtually all cells of hematopoietic lineage may be cultured in vitro. The works of *Bradley and Metcalf* [4] and *Pluznik and Sachs* [42] have ushered in an era of insight into the physical and functional characteristics of morphologically unrecognizable hematopoietic progenitor cells. These include multipotent stem cells [18, 37], progenitors of varying degrees of maturity in the erythroid (e.g., the 8-day and 3-day burst-forming unit and colony-forming unit erythroid) [10, 14, 16, 35, 47] and granulocyte-macrophage lineage (the high proliferative potential colony-forming cell, HPP-CFC [2, 3], the granulocyte-macrophage, GM-CFC, and macrophage colony-forming cells, M-CFC [20, 25, 26, 28, 29]), in addition to the megakaryocyte [38], eosinophil [39], and B and T lymphocyte colony-forming cells [40, 45].

This section will deal with the culture technique, growth characteristics, and properties of the M-CFC, a CFC distinct in many ways from the more primitive GM-CFC and HPP-CFC [2, 3]. There is abundant literature on the growth characteristics and physical properties of the GM-CFC [review, 36] but much less information on the new and interesting HPP-CFC [2, 3].

The M-CFC was initially demonstrated by *Lin and Stewart* [26] in the thioglycollate-stimulated peritoneal exudate of mice [22, 23]. These initial observations were performed in agar cultures while subsequent experiments in liquid culture demonstrated a greater cloning efficiency and decreased lag time before initiation of growth. The ability to clone macrophages in liquid culture has allowed these investigators and others

[6, 8, 9, 20–25, 44, 48] the opportunity to gain a great deal of information on the identity and functional ability of the mononuclear and macrophage progeny of the M-CFC derived from the bone marrow and extramedullary sources. The point to be made here is that this technique allows the investigation of macrophage populations cloned from M-CFCs derived from a variety of sources, including peritoneal and pleural exudate [9, 22, 23, 25], alveolar space [24], thymus and lymph nodes [28, 30], and liver [8] as well as the bone marrow, spleen [9], and peripheral blood [20, 29]. Undoubtedly, there is a significant advantage when one is dealing with the question of macrophage heterogeneity and the possible effect of tissue-specific microenvironment on phenotypic expression of macrophage populations. However, if the requirement is only for a source of marrow-derived macrophages, the most convenient is the liquid culture technique for GM-CFC used with a macrophage colony-stimulating factor such as L-cell-conditioned medium [1] or pregnant mouse uterine extract (PMUE) [5]. The source of the macrophages in this technique are the GM-CFC and M-CFC induced to amplify and differentiate through the action of a macrophage colony-stimulating factor [46]. These may be separated from the progeny of the M-CFC through the use of two differential properties exhibited by the GM- and M-CFC. These will be discussed later. The basic ingredients of the culture technique are the same when assaying for or deriving macrophages from the GM- and M-CFCs. The following is an outline of this technique.

Culture Technique

There exists a great variation in media used today for culture of granulocyte and macrophage colonies, although the variation exists mainly in concentration of basic ingredients rather than in the number of basic ingredients. The list of basics includes:

(a) A tissue culture medium such as RPMI, McCoys 5a, CMRL 1066, alpha MEM, or Eagle's MEM. A 10× formula is required for preparation of 2× medium for agar cultures.

(b) Fetal calf serum. This is an essential ingredient in our hands, and adequate cloning efficiency and growth depend on a good batch of serum. Most companies will let you assay samples of serveral lots or batches before placing an order. This is routine in our laboratory.

(c) Horse serum. It is also recommended that several 'lots' of horse serum be tested to assure maximal culture conditions. Undoubtedly the serum represents an 'alphabet soup' of growth regulators, and serves as one of two sources of variability in the culture medium. The other is the source of colony-stimulating activity (CSA) necessary for growth and differentiation. Recent attempts have been made to replace the need for the fetal calf serum and/or horse serum requirement for colony formation [11, 15, 19]. *Kubota* et al. [19] have shown that they can replace the fetal calf serum in a culture medium required for efficient colony formation of GM-CFC through the addition of bovine serum albumin, transferrin, and cholesterol, *L*-α-phosphatidylcholine. Colony-forming efficiency was 80% of that noted for control cultures containing 20% fetal calf serum.

(d) A suitably prepared factor with macrophage-directed CSA L-cell-conditioned medium [1, 46] or PMUE [5].

Preparation of the medium with 2× osmolarity may proceed as follows:

Ingredient	Amount	Ingredient	Amount
CMRL 1066 (10×)	150 ml	*L*-asparagine	0.06 g
Fetal calf serum	200 ml	Antibiotic-antimycotic (100×)	10 ml
Horse serum	100 ml	Tryptic soy broth	6.0 g
Pyruvate (100×)	20 ml	Sodium bicarbonate	4.4 g
L-serine	0.042 g	q.s. to 1,000 ml with 3× distilled water	

Hints

(1) Careful check of the incubator for proper humidity and CO_2 level. Incubators with 'quick purge' systems are a great help in maintaining CO_2 levels (5–7%) in a frequently used incubator. Use a water-jacketed incubator if the laboratory experiences large changes in temperature.

(2) We routinely place our 35-mm Petri dishes inside 150-mm Petri dishes with covers. Seven 35-mm dishes will fit nicely, with one open dish in the center containing distilled H_2O. This aids in preventing drying as well as organizing and handling of dishes.

(3) Use of the double-layer agar technique in the quantitative assay, although using twice the medium, provides twice the nutrients, and may aid growth by keeping poorly diffusible inhibitors in the bottom layer [7].

(4) Measure the osmolarity of the prepared medium. *Metcalf*[36] has provided an excellent summary of the semi-solid culture technique and its specific requirements. He includes sections on general preparation of cultures, special requirements, information on sources of CSA, incubation procedures, problem areas, and examination of colonies. It is certainly a must for anyone entering the field.

The culture technique used is dependent on the questions being asked. The agar technique provides a quantitative assay for the number of cells defined as M-CFC within a tissue responding to a particular treatment. The technique is reproducible, with the advantage of a semi-solid medium preventing migration and overgrowth of colonies. The colonies can be removed for cytological and functional determinations of the macrophages, but the presence of the agar that coats the cells does make it somewhat difficult. The colonies may be aspirated from the medium with a Pasteur pipette. They can be dispersed in tissue culture medium or fixed for sectioning, and then examined by light and electron microscopy techniques. The dispersed suspension of M-CFC progeny can be either deposited on slides using a cytospin or replated onto Petri dishes. They will adhere to the dish and can be assayed later for functional properties such as phagocytosis and microbicidal or tumoricidal activity as well as surface markers, receptors, or specific enzyme content.

The liquid culture technique can provide large numbers of mononuclear phagocytes without the encumbrance of the agar. It is worth mentioning that the cells grown in agar have ingested a great amount of agar. This should be considered when deciding cytological and functional criteria used for identification. Adaption of liquid growth to large flasks should provide quantities of M-CFC-derived macrophages for further determination of heterogeneity as a function of tissue derivation and/or exposure to growth factor. The assay of growth factors would best be served initially using a microwell method, whereas further use of the progeny would require large numbers of cells.

Growth Characteristics of M-CFC

Colony Formation and Survival without CSA

All M-CFC exhibit two characteristics that allow us to distinguish them from GM-CFC or HPP-CFC [22, 23, 28, 29]. These are the lag period or delay in initiation of colony formation (fig. 1) and their

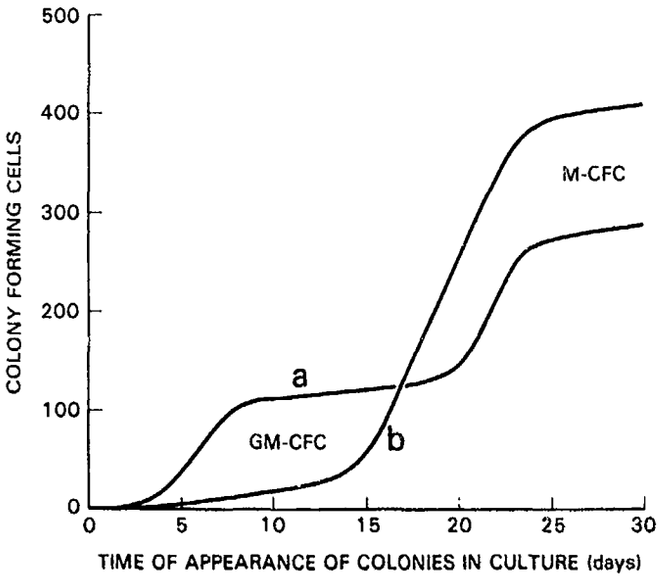

Fig. 1. The appearance of GM-CFC- and M-CFC-derived colonies with time in culture: characteristic GM-CFC- and M-CFC-derived colony growth from bone marrow (a), and characteristic M-CFC-derived colony appearance from extramedullary sources such as peritoneal exudate, thymus and lymph node (b).

resistance to the absence of CSA in the culture system (fig. 2). The duration of delay in initiation of proliferation is variable, but usually in the agar system the initial clusters of cells derived from the M-CFC are not observed until after 5–10 days of culture (fig. 1). This can vary with the tissue source of M-CFC, CSA, and type of culture system (agar or liquid), but the delay or lag is always present. Those using the liquid system have noticed a consistently shorter delay, perhaps as a consequence of the more readily available CSA and adherence of M-CFC. Once colony formation is initiated, growth proceeds at a rate comparable to the GM-CFC and HPP-CFC, with a plateau in total colony formation occurring at approximately 25 days of culture in the agar system and 14 days in the liquid system.

The M-CFC is also characteristically more resistant to the absence of CSA in culture, although the presence of CSA is an absolute requirement (fig. 2). This resistance is most likely a benefit derived from their delay in initiation of proliferation. CSA withheld for 48 h reduces colony

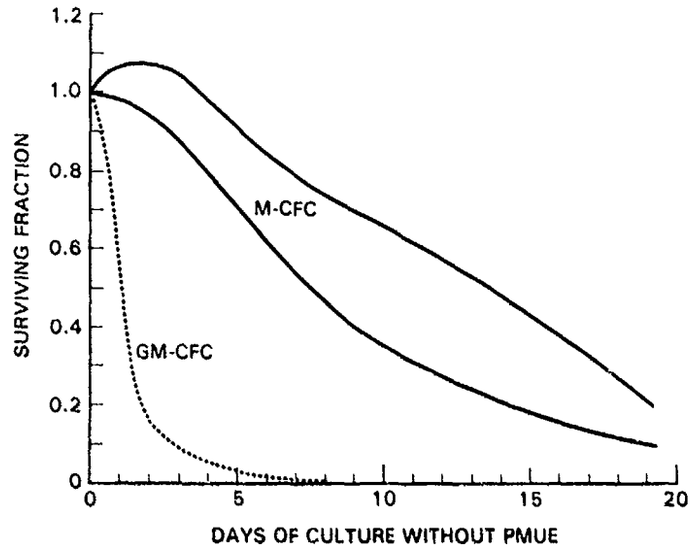

Fig. 2. The differential sensitivity of GM-CFC and M-CFC to the absence of CSA in culture.

formation derived from GM-CFC to approximately 10–20%, while 100% of colony-forming ability is maintained by the M-CFC. This characteristic has proved valuable in separating the growth of colonies derived from a tissue source (bone marrow, spleen, peripheral blood) that contains both GM-CFC and M-CFC. In this situation, we use one culture set to assay GM-CFC and another set (in which CSA is withheld for 2 days) to assay M-CFC.

Morphology of M-CFC-Derived Colonies

Examination of cells present in M-CFC-derived colonies at all stages of growth revealed only mononuclear cells and macrophages. Colonies removed early in culture growth revealed mononuclear cells early in the lineage of mononuclear phagocyte development, with macrophages predominating as time in culture increased [28–30]. The cells derived from mature colonies were morphologically recognizable as mononuclear phagocytes or macrophages by both light and electron microscopy as well as simple functional tests such as phagocytosis of bacteria, yeast and sheep red blood cells, and the presence of Fc receptors.

Incidence of M-CFC

Adult Tissues and Extramedullary Spaces

The murine system has been the most extensively examined. In the mouse, M-CFCs have been detected in bone marrow, spleen, peripheral blood, peritoneal and pleural exudate, alveolar space, liver, cervical and mesenteric lymph nodes, and the thymus. We have also recently detected M-CFC within adherent and nonadherent fractions of brain-derived nerve tissue from both mouse and rat species [unpublished observations]. Shown in table I are relative and absolute values of M-CFC detected in marrow, spleen, peripheral blood, thymus, and resident peritoneal exudate cells of the various strains of mice used in our laboratory. Obvious strain differences exist, whith the highly significant variations noted in femoral, splenic, and resident peritoneal exudate cells. At this point it is an interesting observation that the C57Bl/10ScN and C3H/HeJ strains, both endotoxin-resistant by virtue of possessing the defective LPS gene, have significantly higher content of M-CFC in bone marrow, spleen, and peritoneal exudate cells than do their paired endotoxin-sensitive strains. Shown in table II for comparison are the relative and absolute GM-CFC values obtained during the same culture period. It is noted that, while GM-CFC are detected only within the bone marrow, peripheral blood, and spleen, the M-CFC have been detected in at least nine different organs and tissue spaces of the mouse. It is also noted that if we assume an equivalent plating efficiency for both GM- and M-CFC, the bone marrow, spleen, and peripheral blood contain (respectively) 2–3, 10–30, and 200–500 times the number of M-CFC than GM-CFC.

Although we and others have used the mouse as a tissue source almost exclusively, we have also detected M-CFC in marrow and peripheral blood-derived cells from the rat, dog [43], monkey, baboon, and human [unpublished observations]. The source of CSA used differs with the species being investigated. The other general characteristics of the M-CFC remain the same. All cultures, irrespective of species derivation, show the lag in initiation of growth in culture, they are resistant to the lack of CSA, and all of their progeny are mononuclear phagocytes. The CSA used for rat and dog is endotoxin-stimulated serum or plasma, while that for monkey, baboon, and human can be human placenta-conditioned medium or giant cell tumor-conditioned medium (GIBCO Laboratories, Grand Island, N.Y.).

Table I. The concentration[1] and total content[1] of M-CFC within various tissues and sites within different strains[2] of adult mice

Strain	Concentration / Content				
	femur	spleen	blood	thymus	peritoneal exudate
C57Bl/6J	503	9.4	231	1.2	0
	83,109 ± 11,300	9,869 ± 1,030	7,563 ± 673	1,020 ± 75	0
C57Bl/10Sn	338	9.4	216	1.8	1.3
	68,653 ± 5,430	15,406 ± 1,100	7,776 ± 811	1,575 ± 86	40 ± 11
C57Bl/10ScN	856	39	200	2.4	26
	211,414 ± 16,540	62,228 ± 7,410	10,700 ± 1,245	2,117 ± 405	1,022 ± 48
B6D2F1	538	79	274	2.6	0
	102,336 ± 13,210	105,894 ± 11,418	10,500 ± 893	2,353 ± 135	0
B6CBF1	854	43	210	2.4	2.2
	108,225 ± 18,105	31,640 ± 3,715	9,450 ± 750	1,860 ± 214	62 ± 12
C3Heb/FeJ	599	37	303	2.0	3.2
	86,004 ± 9,930	53,825 ± 6,470	14,100 ± 1,075	1,850 ± 185	100 ± 17
C3H/HeN	979	77	225	3.8	0
	103,475 ± 12,425	122,226 ± 8,750	7,875 ± 825	3,515 ± 310	0
C3H/HeJ	1,143	102	466	3.7	47
	154,647 ± 16,640	183,248 ± 12,225	19,600 ± 1,141	3,386 ± 425	2,115 ± 315

[1] Concentration per 10^5 nucleated cells, total content is per femoral shaft, spleen, thymus, milliliter of blood and total exudate cells (± SEM).
[2] B6D2F1 = C57Bl/6J × DBA/2; B6CBF1 = C57Bl/6J × CBA.
[3] CSA was PMUE at 2.5% v/v.

Table II. The concentration[1] and total content of GM-CFC within various hematopoietic tissues of the adult mouse

Strain	Concentration / Content		
	femur	spleen	blood
C57Bl/6J	243	0.9	0.4
	29,463 ± 2,180	1,016 ± 71	14 ± 3
B6D2F1	259	3.0	0.8
	49,250 ± 3,470	3,105 ± 245	34 ± 7
C3Heb/FeJ	210	11.8	1.6
	30,535 ± 2,450	5,525 ± 610	61 ± 9
C3H/HeJ	281	8.5	2.5
	37,208 ± 3,220	4,404 ± 870	90 ± 9

[1] Concentration per 10^5 nucleated cells, total content per femoral shaft, spleen and milliliter of blood (± SEM).

Shown in table III are the relative and absolute values of GM-CFC and M-CFC derived from the bone marrow, spleen, thymus, and peripheral blood leukocytes of young adult Sprague-Dawley rats. The M-CFC are more numerous than GM-CFC in all of the organs tested. M-CFC have also been detected in the lymph nodes and brain tissue [unpublished observations], but are undetectable within resident peritoneal exudate cells.

Fetal and Neonatal Tissue-Derived M-CFC

We have detected M-CFC in fetal bone marrow, spleen, liver, and thymus [unpublished observations]. Shown in table IV are the relative and absolute values for M-CFC in 16-day-old fetal tissues. The values for GM-CFC detected in the same tissue cell suspensions are also shown. M-CFC concentration and content are significantly greater in each organ, with the exception of the bone marrow where the values are equivalent. GM-CFC are not detectable in the thymus of the normal mouse. The fetal spleen and thymus also have much higher numbers of M-CFC than do the adult tissues (table I), whereas content and concentration of the femoral M-CFC increase with age. Table V shows the con-

Table III. The concentration[1] and total content[1] of GM-CFC and M-CFC within various tissues of the adult rat[2]

	Concentration Total content		
	GM-CFC	M-CFC	TNC ($\times 10^7$)
Bone marrow	124 ± 33	207 ± 34	15.85 ± 1.41
	192,753 ± 14,760	302,941 ± 21,900	
Spleen	0.20 ± 0.04	18.6 ± 2.7	121.99 ± 9.72
	2,285 ± 505	157,997 ± 11,525	
Thymus	ND	10.7 ± 4.1	66.82 ± 1.54
		75,983 ± 7,805	
Peripheral blood	1.4 ± 2	33 ± 6	5.3 ± 0.42
	76 ± 4	1,749 ± 471	

CSA is plasma from rats perviously injected with endotoxin (50 μg, 5% v/v).
[1] Concentration per 10^5 nucleated cells, total content is per femoral shaft, spleen, thymus and per milliliter of peripheral blood (± SEM). ND = None detected.
[2] Sprague-Dawley strain.

centration and content of M-CFC and GM-CFC in 1-, 7-, and 14-day neonatal tissue. The liver shows a decrease in the number of M-CFC that can be assayed after simply mincing and dissociating the hepatic tissue. After approximately 10 days of age, the M-CFC harvested in this manner will not form colonies in culture. The dissociation technique and separation procedure of *Chan* et al. [7] must be used for the detection of the large number of adult liver-derived M-CFC.

These fetal and neonatal M-CFC exhibit the same general characteristics of the adult tissue-derived M-CFC. They require the presence of CSA for growth, they are relatively resistant to the absence of CSA, they exhibit a significant lag in initiation of proliferation in vitro, and their progeny are all mononuclear phagocytes. We have yet to confirm whether these fetal organ-derived M-CFC are heterogeneous with respect to neonatal organ-derived and/or adult organ-derived M-CFC. Early fetal liver GM-CFC have been shown to differ in density and size from the adult GM-CFC and from the late fetal liver GM-CFC [13, 17, 41]. Separation of the early fetal liver GM-CFC by velocity sedimentation has

Table IV. M-CFC and GM-CFC: the realtive[1] and absolute[1] values in 16-day-old fetal tissue of B6D2F1 mice

Organ	GM-CFC		M-CFC	
	concentration	total	concentration	total
Spleen	27±2.0	342± 67	255±48	2,850± 530
Liver	30±3.5	16,032±731	112± 8	56,477±9,450
Femur	13±0.8	200± 43	12± 3	214± 48
Thymus	–	–	63±15	1,584± 241

[1] Concentration is per 10^5 nucleated cells, total content is per spleen, liver, thymus and femoral shaft (±SEM).

Table V. M-CFC and GM-CFC: the relative[1] and absolute[1] values in 1-, 7-, and 14-day-old B6D2F1 neonatal mice

Organ	Age days	GM-CFC		M-CFC	
		concentration	total	concentration	total
Spleen	1	92 ±18	1,470± 185	167±21	2,227± 373
	7	43 ± 9	11,121± 589	50± 6	18,919± 1,097
	14	26 ± 6	19,581± 677	243±30	86,779± 7,450
Liver	1	105 ±21	25,888±1,281	507±33	60,671±11,800
	7	9.5± 3	6,352± 427	43± 8	22,956± 2,412
Femur	1	104 ±12	728± 126	333±16	2,333± 407
	7	45 ± 6	1,905± 204	92± 9	2,836± 600
	14	119 ±11	6,431± 793	392±21	18,235± 808
Thymus	1	–	–	124±11	1,338± 187
	7	–	–	107± 7	3,009± 412
	14	–	–	77± 7	5,091± 610

[1] Concentration is per 10^5 nucleated cells, total content is per spleen, liver, thymus and femoral shaft (±SEM).

shown these GM-CFC to have a very high sedimentation velocity with two peaks at approximately 7.7 and 9.4 mm/h, whereas adult GM-CFC sediment at a rate of 4.5 mm/h [13, 19]. Using adult marrow we have shown the GM-CFC population to sediment at 5.2 mm/h whereas the adult marrow-derived M-CFC sedimented at two distinct rates, 4.1 and

6.5 mm/h [34]. It would be of interest to examine the fetal organ-derived M-CFC relative to the adult tissues. The presence of the M-CFC in many adult tissues would allow comparison of fetal M-CFC derived from marrow, spleen, liver, thymus, and brain. In addition, pure populations of macrophages may be derived from fetal and neonatal tissue, making it possible for the same issues concerning phenotypic heterogeneity and specific tissue-derived inducing factors to be addressed in fetal versus adult tissue and medulla-derived macrophages.

Response of M-CFC in Medullary-Extramedullary Tissue to Antigenic Stimulus

Many studies have shown the influence of antigens, lipopolysaccharide, and other bacterial cell wall products and bacteria on the GM-CFC. The general response is characterized by a transient rise in peripheral blood content, followed by a marked increase in the spleen and stimulation of marrow GM-CFC. GM-CFC are rarely detected outside of the marrow, peripheral blood, and spleen. However, the M-CFC, as mentioned earlier, has been detected in a variety of extramedullary organs and tissue spaces including the blood, spleen, and bone marrow. The potential physiological significance of the M-CFC lies in its ubiquitous presence as a precursor of the macrophage. This large and widely disseminated cell population would provide a maximal increase in potential effector and/or activated macrophages throughout the mononuclear phagocyte system. Data accumulated in our laboratory suggest that the M-CFC, just as the GM-CFC, forms part of the extensive cellular response of the hematopoietic organs to agents such as lipopolysaccharide, *Corynebacterium parvum*, and *Bacille bilié de Calmette-Guérin* [27, 31, 32]. However, the M-CFC also form part of the cellular inflammatory response of the organs and tissue spaces of the mononuclear phagocyte system [27, 33]. Table VI shows the range values of peak responses for organ content of GM-CFC and M-CFC responding to injection of killed *C. parvum* [unpublished results, 27]. This is an incomplete list of responsive organ-derived M-CFC, but it gives an indication of the numbers responding to an inflammatory stimulus. The total number of M-CFC potentially available within the organs of the mononuclear phagocyte system is significantly greater than that for the GM-CFC population as well as the HPP-CFC, although there is an obvious difference in amplifi-

Table VI. The response[1] of mouse GM-CFC[2] and M-CFC[2] to intraperitoneal injection of *Corynebacterium parvum*

	M-CFC		GM-CFC	
	control	*C. parvum*	saline	*C. parvum*
Femoral shaft	45 –80	55 – 90	18 –35	25 – 60
Spleen	21.5–40.5	275 –450	1.5 – 2.5	75 –120
Peripheral blood leukocytes	5 –18	25.0– 33.0	0.03– 0.07	0.3– 0.6
Thymus	1.5– 2.5	4.5– 8.2	ND	ND
Lymph nodes	0.7– 1.5	6.0– 11.0	ND	ND
Peritoneal exudate	ND[3]	250 –400	ND	ND

[1] Range of peak responses of GM-CFC and M-CFC in bone marrow and extramedullary organs to *C. parvum.* Values are ranges calculated from unpublished observations and *MacVittie* [27].

[2] Range values × 10^3 per organ, femoral shaft, milliliter of blood and peritoneal cavity.

[3] None detected.

cation potential between these three CFCs as assayed in vitro. It is also most likely that the organ-derived resident M-CFC are capable of limited self-renewal in the steady state as well as part of the inflammatory response, and are not totally dependent on immigration of blood-borne, marrow-derived M-CFC for maintenance of their number.

Cell Lineage: Relationship to GM-CFC and HPP-CFC

In considering the hierarchy of these CFCs, results in our laboratory as well as others [2, 20, 23, 24, 34, 44, unpublished results] suggest they occupy a position somewhat distant to the GM-CFC and HPP-CFC. These results also emphasize the heterogeneity of the M-CFCs with respect to age or degree of maturation. *Lin and Freeman* [23] and *Reppun* et al. [44], in describing the population of M-CFCs found in peritoneal exudate and alveolar space, have shown that the CFC, with relatively high colony-forming efficiency, is contained within a homogeneous fraction of separated cells identified morphologically as mature macrophages. Their presence in bone marrow, spleen, and peripheral blood suggests that these CFCs are part of a morphologically unidentifiable

Table VII. The cell cycle status[1] of bone marrow-derived HPP-CFC, GM-CFC, and M-CFC: reduction in colony forming ability[2]

Femoral content	HPP-CFC	GM-CFC	M-CFC
Control	5,390 ±585	20,689 ±864	74,980 ±4,915
Hydroxyurea	4,920 ±809	11,844 ±998	43,540 ±2,603
% reduction	10.3± 2.3	38.0± 4.0	45.2± 4.8

[1] Hydroxyurea injected i.p. (900 mg/kg) 2 h prior to sacrifice and assay for marrow-derived CFCs.

[2] Values are means ± SEM of five replicate experiments. All CFCs are assayed from the same marrow samples.

population of mononuclear cells of different sizes, density [23, 34, 44], radiosensitivity [20, 21, 24, 30, unpublished results], and perhaps cycling characteristics. We are in the process of determining the cell cycle characteristics of M-CFCs derived from a variety of tissue sources. Our preliminary data using the phase-specific drug hydroxyurea [unpublished results] to measure the effect on marrow-derived CFCs such as the HPP-CFC, GM-CFC, and M-CFC show that the population of M-CFCs are cycling to the same extent as GM-CFCs (table VII). In contrast, the HPP-CFCs have a smaller percentage of the population in cell cycle, as previously shown by *Baines* et al. [2]. Additional evidence suggesting the M-CFC is a more mature cell is as follows: (a) A lower amplification potential is shown in culture. M-CFC-derived colonies are significantly smaller in size than the GM-CFC-derived and HPP-CFC-derived colonies. Assuming that amplification potential correlates with the degree of maturation, the HPP-CFC are the least mature, followed by GM-CFC, and then by the M-CFC. (b) If HPP-CFC and GM-CFC colonies are harvested after 7–12 days of culture,significant numbers of M-CFC are detected upon reculture of the dispersed cells, whereas HPP-CFC and GM-CFC are not observed. This suggests that as the younger HPP-CFC and GM-CFC proliferate and differentiate in culture, M-CFC are part of their progeny [unpublished results]. (c) M-CFC are not transplantable, as assayed from the hematopoietic organs of bone marrow-, spleen-, or peripheral blood-transplanted mice. Their presence in the spleen and marrow of transplanted hosts coincides with the detection of GM-CFC [unpublished results]. Considering the tissue distribution of M-CFCs

and the available evidence, it is probable that the marrow-derived M-CFC are a heterogeneous population of CFCs with limited self-renewal potential and are derived from the HPP-CFCs and GM-CFCs, while the tissue-derived M-CFC represent populations of a greater degree of maturity and restricted self-renewal.

Characteristics of M-CFC

The M-CFC are a class of CFCs with similar characteristics that distinguish them from hematopoietic stem cells, GM-CFC, and HPP-CFC. Yet they possess characteristics that separate them into subpopulations, and indicate a strong degree of heterogeneity within the class or population of M-CFC that is dependent on tissue derivation.

It is the heterogeneity of the M-CFC that may prove to be the most illuminating aspect of the CFCs. From our standpoint, one of the most interesting questions to be addressed over the next few years is the effect of organ microenvironment on macrophage heterogeneity. Do the M-CFCs derived from the hematopoietic organs differ functionally, metabolically, morphologically, etc., from the M-CFCs derived from extramedullary tissues such as thymus, lymph nodes, liver, and brain? Are differences, once defined, phenotypically induced by the organ-specific microenvironment in which the M-CFCs reside? The ability of the M-CFC to produce colonies of macrophage progeny, coupled with the advent of monoclonal antibodies and better physical sorting capabilities, will shed some light on these very basic and most interesting questions.

The heterogeneity of M-CFCs has already been indicated by a number of investigations [12, 21, 24, 30, 34, 44, 48]. M-CFCs derived from bone marrow, spleen, peripheral blood, and alveolar space can be separated based on size [34, 44]. We have shown that marrow-derived M-CFCs are of two sizes, one sedimenting at 4.1 mm/h and the other at 6.5 mm/h. Spleen- and blood-derived M-CFCs are homogeneous in size and sediment at 4.1 mm/h, while peritoneal exudate-derived M-CFCs sediment at 6.5 mm/h. The marrow-derived GM-CFCs sediment at 5.2 mm/h [34]. *Reppun* et al. [44] also observed size differences between alveolar- and blood-derived M-CFCs. The blood-derived M-CFCs sedimented slower than the larger alveolar M-CFCs. These results confirm ours regarding the blood-derived M-CFC, and place the alveolar-derived M-CFC in a class similar to that of the peritoneal exudate.

The radiosensitivity of these cells is another parameter that indicates significant heterogeneity within the population of M-CFC that is dependent on tissue origin. M-CFCs derived from marrow [unpublished], spleen [unpublished], thymus, and lymph node [30] are most radiosensitive, with D_o values approximating 75 rad, and they fall into a class with the stem cell, the GM-CFC, and the HPP-CFC [unpublished]. In contrast, the M-CFCs derived from the liver, peritoneal exudate, and pleural space [8, 21, 23] are intermediate in radiosensitivity, with D_o values of approximately 120 rad. The M-CFCs from blood and alveolar space are the most resistant, with D_o values of approximately 200 rad [20, 24].

The application of monoclonal antibodies, fluorescent probes, and cell sorting will allow correlation of specific macrophage progeny with subpopulations of M-CFC, tissue derivation, state of maturation, and activation. In addition, such techniques will enable insight into the induction process of these markers by specifically derived growth, differentiation, and/or inducing factors.

The physiological significance of the cell (M-CFC) assayed in vitro by its ability to form colonies of mononuclear phagocytes remains to be determined. Does it simply represent a population of macrophages that are able to respond to CSA and multiply in vitro? Are there differences between M-CFC derived from hematopoietic tissue, marrow, and spleen, versus extramedullary tissues such as thymus, liver, alveolar and peritoneal space, lymph nodes, and brain? Do these M-CFC represent local tissue-specific subsets of macrophages or mononuclear cells capable of local proliferation in steady state and in response to stress, or are the tissue macrophages supplied by blood-borne, marrow-derived M-CFC? Can tissue-specific M-CFC be separated and isolated from tissue macrophages as well as from other tissue-derived M-CFC? Do tissue-specific CSAs exist that can induce a tissue-specific phenotype upon M-CFC derived from different tissue sources? What are the microenvironmental factors that induce macrophage heterogeneity? Can these be detected at the level of the M-CFC? As mentioned earlier in the text, the use of monoclonal antibodies and sophisticated cell-separating techniques should shed light on some of these intriguing questions. Our laboratory is actively pursuing these questions, and with specific use of the BudR labeling technique [*Hagan*, this book], we hope to determine the in vivo turnover times of marrow-derived versus tissue-derived M-CFC populations.

References

1 Austin, P.E.; McCulloch, E.A.; Till, J.E.: Characterization of the factor in L-cell conditioned medium capable of stimulating colony formation by mouse marrow cells in culture, J. cell. Physiol. *77:* 121–134 (1971).

2 Baines, P.; Bol, S.; Rosendaal, M.: Charcterization of a developmentally early macrophage progenitor found in normal mouse marrow. Br. J. Haemat. *48:* 147–153 (1981).

3 Bradley, T.R.; Hodgson, G.S.: Detection of primitive macrophage progenitor cells in mouse bone marrow. Blood *54:* 1446–1450 (1979).

4 Bradley, T.R.; Metcalf, D.: The growth of mouse bone marrow cells in vitro. Aust. J. exp. Biol. med. Sci. *44:* 287–300 (1966).

5 Bradley, T.R.; Stanley, E.R.; Sumner, M.A.: Factors from mouse tissues stimulating colony growth of mouse bone marrow cells in vitro. Aust. J. exp. Biol. med. Sci. *49:* 595–603 (1971).

6 Buhles, W.C.: Studies on mononuclear phagocyte progenitor cells: morphology of cells and colonies in liquid culture of mouse bone marrow. J. reticuloendoth. Soc. *25:* 363–378 (1979).

7 Chan, S.H.; Metcalf, D.; Stanley, E.R.: Stimulation and inhibition by normal human serum of colony formation in vitro by bone marrow cells. Br. J. Haemat. *20:* 329–341 (1971).

8 Chen, D.M.; Lin, H.S.; Stahl, P.; Stanley, E.R.: Clonal growth in vitro by mouse Kupffer cells. Expl Cell Res. *121:* 103–109 (1979).

9 Chu, J.Y.; Lin, H.S.: Induction of macrophage colony-forming in the pleural cavity. J. reticuloendoth. Soc. *20:* 299–305 (1976).

10 Gregory, C.J.; Eaves, A.C.: Three stages of erythropoietic progenitor cell differentiation distinguished by a number of physical and biological properties. Blood *51:* 527–535 (1978).

11 Guilbert, L.J.; Iscove, N.N.: Partial replacement of serum by selenite, transferrin, albumin, and lecithin in haemopoietic cell cultures. Nature, Lond. *263:* 594–595 (1976).

12 Haskill, S.; Becker, S.: Flow cytometric analysis of macrophage heterogeneity and differentiation: utilization of electronic cell volume and fluorescent substrates corresponding to common macrophage markers. J. reticuloendoth. Soc. *32:* 272–285 (1982).

13 Haskill, J.S.; Moore, M.A.S.: Two dimensional cell separation: comparison of embryonic and adult haemopoietic stem cells. Nature, Lond. *226:* 853–854 (1970).

14 Heath, D.S.; Axelrad, A.A.; McLeod, D.L.; Shreeve, M.M.: Separation of the erythropoietin-responsive progenitors BFU-E and CFU-E in mouse bone marrow by unit gravity sedimentation. Blood *47:* 777–792 (1976).

15 Iscove, N.N.; Guilbert, L.J.; Weyman, C.: Complete replacement of serum in primary cultures of erythropoietin-dependent red cell precursors (CFU-E) by albumin, transferrin, iron, unsaturated fatty acid, lecithin and cholesterol. Expl Cell Res. *126:* 121–126 (1980).

16 Iscove, N.N.; Sieber, F.; Winterhalter, K.H.: Erythroid colony formation in cultures of mouse and human bone marrow. Analysis of the requirement for erythropoietin by

gel filtration and affinity chromatography on agarose-concanavalin A. J. cell. Physiol. *83:* 309–320 (1974).

17 Johnson, G.R.; Metcalf, D.: Characterization of mouse fetal liver granulocyte-macrophage colony-forming cells (GM-CFC) by velocity sedimentation at unit gravity. Exp. Hematol. *6:* 246–253 (1978).

18 Johnson, G.R.; Metcalf, D.: Pure and mixed erythroid colony formation in vitro stimulated by spleen cell conditioned medium with no detectable erythropoietin. Proc. natn. Acad. Sci. USA *74:* 3879–3888 (1977).

19 Kubota, K.; Motoyosh, K.; Kajagaya, S.; Suda, T.; Saito, M.; Muura, Y.: Morphological examinations of murine granulocyte/macrophage colonies grown in serum-free cultures. Exp. Hematol. *11:* 364–370 (1983).

20 Lin, H.-S.: Colony formation in vitro by mouse blood monocytes. Blood *49:* 593–598 (1977).

21 Lin, H.-S.: Peritoneal exudate cells. III. Effect of gamma-irradiation of mouse peritoneal colony-forming cells. Radiat. Res. *63:* 560–566 (1975).

22 Lin, H.-S.: Peritoneal exudate cells. I. Growth requirements of cell capable of forming colonies in soft agar. J. cell. Physiol. *83:* 369–378 (1974).

23 Lin, H.-S.; Freeman, P.: Peritoneal exudate cells. IV. Characterization of colony-forming cells. J. cell. Physiol. *90:* 407–414 (1976).

24 Lin, H.-S.; Kun, C., III; Chen, D.-M.: Radiosensitivity of pulmonary alveolar macrophage colony-forming cells. Radiat. Res. *89:* 283–290 (1982).

25 Lin, H.-S.; Kuhn, C.; Kuo, T.T.: Clonal growth of hamster free alveolar cells in soft agar. J. exp. Med. *142:* 877–886 (1975).

26 Lin, H.-S.; Stewart, C.C.: Colony formation by mouse peritoneal exudate cells in vitro. Nature, Lond. *243:* 176–177 (1973).

27 MacVittie, T.J.: Alterations induced in macrophage and granulocyte-macrophage colony-forming cells by a single injection of mice with *Corynebacterium parvum.* J. reticuloendoth. Soc. *26:* 479–490 (1979).

28 MacVittie, T.J.; McCarthy, K.F.: The detection of in vitro monocyte-macrophage colony-forming cells in mouse thymus and lymph nodes. J. cell. Physiol. *92:* 203–208 (1977).

29 MacVittie, T.J.; Porvaznik, M.: Detection of in vitro macrophage colony-forming cells (M-CFC) in mouse bone marrow, spleen, and peripheral blood. J. cell. Physiol. *97:* 305–314 (1978).

30 MacVittie, T.J.; Weatherly, T.L.: Characteristics of the in vitro monocyte-macrophage colony-forming cells detected within mouse thymus and lymph nodes; in Baum, Ledney, Experimental hematology today, pp. 147–156 (Springer, New York 1977).

31 MacVittie, T.J.; Weinberg, S.R.: An LPS responsive cell in C3H/HeJ mice: the peritoneal exudate-derived macrophage colony-forming cell (M-CFC); in Skamene, Perspectives in immunology, pp. 511–518 (1980).

32 MacVittie, T.J.; Weinberg, S.R.: Murine Hemopoiesis: responses of pluripotent stem cells (CFU-s) and granulocyte/macrophage colony-forming cells (GM-CFC) to endotoxin in C3H/FeJ and C3H/HeJ mice; in Baum, Ledney, van Bekkum, Experimental hematology today, pp. 19–28 (Karger, New York 1980).

33 MacVittie, T.J.; Weinberg, S.R.: The response of murine macrophage colony-forming cells to endotoxin in C3Heb/FeJ and C3H/HeJ mice. J. reticuloendoth. Soc. *29:* 413–422 (1981).

34 McCarthy, K.F.; MacVittie, T.J.: Velocity sedimentation studies on monocyte-macrophage colony-forming cells from marrow, spleen, blood and peritoneal exudate. J. reticuloendoth. Soc. *24:* 263–269 (1978).

35 McLeod, D.L.; Shreeve, M.M.; Axelrad, A.A.: Improved plasma culture system for production of erythrocytic colonies in vitro: quantitative assay method for CFU-E. Blood *44:* 517–534 (1974).

36 Metcalf, D.: Techniques for clonal culture of hemopoietic cells in semisolid medium; in Hemopoietic colonies. In vitro cloning of normal and leukemic cells, pp. 12–35 (Springer, Heidelberg 1977).

37 Metcalf, D.; Johnson, G.R.; Mandel, T.E.: Colony formation in agar by multipotential hemopoietic cells. J. cell. Physiol. *98:* 401–407 (1979).

38 Metcalf, D.; MacDonald, H.R.; Ordartchenko, N.; Sordat, B.: Growth of mouse megakaryocyte colonies in vitro. Proc. natn. Acad. Sci. USA *72:* 1744–1748 (1975).

39 Metcalf, D.; Parker, J.; Chester, H.M.; Kincade, P.W.: Formation of eosinophil-like granulocytic colonies by mouse bone marrow cells in vitro. J. cell. Physiol. *84:* 275–290 (1974).

40 Metcalf, D.; Warner, N.L.; Nossal, G.J.; Miller, J.F.A.P.; Shortman, K.; Rabellino, E.: Growth of B-lymphocyte colonies in vitro from mouse lymphoid organs. Nature, Lond. *255:* 630–532 (1975).

41 Moore, M.A.S.; McNeill, T.A.; Haskill, J.S.: Density distribution analysis of in vivo and in vitro colony-forming cells in developing fetal liver. J. cell. Physiol. *75:* 181–192 (1970).

42 Pluznik, D.H.; Sachs, L.: The cloning of normal 'mast' cells in tissue culture. J. cell. comp. Physiol. *66:* 319–324 (1965).

43 Porvaznik, M., MacVittie, T.J.: Detection of gap junctions between the progeny of a canine macrophage colony-forming cell in vitro. J. Cell Biol. *8:* 555–564 (1979).

44 Reppun, T.S.; Lin, H.-S.; Kuhn, C.: Isokinetic separation and characterization of mouse pulmonary alveolar colony-forming cells. J. reticuloendoth. Soc. *25:* 379–387 (1979).

45 Rosenszajn, L.A.; Shoham, D.; Kalechman, I.: Clonal proliferation of PHA-stimulated human lymphocytes in soft agar culture. Immunology *29:* 1041–1055 (1975).

46 Stanley, E.R.; Cifone, M.; Heard, P.M.; Defendi, V.: Factors regulating macrophage production and growth: identity of colony stimulating factor and macrophage growth factor. J. exp. Med. *143:* 631–647 (1976).

47 Stephenson, J.R.; Axelrad, A.A.; McLeod, D.L.; Shreeve, M.M.: Induction of colonies of hemoglobin-synthesizing cells by erythropoietin in vitro. Proc. natn. Acad. Sci. USA *68:* 1542–1548 (1971).

48 Meer Jos, W.M. van der: Characteristics of mononuclear phagocytes in culture; in Carr, Daems, The reticuloendothelial system, vol. 1, pp. 735–771 (Plenum Publishing Corp., New York 1980).

T.J. MacVittie, PhD, Armed Forces Radiobiology Research Institute, Experimental Hematology Department, Bethesda, MD 20814 (USA)

Agents and Actions, vol. 15, 3/4 (1984)

Early kinetics of Ca^{2+} fluxes and histamine release in rat mast cells stimulated with compound 48/80

DAVID E. MCCLAIN, MILDRED A. DONLON, THOMAS A. HILL and GEORGE N. CATRAVAS

Biochemistry Department, Armed Forces Radiobiology Research Institute, Bethesda, MD 20814

Abstract

The kinetics of Ca^{2+} uptake and efflux have been measured in rat peritoneal mast cells stimulated with compound 48/80 using rapid mixing and a silicone oil centrifugation technique. Responses at one-second time intervals were resolved beginning as early as three seconds after initial stimulation. The results clearly demonstrate that Ca^{2+} uptake occurs after the initiation of histamine release. Ca^{2+} efflux occurs simultaneously with histamine release. The implications of these findings are discussed and the technique is described.

Introduction

As a part of our laboratory's investigation of the role of the mast cell in radiation injury we are studying aspects of the biochemistry of the secretion process. The absolute requirement for calcium in many secretory processes including histamine release by mast cells is well established [1]. In the mast cell there is an uptake and release of Ca^{2+} associated with the release of histamine stimulated by a variety of releasing agents. There have been several reports detailing the measurement of the time course of histamine release in compound 48/80-stimulated mast cells [2–4] and the Ca^{2+} fluxes associated with stimulation [5]. However, the fact that compound 48/80-stimulated histamine release is completed in approximately 10 sec has made it difficult to determine the sequence of events occurring in the critical first few seconds after stimulation. Simultaneous measurements of compound 48/80-stimulated histamine release and associated Ca^{2+} fluxes which demonstrate the time relationship of these events have not been reported.

In this report we describe the simultaneous measurement of Ca^{2+} fluxes and histamine release in the rat peritoneal mast cell in the period immediately after stimulation with compound 48/80.

Materials and methods

Solutions

Tyrodes A buffer contained 137 m*M* NaCl, 2.7 m*M* KCl, 0.33 m*M* NaH_2PO_4, 12 m*M* $NaHCO_3$, and 1 g/l glucose (anhydrous). The buffer for peritoneal extractions was Tyrodes A, containing 10 i.u./ml of heparin (Riker Labs, St. Louis, MO) and 0.25% (w/v) bovine serum albumin (fatty acid-free, fraction V, Miles Laboratories, Elkhart, IN). Hanks buffer was prepared with Hanks Balanced Salt Solution (Gibco Labs, Grand Island, NY; without Ca^{2+}, Mg^{2+} and phenol red) to which was added 0.8 m*M* Ca^{2+}, 0.8 m*M* Mg^{2+}, and 1 mg/ml bovine serum albumin (fatty acid-free). Compound 48/80 (Sigma Chemicals, St Louis, MO) was dissolved in Hanks buffer. $^{45}CaCl_2$ (10 mCi/ml, 39.2 mCi/mg, New England Nuclear, Boston, MA) was prepared as a 1.0 mCi/ml stock solution in water.

Mast cell purification

Male Sprague–Dawley rats (200–400 g) were sacrificed by carbon dioxide inhalation. Tyrodes A extraction buffer (20 ml) was injected into the peritoneal cavity, and the fluid was drained through an incision. The resulting cell suspension contained 3–7% mast cells and after centrifugation through a 38% albumin gradient [6] mast cells were recovered with a purity of greater than 95%. Cell viability (trypan blue dye exclusion) was greater than 93%. Each animal yielded $1–1.5 \times 10^6$ mast cells (direct cell count).

Preincubation for Ca^{2+} uptake experiments

For Ca^{2+} uptake experiments the purified cells were incubated at 37°C in Hanks buffer for 45 min to re-equilibrate Ca^{2+} levels in the cell after the isolation procedure. A minimum 30 min incubation in Hanks buffer is required under these conditions for the cell to maximize the Ca^{2+} association. The cell suspension was then centrifuged at $1000 \times g$ for 5 min at 8°C to pellet the cells. The supernatant was removed and the pellet stored at 4°C until used.

Preincubation for Ca^{2+} efflux experiments

For Ca^{2+} efflux experiments $^{45}Ca^{2+}$ (10.0 μCi/ml) was added to the pre-incubation buffer during Ca^{2+} re-equilibration in order to label the cells with $^{45}Ca^{2+}$. The cells were then separated from the radioactive medium by first layering the cells over silicone oil (Versilube F50, General Electric Co., Waterford, NY; 2 ml cells per 2 ml of oil) and centrifuging the cells at 2000 × *g* for 10 min at 25°C. The radioactive incubation medium and oil layer were carefully aspirated from over the cell pellet. The pellet was resuspended in $^{45}Ca^{2+}$-free Hanks buffer (approximately 10^6 cells/ml) and incubated an additional 15 min at 37°C to remove loosely bound $^{45}Ca^{2+}$. This step reduces the background radioactivity during efflux measurements. The cell suspension was then centrifuged (1000 × *g* for 5 min at 8°C), the supernatant removed, and the pellet stored at 4°C until used.

Rapid sampling technique

The sampling technique in these experiments is derived from the silicone oil centrifugation method of WOHLHUTTER et al. [7], modified by us to allow simultaneous measurement of histamine release and Ca^{2+} fluxes in the mast cell.

Hanks buffer (0.45 ml) containing 0.8 m*M* Ca^{2+} (with or without 1.8 μCi/ml $^{45}Ca^{2+}$) was layered over 0.2 ml of silicone oil in a microfuge tube (1.5 ml polypropylene Eppendorf style). Up to 12 tubes were loaded into a microfuge rotor (Brinkman, Model 5413) which was placed into a water bath at 37°C for 10 min. Experiments were begun by quickly returning the rotor to the microfuge and carefully injecting (see below) 0.05 ml of a mast cell suspension (6 × 10^6 cells/ml, previously equilibrated to 37°C) into each tube. Samples were centrifuged (13,500 × *g*) for 30 sec, which forces cells out of the reaction medium and into the oil, stopping the reaction. The cells form a pellet at the bottom of the microfuge tube. Both the pellet and the aqueous phase were then processed independently.

No detectable temperature change was observed in the reaction medium during the time required to deliver and react the cells. Measurements at 2 sec intervals were obtained in these experiments. However, it was found that 1 sec intervals could be easily and reproducibly obtained.

Cell delivery technique

The cell suspension was delivered to the reaction mixture by means of a repeating syringe (Model P600, Hamilton Co.) fitted with a siliconized, 1 ml gas-tight syringe (Model 1001, Hamilton Co.). A 1.5 in. no. 18 syringe needle was modified to serve as an injector nozzle by removing the point and polishing the end before bending the needle 45 degrees off line at a point about 5 mm from the polished end. This particular construction serves two purposes. First, the injector has the proper overall length to provide controllable access to the reaction mixture in the microfuge tube, and, second, the bend in the injector needle allows the direct injection of the cell suspension into the medium without disrupting the oil-aqueous phase interface. It is important that the injector be held at an appropriate angle such that the cell suspension, when injected, does not form cell-containing droplets beneath the interface. Formation of these droplets in the oil can prevent the cells from being adequately exposed to the reaction mixture above the oil. In addition, some of these cell-containing droplets can have sufficient density to be carried down to the pellet during centrifugation. This can result not only in a loose pellet that is easily disrupted when the oil layer is aspirated, but also, in the case of Ca^{2+} uptake experiments, $^{45}Ca^{2+}$ carried from the reaction mixture can contaminate the pellet with unincorporated $^{45}Ca^{2+}$. For these two reasons improper injection technique can lead to errors of sufficient magnitude to make good time resolution impossible.

Microfuge tube processing

The following steps apply to both uptake and efflux experiments unless otherwise noted. After completion of the centrifugations, 0.10 ml of the reaction medium was withdrawn to determine the amount of histamine released by the mast cells. For the efflux experiments an additional 0.20 ml was withdrawn to measure the amount of $^{45}Ca^{2+}$ released from the cells.

The remaining aqueous phase was removed and discarded, using a Pasteur pipette attached to a vacuum source. The oil layer was aspirated using a circular motion along the walls of the tube to help ensure, in the case of uptake experiments, that no $^{45}Ca^{2+}$ medium travels down the walls of the tube to contaminate the pellet. It is desirable to remove as much oil as possible from the tube as long as the pellet is not disturbed.

Before processing, the cell pellet was removed from the microfuge tube by cutting off the tip using a rat guillotine (Harvard Apparatus, Dover, MA). This avoids contamination of the pellet with any radioactivity remaining on the walls of the tube.

The pellet was then disrupted to determine the amount of histamine remaining in the cells, and, in the case of Ca^{2+} uptake experiments, the amount of $^{45}Ca^{2+}$ associated with the cells. A solution (0.50 ml), containing 1% (w/v) Triton X-100 (New England Nuclear) and 1% (v/v) Acationox (American Scientific Products, McGraw Park, IL), was added to a microfuge tube containing the cut tube tip and pellet. The tube was allowed to stand for at least an hour to soften the pellet before the tube was vortexed to ensure suspension of the disrupted cells. A portion of this suspension (0.10 ml) was then removed, diluted to 1.00 ml with water, and used for histamine determination. In the case of Ca^{2+} uptake measurements the remainder of the suspension was conserved to measure the amount of $^{45}Ca^{2+}$ incorporated into the pellet.

$^{45}Ca^{2+}$ Determination

To determine the amount of Ca^{2+} released from the cells during efflux experiments an aliquot of the supernatant (0.20 ml) was added to 18 ml of Aquasol liquid scintillation cocktail (New England Nuclear). For the uptake experiments the entire microfuge tube containing the processed pellet fraction was place into a scintillation vial with 18 ml of Aquasol for counting. Radioactivity in the samples was determined with a Hewlett-Packard Mark III Liquid Scintillation Counter. Counting efficiences were generally 60% and constant for a given experiment.

To calculate the amount of Ca^{2+} taken up or released by the mast cells, raw $^{45}Ca^{2+}$ counts per minute (c.p.m.) were first adjusted to account for the variable number of cells present in each assay tube. This was done by dividing c.p.m. by the total histamine present in both the supernatant and pellet fractions (approximately 10 μg per 3 × 10^5 cells) and expressing the amount of Ca^{2+} as c.p.m. per 10 μg histamine. The c.p.m. from untreated cells was subtracted from that of cells exposed to compound 48/80 to give *net* c.p.m. of Ca^{2+} uptake or efflux. Percent maximum response was determined by comparing the net c.p.m. of Ca^{2+} at each

sampling time to the average net c.p.m. measured at 20 and 22 sec after initial stimulation, which were plateau points in all experiments.

Histamine determination

Samples were analysed fluorometrically for histamine on a Technicon Auto-Analyzer II system (Tarrytown, NY), using the method of Siraganian [8, 9]. The amount of histamine released was calculated as a percent of the total histamine in the cell. *Net* histamine release was determined by subtracting the histamine release from untreated cells (approximately 4%) from the amount released from treated cells. The percent maximum response of histamine release was calculated by comparing the net histamine release at each sampling time with that observed 20 and 22 sec after initial stimulation (plateau points).

Calcium and histamine data were fitted by a logistic curve fitting program derived from PARKER and WAUD [10, 11]. The program calculates three characteristic parameters which describe each curve (the plateau point: R_{max}; the slope function; and time of half-maximal response: t_{50}), computes an analysis of variance to test for a common slope function among the group of curves to be compared, and computes individual values of t_{50} for each curve using the common slope function. A direct comparison of t_{50} is allowed if there is a common slope function and common R_{max} (always 100% here, as the result of the normalization calculation). The mean values of t_{50} for each group of curves are calculated and the means of simultaneously derived histamine and calcium data compared using the Mann–Whitney U-test.

Results

Figure 1 shows the results of experiments simultaneously measuring histamine release and Ca^{2+} uptake in mast cells stimulated with 1.0 μg/ml compound 48/80. Each curve shown is a composite of 10 individual experiments with common slope functions and R_{max}. The mean ± SD of slope function for the histamine and calcium composites, 4.97 ± 0.33 and 4.18 ± 0.25, respectively, were not significantly different (Mann–Whitney U-test: $P < 0.002$). Cells incubated without the secretagogue did not show histamine release or Ca^{2+} uptake above average background levels (4.3 ± 0.6% and 35 pmoles per 10^6 cells, respectively) over the time period tested. Data are expressed as a percentage of maximum response vs time after stimulation. The respective plateau levels represent a net histamine release of 50.6 ± 1.2% and a net Ca^{2+} uptake of 56 pmoles per 10^6 mast cells. There is a finite time between switching on the microfuge and the cells becoming effectively separated from the incubation medium. This time has been estimated to be 2 sec in a system similar to ours [7]. The time intervals in all figures reflect this delay.

Histamine release is completed within 12 to 14 sec with half of the release completed by 5.7 ± 0.5 sec (mean ± SD). This is in the range of previously reported observations [4]. Ca^{2+} uptake is completed within 18 sec with half of the association occurring by 6.9 ± 0.7 sec (mean ± SD). Thus, Ca^{2+} uptake begins after the initiation of histamine release with a lag time of approximately 1.2 sec. This difference in t_{50} between the curves is significant (Mann–Whitney U-test, $p < 0.002$).

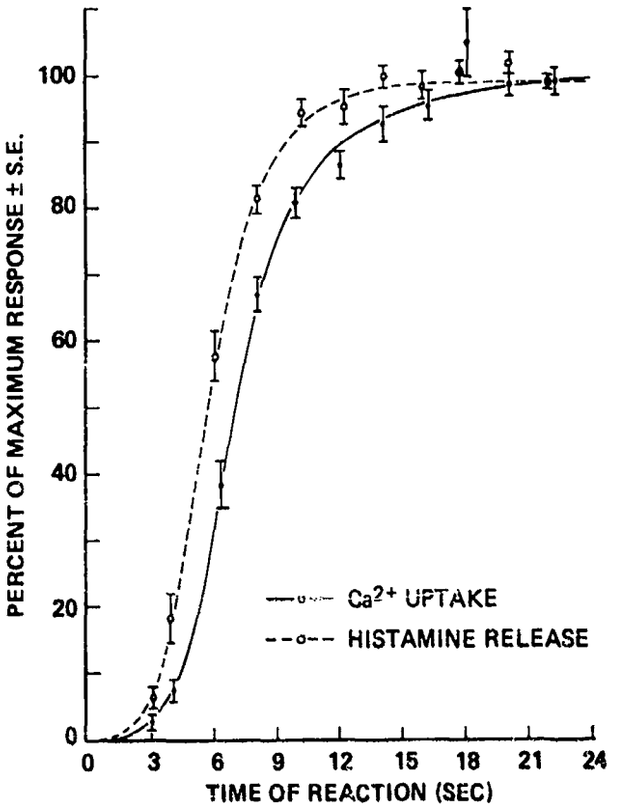

Figure 1
Simultaneous measurement of histamine release and Ca^{2+} uptake in mast cells incubated with 1.0 μg/ml compound 48/80. Cells incubated without the secretagogue showed no net histamine release or Ca^{2+} uptake over the time period shown. Each point represents the mean ± SE of 10 determinations.

It should be noted (Fig. 1) that although the Ca^{2+} uptake curve reaches an apparent plateau by 22 sec, it does not reach an absolute plateau over the short time course of these experiments. This fast, stimulus-related uptake is followed by a much slower association of $^{45}Ca^{2+}$ with the cell continuing for approximately 30 min [5, and unpublished data]. It is likely that this reflects an exchange of $^{45}Ca^{2+}$ from the medium with cellular Ca^{2+} pools not equilibrated with the isotope.

Figure 2 shows the results of simultaneously measuring histamine release and Ca^{2+} efflux from

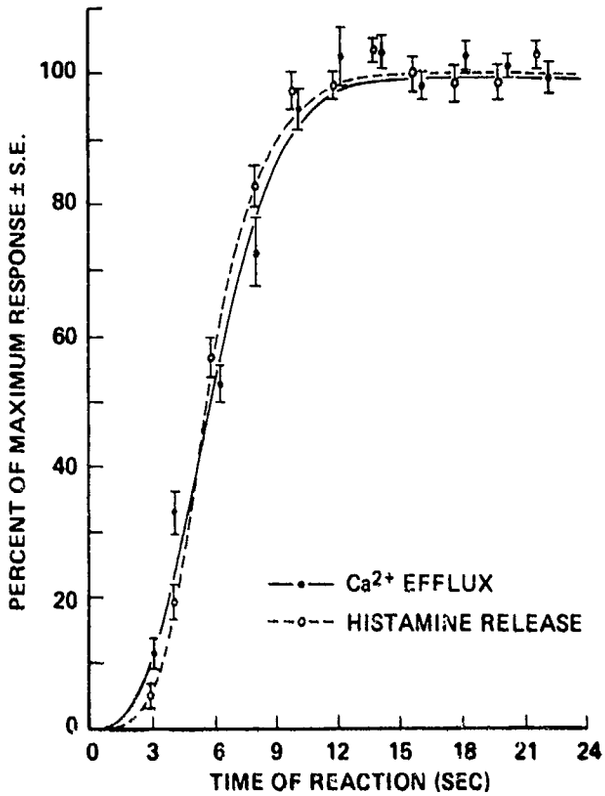

Figure 2
Simultaneous measurement of histamine release and calcium efflux in mast cells incubated with 1.0 μg/ml compound 48/80. Cells incubated without the secretagogue showed no net histamine release or calcium efflux over the time period shown. Each point represent the mean ± SE of 9 determinations.

cells preloaded with $^{45}Ca^{2+}$ then stimulated with 1.0 μg/ml compound 48/80. Each curve shown is a composite of 9 individual experiments with common slope functions and R_{max}. The mean ± SD of slope function for the histamine release and calcium efflux composite curves, 4.94 ± 0.33 and 4.65 ± 0.16, respectively, were not significantly different (Mann–Whitney U-test: $p < 0.002$). Ca^{2+} efflux occurs simultaneously with histamine release and follows a similar time course until completion of the reaction at 12 to 14 sec after stimulation. The t_{50} for histamine release, 5.5 ± 0.3 sec (mean ± SD) and the t_{50} for calcium efflux, 5.7 ± 0.4 sec (mean ± 0.4 sec (mean ± SD) were not significantly different (Mann–Whitney U-test, $p < 0.05$). Cells incubated without the secretagogue did not show histamine release or a Ca^{2+} efflux above the average background levels (4.0 ± 0.7% and 1495 c.p.m. of $^{45}Ca^{2+}$ per 10^6 cells, respectively) over the time period tested. In these experiments the plateau level represents a net histamine release of 50.1 ± 2.3%. Since we are unable to determine how effectively the intracellular calcium pools are saturated during the preincubation step with $^{45}Ca^{2+}$ we could not calculate the absolute amount of Ca^{2+} released upon stimulation. The plateau level in Fig. 2 corresponds to a net release of 5275 c.p.m. of $^{45}Ca^{2+}$ per 10^6 cells.

Histamine release and Ca^{2+} uptake and efflux appear to have a lag time of approximately 3 sec following initial stimulation. This is consistent with previous observations [4]. No attempts were made to interpret the nature of this delay.

Discussion

Compound 48/80 is a non-immunologic secretagogue commonly employed to study the mechanisms involved in histamine release from mast cells. Early attempts to measure the rate of compound 48/80-induced histamine release were unsuccessful since the techniques used were too slow to detect the rapid changes occurring in the cells after stimulation. MORAN et al. [2] reported compound 48/80-induced release in mast cells occurred within 20 sec at 22°C, but it was not known how the time course of the release was influenced by the non-physiological temperatures. BLOOM et al. [3] obtained a reproducible measurement of histamine release as early as 5 and 10 sec after stimulation with compound 48/80. These early time intervals were obtained by terminating the incubation with the addition of a tenfold excess of cold buffer, thus lowering the temperature and diluting the concentration of secretagogue to non-releasing levels. In these experiments histamine release was shown to be completed within 10 sec at 37°C. BLOOM and CHAKRAVARTY [4] later were able to obtain 3, 5, and 8 sec samples using the same dilution techniques. They showed histamine release to be initiated in 3 sec and completed within 8 sec, times roughly comparable to those we report here. Their techniques were not suitable for detecting the Ca^{2+} uptake and efflux which occurs as rapidly as histamine release in compound 48/80-stimulated mast cells.

Attempts have been made to examine the role of Ca^{2+} in the secretion process by trying to determine the relative sequence of histamine release and Ca^{2+} uptake occurring in the stimulated mast cell, but results were often contradictory GROSMAN and DAIMANT [5] correlated the binding of $^{45}Ca^{2+}$ in rat mast cells stimulated with compound 48/80 and other releasing agents

with histamine release in parallel samples, using the same pool of mast cells. Their measurement techniques were not capable of elucidating events occurring in the seconds immediately after stimulation, but their results suggested histamine release occurred more rapidly than Ca^{2+} uptake, a fact which seemingly contradicted some of the notions of stimulus-secretion coupling as originally proposed [12]. In support of these findings SUGIYAMA [13] detected a late association of Ca^{2+} in rat mast cells stimulated with compound 48/80. It was suggested that the Ca^{2+} uptake might be occurring as a result of exocytosis. However, RANADIVE and DHANANI [14] performed experiments which showed Ca^{2+} did not diffuse into cells previously degranulated with compound 48/80. Therefore, whether Ca^{2+} uptake represents the Ca^{2+} which triggers secretion or merely occurs as a consequence of exocytosis, whereby non-specific binding sites for Ca^{2+} are made available, is still a matter in dispute.

In our attempt to resolve some of these questions we have demonstrated the capability of differentiating the temporal sequences of the histamine release reaction and associated Ca^{2+} fluxes at several consecutive time intervals during the early stages of histamine release. This technique allows the monitoring of both histamine release and Ca^{2+} fluxes in the same tube, with the ability to correct the Ca^{2+} data for the number of mast cells present in the assay.

It is clear that Ca^{2+} uptake begins after the initiation of histamine release, suggesting that at least the bulk of the Ca^{2+} that becomes associated with the cell after stimulation with compound 48/80 is not responsible for triggering histamine release. The Ca^{2+} association seen here is not spontaneous or non-specific since control cells incubated without compound 48/80 did not show any significant net Ca^{2+} uptake or efflux over the time course studied.

Compound 48/80-stimulated histamine release is in many ways different from the release stimulated by other releasing agents. Therefore, it is only speculation at this point to suggest that the sequences of Ca^{2+} fluxes and histamine release observed with compound 48/80 might reflect the sequences occurring in mast cells stimulated with the more physiologically interesting immunologic secretagogues. For example, although compound 48/80 will stimulate the uptake of Ca^{2+} from the incubation medium when external Ca^{2+} is available [15], histamine release will occur at almost optimal levels in the absence of external Ca^{2+} [16], provided the internal stores of Ca^{2+} are intact [17, 18]. This is unlike the histamine release stimulated by the antigen–antibody reaction which requires Ca^{2+} in the incubation medium before any significant histamine release will occur [19], though exeptions to this observation have been reported [20]. Other workers [21] have presented data supporting the stimulus-secretion coupling notion that a Ca^{2+} influx precedes histamine release in immunologically-stimulated cells, but their data do not provide information at a stage early enough in the release process to allow one to determine whether Ca^{2+} uptake or the histamine release process begins first. The methods outlined in this report will assist in answering this question.

In terms of the time sequence of Ca^{2+} efflux relative to that of histamine release stimulated by compound 48/80, these experiments show that the efflux occurs simultaneously with histamine release. This suggests that these two events might occur as the result of some common process. Recent findings [22, 23] suggests that the granule matrix contains concentrations of Ca^{2+} several times greater than the cytoplasmic concentration. It is therefore possible that granule-associated Ca^{2+} is released at the time the granule matrix is exposed to the external medium. The extrusion of Ca^{2+} from the granule may represent one of the mechanisms the cell utilizes to return cytoplasmic concentrations of Ca^{2+} back to pre-stimulation levels.

We report here a rapid sampling technique for the simultaneous measurement of histamine release and Ca^{2+} fluxes in the rat mast cell during the first several seconds following stimulation by compound 48/80. It is an inexpensive and reasonably simple technique that is quite precise if samples are carefully processed. It allows the resolution of one-sec time intervals beginning approximately 3 sec after initial stimulation of the cell, providing the most precise and accurate measurement reported for Ca^{2+} fluxes and histamine release occurring in the stimulated mast cell.

Acknowledgment

We wish to thank L. May and J. K. Poplack for their helpful suggestions during the preparation of this manuscript.

Received 25 July 1983; accepted 18 November 1983

[1] R. P. RUBIN, *Calcium and Cellular Secretion*, Plenum Press, New York 1982.

[2] N.C. MORAN, B. UVNÄS and B. WESTERHOLM, *Release of 5-hydroxytryptamine and histamine from rat mast cells*, Acta physiol. scand. *56*, 26–41 (1962).

[3] G.D. BLOOM, B. FREDHOLM and O. HAEGERMARK, *Studies on the time course of histamine release and morphological changes induced by histamine liberators in rat peritoneal mast cells*, Acta physiol. scand. *71*, 270–282 (1967).

[4] G.D. BLOOM and N. CHAKRAVARTY, *Time course of anaphalactic histamine release and morphological changes in rat peritoneal cells*, Acta physiol. scand. *78*, 410–419 (1970).

[5] N. GROSMAN and B. DIAMANT, *Binding of 45-calcium to isiolated rat mast cells in connection with histamine release*, Agents and Actions *8*, 338–346 (1978).

[6] T.J. SULLIVAN, K.L. PARKER, W. STENSON and C.W. PARKER, *Modulation of cyclic AMP in purified rat mast cells. I. Responses to pharmacologic, metabolic and physical stimuli*, J. Immun. *114*, 1473–1479 (1975).

[7] R.M. WOHLHUTTER, R. MARZ, J.C. GRAFF, and P.G.W. PLAGEMANN, A rapid mixing technique to measure transport in suspended animal cells: applications to nuclelotide transport in Novikoff rat hepatoma cells. In *Methods in Cell Biology*, vol. 20, pp. 211–236. (Ed. D.M. PRESCOTT). Academic Press, New York 1978.

[8] R.P. SIRAGANIAN, *An automated continuous-flow system for the extraction and fluorometric analysis of histamine*, Analyst. Biochem. *57*, 383–394 (1974).

[9] R.P. SIRAGANIAN and W.A. HOOK, Histamine release and assay methods for the study of human allergy. In *Manual for Clinical Immunology*, pp. 808–821 (Eds N.E. ROSE and H. FRIEDMAN). American Society for Microbiology, Washington, D.C. 1980.

[10] R.B. PARKER and D.R. WAUD, *Pharmacological estimation of drug-receptor dissociation constants. Statistical evaluation. I. Agonists*, J. Pharmac. exp. Ther. *177*, 1–13 (1971).

[11] D.R. WAUD and R.B. PARKER, *Pharmacological estimation of drug-receptor dissociation constants. Statistical evaluation. II. Competitive antagonists*. J. Pharmac. exp. Ther. *177*, 13–24 (1971).

[12] W.W. DOUGLAS, *Stimulus-secretion coupling: the concepts and clues from chromaffin and other cells*, Br. J. Pharmac. *34*, 451–463 (1968).

[13] K. SUGIYAMA, *Significance of ATP-splitting activity of rat peritoneal cells in the histamine release induced by exogenous ATP*, Jap. J. Pharmac. *21*, 531–538 (1971).

[14] N.S. RANADIVE and N. DHANANI, *Movement of calcium ions and release of histamine from rat mast cells*, Int. Archs Allergy appl. Immun. *61*, 9–18 (1980).

[15] A.C. SPATARO and H.B. BOSMANN, *Mechanism of action of disodium cromoglycate – mast cell calcium influx after a histamine releasing stimulus*, Biochem. Pharmac. *25*, 505–510 (1976).

[16] D.E. COCHRANE and W.W. DOUGLAS, *Calcium-induced extrusion of secretory granules in mast cells exposed to 48/80 or the ionophores A-23187 and X-536-A*, Proc. natn. Acad. Sci. USA *71*, 408–412 (1974).

[17] B. DIAMANT and S.A. PATKAR, *Stimulation and inhibition of histamine release from isolated rat mast cells. Dual effects of the ionophore A-23187*, Int. Archs. Allergy appl. Immun. *49*, 183–207 (1975).

[18] G. ATKINSON, M. ENNIS and F.L. PEARCE, *The effect of alkaline earth cations on the release of histamine from rat peritoneal mast cells treated with compound 48/80 and peptide 401*, Br. J. Pharmac. *65*, 395–402 (1979).

[19] J.C. FOREMAN and J.L. MONGAR, *The role of alkaline earth ions in anaphalactic histamine secretion*, J. Physiol., Lond. *224*, 753–769 (1972).

[20] J.R. WHITE and F.L. PEARCE, *Characteristics of histamine secretion from rat peritoneal mast cells sensitized to the nematode Nippostrongulus brasiliensis*, Immunology *46*, 353–359 (1982).

[21] J.C. FOREMAN, M.B. HALLETT and J.L. MONGAR, *The relationship between histamine secretion and 45-calcium uptake by mast cells*, J. Physiol., Lond. *271*, 193–214 (1977).

[22] E.S. CHOCK, M.A. DONLON, C.E. FIORI and G.N. CATRAVAS, *Elemental analysis for calcium in rat peritoneal mast cells*, J. Cell Biol. *95*, 409a (1982).

[23] A. HEIN and J.P. CAULFIELD, *Sulphur and calcium detection in rat peritoneal mast cell granules*, J. Cell Biol. *95*, 397a (1982).

J. Membrane Biol. 82, 59–65 (1984)

The Journal of
Membrane Biology
© Springer-Verlag 1984

Hexose Regulation of Sodium-Hexose Transport in LLC-PK$_1$ Epithelia: The Nature of the Signal

A. Moran, R.J. Turner†, and J.S. Handler†

Physiology Department, Armed Forces Radiobiology Research Institute, Bethesda, Maryland 20814, and †National Heart, Lung and Blood Institute, National Institutes of Health, Bethesda, Maryland 20205

Summary. We have shown previously that the concentration of glucose in the growth medium regulates sodium-coupled hexose transport in epithelia formed by the porcine renal cell line LLC-PK$_1$. Assayed in physiological salt solution, the ratio of the concentration of α-methyl glucoside (AMG) accumulated inside the cell at steady state to its concentration outside, and the number of glucose transporters, as measured by phlorizin binding, was inversely related to the glucose concentration in the growth medium. In this study, using a cloned line of LLC-PK$_1$ cells, we provide evidence that the difference in AMG concentrating capacity is the result of a regulatory signal and not simply due to a selection process where the growth of cells with enhanced glucose transport is favored by low glucose medium or vice-versa. By adding glucose to conditioned medium (collected after 48 hr incubation with cells and therefore containing less than 0.1 mM glucose), we demonstrate that the signal in the growth medium is indeed the concentration of glucose rather than another factor secreted into or depleted from the medium. Fructose and mannose, two sugars not transported by the sodium-dependent glucose transporter, can substitute for glucose as a carbohydrate source in the growth medium and have a modest glucose-like effect on the transporter. Growth in medium containing AMG does not affect the transporter, indicating that the regulatory signal is not a direct effect of the hexose on its carrier but involves hexose metabolism.

Key Words cultured epithelia · hexose transport · transport regulation

Introduction

LLC-PK$_1$ is a continuous epithelial cell line derived from porcine kidney [5]. The cells grow with their basal surface oriented toward the supporting substrate and form confluent epithelia with many characteristics of the proximal tubule [6, 12–14]. In particular, they exhibit a sodium-coupled hexose transport system in their apical plasma membrane [1, 7, 9, 10] with properties similar to the apical plasma membrane D-glucose transporter identified in the late proximal tubule [8, 9, 16, 17]. The ability of LLC-PK$_1$ cells to transport α-methyl glucose (AMG), a nonmetabolized glucose analogue, develops slowly with time after seeding, reaching a maximum after 3 to 4 weeks [4, 9, 11]. These changes presumably reflect increasing expression of the sodium-coupled hexose carrier. Recently we have shown that sodium-dependent hexose transport in this cell line is affected by the concentration of glucose in the growth medium [10]. Epithelia grown in medium containing low concentrations of glucose develop a much higher transport capacity for AMG than cells grown in medium containing a high concentration of glucose. Furthermore, this phenomenon is reversible. When epithelia grown in high glucose medium are switched to low glucose medium, or vice versa, the transport capacity of the epithelium for AMG increases or decreases accordingly. These changes, like the development of the sodium-coupled hexose transport system itself, are slow, requiring more than 48 hr before significant effects on AMG transport capacity are apparent. Phlorizin binding measurements indicate that it is the number of sodium-dependent glucose transporters that is affected; epithelia grown in low glucose have more carriers than epithelia grown in high glucose [10]. In the present study, we investigate the mechanism underlying this phenomenon. We provide evidence that the difference in AMG transport capacity is the result of a regulatory signal and not simply due to a selection process where the growth of cells with enhanced glucose transport is favored by low glucose medium or vice-versa. Furthermore, we show that the regulatory signal is the glucose concentration itself rather than the presence or absence of some other factor secreted into or depleted from the medium as a result of the glucose concentration. Finally, we rule out the possibility that the regulatory role of D-glucose is due to

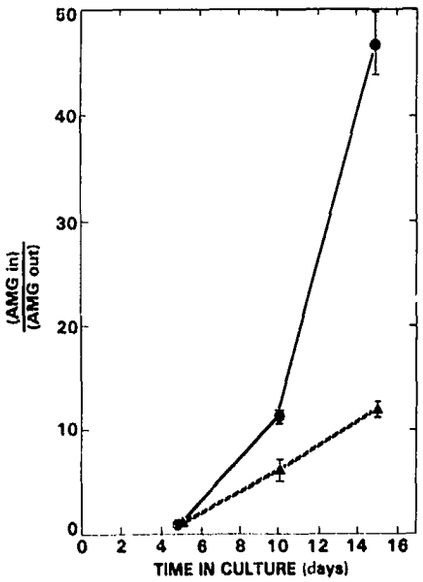

Fig. 1. Steady-state AMG-concentrating capacity of a cloned cell line as a function of time in culture. The cells were grown in media containing 5 mM (●) or 25 mM (▲) glucose

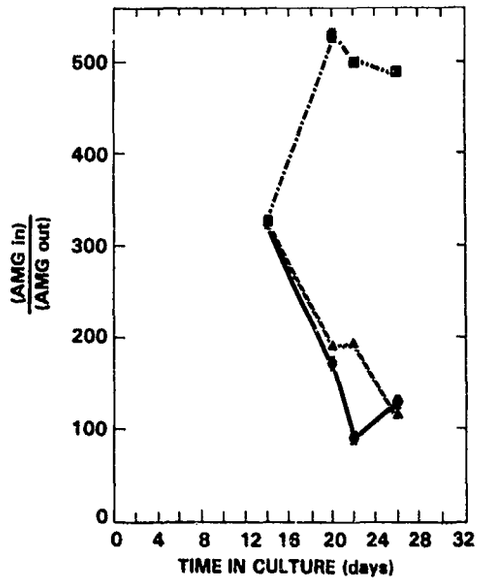

Fig. 2. Regulation of AMG-concentrating capacity in fresh and conditioned media (medium collected after exposure to cells for 48 hr). Epithelia grown for 14 days in medium containing 5 mM glucose were switched to different media: (▲) switched to fresh medium containing 25 mM glucose, (●) switched to conditioned medium supplemented with 25 mM glucose, and (■) continued growth in medium with 5 mM glucose

a direct effect of transported substrate on the carrier.

Materials and Methods

Cells were grown in cluster-12 wells as previously described [9, 10]. We assayed sodium-coupled hexose transport by measuring the steady-state concentrating capacity for AMG as described earlier [9, 10]. Briefly, on the day of the experiment the epithelia were rinsed with phosphate buffered saline (PBS) and then incubated with PBS containing 0.1 mM [^{14}C]-AMG and 0.1 mM [^{3}H]-raffinose (an extracellular marker) on a mechanical shaker at room temperature for 5 hr until a steady-state condition had been achieved. The incubation media were sampled and the cells rinsed and then solubilized using 0.5% Triton X-100 in water. Samples for counting radioactivity and for protein determination were taken. Cell volume was measured using the nonmetabolizable sugar 3-O-methyl glucoside (3OM) that does not accumulate in these cells. Glucose concentration was measured using a Beckman glucose analyzer. The AMG concentrating capacity is expressed as the steady-state ratio of AMG accumulated in cell water to that in the incubation medium. To estimate the number of cells in a plate the epithelia were suspended by trypsin and the cells were counted with a hemocytometer. The data points illustrated in the figures are the mean and standard deviation determined from three wells. Results of representative experiments are shown.

Materials

[^{14}C]-AMG, 3OM and [^{3}H]-raffinose were obtained from New England Nuclear (Boston, MA). Unlabeled raffinose and 3OM were from Cal Biochem. (La Jolla, CA). Uridine and unlabeled monosaccharides were from Sigma Chemicals (St. Louis, MO). Other chemicals were of the highest purity available from commercial sources. A cloned cell line of LLC-PK$_1$ was kindly given to us by Dr. John Cook of Oak Ridge, TN. The cells were cloned by repeated limiting dilution by Dr. Kurt Amsler in Dr. Cook's laboratory. The cells were grown in medium containing 25 mM glucose for two passages and then subcultured into two different media in Cluster-12 wells.

Results

In previous studies [10] we have observed that the change in AMG concentrating capacity of LLC-PK$_1$ epithelia in response to a shift in the concentration of glucose in the growth media is not evident for at least 48 hr. A slow response such as that might result if the glucose concentration in the medium selects cells from a heterogenous population. To evaluate this possibility, we used a cloned line of LLC-PK$_1$ cells. Figure 1 shows concentrating capacity of the cloned cell line as a function of days in growth media prepared to contain 5 or 25 mM glucose. As we have previously shown for the parent cell line [10], cloned cells grown in 5 mM glucose attained a much higher concentrating capacity than the same cells grown in medium containing 25 mM glucose. Thus, it is unlikely that growth medium with a low concentration of glucose acts merely by selecting against cells with a low number of glucose transporters.

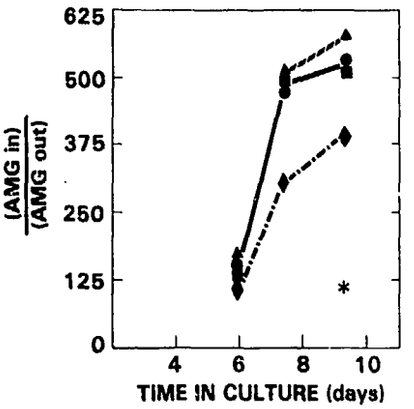

Fig. 3. Effect of glucose concentration on the AMG-concentrating capacity. Epithelia were grown (from day 0) in media containing: 5 mM glucose + 5 mM uridine (♦, ▲) and 5 mM uridine (●, ■), and 25 mM glucose (*). Some epithelia (♦, ●) were fed every 8 to 12 hr; the others were fed every 48 hr

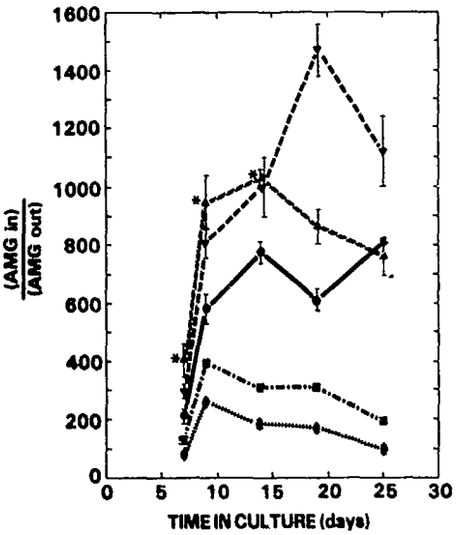

Fig. 4. The effect of different substrates in the growth medium on the AMG-concentrating capacity. 5 mM glucose (▲), 25 mM glucose (♦), 25 mM glucose + 5 mM uridine (■), 5 mM uridine (▼), 25 mM mannose (●), and 5 mM glucose + 5 mM uridine (*)

To identify the factor in the growth medium responsible for the regulation of glucose transport, we compared the effect of fresh medium with that of conditioned medium. The conditioned medium used in these experiments initially contained 5 mM glucose and was collected from LLC-PK$_1$ epithelia after 48 hr in culture. Consequently, it contained less than 0.1 mM glucose. It should also contain or be depleted of any other factors that signal the epithelium to develop more hexose transporters. Epithelia grown in the usual fashion in 5 mM glucose for 14 days were switched into either conditioned medium supplemented with 25 mM glucose or into fresh medium containing 25 mM glucose. As depicted in Fig. 2, conditioned medium supplemented with 25 mM glucose caused the same suppression of the AMG concentrating capacity as fresh medium containing 25 mM glucose. Since the conditioned medium should contain (or lack) any substance that was secreted into or depleted from the medium by the cells, we conclude that glucose, the only supplement, is the cause of the suppression of concentrating capacity observed in this experiment.

In an attempt to quantitatively relate the concentrating capacity of the cells to the concentration of glucose in the medium throughout the growth period, we used frequent feeding as a means of keeping the glucose concentration within known limits (albeit not constant). Epithelia were assigned to two groups. One group was fed with medium containing 5 mM glucose, the other with medium containing no glucose. Half the epithelia within each group were fed every 8–12 hr, the other as usual, every 48 hr. The concentration of glucose in the medium was monitored throughout the experiment. The glucose concentration in medium prepared to contain 5 mM and exchanged every 48 hr decreased below 0.1 mM after 15 hr (data not shown). By feeding the cells every 8–12 hr with medium containing 5 mM glucose, the concentration of glucose in the medium was maintained above 1 mM. All media in this experiment were supplemented with 5 mM uridine, which has been shown to support cell growth in the absence of glucose or other carbohydrates in the growth medium [3]. Fig. 3 depicts the result of this series of experiments. There is no difference between the concentrating capacity of epithelia fed in the customary fashion (every 48 hr) with 5 mM glucose and those fed with glucose-free medium containing uridine regardless of how often the latter were fed (cells were in media containing zero or less than 0.1 mM glucose most of the time). However, when the glucose concentration in the growth medium was kept above 1 mM by frequent feeding, the AMG concentrating capacity was lower. Cells which were grown in 25 mM glucose (where glucose concentration in the medium was always above 5 mM) attained even lower AMG-concentrating capacity, which indicates that the regulatory effect of the concentration of glucose is monotonic: the higher the concentration of glucose in the medium the lower the AMG-accumulating capacity achieved.

To test whether growth in the complete absence of glucose would evoke a higher AMG-concentrating capacity than growth in 5 mM glucose, we measured the AMG-concentrating capacity of epithelia fed medium without glucose but supplemented with 5 mM uridine for over 2 weeks (the time AMG-concentrating capacity reaches a plateau). Figure 4

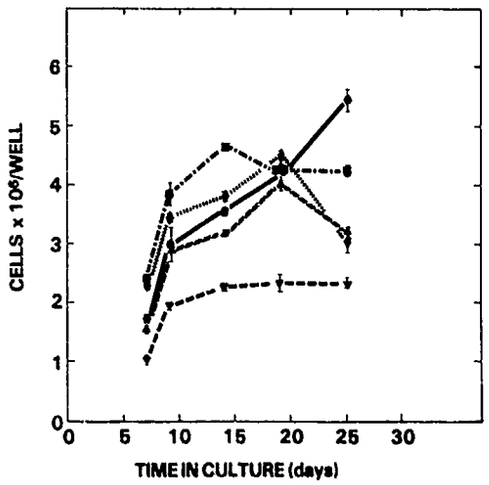

Fig. 5. Density of cells in different growth media. Number of cells per well (4 cm^2) as a function of time in culture. Data from experiment shown in Fig. 4

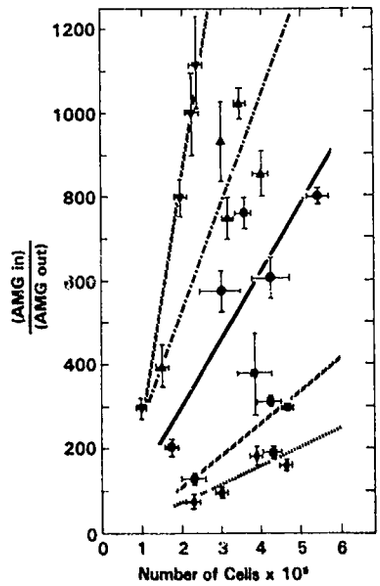

Fig. 6. The AMG-concentration capacity as a function of cell density. Data from Figs. 4 and 5. Lines drawn by linear regression analysis yield the following values for the accumulating capacity to 10^6 cell ratio (mean ± SE): 5 mM glucose, 643 ± 61 (▼); 25 mM glucose, 46 ± 6 (◆); 25 mM glucose + 5 mM uridine, 83 ± 17 (■); 5 mM uridine, 233 ± 34 (▲); 25 mM mannose, 143 ± 14 (●)

shows the concentrating capacity of cells as a function of days in culture in different media. Cells grown in 25 mM glucose exhibit the lowest AMG-concentrating capacity, whereas those grown in 5 mM glucose the highest. When uridine is added to medium containing 25 mM glucose it elicits a significant increase in the concentrating capacity of the epithelia. In contrast, when added to medium containing 5 mM glucose uridine does not affect the concentrating capacity of the epithelia over the first 2 weeks. The concentrating capacity of cells fed with uridine alone (5 mM) is not significantly different from the concentrating capacity of cells fed with 5 mM glucose alone, at least for the first 2 weeks after seeding.

The different growth conditions result in the formation of epithelia with different population densities, which also change with age. To evaluate the correlation between cell density and the AMG-concentrating capacity attained in these studies, we followed the change in cell number as a function of the carbohydrate concentration in the growth medium and time after subculture. In Fig. 5, we plot the number of cells per well as a function of time in the experiment depicted in Fig. 4. The number of cells per well increases with the concentration of carbohydrate in the medium. Regardless of composition of the medium, the density of cells in a well reaches a plateau at approximately the same time as the AMG-accumulating capacity. In Fig. 6, the concentrating capacity attained in the epithelia described in Fig. 4 is plotted as a function of the number of cells per well from Fig. 5. For each growth condition the epithelia attained a different concentrating capacity despite comparable cell density. However, in each medium there is a linear relationship between cell density and the AMG-concentrating capacity achieved: the higher the cell density the greater the AMG-concentrating capacity. This relationship appears to be independent of cell age; as shown in Fig. 5, in some cases cell density actually decreased with cell age.

Does the regulation involve a direct effect of the substrate on its carrier or is it a process in which the glucose concentration serves as a primary trigger? To address this question we replaced glucose in the growth medium with the metabolizable sugars mannose and fructose, which are not transported by the sodium-dependent hexose transporter [15], and AMG, which shares the transporter but is not metabolizable. The AMG-concentrating capacity achieved with 25 mM mannose is higher than the concentrating capacity the cells reached when fed with medium containing the same concentration of glucose (Fig. 4). Figure 7, shows the result of an experiment in which epithelia grown for 13 days in 25 mM glucose were switched to media containing either 5 mM glucose, 25 mM mannose, or 25 mM fructose or continued in 25 mM glucose. Clearly, mannose and fructose, sugars that are not substrates for the sodium coupled glucose transporter [15], had a modest effect like that of glucose in down regulating the AMG-concentrating capacity.

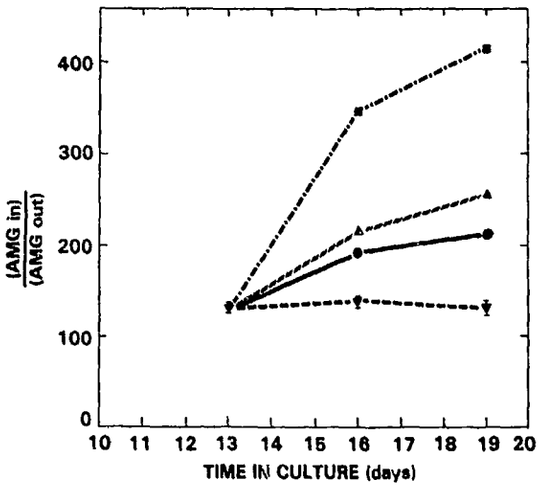

Fig. 7. AMG-concentrating capacity of epithelia grown for 13 days in medium containing 25 mM glucose and then switched to media supplemented with different hexoses. (●) 25 mM fructose, (▲) 25 mM mannose, (■) 5 mM glucose, and (▼) continued in 25 mM glucose

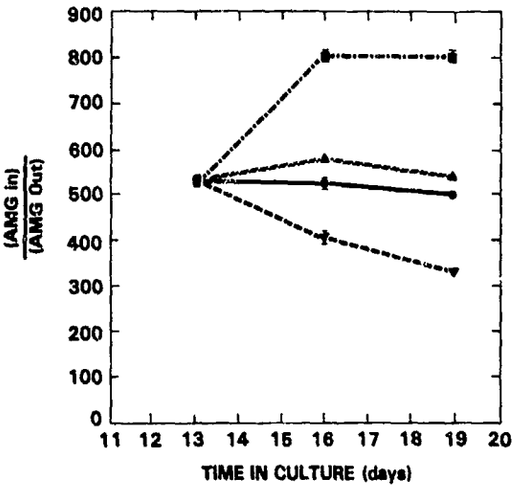

Fig. 8. AMG-concentrating capacity of epithelia grown for 13 days in medium containing 5 mM glucose and then switched to media supplemented with different hexoses: (●) 25 mM fructose, (▲) 25 mM mannose, (▼) 25 mM glucose, and (■) continued in 5 mM glucose

In a similar experiment (Fig. 8), we observed that switching epithelia grown in 5 mM glucose to media containing 25 mM mannose or 25 mM fructose results in a decrease in their concentrating capacity, which was, however, less than the decrease in epithelia switched into 25 mM glucose. Thus the absence of substrate-carrier interaction did not prevent the regulatory effect.

Next we tested the effect of a high concentration of AMG on the development of the concentrating capacity. Epithelia were grown for 14 days in medium containing 25 mM glucose. At that time one third of the epithelia were switched to medium containing 5 mM glucose, one third to medium containing 5 mM glucose + 20 mM AMG, and the remaining cells continued in medium containing 25 mM glucose. Uptake measurements in epithelia growing in media containing AMG will show a false reduction in AMG-concentrating capacity. AMG accumulating in the cells interferes with the uptake measurements unless the excess AMG is eliminated from the cells preceding the assay for AMG-concentrating capacity. Therefore AMG was chased by incubating the epithelia with medium containing 25 mM glucose for 4 hr prior to the assay. As we showed previously, no change in the concentrating capacity is detectable in less than 48 hr after changing the medium from one concentration of glucose to another [10]. Thus, 4 hr of 25 mM glucose did not affect the measurements. We found no difference between the concentrating capacity of cells grown in media containing either 5 mM glucose or 5 mM glucose + 20 mM AMG (245 ± 12 and 258 ± 10, respectively). Thus a substrate-carrier interaction with substrate in high concentration during incubation with low glucose did not suppress the development of high AMG-concentrating capacity. In view of the effect of mannose and fructose and the absence of an effect of AMG on the regulatory process, we conclude that the regulation does not require a direct interaction of the sugar substrate with the carrier, but involves another mechanism.

Discussion

In this study we deal with two main questions concerning the regulation of the sodium-coupled glucose transport system of LLC-PK$_1$ epithelia in culture: (i) Is the concentration of glucose in the medium the factor responsible for the regulation of the transport system? (ii) Is the regulation mediated by the effect of the substrate on its carrier, or rather some other mechanism?

Before addressing these two basic problems, other questions inherent in the tissue culture technique have to be resolved. In many cases, by manipulating the culture medium, one selects cells with certain properties. The possibility that the concentration of glucose in the growth medium promotes the growth of cells with certain glucose transport characteristics is always a possibility that has to be taken into account. The fact that a cloned cell line manifested the same basic regulatory characteristic makes this possibility very unlikely. In addition, the fact that the phenomenon of up and down

regulation is completely reversible upon changing the growth conditions also supports this conclusion.

Population density is also known to affect cell properties [11]. In the present work we find a linear relationship between the population density and the concentrating capacity within each treatment: the higher the population density the greater the AMG-concentrating capacity achieved. On the other hand, the differences in the AMG-concentrating capacity between cells grown in media containing 5 or 25 mM glucose are not the result of differences in population density.

To explore the nature of the extracellular regulatory signal, we used a conditioned medium in which cells that expressed increased AMG-concentrating capacity had been grown. The results eliminated all metabolites but glucose as the primary effector in the regulation. The only difference between the medium that caused an elevation in the concentrating capacity and the medium that suppressed it was the presence of a high concentration of glucose in the latter. By using frequent feeding for replenishment of consumed glucose, three growth conditions were created: (i) the concentration of glucose in the medium was virtually zero, (ii) it was maintained between 5 and 1 mM, and (iii) it was between 25 and 5 mM. The three growth conditions result in three different AMG-concentrating capacities related inversely to the glucose concentrations in the media.

In nonpolarized cells, such as fibroblasts, there is evidence that the metabolic state of the cell plays a role in the regulation of glucose transport [2, 18]. Our observation that sugars that are not transported by the sodium-dependent glucose transporter do affect the AMG-concentrating capacity of LLC-PK_1 epithelia, whereas a sugar that is transported by this transport system but is not metabolized does not, indicates that the regulation of this transport system involves hexose metabolism rather than an interaction with the transporter itself. One reasonable candidate for a second messenger in this regulatory system is intra- or extracellular pH. Since LLC-PK_1 epithelia have a high rate of glycolysis, cells grown in high glucose acidify the medium more than cells grown in low glucose. However, hydrogen ion concentration cannot completely explain the regulatory effect of medium glucose concentration since media that contained mannose or fructose became as acidic as the medium containing high glucose, yet the concentrating capacity was significantly higher in mannose or fructose media.

Although aspects of the regulation of the sodium-coupled hexose transport have been established, additional studies are required for further understanding. For example, it is not clear whether the electrochemical gradient for sodium entry across the apical membrane, i.e., the driving force for this hexose transport, is also regulated. Furthermore, it remains to be determined whether regulation occurs in mature cells or only in dividing cells.

This work was supported by Armed Forces Radiobiology Research Institute, Defense Nuclear Agency, under Research Work Unit MJ 00106. The views presented in this paper are those of the author. No endorsement by the Defense Nuclear Agency has been given or should be inferred.

A.M. was supported by a National Research Council Fellowship.

References

1. Amsler, K., Cook, J.S. 1982. Development of Na^+ dependent hexose transport in a culture line of porcine kidney cells. *Am. J. Physiol.* **242**:C94–C101
2. Bader, J.P., Brown, N.R., Ray, D.A. 1981. Increased glucose uptake capacity of Rous-transformed cells and the relevance of deprivation depression. *Cancer Res.* **41**:1702–1709
3. Burton, M.W., Reitzer, L.J., Kennell, D. 1981. The continuous growth of vertebrate cells in the absence of sugars. *J. Biol. Chem.* **256**:7812–7819
4. Cook, J.S., Amsler, K., Weiss, E.R., Shaffer, C. 1982. Development of Na^+ hexose transport *in vitro*. *In:* Membranes in Growth and Development. J.F. Hoffman, G. Giebisch, and L. Bolix, editors. pp. 551–567. A.R. Liss, New York
5. Hull, R.N., Cherry, W.R., Weaver, G.W. 1976. The origin and characteristics of a pig kidney cell strain LLC-PK_1. *In Vitro* **12**:670–677
6. Mills, J.W., Macknight, A.D.C., Jarrell, J.A., Dayer, J.M., Ausiello, D.A. 1981. Interaction of ouabain with the Na^+ pump in intact epithelial cells. *J. Cell Biol.* **88**:637–643
7. Misfeldt D.S., Sanders, M.J. 1981. Transepithelial transport in cell culture: D-glucose transport by a pig kidney cell line (LLC-PK_1). *J. Membrane Biol.* **59**:13–18
8. Misfeldt, D.S., Sanders, M.J. 1983. Transepithelial transport in cell culture: Stoichiometry of Na/phlorizin binding and Na/D-glucose cotransport. A two-step, two-sodium model of binding and translocation. *J. Membrane Biol.* **70**:191–198
9. Moran, A., Handler, J.S., Turner, R.J. 1982. Na^+ dependent hexose transport in vesicles from cultured renal epithelial cell line. *Am. J. Physiol.* **243**:C293–C298
10. Moran, A., Turner, R.J., Handler, J.S. 1983. Regulation of sodium coupled glucose transport by glucose in a cultured epithelium. *J. Biol. Chem.* **258**:15087–15090
11. Mullin, J.M., Weibel, J., Diamond, L., Kleinzeller, A. 1980. Sugar transport in the LLC-PK_1 renal epithelial cell line: Similarity to mammalian kidney and the influence of cell density. *J. Cell Physiol.* **104**:375–389
12. Rabito, C.A. 1980. Phosphate transport by a kidney epithelial cell line. *J. Gen. Physiol.* **76**:20a
13. Rabito, C.A. 1981. Localization of the Na^+ sugar cotransport system in a kidney epithelial cell line (LLC-PK_1). *Biochim. Biophys. Acta.* **649**:286–297
14. Rabito, C.A., Karish, M.V. 1982. Polarized amino acid transport by an epithelial cell line of renal origin (LLC-PK_1). The basolateral system. *J. Biol. Chem.* **257**:6802–6808

15. Sanders, M.J., Simon, L.M., Misfeldt, D.S. 1982. Transepithelial transport in cell culture: Bioenergetics of Na, D-glucose coupled transport. *J. Cell Physiol.* **114**:263-266
16. Turner, R.J., Moran, A. 1982. Heterogeneity of sodium dependent D-glucose transport sites along the proximal tubule. *Am. J. Physiol.* **242**:F406–F414
17. Turner, R.J., Moran, A. 1982. Further studies of proximal tubular brush border membrane D-glucose transport heterogeneity. *J. Membrane Biol.* **70**:37–45
18. Ullrey, D., Gammon, M.T., Kalckar, H.M. 1975. Uptake patterns and transport enhancements in cultures of hamster cells deprived of carbohydrates. *Arch. Biochem. Biophys.* **167**:410–416

Received 2 February 1984; revised 21 June 1984

Reprint from

Agents and Actions

Plasma histamine and hemodynamic responses following administration of nalbuphine and morphine

S. M. Muldoon, M. A. Donlon, R. Todd, E. A. Helgeson and W. Freas (USA)

Vol. 15
No. 3/4
October 1984
pages 229–234

Birkhäuser Verlag
Basel · Boston · Stuttgart

Agents and Actions, vol. 15, 3/4 (1984)

Plasma histamine and hemodynamic responses following administration of nalbuphine and morphine

S.M. MULDOON,* M.A. DONLON,† R. TODD,* E.A. HELGESON,† and W. FREAS*

* Department of Anesthesiology, Uniformed Services University of the Health Sciences, Bethesda, MD 20814, USA
† Department of Biochemistry, Armed Forces Radiobiology Research Institute Bethesda, MD 20814, USA

Abstract

A comparative study of plasma histamine levels following administration or morphine and nalbuphine in pentobarbital anesthetized dogs was performed. Two concentrations, 3 mg/kg and 0.3 mg/kg of these drugs were investigated. High dose morphine caused an immediate marked increase in plasma histamine from 5.0 ± 0.4 to 340 ± 72 ng/ml. Simultaneous with this increase in plasma histamine was a marked decrease in mean arterial blood pressure within the first minute. In contrast significant alterations in plasma histamine levels were not observed with high or low doses of nalbuphine. A low dose of morphine (0.3 mg/kg) did not increase plasma histamine levels. Heart rate was not changed by any drug treatment. The use of compound 48/80 a specific mast cell degranulating agent allowed for the identification of a specific pool of mast cells capable of responding to morphine. *In vitro* exposure of purified dog leukocytes to high doses of morphine did not result in histamine release. These results indicate that nalbuphine does not increase plasma histamine, while morphine does, and that the source of the increase in plasma histamine is from tissue mast cells.

Introduction

Moderate to large doses of opiates are being increasingly used either as principal anesthetic agents or to supplement general anesthesia particularly for patients with minimal circulatory reserve [1–4]. However, the usefulness of morphine, a pure opiate receptor agonist is limited because of significant hemodynamic alterations, particularly hypotension most commonly attributed to histamine release [5, 6]. In contrast, it has been recently reported that the synthetic narcotic agonist–antagonist analgesic nalbuphine even in high doses does not cause significant hemodynamic alterations in man [7].

This work has been supported in part by NIH grant GM 25926 and USUHS grant RO8004.

We postulated that the differences between nalbuphine and morphine may be related to their capability to release histamine *in vivo*. The present study was undertaken to determine the quantitative effect of intravenous administration of nalbuphine, as compared to similar doses of morphine on plasma histamine levels, and mean arterial pressure. In addition selected *in vitro* studies using purified dog leukocytes were performed to delinate the source of elevated plasma histamine following treatment with morphine.

Methods

Twenty-one mongrel dogs of either sex were anesthetized with sodium pentobarbital 30 mg/kg i.v. A femoral artery cannula was utilized for continuous direct measurement of arterial blood pressure and for periodic sampling of blood for gas analysis. Heart rate was calculated from the arterial pressure tracing. The right femoral vein was cannulated for drug and fluid administration. All animals were given 5% dextrose in lactated Ringer's solution at an approximate rate of 18 ml/kg/h for the duration of the experiment. To obtain venous blood for determination of plasma histamine levels, the contralateral femoral vein was cannulated and the tip of this cannulae was advanced into the inferior vena cava. An endotracheal tube was inserted in all animals and ventilation controlled with a Harvard respiratory pump. Arterial blood gases were repeatedly checked and Pao_2, $Paco_2$ and pH was maintained within normal limits. Animals that became severely hypotensive and developed metabolic acidosis were administered increments of sodium bicarbonate, to return pH to normal levels. Rectal temperature was maintained at 37°C by use of a heating blanket.

Experimental design

The effect of administration of two concentrations (0.3 and 3 mg/kg in 6.0 ml saline solution) of nalbuphine or morphine was determined in anesthetized dogs. Venous blood samples from plasma histamine determinations were obtained approximately 30 min post induction of anesthesia.

Following administration of nalbuphine or morphine samples for plasma histamine determinations were obtained at the following time intervals: 0.5, 1, 5, 10, 15, 20, 30, 45, 60, and 120 min. Blood samples were removed with plastic syringes via stopcocks connected to the catheters and transferred to chilled collection tubes containing disodium ethylenediaminetetraacetate (EDTA). The tubes were inverted gently and stored on ice. The blood was centrifuged for 10 min at 3000 r.p.m. within 1 h following removal from the dog. Then plasma was transferred to polypropylene tubes and frozen at −80°C until analyzed. Plasma histamine content was determined after treatment with 0.4 *N* perchloric acid. The samples were centrifuged at 13,000 × *g* for 45 min and the supernatant was analyzed for histamine content using the Technicon II automated fluorometric technique developed by SIRAGANIAN [8, 9]. To verify that the fluorescent compound in plasma seen after drug treatment was authentic histamine, 7.5 units of diamine oxidase (DAO) (Sigma Chem. Co.) was added to 500 µl of plasma and incubated for 60 min at 37°C. The reaction was terminated by the addition of perchloric acid (final concentration 0.4 *N*) and treated in an identical manner as the non-DAO samples. DAO degrades histamine and allows the subtraction of any non-specific background fluorescence which is not attributed to histamine. Basal plasma histamine values in each animal were not affected by morphine, nalbuphine or by addition of the histamine releasing agent compound 48/80 to the sample. Two hours post administration of nalbuphine and morphine, the compound 48/80 (0.5 mg/kg i.v.) was administered. Blood samples for plasma histamine were withdrawn at 1, 2, 4, 7, and 10 min following this treatment.

Blood leukocyte histamine release

Histamine release measurements were made on dextran purified leukocytes obtained by fractionation of 100 ml of whole dog blood. The leukocyte layer was collected and washed twice in Hanks balanced salt solution (25°C) as described by MAY et al. [10], and the cells counted on a Coulter counter. Cell suspensions were then divided, centrifuged, and the cell pellets resuspended in prewarmed (37°C) Tyrode's buffer (0.033% fatty acid free bovine serum albumin) containing either morphine (1×10^{-3} *M*), nalbuphine (1×10^{-3} *M*) or buffer controls. The cells were incubated (37°C) for 30 min. The reaction was terminated by centrifugation (1000 r.p.m., 5 min) and the supernatants were removed. The cell pellet was resuspended in distilled water and heated at 90°C for 10 min. The supernatants and pellets were stored frozen (−70°C) until histamine analysis. Neither morphine nor nalbuphine interfered with the fluorometric analysis of histamine under the experimental conditions employed. The percent histamine release for each sample was determined by calculation according to the following formula:

$$\% \text{ histamine release} = \frac{\text{supernatant histamine}}{\text{total histamine}} \times 100\%.$$

Analysis of data

Mean values are given, with standard error of the mean. For statistical evaluation of the data Student's *t* test was used. *P* values less than 0.05 were considered significant.

Results

Plasma histamine levels and the associated changes in mean arterial pressure (MAP) following an acute administration of morphine (3 mg/kg i.v.) are shown in Fig. 1. An immediate and maximal increase in plasma histamine from 5.0 ± 0.4 ng/ml to 340.5 ± 72.2 ng/ml was observed within the first minute post-injection. This was followed by a continued gradual decline in plasma histamine levels to 81.3 ± 18.9 ng/ml at 10 min with a return to pre-morphine levels after 60 min. Simultaneous with the initial maximal increase in plasma histamine levels was an immediate and marked decrease in MAP from 115 ± 7 mmHg to 29 ± 4 mmHg at 1 min post-injection. At this time there was a significant correlation between the change in plasma histamine levels and MAP depression ($r = -0.95$). Following the initial rapid decrease, MAP increased slowly to 34 ± 2 mmHg at 5 min, and 64 ± 8 mmHg at 30 min post-injection. At 60 min when plasma histamine levels had returned to basal levels, MAP (89 ± 8 mmHg) had not returned to pre-injection levels and even at 120 min MAP remained significantly depressed. Morphine administration did not cause a significant change in heart rate within the first 30 min; heart rate was however significantly elevated at 60 and 120 min post drug.

A strikingly different pattern of plasma histamine values and MAP was observed following

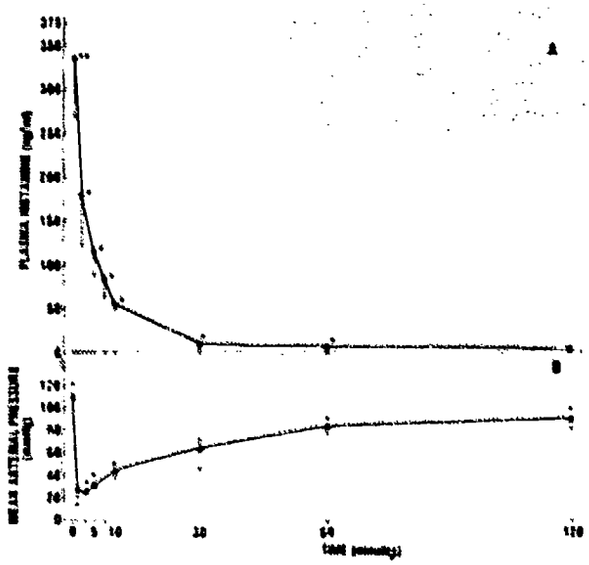

Figure 1
Time course of plasma histamine ● (A), and MAP ▲ (B) measurements in dogs administered 3 mg/kg morphine sulphate i.v. ($n = 6$). Data presented as mean + SEM. * Indicates significant difference from pre-morphine levels $P < 0.05$; ** $P < 0.01$.

the i.v. administration of nalbuphine 3 mg/kg (Fig. 2). Significant alterations in plasma histamine level were not observed in any of these animals at any time intervals. However, in the six animals studied a small decrease in MAP was observed within the first minute from 108.7 ± 9.9 mmHg to 98.7 ± 8.7 mmHg, but at all subsequent intervals the MAP remained constant. There was no significant changes in heart rate.

Three animals served as control shams for these studies and the results are presented in the Table. Blood samples were drawn for plasma histamine at similar time intervals as in the drug-treated groups. There were no significant changes in plasma histamine, heart rate or MAP measurements during the duration of the experiment.

Two other groups of animals ($n = 3$) received a lower concentration of morphine (0.3 mg/kg) and nalbuphine (0.3 mg/kg i.v.). There was no significant change in plasma histamine or MAP with these concentrations.

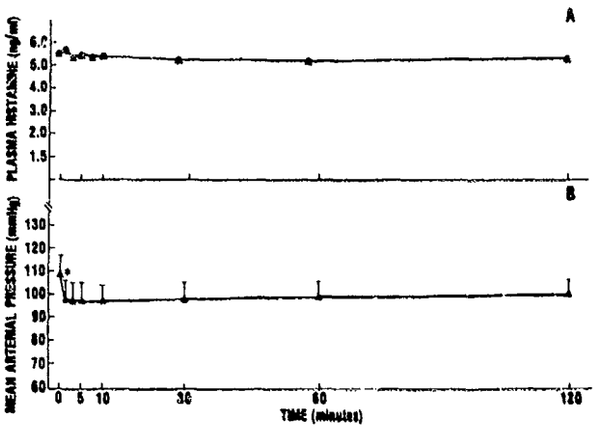

Figure 2
Time course of plasma histamine ● (A), and MAP ▲ pressure (B) measurement in dogs administered 3 mg/kg nalbuphine i.v. ($n = 6$). Results presented as mean ± SEM *Indicates significant difference from pre-nalbuphine value.

In order to compare the response of mast cells in the high dose morphine-treated and control animals compound 48/80 a specific mast cell degranulating agent was administered i.v. (0.5 mg/kg) at 120 min. As shown in Fig. 3 at 1 min post-injection there was no difference in the initial rate of appearance of histamine in plasma between the two groups. However, at all subsequent time intervals the response of morphine-treated animals was depressed as compared to control animals. Nalbuphine-treated animals responded to 48/80 in a manner similar to control dogs.

To further investigate the source of plasma histamine in morphine-treated animals, canine leukocytes were purified and exposed to high

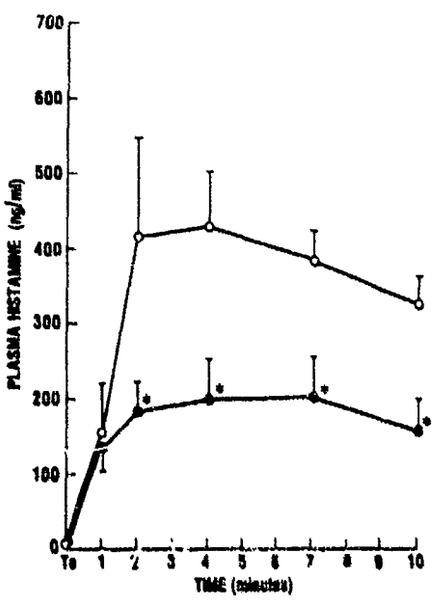

Figure 3
Comparison of plasma histamine response to compound 48/80 (0.5 mg/kg i.v.) in dogs pre-treated with morphine (3 mg/kg i.v.) closed circles, and sham-injected animals (6 ml saline) open circles ($n = 3$ in each group). Data presented as mean ± SEM. *Indicates significant difference between the control and morphine-treated groups.

Table
Effect of sham injection on plasma histamine and mean arterial pressure (MAP).

Minutes after sham injection	−5	1	2	4	10	30	120
Histamine ng/ml	4.05 ± 0.26	3.83 ± 0.60	4.12 ± 0.24	4.16 ± 0.11	3.70 ± 0.37	3.96 ± 0.13	4.22 ± 0.39
MAP	98.7 ± 2.9	96.7 ± 5.7	96.7 ± 5.7	96.0 ± 4.0	100.7 ± 4.4	109.7 ± 6.5	109.0 ± 0.3

Results are expressed as mean ± SEM ($n = 3$).
Sham injection is 6 ml of normal saline (the vehicle for morphine and nalbuphine).

concentrations (1×10^{-3} *M*) of morphine (Experiment I) and nalbuphine (Experiment II) *in vitro*. Leukocytes were incubated (37°C, 30 min) in either buffer only, nalbuphine, or morphine. The percent histamine release in Experiment I was 2.8%, 3.6% and 5.5% and Experiment II was 0.6%, 1.0% and 1.0%, respectively. The results from two separate histamine release experiments showed no substantial histamine release in cells exposed to these drug concentration.

Discussion

This study demonstrates unequivocally that nalbuphine even in doses up to 3 mg/kg does not increase in plasma histamine when administered to anesthetized dogs. In contrast, equivalent doses of morphine elicit profound alterations in both plasma histamine and mean arterial blood pressure. Morphine has been shown to increase plasma histamine levels both in man and animals [5, 6, 11], and this increase is considered to be the main causative factor in hypotensive episodes following morphine administration [6]. Further, H_1 and H_2-receptor antagonists attenuate the hypotensive response to morphine [12]. The results of this study indicate a high correlation between the initial increase in plasma histamine, and the decrease in the mean arterial pressure within the first minute following administration of morphine. Correlations between these two parameters after 1 min, however, did not demonstrate a high correlation coefficient. Since the metabolism of histamine in plasma occurs extremely rapidly ($T_{1/2} \approx 1.8$ min) [13], additional experiments are necessary to explain the substained decrease in blood pressure which was unrelated to the plasma histamine levels.

For accurate fluorometric determination of plasma histamine, non-specific background must be subtracted from the sample fluorescence. Two methods for determining this non-specific background fluorescence involve the use of the enzymes diamine oxidase (DAO) and histamine methyl transferase (HMT). LORENZ et al. [14] compared these two methods and demonstrated that the procedure utilizing HMT results in lower authentic histamine values in plasma than those obtained using DAO. In the present studies the basal plasma histamine levels in the dog were not treated with DAO. These values (4 to 6 ng/ml) are therefore higher than those reported following treatment with either DAO or HMT [14]. Although the fluorescence assay of SIRAGANIAN [8, 9] is not a highly specific test for authentic plasma histamine, the reported increases in these values with morphine and compound 48/80 are attributed to authentic histamine, since DAO treatment returned these to pretreatment basal values. Further confirmation that the plasma compound released by morphine and compound 48/80 is indeed histamine, is demonstrated by the simultaneous decrease in mean arterial blood pressure coincident with the elevation in plasma histamine. Decreases in arterial blood pressure with elevations in plasma histamine obtained either by release of histamine from endogenous stores [12], or following administration of exogenous histamine are well documented physiological responses [15].

Despite the fact that the plasma histamine levels were markedly elevated and blood pressure markedly depressed, the heart rate was unchanged during the first 30 min post-morphine. Histamine-induced increases in heart rate are known to exhibit a high degree of species specificity, and it has been previously reported that dog heart rate is non-responsive to doses of histamine that produce marked changes in blood pressure [15, 16]. Furthermore, in dogs treated with high doses of compound 48/80 (1 mg/kg) no increases in heart rate were observed in the first 15 min in spite of the fact that blood pressure had decreased by more than 50% [17].

Systemic administration of compound 48/80, a synthetic polyamine results in a marked hypotensive response and increased plasma histamine levels in a variety of experimental animals [18]. This response is accompanied by a profound degranulation of mast cells in specific tissues of the body and a resultant depletion of histamine content in these areas [19–21]. Compound 48/80 was used for two purposes in the experimental design. First, to demonstrate that animals previously treated with high doses of nalbuphine were indeed capable of responding to this specific mast cell degranulating agent, and secondly, as a pharmacological tool to identify the origin of the plasma histamine observed following high dose morphine administration. We reasoned that morphine may deplete a preexisting pool of compound 48/80 sensitive mast cells within these animals and the subsequent administration of a predetermined amount of compound 48/80 (0.5 mg/kg) may allow us to identify this pool. It is well documented that the ability of compound 48/80 to release histamine is tissue and species

specific [22, 23]. For example, rat intestinal cells are unresponsive to this compound [24], as well as lung mast cells and circulating basophils in a variety of species [25].

In the present experiments there is no significant difference in the initial response to compound 48/80 during the first minute in both control and drug-treated animals. However, after the first minute a striking difference is seen in the flattened response of the morphine-treated animals which implies that morphine releases histamine from the same mast cell stores as compound 48/80 i.e. from skin and muscles as has been shown by PATON [26].

Further evidence to support this hypothesis is obtained from studies on histamine release utilizing isolated dog leukocytes. The basophil is another potential source of plasma histamine in morphine-treated animals. Dogs have an extremely low whole blood histamine content due to a low concentration of basophils in their blood [27]. Administration of morphine to the *in vitro* leukocyte preparation did not effect histamine release from these cells. These *in vitro* results together with the compound 48/80 *in vivo* study support the conclusion that the increases in plasma histamine observed following systemic morphine administration is derived from mast cells.

Nalbuphine is a new narcotic analgesic that is chemically and pharmacologically related to both the opioid oxymorphine, and the narcotic antagonist, naloxone [28]. Following intramuscular injections in man BEAVER and FEISE [29] reported that nalbuphine is as effective as morphine with the same onset, peak and duration of action. Its advantages over morphine are a lower abuse potential, less respiratory depression [30], and little hypotensive effect in patients with acute myocardial infarction [31]. LAKE et al. [7] examined the cardiovascular effects of nalbuphine administered intravenously to patients with myocardial disease. Acute administration of a high dose of nalbuphine (2–3 mg/kg) did not cause significant changes in any of the major hemodynamic variables; however, at these concentrations morphine does produce significant changes in hemodynamic patterns [3, 12].

The small decrease in mean arterial pressure following administration of nalbuphine is not believed to be the result of small undetectable changes in histamine levels [13], but rather to a direct venodilating action of nalbuphine on the vascular tissue. High concentrations of nalbuphine have been shown to inhibit release of endogenous norepinephrine in isolated veins and may therefore cause decrease in venomotor tone [32].

In summary, the results of this study indicate that nalbuphine unlike morphine does not increase plasma histamine or cause major decreases in arterial blood pressure, which suggests that nalbuphine may be a logical alternative to morphine when high dose narcotic anesthesia is desired.

Received 25 June 1983.

References

[1] E. LOWENSTEIN, P. HALLOWELL, F.H. LEVINE, W.M. DAGGETT, W.G. AUSTEN and M.B. LAVER, *Cardiovascular response to large doses of intravenous morphine in man*, New Engl. J. Med. *281*, 1389–1393 (1969).

[2] T.H. STANLEY, N.H. GRAY, W. STANFORD and R. ARMSTRONG, *The effect of high dose morphine on fluid and blood requirements in open heart operations*, Anesthesiology *38*, 536–541 (1973).

[3] K.C. WONG, W.E. MARTIN, T.F. HORBEIN, F.G. FREUND and J. EVERETT, *The cardiovascular effect of morphine with oxygen and with nitrous oxide in man*, Anesthesiology *38*, 542–549 (1973).

[4] T.H. STANLEY and L.R. WEBSTER, *Anesthetic requirement and cardiovascular effect of fentanyl oxygen and fentanyl diazepam oxygen anesthesia in man*, Anesth. Analg. (Cleve) *57*, 411–416 (1978).

[5] J.E. ECKENHOFF and S.R. OECH, *The Effects of narcotics and antagonist upon respiration and circulation in man*, Clin. Parmac. Ther. *1*, 483–524 (1960).

[6] C.E. ROSOW, J. MOSS, D.M. PHILBIN and J.J. SAVARESE, *Histamine release during morphine and fentanyl anesthesia*, Anesthesiology *56*, 93–96 (1982).

[7] C.L. LAKE, E.N. DUCKWORTH, C.A. DIFAZIO, C.G. DURBIN and M.R. MAGRUDER, *Cardiovascular effects of nalbuphine in patients with coronary or valvular heart disease*, Anesthesiology *37*, 498–503 (1982).

[8] R.P. SIRAGANIAN, *An automated continuous-flow system for the extraction and fluorometric analysis of histamine*, Analyt. Biochem. *57*, 383–394 (1974).

[9] R.P. SIRAGANIAN, Histamine release and assay methods for the study of human allergy. In *Manual of Clinical Immunology*, pp. 603–625. (Eds N.R. ROSE and H. FRIEDMAN) American Society for Microbiology, Washington, DC 1976.

[10] C.D. MAY, M. LYMAN, R. ALBERTO and F. CHENG, *Procedures for immunochemical study of histamine release from leukocytes with small blood volume*, J. Allergy *46*, 12–20 (1970).

[11] J.E. SCHURIG, R.L. CAVANAGH and J.P. BUYNISKI, *Effect of butorphanol and morphine on pulmonary mechanics, arterial blood pressure and venous plasma histamine in the anesthetized dog*, Archs. int. Pharmacodyn. Ther. *233*, 296–304 (1978).

[12] D.M. PHILBIN, J. MOSS, C.W. AKINS, C.E. ROSOW, K. KONO, R.C. SCHNEIDER, T.R. VERLEE and J.J.

SAVARESE, *The use of H_1 and H_2 histamine antagonists with morphine anesthesia: a double-bind study*, Anesthesiology *55*, 292–296 (1981).

[13] W. LORENZ, H. BARTH, M. THERMANN, A. SCHMAL, P. DORMANN and I. NIEMEYER, *Fluorometric histamine determination in canine plasma under normal conditions, following application of exogenous histamine, and during histamine release by Haemaccel*, Hoppe-Seyler's Z. Physiol. Chem. *355*, 1097–1111 (1974).

[14] W. LORENZ, M. THERMANN, K. MESSMER, A. SCHMAL, P. DORMANN, J. KUSCHE, H. BARTH, R. TAUBER, M. HUTZEL, G. MANN and R. UHLIG, *Evaluation of histamine elimination curves in plasma and whole blood of several circulatory regions: a method for studying kinetics of histamine release in the whole animal*, Agents and Actions *4*, 336–356 (1974).

[15] D.A.A. OWEN, C.A. HARVEY and M.J. BOYCE, *Effects of histamine on the circulatory system*, Klin. Wschr. *60*, 972–977 (1982).

[16] J.P. TRZECIAKOWSKI and R. LEVI, *Cardiac histamine: a mediator in search of a function*, Trends in Pharmacol. Sciences *2*, 14–17 (1981).

[17] J.W. CONSTANTINE and W.S. LEBEL, *Histamine release in dogs by Emulphor EL620*, Experientia *35*, 338–339 (1978).

[18] W. KAZIMIERCZAK and B. DIAMONT, *Mechanisms of histamine release in anaphylactic and anaphylactoid reactions*, Prog. Allergy *24*, 295–365 (1978).

[19] P.B. DEWS, A.L. WNUCK, R.V. FANELLI, A.E. LIGHT, J.A. TORNABER, S. NORTON, C.H. ELLIS and E.J. DEBEER, *The pharmacology of 48/80 a long acting vasodepressor drug*, J. Pharmac. exp. Ther. *107*, 1–11 (1953).

[20] A.N. SMITH, *Release of histamine by the histamine liberator compound 48/80 in cats*, J. Physiol., Lond. *121*, 517–538 (1953).

[21] W. FELBERG and J. TALESNIK, *Reduction of tissue histamine by compound 48/80*, J. Physiol. Lond. 20, 550–568 (1953).

[22] W. LORENZ, J.V. PARKIN, H. ROHDE, H. BARTH, H. TROIDL, K. THON, E. HINTERLANG, D. WEBER, R. ALBRECHT and H. ROHER, Histamine in gastric secretory disorders: the relevance of the mucosal histamine content and the origin of histamine in gastric aspirate. In *Gastric Secretion, Basic and Clinical Aspects* (Eds S.J. KONTUREK and W. DOMSCHKE). Georg Thieme Verlag, Stuttgart–New York, Thieme-Stratton Inc., New York 1981.

[23] W. LORENZ, K. MOHRI, H.-J. REIMANN, H. TROIDL, H. ROHDE and H. BARTH, Intramucosal mechanisms: relevance of the mast cell concept, Inter. Congress Series 537, *Advances in Ulcer Disease*, pp. 177–191. Excerpta Medica, Amsterdam–Oxford–Princeton 1981.

[24] L. ENERBACK, *Mast cells in rat gastrointestinal mucosa. III. Reactivity towards compound 48/80*, Acta Path. Microbiol. Scand. *66*, 316 (1966).

[25] F.L. PEARCE, *Mast cell heterogeneity*, Trends in Pharmacol. Sciences *4*, 165–166 (1983).

[26] W.D.M. PATON, *The release of histamine*, Prog. Allergy *5*, 79–148 (1958).

[27] W. LORENZ and A. DOENICKE, *Histamine release in clinical conditions, The Mount Sinai*, J. Med. *45*, 357–386 (1978).

[28] R.R. MILLER, *Evaluation of nalbuphine hydrochloride*, Am. J. Hosp. Pharm. *37*, 942–949 (1980).

[29] W.T. BEAVER and G.A. FEISE, *A comparison of the analgesic effect of intramuscular nalbuphine and morphine in patients with postoperative pain*, J. Pharmac. Exp. Ther. *204*, 487–496 (1978).

[30] A ROMAGNOLI and A.S. KEATS, *Ceiling effect for respiratory depression by nalbuphine*, Clin. Pharmac. Ther. *27*, 478–485 (1980).

[31] G. LEE, R.I. LOW, E.A. AMSTERDAM, A.N. DEMARIA, P.W. HUBER and D.T. MASON, *Hemodynamic effects of morphine and nalbuphine in acute myocardial infaction*, Clin. Pharmac. Ther. *29*, 576–581 (1981).

[32] S.M. MULDOON, J. OTTO, W. FREAS and R.L. WATSON, *The effect of morphine, nalbuphine and butorphanol on adrenergic function in canine saphenous veins*, Anesth. Analg. *62*, 21–28 (1983).

0022-3565/85/2322-0413$00.00/0
THE JOURNAL OF PHARMACOLOGY AND EXPERIMENTAL THERAPEUTICS

Actions of Ethanol on Voltage-Sensitive Sodium Channels: Effects on Neurotoxin-Stimulated Sodium Uptake in Synaptosomes

MICHAEL J. MULLIN[1] and WALTER A. HUNT

Behavioral Sciences Department, Armed Forces Radiobiology Research Institute, National Naval Medical Center, Bethesda, Maryland

Accepted for publication October 30, 1984

ABSTRACT

Exposure of rat brain synaptosomes to ethanol *in vitro* reduced the neurotoxin-stimulated uptake of $^{22}Na^+$. This effect of ethanol was concentration-dependent, occurred with concentrations of ethanol achieved *in vivo* and was fully reversible. The inhibitory effect of ethanol on neurotoxin-stimulated sodium uptake was due to a decrease in the maximal effect of the neurotoxins. Ethanol reduced the rate of batrachotoxin-stimulated sodium uptake when measured at 3, 5 and 7 but not 10 or 20 sec after the addition of $^{22}Na^+$. In a series of aliphatic alcohols, there was a good correlation between potency for inhibition of batrachotoxin-stimulated $^{22}Na^+$ uptake and the membrane/buffer partition coefficient, suggesting that a hydrophobic site in the membrane was involved in the action of the alcohols. Ethanol did not affect the scorpion venom-induced enhancement of batrachotoxin-stimulated sodium uptake. The inhibitory potency of tetrodotoxin was also unaffected by ethanol. These results demonstrate that ethanol has an inhibitory effect on neurotoxin-stimulated sodium influx occurring in voltage-sensitive sodium channels of brain tissue.

The exact mechanisms by which ethanol causes depression of the CNS and the subsequent behavioral manifestations of intoxification remain undefined. In recent years, a great deal of research has focused on the effects of ethanol on the physical properties of artificial and biological membranes (Seeman, 1972; Goldstein *et al.*, 1980). Through the use of techniques such as electron paramagnetic resonance (Chin and Goldstein, 1977a) and fluorescence spectroscopy (Harris and Schroeder, 1981), it has been demonstrated that pharmacologically relevant concentrations of ethanol *in vitro* cause disordering of membrane lipids as inferred from the measurements of the properties of molecular probes inserted into membranes. By using a variety of molecular probes that insert at different depths in the membrane, it has been shown that the fluidizing effect of ethanol is greater at the hydrophobic inner core than at the superficial membrane surface (Chin and Goldstein, 1981; Harris and Schroeder, 1981). This is somewhat surprising because ethanol is a relatively small, neutral, hydrophilic molecule.

Further evidence that membrane disordering is involved in the intoxicating effects of ethanol has been based on a number of studies that have provided genetic (Goldstein *et al.*, 1982), pharmacological (Lyon *et al.*, 1981) and temporal (Chin and Goldstein, 1977b) correlations between *in vivo* effects and the membrane disordering effect of ethanol *in vitro*. However, because the magnitude of membrane lipid disordering by ethanol is relatively small (Chin and Goldstein, 1977a), it is probable that membrane-mediated biological responses would involve functional entities in membranes. Consequently, ethanol would be expected to interact directly or indirectly with these entities, so that alterations in the functional properties of membrane proteins may also play an important role in the changes in neuronal activity and synaptic function associated with ethanol-induced depression of the CNS. Alterations in lipid fluidity are known to influence the activities of membrane proteins (Lenaz, 1977) and this may represent a mechanism by which the lipid disordering effect of ethanol could be translated into the biochemical and behavioral effects of ethanol.

In the present study, a basic functional unit related to neuronal excitation was investigated with respect to its possible involvement in the actions of ethanol on the brain. An important mechanism in the control of neuroexcitability is the regulation of ion movements at the level of the excitable membrane. Using the squid giant axon, Hodgkin and Huxley (1952) demonstrated that the changes in membrane voltage associated with an action potential were due to a transient increased

Received for publication April 30, 1984.
[1] Supported in part by a Postdoctoral Fellowship from the National Academy of Sciences/National Research Council.

ABBREVIATIONS: CNS, central nervous system; TTX, tetrodotoxin; BTX, batrachotoxin; VER, veratridine; ScV, scorpion venom; HEPES, 4-(2-hydroxyethyl)-1-piperazineethanesulfonic acid.

permeability to sodium followed by an increased permeability to potassium. Apparently, separate channels are utilized by sodium and potassium ions (Hille, 1970; Ulbricht, 1977). The inward movement of sodium ions during excitation occurs through voltage-sensitive sodium channels. The sodium channels that traverse the excitable membrane are composed of complex glycoproteins with multiple polypeptide subunits and contain three distinct receptor sites for various neurotoxins (Catterall, 1980). One receptor site, thought to be located on the extracellular side of the channel (Narahashi, 1966), binds the specific inhibitors saxitoxin and TTX which inhibit the inward movement of sodium (Ritchie and Rogart, 1977). The second neurotoxin receptor site binds the lipid soluble toxins, BTX and VER, which cause persistent activation of sodium channels by blocking the process of channel inactivation and by shifting the voltage-dependence of channel activation to more negative membrane potentials. The third neurotoxin receptor binds small polypeptide toxins present in sea anemone and ScVs. The polypeptide toxins slow channel inactivation and also enhance the effects of BTX and VER. Because the neurotoxins bind to their receptor sites with high affinity and specificity, they have been widely used as chemical tools to study the structure and functional properties of voltage-sensitive sodium channels in a variety of excitable membranes (Narahashi, 1974; Catterall, 1982).

We have studied the effects of ethanol *in vitro* on the functional properties of voltage-sensitive sodium channels in whole rat brain synaptosomes. Ion flux measurements were used as an estimate of sodium ($^{22}Na^+$) ion permeability to assess the function of synaptosomal sodium channels.

Methods

Animals and chemicals. Male Sprague-Dawley rats (200–400 g) were obtained from Charles River Breeding Laboratories, Inc. (Wilmington, MA) and were housed two per cage with free access to water and standard laboratory chow before being used for the experiments. Chemicals and suppliers were as follows: ScV (Leiurus quinquestriatus), TTX and VER from Sigma Chemical Co. (St. Louis, MO); carrier-free $^{22}NaCl$ from New England Nuclear (Boston, MA). BTX was kindly supplied by Dr. John Daly (National Institute of Arthritis, Metabolism and Digestive Diseases, National Institutes of Health, Bethesda, MD). All other chemicals were obtained from commercial sources and were of analytical grade.

Preparation of synaptosomes. A crude synaptosomal (P_2) fraction was prepared by a modification of the method of Gray and Whittaker (1962). Rats were decapitated and the whole brains were removed and homogenized in ice-cold 0.32 M sucrose and 5 mM K_2HPO_4, pH 7.4 (10 ml/g wet wt.), with 10 strokes of a motor-driven Teflon-glass homogenizer. The homogenate was then centrifuged at 1000 × *g* for 10 min. The resulting supernatant was then centrifuged at 17,000 × *g* for 60 min. The final pellet was resuspended in ice-cold incubation buffer (8–10 ml/brain) containing (millimolar): KCl, 5.4; $MgSO_4$, 0.8; glucose, 5.5; HEPES-Tris (pH 7.4), 50; and choline chloride, 130. Ten strokes of a loose fitting glass-glass homogenizer were used to resuspend the final pellet. Synaptosomes were kept on ice and were used immediately after preparation.

Measurement of $^{22}Na^+$ uptake. Synaptosomal sodium uptake was determined by a modification of the method of Tamkun and Catterall (1981). Aliquots (50 μl) of the synaptosomal suspension were preincubated at 36°C for 2 min, except in the time course experiments, with incubation buffer or incubation buffer containing the indicated concentration of ethanol. Immediately after the preincubation with ethanol, the indicated concentration of activator toxin (BTX or VER) was added and the samples were incubated for 10 min at 36°C. After 10 min the samples were diluted with a solution containing (final concentration) the indicated concentration of toxin (millimolar): KCl, 5.4; $MgSO_4$, 0.8; glucose, 5.5; HEPES-Tris (pH 7.4), 50; choline chloride, 128; NaCl, 2; ouabain, 5; and 1.3 μCi of carrier-free $^{22}NaCl$ per ml and the indicated concentration of ethanol. After a 5-sec incubation (except where noted), uptake was terminated by the addition of 3 ml of an ice-cold wash solution containing (millimolar): choline chloride, 163; $MgSO_4$, 0.8; $CaCl_2$, 1.8; HEPES-Tris (pH 7.4), 5; and bovine serum albumin, 1 mg/ml. The mixture was filtered rapidly under vacuum through an Amicon 0.45-μm cellulose filter (Amicon, Lexington, MA) and the filters were washed twice with 3 ml of wash solution. The entire halt-filter-wash cycle took less than 10 sec to complete. The filters were placed in scintillation vials, 15 ml of scintillation cocktail were added and filter radioactivity was determined by liquid scintillation spectrometry. The data are presented as corrected specific uptake after subtraction of nonspecific uptake (TTX, 1 μM present in incubation and uptake buffers).

Data analysis. Double reciprocal analysis of the data was performed as described by Catterall (1975) using a modified Michaelis-Menton equation of the form:

$$v = VA/(K_{0.5} + A)$$

where v is the uptake rate at various activator toxin concentrations A, V is maximal uptake rate and $K_{0.5}$ is the apparent dissociation constant of the activator toxin. Statistical analysis was performed using Student's t test for paired samples. Multiple comparisons with a control were done by analysis of variance and Dunnett's test (1964).

Other methods. Drug concentrations in the aqueous and membrane phases were calculated as described by Lyon *et al.* (1981). The membrane/buffer partition coefficients were derived from the data of McCreery and Hunt (1978). Solutions of ScV were prepared according to Catterall (1976). A stock solution of BTX was prepared in absolute ethanol and aliquots were diluted in the appropriate buffer. The final concentration of ethanol in the assay from the addition of BTX was never greater than 0.13 mM. Protein concentrations were determined by the method of Lowry *et al.* (1951). Bovine serum albumin was used as the protein standard.

Results

Preincubation of whole brain synaptosomes with ethanol *in vitro* caused a concentration-dependent inhibition of BTX-stimulated $^{22}Na^+$ uptake (fig. 1). Over the concentration range of ethanol used, the reduction in $^{22}Na^+$ uptake was a linear function of the concentration of ethanol ($r = -0.95$). The inhibitory effect of ethanol occurred at pharmacologically relevant concentrations of ethanol and was fully reversible when ethanol was removed from the sample by washing and centrifugation (fig. 2). Neither the nonspecific (1 μM TTX present) nor the passive, unstimulated (no toxins present) uptake of $^{22}Na^+$ were affected by ethanol *in vitro* (data not shown).

The effects of ethanol on $^{22}Na^+$ uptake were also studied over a range of concentrations of the alkaloid toxins BTX and VER. There was a 6-fold increase in synaptosomal sodium uptake when the concentration of BTX was raised from 0.1 to 5 μM. Ethanol (100 and 400 mM) inhibited $^{22}Na^+$ uptake in synaptosomes exposed to more than 0.1 μM BTX (fig. 3). When VER was used to activate sodium channels and promote $^{22}Na^+$ uptake, a similar effect of ethanol was observed, as shown in figure 4. In order to assess indirectly the interaction of ethanol with the channel receptor site for BTX and VER, we performed a double reciprocal analysis of concentration-effect curves for BTX- and VER-stimulated $^{22}Na^+$ uptake in the absence (control) and presence of two concentrations of ethanol (100 and 400 mM). The data from the double reciprocal analysis are

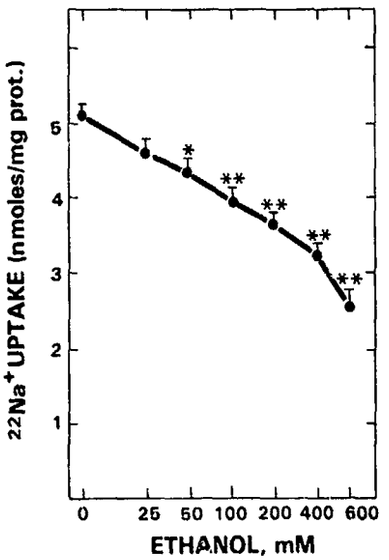

Fig. 1. Concentration-effect curve for inhibition of BTX-stimulated $^{22}Na^+$ uptake. Triplicate samples of whole brain synaptosomes were preincubated for 2 min with the indicated concentration of ethanol followed by a 10-min incubation with 1 μM BTX. Symbols represent the means ± S.E.M., $N = 5$ experiments. The corrected specific uptake of $^{22}Na^+$ during a 5-sec period is shown on the ordinate. The concentration of ethanol is shown on the abscissa, log scale. *$P < .01$ (Dunnett's test) compared to uptake measured in the absence of ethanol. prot., protein.

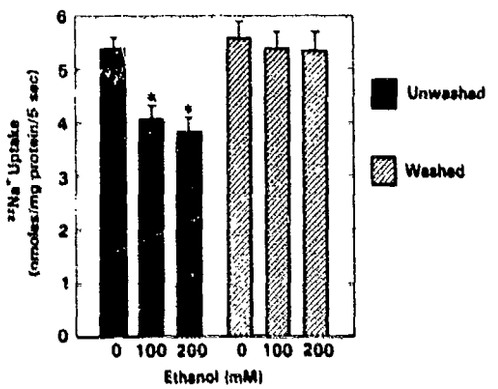

Fig. 2. Reversibility of the inhibitory effect of ethanol on BTX-stimulated $^{22}Na^+$ uptake. After a 2-min preincubation with ethanol, one-half of the samples were centrifuged (1000 × g for 5 min), washed and resuspended in incubation buffer. BTX (1 μM) was added, samples were incubated at 36°C for 10 min and $^{22}Na^+$ uptake was measured as described. The data are expressed as the means ± S.E.M., $N = 4$ experiments. The corrected specific uptake of $^{22}Na^+$ is shown on the ordinate. The concentration of ethanol is shown on the abscissa. *$P < .01$ (Dunnett's test) compared to uptake in control samples.

summarized in table 1. When sodium channels were activated by BTX, ethanol acted as a noncompetitive inhibitor as the maximum uptake of $^{22}Na^+$ was reduced with no change in the concentration of BTX required for 50% of maximum uptake ($K_{m's}$). The effects of ethanol on VER-stimulated $^{22}Na^+$ uptake are somewhat more difficult to interpret. Clearly, ethanol significantly reduced the maximum effect of VER. In addition, ethanol reduced the $K_{m's}$ values for VER but the difference from control was not significant.

The time courses for $^{22}Na^+$ uptake with 1 μM BTX alone and with 1 μM BTX plus 200 mM ethanol are illustrated in figure 5. In the presence of ethanol, the BTX-stimulated uptake of $^{22}Na^+$ was significantly reduced at uptake times of 3, 5 and

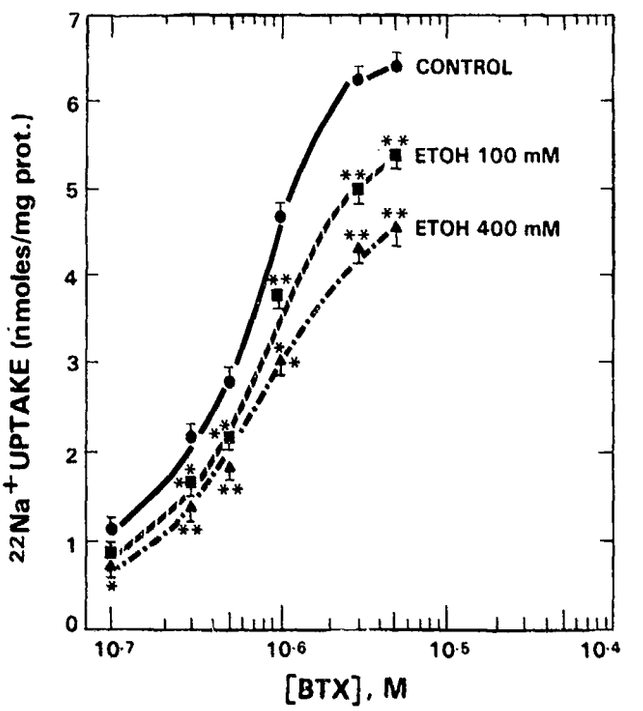

Fig. 3. Effect of ethanol on concentration-effect curve for BTX-stimulated $^{22}Na^+$ uptake. Synaptosomes were preincubated with buffer only or buffer containing ethanol (100 and 400 mM) for 2 min. The indicated concentration of BTX was added and samples were incubated for an additional 10 min and $^{22}Na^+$ uptake was measured for 5 sec as described under "Methods." Symbols represent the means ± S.E.M., $N = 6$ experiments. *$P < .05$; **$P < .01$ (Dunnett's test) compared to corresponding control. prot., protein.

7 sec, but not at 10 or 20 sec. Thus, the effect of ethanol on $^{22}Na^+$ uptake is an inhibitory effect on the initial rates of $^{22}Na^+$ uptake. We were unable to measure $^{22}Na^+$ uptake at uptake times shorter than 3 sec with acceptable precision. The results in table 2 demonstrate that the duration of the preincubation period with ethanol was not an important determinant of the inhibitory effect of ethanol. An ethanol concentration of 200 mM reduced the specific uptake to 77.2, 79.3, 74.5 and 77.4% after 0, 0.5, 2 and 10 min, respectively. Thus, the onset of action was immediate and was unchanged over the time periods studied.

The effect of increasing lipid solubility on potency for inhibition of BTX-stimulated $^{22}Na^+$ uptake was studied for a series of aliphatic alcohols. Membrane-buffer partition coefficients were used to calculate the concentration of each alkanol that would result in a similar molar concentration in the nonaqueous (membrane) phase (Lyon *et al.*, 1981). Concentration-effect curves were constructed for each alkanol as percentage of control uptake *vs.* log of the alkanol concentration. Linear regression analysis was used to determine the correlation coefficients, slopes and the concentration of alkanol that inhibited control uptake by 50% (IC_{50}). These values are shown in table 3. For each alkanol tested, the reduction in $^{22}Na^+$ uptake was a linear function of the concentration of alkanol.

The IC_{50} and membrane/buffer partition coefficient values for each alkanol were plotted on a log-log scale (fig. 6). There was a good correlation ($r^2 = 0.997$) between the two parameters, indicating that the ability to partition into a hydrophobic region of the membrane was an important determinant of the potency for inhibition of BTX-stimulated $^{22}Na^+$ uptake.

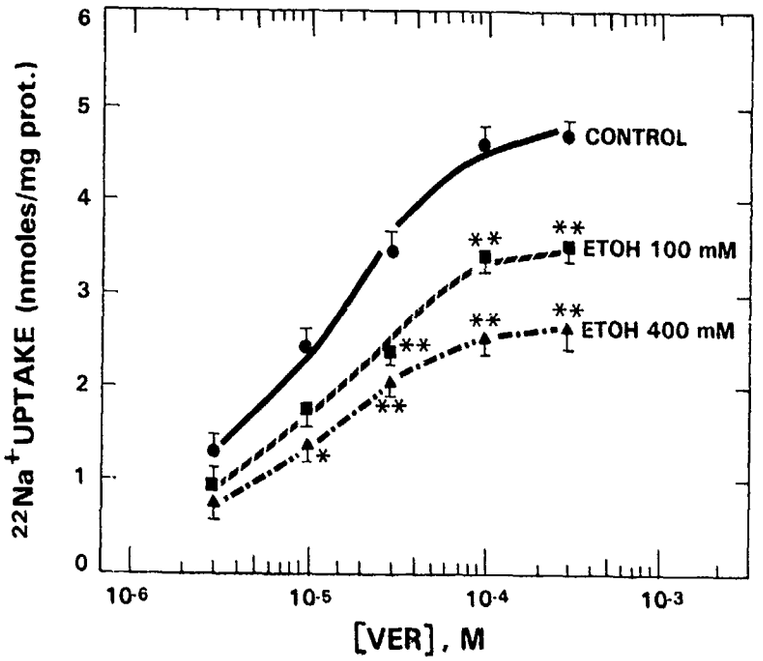

Fig. 4. Effect of ethanol on concentration-curve for VER-stimulated $^{22}Na^+$ uptake. Synaptosomes were preincubated with buffer only or buffer containing ethanol (100 and 400 mM) for 2 min. The indicated concentration of VER was added, samples were incubated for an additional 10 min and $^{22}Na^+$ uptake was measured for 5 sec as described under "Methods." Symbols represent the means ± S.E.M., $N = 4$ experiments. *$P < .05$; **$P < .01$ (Dunnett's test) compared to corresponding control. prot., protein.

TABLE 1

Double reciprocal analysis of alkaloid toxin activation of sodium channels

Alkaloid Toxin	Ethanol Conc.	N	V*	$K_{0.5}$*
	mM		*nmol/mg protein/5 sec*	*μM*
BTX	0	6	6.43 ± 0.27†	0.430 ± 0.024
BTX	100	6	4.84 ± 0.15*	0.439 ± 0.042
BTX	400	6	4.09 ± 0.10*	0.431 ± 0.022
VER	0	4	4.62 ± 0.22	9.33 ± 0.70
VER	100	4	3.30 ± 0.29*	7.83 ± 0.94
VER	400	4	2.50 ± 0.12*	6.58 ± 0.63

* Values for maximum uptake (V) and $K_{0.5}$ were calculated using a modified Michaelis-Menton equation as described under "Methods."
† Values are means ± S.E.M. N = number of experiments.
* Significantly different from control, $P < .01$.

ScV alone does not promote sodium influx. However, ScV enhances alkaloid toxin-stimulated $^{22}Na^+$ uptake, presumably by an allosteric mechanism (Catterall, 1980; Tamkun and Catterall, 1981). The effect of ethanol on the ScV-BTX interaction is shown in figure 7. In control samples, ScV at concentrations of 1 and 10 μg/ml increased BTX-stimulated $^{22}Na^+$ uptake by 26.5 ± 1.6 and 62.5 ± 1.7%, respectively. In the presence of ethanol, a similar enhancement of BTX-stimulated $^{22}Na^+$ uptake was noted (1 μg/ml, 27.3 ± 3.8; 10 μg/ml, 54.2 ± 3.8%). Thus, ethanol does not have a significant effect on the allosteric interaction of ScV and BTX.

The effect of ethanol on the inhibition of BTX-stimulated $^{22}Na^+$ uptake by TTX is shown in figure 8. An ethanol concentration of 200 mM did not affect the potency of the specific inhibitor TTX. The concentration of TTX necessary for a 50% reduction in BTX-stimulated $^{22}Na^+$ uptake in control samples was 12.72 ± 0.61 nM. In the presence of ethanol, a similar value (12.60 ± 0.59 nM) was measured.

Discussion

Incubation of synaptosomes with ethanol *in vitro* caused a significant inhibition of the initial rates of neurotoxin-stimulated sodium uptake. This effect of ethanol was concentration-

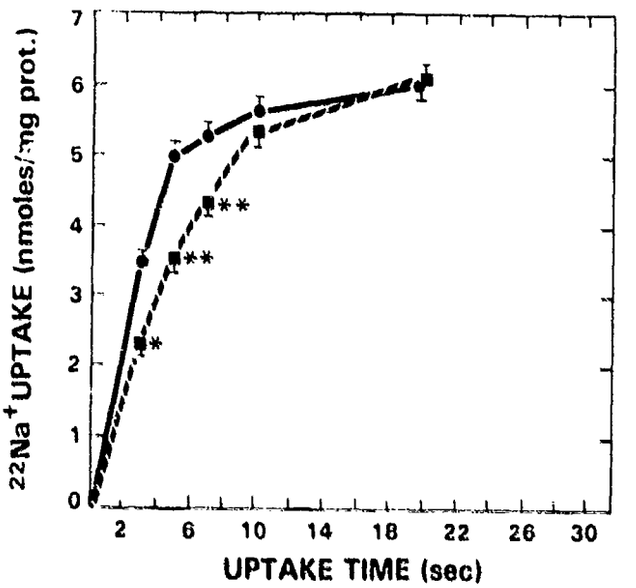

Fig. 5. Effect of ethanol on the time course of BTX-stimulated $^{22}Na^+$ uptake. Synaptosomes were preincubated with buffer only or buffer containing ethanol (200 mM) for 2 min. BTX (1 μM) was added and samples were incubated for an additional 10 min and $^{22}Na^+$ uptake was measured for the indicated time. Symbols represent the means ± S.E.M., $N = 5$ experiments. *$P < .05$; **$P < .01$ (paired t test) compared to corresponding control. prot., protein.

TABLE 2

Effect of preincubation time with ethanol on inhibition of BTX-stimulated $^{22}Na^+$ uptake; duration of preincubation*

	0 min	0.5 min	2.0 min	10 min
Control	4.72 ± 0.35†	4.82 ± 0.39	5.22 ± 0.17	4.65 ± 0.25
Ethanol, 200 mM	3.04 ± 0.39*	3.82 ± 0.38*	3.89 ± 0.20*	3.60 ± 0.21*

* Refers to the duration of preincubation of tissue with buffer or buffer containing ethanol (200 mM) before the addition of BTX (1 μM).
† Values are means ± S.E.M., $N = 3$ experiments. units are nanomoles of $^{22}Na^+$ per milligram of protein per 5 sec.
* Significantly different from corresponding control, $P < .01$.

TABLE 3

Effects of aliphatic alcohols *in vitro* on BTX-stimulated $^{22}Na^+$ uptake

Alcohol	Pm/b[a]	IC_{50}[b]	Slope[b]	r^2
Ethanol	0.096	582.8 ± 51.8	−71.1 ± 7.2	0.980
Propanol	0.438	104.0 ± 13.6	−72.8 ± 6.9	0.983
Butanol	1.52	35.9 ± 5.4	−65.1 ± 9.2	0.993
Pentanol	5.02	6.6 ± 0.6	−55.9 ± 6.6	0.940
Hexanol	21.4	1.2 ± 0.06	−60.0 ± 9.6	0.936

[a] Membrane/buffer partition coefficient ($P_{m/b}$) values are from McCreery and Hunt (1978).

[b] Values are the means ± S.E.M., N = 4–8 experiments. In each experiment, three or four concentrations of each alkanol were tested. IC_{50}, the concentration of each alcohol necessary to reduce control BTX-stimulated uptake by 50%. Values were derived from linear regression analysis of percentage of control uptake *vs.* log [alkanol].

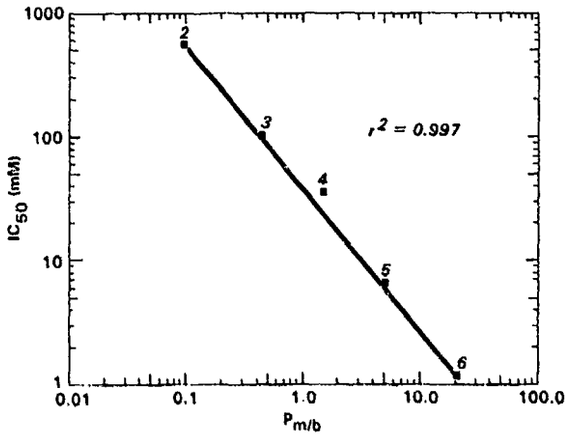

Fig. 6. Correlation of the inhibitory potency of aliphatic alcohols on BTX-stimulated $^{22}Na^+$ uptake with their membrane/buffer partition ($P_{m/b}$) coefficient. The concentration of each alcohol that inhibits BTX-stimulated $^{22}Na^+$ uptake by 50% (IC_{50}, millimolar) is presented on the ordinate. The $P_{m/b}$s are shown on the abscissa. The number above each symbol represents the chain length of the alcohol: 2, ethanol; 3, *n*-propanol; 4, *n*-butanol; 5, *n*-pentanol; and 6, *n*-hexanol. The line was fit by linear regression analysis with a correlation coefficient, r^2 = 0.997. See table 3 for details.

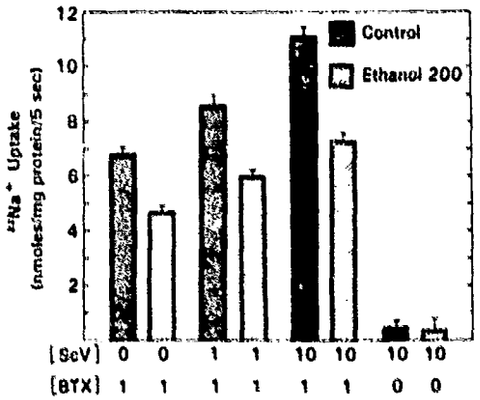

Fig. 7. The effect of ethanol *in vitro* on the BTX-ScV interaction. An aliquot of synaptosomes was preincubated for 2 min with buffer (control) or buffer containing ethanol. The indicated concentrations of BTX and ScV were added and $^{22}Na^+$ uptake was measured as described. The units of concentration for ScV and BTX were micrograms per milliliter and micromolar, respectively. The data are presented as the means ± S.E.M., N = 4 experiments.

dependent, occurred with pharmacologically relevant (50 mM) concentrations of ethanol and was fully reversible when ethanol was removed from the system. In addition, there was a good correlation between potency for inhibition of BTX-stimulated

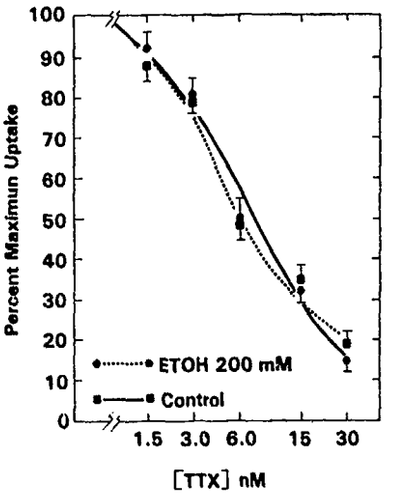

Fig. 8. Effect of ethanol on the inhibition of BTX-stimulated $^{22}Na^+$ uptake by TTX. Triplicate samples of whole brain synaptosomes were preincubated for 2 min with buffer (control) or with buffer containing ethanol. The indicated concentration of TTX was added and 3 min later BTX (1 μM) was added and all samples were incubated for an additional 10 min. Symbols represent the means ± S.E.M., N = 4 experiments. Maximum uptake for control and ethanol samples was 6.50 ± 0.13 and 4.33 ± 0.13 nmol of $^{22}Na^+$ per mg of protein per 5 sec, respectively.

$^{22}Na^+$ uptake and the membrane/buffer partition coefficients for a series of aliphatic alcohols, suggesting that a hydrophobic area of the sodium channel microenvironment was involved in the action of the alkanols. Inasmuch as the neurotoxin-stimulated uptake of sodium was blocked by the specific inhibitor TTX with a $K_{0.5}$ of approximately 13 nM, it appears that the neurotoxin-stimulated sodium uptake that was inhibited by ethanol occurred through voltage-sensitive sodium channels in synaptosomes (Catterall, 1980). Our results with ethanol are consistent with the work of Harris (1984) which showed that a variety of intoxicant anesthetics agents reduced neurotoxin-stimulated sodium uptake.

In the CNS, ionic channels for calcium, potassium and sodium are involved intimately in the control of excitability and each plays an essential role in signal transduction and information processing (Catterall, 1984). At the present time, the structural and functional properties of the voltage-sensitive sodium channels are understood most completely. This is due in part to the existence of a variety of neurotoxins that can be used as tools to study the sodium channel (Narahashi, 1974). In this regard, BTX has been defined as a full agonist (Catterall, 1980; Tamkun and Catterall, 1981) because it activates a larger number of sodium channels and is also more potent ($K_{0.5}$ value is smaller) than the partial agonist VER.

There appeared to be slight differences in the effect of ethanol when different neurotoxins were used to stimulate sodium uptake. When BTX was used to stimulate sodium uptake, the maximum effect of BTX was reduced by ethanol with no change in the $K_{0.5}$ value. Also, the minimum effective concentration of ethanol was 50 mM and the concentration of ethanol required for 50% inhibition (IC_{50}) was approximately 583 mM. VER-stimulated sodium uptake was more sensitive to inhibition by ethanol because the minimum effective concentration of ethanol was 25 mM and the IC_{50} value was approximately 345 mM (Mullin and Hunt, 1984). Ethanol reduced the maximum effect of VER and there was also a clear trend toward reducing the $K_{0.5}$ value of VER. It would be desirable to perform

more experiments with VER to investigate further this point, but during the course of this study VER became unavailable commercially. Even though it is well known that BTX and VER compete for the same binding site in the channel (Catterall, 1975), the mechanism by which each neurotoxin stimulates sodium uptake may be slightly different because of other properties of the toxins (Miller, 1983; Tanaka *et al.*, 1983).

The action of ethanol on the voltage-sensitive sodium channels in synaptosomes appears to be somewhat selective for the site that binds BTX and VER. Ethanol did not interfere with the allosteric interaction that occurred between BTX and ScV. Similarly, the presence of ethanol did not alter the concentration of TTX required to inhibit BTX-stimulated sodium uptake by 50%. However, it must be noted that these findings concerning the effects of ethanol on neurotoxin receptor sites I (TTX) and III (ScV) are based on indirect measurements. Direct measurement using radiolabeled neurotoxins should clarify these points.

Recent studies with fluorescent derivatives of sodium channel neurotoxins (Angelides and Nutter, 1983, 1984) in conjunction with published biochemical evidence (Hartshorne and Catterall, 1981, 1984; Ellisman *et al.*, 1982) have advanced our knowledge of the molecular arrangement of the functional components of the sodium channel. Angelides and Nutter (1984) have proposed a model wherein the TTX binding site resides in a highly polar, hydrophilic area at the extracellular side of the membrane. The binding site for ScV may be located in a more hydrophobic region that is not lipid in nature and may extend 15 A into the cell membrane. The final neurotoxin receptor site (for BTX and VER) is placed in a hydrophobic area directly interacting with the subunit of the channel and the interior of the lipid bilayer. Thus, in this model, the BTX/VER binding site is located in the area of the membrane in which the fluidizing effect of ethanol is greatest (Harris and Schroeder, 1981). An explanation for the observed effects of ethanol on neurotoxin-stimulated sodium uptake may involve changes in the fluidity of the neuronal membrane as a number of other membrane perturbants inhibit sodium uptake with potency for inhibition of sodium uptake being related to lipid solubility (Harris, 1984). Ethanol may alter the arrangement of membrane lipids or hydrophobic proteins in a specific area of the sodium channel microenvironment. In addition, disruption of important lipid-protein interactions by ethanol may result in suboptimal conditions that would adversely affect sodium channel function. Further studies of sodium channel function in systems in which the lipid and protein components are more tightly controlled may answer some of these questions.

It is difficult to determine how important the effect of ethanol on sodium channels is to the intoxicating effect of ethanol. In this study and that of Harris and Bruno (1985), an ethanol concentration of 50 to 100 mM was required to produce a significant inhibitory effect. Previous work from our laboratory demonstrated that an ethanol concentration of 25 mM which is commonly achieved *in vivo* and is associated with moderate intoxication was sufficient to cause a significant inhibition of VER-stimulated $^{22}Na^+$ uptake (Mullin and Hunt, 1984). Additionally, it appears that brain regions differ in sensitivity to this effect of ethanol (Harris and Bruno, 1985).

We have used an ion flux assay to study the effects of ethanol on sodium channel function in synaptosomes in which electrophysiological methods are not practical. Because it is necessary to use toxins to activate the sodium channels, one must consider the possibility that ethanol is interfering with the binding of the toxins to their receptors in the channel. This could explain the results we have presented. This question is currently under study in our laboratory using radiolabeled toxins.

Acknowledgments

The authors thank Dr. John Daly for generously providing BTX, Mr. Tom Dalton for technical assistance, Mrs. Marion Golightly for preparing the manuscript and Drs. R. Adron Harris and E. Majchrowicz for their comments.

References

ANGELIDES, K. J. AND NUTTER, T. J.: Mapping the molecular structure of the voltage-dependent sodium channel: Distances between the tetrodotoxin and Leiurus quinquestriatus scorpion toxin receptors. J. Biol. Chem. **258:** 11958–11967, 1983.

ANGELIDES, K. J. AND NUTTER, T. J.: Molecular and cellular mapping of the voltage-dependent sodium channel. Biophys. J. **45:** 31–34, 1984.

CATTERALL, W. A.: Activation of the action potential Na^+ ionophore of cultured neuroblastoma cells by veratridine and batrachotoxin. J. Biol. Chem. **250:** 4053–4059, 1975.

CATTERALL, W. A.: Purification of a toxic protein from scorpion venom which activates the action potential Na^+ ionophore. J. Biol. Chem. **251:** 5528–5536, 1976.

CATTERALL, W. A.: Neurotoxins that act on voltage-sensitive sodium channels in excitable membranes. Annu. Rev. Pharmacol. Toxicol. **20:** 15–43, 1980.

CATTERALL, W. A.: The emerging molecular view of the sodium channel. Trends Neurosci. **5:** 303–306, 1982.

CATTERALL, W. A.: The molecular basis of neuronal excitability. Science (Wash. DC) **223:** 653–661, 1984.

CHIN, J. H. AND GOLDSTEIN, D. B.: Effects of low concentrations of ethanol on the fluidity of spin-labeled erythrocytes and brain membranes. Mol. Pharmacol. **13:** 435–441, 1977a.

CHIN, J. H. AND GOLDSTEIN, D. B.: Drug tolerance in biomembranes: A spin label study of the effects of ethanol. Science (Wash. DC) **196:** 684–685, 1977b.

CHIN, J. H. AND GOLDSTEIN, D. B.: Membrane-disordering action of ethanol: Variation with membrane cholesterol content and depth of the spin label probe. Mol. Pharmacol. **19:** 425–431, 1981.

DUNNETT, C. W.: New tables for multiple comparisons with a control. Biometrics **20:** 482–491, 1964.

ELLISMAN, M. H., AGNEW, W. S., MILLER, J. A. AND LEVINSON, S. R.: Electron microscopic visualization of the tetrodotoxin-binding protein from Electrophorus electricus. Proc. Natl. Acad. Sci. U.S.A. **79:** 4461–4465, 1982.

GOLDSTEIN, D. B., CHIN, J. H. AND LYON, R. C.: Ethanol disordering of spin-labeled mouse brain membranes: Correlation with genetically determined ethanol sensitivity of mice. Proc. Natl. Acad. Sci. U.S.A. **79:** 4231–4233, 1982.

GOLDSTEIN, D. B., CHIN, J. H., MCCOMB, J. A. AND PARSONS, L. M.: Chronic effects of alcohols on mouse biomembranes. *In* Biological Effects of Alcohol, ed. by H. Begleiter, pp. 1–6, Plenum Press, New York, 1980.

GRAY, E. G. AND WHITTAKER, V. P.: The isolation of nerve endings from brain: An electron-microscopic study of cell fragments derived by homogenization and centrifugation. J. Anat. **96:** 79–87, 1962.

HARRIS, R. A.: Differential effects of membrane perturbants on voltage-activated sodium and calcium channels and calcium-dependent potassium channels. Biophys. J. **45:** 132–134, 1984.

HARRIS, R. A. AND BRUNO, P.: Effects of ethanol and other intoxicant-anesthetics on voltage-dependent sodium channels of brain synaptosomes. J. Pharmacol. Exp. Ther. **232:** 401–406, 1985.

HARRIS, R. A. AND SCHROEDER, F.: Ethanol and the physical properties of brain membranes: Fluorescence studies. Mol. Pharmacol. **20:** 128–137, 1981.

HARTSHORNE, R. P. AND CATTERALL, W. A.: Purification of the saxitoxin receptor of the sodium channel from rat brain. Proc. Natl. Acad. Sci. U.S.A. **78:** 4620–4624, 1981.

HARTSHORNE, R. P. AND CATTERALL, W. A.: The sodium channel from rat brain: Purification and subunit composition. J. Biol. Chem. **259:** 1667–1675, 1984.

HILLE, V.: Ionic channels in nerve membranes. Prog. Biophys. Mol. Biol. **21:** 1–32, 1970.

HODGKIN, A. L. AND HUXLEY, A. F.: A quantitative description of membrane current and its application to conduction and excitation in nerve. J. Physiol. (Lond.) **117:** 500–544, 1952.

LENAZ, G.: Lipid properties and lipid-protein interactions. *In* Membrane Proteins and Their Interactions with Lipids, ed. by R. A. Capaldi, pp. 47–150, Marcel Dekker, New York, 1977.

LOWRY, O. H., ROSEBROUGH, N. J., FARR, A. L. AND RANDALL, R. J.: Protein measurement with the Folin phenol reagent. J. Biol. Chem. **193:** 265–275, 1951.

LYON, R. C., MCCOMB, J. A., SCHREURS, J. AND GOLDSTEIN, D. B.: A relationship between alcohol intoxication and the disordering of brain membranes by a series of short-chain alcohols. J. Pharmacol. Exp. Ther. **21:** 669–675, 1981.

MCCREERY, M. J. AND HUNT, W. A.: Physicochemical correlates of alcohol intoxication. Neuropharmacology **17:** 451–461, 1978.

MILLER, C.: Integral membrane channels: Studies in model membranes. Physiol. Rev. **63:** 1209–1242, 1983.

MULLIN, M. J. AND HUNT, W. A.: Ethanol inhibits veratridine-stimulated sodium uptake in synaptosomes. Life Sci. **34:** 287–292, 1984.

NARAHASHI, T.: Chemicals as tools in the study of excitable membranes. Physiol. Rev. **54:** 813–889, 1974.

NARAHASHI, T., ANDERSON, N. C. AND MOORE, J. W.: Tetrodotoxin does not block excitation from inside the nerve membrane. Science (Wash. DC) **153:** 765–767, 1966.

RITCHIE, J. M. AND ROGART, R. B.: The binding of saxitoxin and tetrodotoxin to excitable tissue. Rev. Physiol. Biochem. Pharmacol. **79:** 1–51, 1977.

SEEMAN, P.: The membrane actions of anesthetics and tranquilizers. Pharmacol. Rev. **24:** 583–655, 1972.

TAMKUN, M. M. AND CATTERALL, W. A.: Ion flux studies of voltage-sensitive sodium channels in synaptic nerve-ending particles. Mol. Pharmacol. **19:** 78–86, 1981.

TANAKA, J. C., ECCLESTON, J. F. AND BARCHI, R. L.: Cation selectivity characteristics of the reconstituted voltage-dependent sodium channel purified from rat skeletal muscle sarcolemma. J. Biol. Chem. **25:** 7519–7526, 1983.

ULBRICHT, W.: Ionic channels and gating currents in excitable membranes. Annu. Rev. Biophys. Bioeng. **6:** 7–31, 1977.

Send reprint requests to: Dr. Michael J. Mullin, Behavioral Sciences Department, Armed Forces Radiobiology Research Institute, Naval Medical Command, National Capital Region, Bethesda, MD 20814-5011.

Journal of Biological Response Modifiers
3:627–633 © 1984 Raven Press, New York

Short Communication

Soluble Polyglycans Enhance Recovery from Cobalt-60–Induced Hemopoietic Injury

M. L. Patchen, *N. R. DiLuzio, †P. Jacques, and T. J. MacVittie

*Armed Forces Radiobiology Research Institute, Experimental Hematology Department, Bethesda, Maryland; *Tulane University School of Medicine, Department of Physiology, New Orleans, Louisiana, U.S.A.; and †Catholic University of Louvain, Biochemical Cytology, Brussels, Belgium*

Summary: Six soluble polyglycans (glucan-C, glucan-F, glucan-S, krestin, lentinan, and schizophyllan), two soluble polymannans (mannan-A and mannan-R), and one soluble polyfructan (levan) were assayed for their ability to enhance hemopoietic recovery in C3H/HeN mice when administered either 1 h before or 1 h after a 6.5-Gy dose of cobalt-60 radiation. Hemopoietic recovery was measured by the endogenous spleen colony assay and was compared with recovery in both radiation control mice and irradiated mice treated with glucan-P (a particulate polyglycan previously shown to enhance recovery from radiation-induced hemopoietic injury). Compared with radiation controls, when administered before irradiation, mannan-A, glucan-F, and glucan-S enhanced endogenous colony formation 4.2–5.1-fold (equivalent to glucan-P), and levan and schizophyllan ~2.7-fold. Lentinan, krestin, mannan-R, and glucan-C did not enhance hemopoietic recovery above radiation controls under these conditions. When polyglycan administration was delayed until after irradiation, endogenous colony formation was enhanced 3.0–3.9-fold by mannan-A, schizophyllan, glucan-S, krestin, and glucan-F (at least comparable with glucan-P) but not at all by mannan-R, levan, lentinan, or glucan-C. **Key Words:** Fructan—Glucan—Hemopoiesis—Mannan—Polyglycans—Radiation recovery.

Glucan-P, a particulate β-1,3–linked polyglycan isolated from the yeast *Saccharomyces cerevisiae* (1,2) has been shown to enhance a variety of biological responses in mice, including reticuloendothelial functions (3,4), humoral- and cell-mediated immune functions (5–8), and hemopoietic proliferation and differentiation (9–13). Glucan-P has also been shown to enhance murine endogenous and exogenous pluri-

Received January 9, 1984; accepted June 21, 1984.

Views presented in this report are those of the authors. No endorsement by the Defense Nuclear Agency has been given or should be inferred.

Address correspondence and reprint requests to Dr. M. L. Patchen at Experimental Hematology Department, Armed Forces Radiobiology Research Institute, Bethesda, MD 20814, U.S.A.

potent stem cell (E-CFU, CFU-s), granulocyte-macrophage and pure macrophage progenitor cell (GM-CFU, M-CFU), and erythroid colony– and burst-forming cell (CFU-e, BFU-e) recovery when administered either before or after exposure to a hemopoietically damaging dose (6.5 Gy) of cobalt-60 radiation (14).

Despite all of these desirable effects, the intravenous use of glucan-P in humans has been restricted because of possible side effects related to glucan-P's particulate nature. Granuloma formation and hepatosplenomegaly have been reported (3,12). Additionally, "occlusion-type" neurovascular side effects due to microembolism may also occur after intravenous administration of large doses of concentrated solutions of glucan-P. Recently, several soluble polyglycans have been produced, and preliminary results suggest that at least some of these compounds also maintain reticuloendothelial-, immunologic-, and hemopoietic-enhancing capabilities similar to those of glucan-P. Thus, the purpose of this study was to screen and to compare nine such soluble polyglycans for their ability to enhance hemopoietic recovery following a hemopoietically damaging dose of cobalt-60 radiation.

METHODS

Since, in previous studies, the endogenous spleen colony assay described by Till and McCulloch (15) accurately predicted the overall ability of glucan-P to enhance recovery of the various specific hemopoietic stem and progenitor cells (16,17), this assay was used to screen for the hemopoiesis-enhancing capacity of the soluble polyglycans. In this assay, following irradiation in the range of 450–900 rad, colonies of hemopoietic cells arise from the clonal proliferation of surviving pluripotent stem cells (E-CFU) and become grossly visible on the spleens of irradiated mice as recovery from radiation progresses (15,18–20). The number of colonies arising from E-CFU is inversely related to radiation dose; at a chosen radiation dose, the ability of an agent to increase the number of detectable colonies reflects its hemopoiesis-enhancing capacity.

For each experiment five to eight female C3H/HeN mice, 6–8 weeks old, were injected intravenously with 0.4 mg (~20 mg/kg) saline-diluted glucan-P or 0.4 mg of the various soluble polyglycans (Table 1). Mice were exposed to 6.5 Gy (0.4 Gy/min) of bilateral, total-body irradiation from the AFRRI cobalt-60 source at either 1 h before or 1 h after polyglycan treatment. Mice were exsanguinated 8 days later, the spleens were removed and stained in Bouin's fixative, and the number of grossly visible spleen colonies derived from E-CFU were counted. Data are expressed as the mean ± 1 SEM of results obtained from three replicate experiments, and data were statistically analyzed using nonparametric methods. Specifically, one-sided comparisons were made between each polyglycan-treated group of animals and radiation controls using Dunn's Test (21) to determine if treatments elevated the E-CFU response above that of radiation controls.

RESULTS

The effects of the various polyglycans on E-CFU response when administered before irradiation are presented in Table 2. As can be seen, radiation controls (saline-injected and irradiated) exhibited 4.5 ± 1.2 E-CFU per spleen. The various polyglycan-treated animals exhibited an E-CFU response that placed them into one of three groups based on their degree of hemopoietic enhancement when compared with

TABLE 1. *Biological and physical characteristics of 10 polyglycans*

Compound	Soluble	Biological source	Structure	Approximate molecular weight	Obtained from
Glucan-C	Yes	*Sclerotium glucanium*	β-1,3 glucan β-1,6 glucan	5×10^5	N. R. Di Luzio, New Orleans, LA, U.S.A.
Glucan-F	Yes	*Saccharomyces cerevisiae*	β-1,3 glucan	10×10^5	N. R. Di Luzio
Glucan-P	No	*S. cerevisiae*	β-1,3 glucan β-1,6 glucan	1–2-μm particle	Accurate Chemical & Scientific Co., Westbury, NY, U.S.A.
Glucan-S	Yes	*S. cerevisiae*	β-1,3 glucan	1×10^5	N. R. Di Luzio
Krestin (PSK)	Yes	*Coriolus versicolor*	β-1,4 glucan β-1,3 glucan β-1,6 glucan (25–38% protein)	1×10^5	Kureha Chemical Co., Tokyo, Japan
Lentinan	Yes	*Lentinus edodes*	β-1,3 glucan	5×10^5	Ajinomoto Co., Yokohama, Japan
Levan	Yes	*Aerobacter leranicum*	β-2,6 fructan	200×10^5	P. Jacques, Brussels, Belgium
Mannan-A	Yes	—	β-mannan	—	P. Jacques
Mannan-R	Yes	*Rhodotorulum rubrum*	β-1,3 mannan β-1,4 mannan	—	P. Jacques
Schizophyllan (SPG)	Yes	*Schizophyllum commune* media	β-1,3 glucan β-1,6 glucan	5×10^5	Kaken Co., Tokyo, Japan

TABLE 2. *Effects of polyglycans on endogenous colony formation (E-CFU) when administered 1 h before 6.5 Gy cobalt-60 radiation*

Group[a]	Compound	E-CFU	Enhancement factor[b]	Spleen weight (mg)
Control	Saline (radiation control)	4.5 ± 1.2	1.0	37 ± 1
1	Mannan-A	23.0 ± 5.3	5.1	56 ± 5
	Glucan-F	21.1 ± 3.6	4.7	49 ± 8
	Glucan-S	18.9 ± 2.6	4.2	45 ± 4
	Glucan-P	17.8 ± 2.1	4.0	55 ± 5
2	Levan	12.6 ± 1.6	2.8	42 ± 1
	SPG	12.0 ± 2.1	2.7	45 ± 2
3	Lentinan	10.7 ± 1.6	2.3	41 ± 2
	PSK	10.2 ± 2.2	2.2	42 ± 3
	Mannan-R	6.4 ± 1.2	1.4	40 ± 6
	Glucan-C	5.3 ± 1.2	1.2	39 ± 2

Abbreviations as in Table 1.

[a]With respect to radiation control E-CFU values: group 1, $p < 0.001$; group 2, $p < 0.01$; and group 3, no statistical difference.

[b]Enhancement factor = mean E-CFU polyglycan/mean E-CFU radiation control.

radiation controls. The first group consisted of mice treated with the polyglycans mannan-A, glucan-F, glucan-S, and glucan-P. Endogenous colony formation in these mice was enhanced 4.0–5.1-fold over radiation controls, and resulted in 23.0 ± 5.3, 21.1 ± 3.6, 18.9 ± 2.6, and 17.8 ± 2.1 E-CFU per spleen, respectively. The second group consisted of mice treated with levan and schizophyllan (SPG). These compounds, respectively, produced 12.6 ± 1.6 and 12.0 ± 2.1 E-CFU per spleen to enhance colony formation 2.8- and 2.7-fold. Lentinan, krestin (PSK), mannan-R, and glucan-C (group 3) did not increase E-CFU colony formation above that of radiation controls. When spleen weights were determined, the greatest increase was observed in group 1, followed in decreasing order by groups 2 and 3. However, differences in spleen weights were not as obvious as differences in E-CFU numbers. Thus, when administered before irradiation, three of the soluble polyglycans (mannan-A, glucan-F, and glucan-S) provided hemopoiesis-enhancing effects at least equivalent to those of glucan-P.

The effects of various polyglycans on E-CFU colony formation when administered after irradiation are presented in Table 3. The various polyglycan-treated mice again exhibited E-CFU numbers that placed them into one of three groups with respect to radiation controls. Group 1 consisted of only glucan-F–treated mice. These mice exhibited 17.6 ± 1.8 E-CFU per spleen or a 3.9-fold increase over radiation control E-CFU values. Group 2 was comprised of mice treated with glucan-P, PSK, glucan-S, SPG, and mannan-A. These mice, respectively, exhibited 14.8 ± 2.3, 14.7 ± 2.7, 14.4 ± 2.6, 13.9 ± 2.2, and 13.6 ± 3.1 E-CFU per spleen to produce a 3.0–3.3-fold increase in the number of endogenous colonies. Mice injected with mannan-R, levan, lentinan, and glucan-C (group 3) exhibited no increase in E-CFU numbers relative to radiation controls. As with preirradiated polyglycan-treated mice, the spleen weights also reflected the progressive decrease in E-CFU numbers from groups 2 through 3.

TABLE 3. *Effects of polyglycans on endogenous colony formation (E-CFU) when administered 1 h after 6.5 Gy cobalt-60 radiation*

Group	Compound	E-CFU	Enhancement factor	Spleen weight (mg)
Control	Saline (radiation control)	4.5 ± 1.2	1.0	37 ± 1
1	Glucan-F	17.6 ± 1.8	3.9	45 ± 1
2	Glucan-P	14.8 ± 2.3	3.3	49 ± 7
	PSK	14.7 ± 2.7	3.2	46 ± 5
	Glucan-S	14.4 ± 2.6	3.2	45 ± 2
	SPG	13.9 ± 2.2	3.1	45 ± 2
	Mannan-A	13.6 ± 3.1	3.0	44 ± 3
3	Mannan-R	8.2 ± 1.6	1.8	40 ± 3
	Levan	8.0 ± 1.6	1.8	41 ± 2
	Lentinan	6.1 ± 3.0	1.4	43 ± 7
	Glucan-C	4.3 ± 0.7	1.0	41 ± 2

See Tables 1 and 2 for abbreviations and explanations.

DISCUSSION

There are obvious practical reasons for discovering agents that can modify radiation injury and/or the consequent sequelae in mammalian systems. Concern exists especially for the protection of humans who may have to be exposed to external irradiation during medical treatment, for example, as well as protection of those persons who may have been exposed to external irradiation resulting from, for instance, occupational hazards or nuclear accidents.

The type and severity of injuries produced by radiation depend on the dose, dose rate, radiation quality, and type (e.g., local vs. whole body) of exposure. In mice, death following whole-body irradiation in the 700–1,000-rad dose range usually occurs 10 days or longer after exposure, and results from irreversible bone marrow damage (i.e., the hemopoietic syndrome) (22–25). Thus, depletion of hemopoietic stem and progenitor cells results in sustained erythrocytopenia, lymphocytopenia, and granulocytopenia. Ultimately, death results from consequences secondary to the hemopoietic injury, such as immunosuppression and the inability to resist even common infections. Hence, it is generally agreed that survival in the hemopoietic syndrome radiation dose range depends primarily on hemopoietic recovery.

Although many chemical and biological substances have been shown to enhance hemopoietic recovery when administered before radiation exposure, fewer compounds have been shown to be effective when administered after irradiation. A classic example of a biological radioprotectant that possesses both capabilities is bacterial lipopolysaccharide (LPS) (26–28). Recently, the particulate polyglycans glucan-P (14,16,17) and mannozym (M. L. Patchen, unpublished observations) have also been shown to enhance hemopoietic recovery when administered either before or after sublethal radiation exposure. In addition, glucan-P has been shown to dramatically enhance long-term survival of mice receiving an otherwise lethal dose of radiation (14). Glucan-P is capable of modifying host resistance to a variety of bacterial, viral, fungal, and parasitic infections (29–31) and, in fact, the radioprotective effect of glucan-P appears to result not only from its ability to enhance hemopoietic recovery but also from its ability to decrease susceptibility to infections (32).

Although the hemopoietic and radioprotective effects of LPS, mannozym, and glucan-P are impressive, the administration of these agents to humans is not practical owing to their undesirable side effects. Specifically, mannozym and glucan-P have side effects associated with their particulate nature (M. L. Patchen, unpublished observations), and LPS is toxic at high doses (33). The present study clearly indicates that several immunomodulating polyglycans (all of which are soluble and most of which are nontoxic even at doses as high as 5–10 mg/mouse) are also capable of enhancing hemopoietic recovery when administered either before or after radiation exposure. The compounds shown to be effective were mannan-A, glucan-F, glucan-S, SPG, and PSK.

It is interesting to note that no apparent correlation exists between the molecular size of the various polyglycans and their ability to induce hemopoietic recovery. However, when administered before irradiation, glucans isolated from *S. cerevisiae* appeared to exert a greater effect on E-CFU response than did glycans isolated from higher fungi or *Sclerotium glucanium*.

Based on these preliminary studies, little can be concluded concerning the exact mechanisms by which these soluble polyglycans enhance recovery from hemopoietic radiation damage, or if these substances will effectively enhance survival after exposure to otherwise lethal irradiation. Such studies are currently in progress in our laboratory. To date, the only soluble polyglycan able to enhance survival following an otherwise lethal dose of radiation as effectively as glucan-P has been glucan-F (M. L. Patchen, unpublished observations). However, because of the overall similarity in immunological and hemopoietic responses elicited by glucan-P and these soluble polyglycans, and because of the obvious advantages of the soluble polyglycans over historical hemopoietic radioprotectants, we believe the potential for the use of these substances as radioprotectants is great and that research in this area should be pursued.

Acknowledgment: The authors would like to acknowledge the excellent technical assistance of Brenda Watkins and James Atkinson and the typing and editorial assistance of Terrie Hunt, Helen Speight, Junith Van Deusen, Steve Gordon, and Lisa Hunt. This research was supported by Armed Forces Radiobiology Research Institute, Defense Nuclear Agency, under Research Work Unit MJ00029. Research was conducted according to the principles enunciated in the *Guide for the Care and Use of Laboratory Animals* prepared by the Institute of Laboratory Animal Resources, National Research Council.

REFERENCES

1. Hassid W, Joslyn M, McCready M. The molecular constitution of an insoluble polysaccharide from yeast *Saccharomyces cerevisiae*. *J Am Chem Soc* 1941;63:295–8.
2. DiLuzio N, Williams D, McNamee R, Edwards B, Kitahama A. Comparative tumor-inhibitory and antibacterial activity of soluble and particulate glucan. *Int J Cancer* 1979;24:773–9.
3. Riggi S, DiLuzio N. Identification of a reticuloendothelial stimulating agent in zymosan. *Am J Physiol* 1961;200:297–300.
4. DiLuzio N. Pharmacology of the reticuloendothelial system: accent on glucan. In: Reichard S, Escobar M, Friedman H, eds. *The reticuloendothelial system in health and disease: functions and characteristics*. New York: Plenum Press, 1976:412–21.
5. Wooles W, DiLuzio N. Reticuloendothelial function and the immune response. *Science* 1963;141:1078–80.
6. DiLuzio N. Evaluation of the graft-vs-host reaction on the immune competence of lymphoid cells of mice with altered reticuloendothelial function. *J Reticuloendothel Soc* 1967;4:459–75.
7. Cook J, Taylor D, Cohen C, Rodriguez J, Malshet V, DiLuzio N. Comparative evaluation of the role of macrophages and lymphocytes in mediating the anti-tumor action of glucan. In: Chirigos M, ed. *Immune modulation and control of neoplasia by adjuvant therapy*. New York: Raven Press, 1978:183–94. (Progress in cancer research and therapy; vol 19).

8. Lotzová E, Gutterman J. Effect of glucan on natural killer (NK) cells: further comparison between NK and bone marrow effector cell activities. *J Immunol* 1979;123:607–11.
9. Burgaleta C, Golde D. Effect of glucan on granulopoiesis and macrophage genesis in mice. *Cancer Res* 1978;37:1739–42.
10. Niskanen E, Burgaleta C, Cline M, Golde D. Effect of glucan, a macrophage activator, on murine hemopoietic cell proliferation in diffusion chambers in mice. *Cancer Res* 1978;38:1406–9.
11. Patchen M, Lotzová E. Modulation of murine hemopoiesis by glucan. *Exp Hematol* 1980;8:409–22.
12. Deimann W, Fahimi H. Induction of focal hemopoiesis in adult rat liver by glucan, a macrophage activator. *Lab Invest* 1980;42:217–24.
13. Patchen M, Lotzová E. The role of macrophages and T-lymphocytes in glucan-mediated alteration of murine hemopoiesis. *Biomedicine* 1981;34:71–7.
14. Patchen M. Immunomodulation and hemopoiesis. *Surv Immunol Res* 1983;2:237–42.
15. Till J, McCulloch E. Early repair processes in marrow cells irradiated and proliferating *in vivo*. *Radiat Res* 1963;18:96–105.
16. Patchen M, MacVittie T. Use of glucan to enhance hemopoietic recovery after exposure to cobalt-60 irradiation. In: Norman S, Sorkin E, eds. *Macrophage and NK cell regulation and function*. London: Plenum Publications, 1982:267–72.
17. Patchen M, MacVittie T, Wathen L. Effects of pre- and post-irradiation glucan treatment on pluripotent stem cells, granulocyte, macrophage and erythroid progenitor cells, and hemopoietic stromal cells. *Experientia* 1984 (in press).
18. Marsh J, Boggs D, Bishop C, Chervenick P, Cartwright L, Wintrobe M. Factors influencing hemopoietic spleen colony formation in irradiated mice. *J Exp Med* 1967;126:833–48.
19. Smith W, Budd R, Cornfield J. Estimation of radiation dose-reduction factor for beta-mercapto-ethylamine by endogenous spleen counts. *Radiat Res* 1966;27:363–8.
20. Kinnamon K, Ketterling L, Stampfli H, Grenan M. Mouse endogenous spleen counts as a means of screening for anti-radiation drugs. *Proc Soc Exp Biol Med* 1982;164:370–3.
21. Hollander M, Wolfe D, eds. *Nonparametric statistical methods*. New York: Wiley and Sons, 1973.
22. Jacobson L. The hemopoietic effects of ionizing radiation. In: Hollander A, ed. *Radiation biology*. New York: McGraw-Hill, 1954:1029–90.
23. Congdon C. Bone marrow transplantation in animals exposed to whole body irradiation. *J Cell Comp Physiol* 1957;50:103–8.
24. Fabrikant J, ed. *Radiobiology*. Chicago: Year Book Medical Publishers, 1972.
25. Arena V, ed. *Ionizing radiation and life*. St. Louis: Mosby, 1971.
26. Smith W, Alderman I, Gillespie R. Hematopoietic recovery induced by bacterial endotoxin in irradiated mice. *Am J Physiol* 1958;192:549–56.
27. Smith W, Biecher G, Budd R, Fred S. Effects of bacterial endotoxin on occurrence of spleen colonies in irradiated mice. *Radiat Res* 1966;27:369–74.
28. Boggs D, Marsh J, Chervenick P, Cartwright G, Wintrobe M. Factors influencing hematopoietic spleen colony formation in irradiated mice IV: the different effect of foreign plasma, endotoxin, and bleeding on colony-forming cell kinetics. *Radiat Res* 1968;35:68–77.
29. Lahnborg G, Hedstrom K, Nord C. The effect of glucan—a host resistance activator—and ampicillin on experimental intraabdominal sepsis. *J Reticuloendothel Soc* 1982;32:347–53.
30. Williams D, Browder W, DiLuzio N. Immunotherapeutic modification of *Escherichia coli*-induced experimental peritonitis and bacteremia by glucan. *Surgery* 1983;93:448–54.
31. DiLuzio N. Immunopharmacology of glucan: a broad spectrum enhancer of host defense mechanisms. *Trends Pharmacol Sci* 1983;4:344–7.
32. Patchen M, Walker R, Brook I, MacVittie T. Glucan, an immunologic and hemopoietic agent, inhibits sepsis and enhances survival of lethally irradiated mice. In: Broerse J, Barendsen G, Kal H, Van der Kogel A, eds. *Proceedings of the Seventh International Congress of Radiation Research*. The Netherlands: Martinus Nijhoff, 1983:D5–30.
33. Morrison DC, Ulevitch RJ. The effects of bacterial endotoxin on host mediation systems. *Am J Pathol* 1978;93:527–617.

Experientia 40 (1984), Birkhäuser Verlag, CH-4010 Basel/Switzerland

Effects of pre- and post-irradiation glucan treatment on pluripotent stem cells, granulocyte, macrophage and erythroid progenitor cells, and hemopoietic stromal cells

M. L. Patchen, T. J. MacVittie and L. M. Wathen

Experimental Hematology Department, Armed Forces Radiobiology Research Institute, Bethesda (Maryland 20814, USA), 12 April 1983

Summary. Glucan, a beta-1,3 polyglucose, was administered to mice either 1 h before or 1 h after a 650 rad exposure to cobalt-60 radiation. Compared to radiation controls, glucan-treated mice consistantly exhibited a more rapid recovery of pluripotent stem cells and committed granulocyte, macrophage, and erythroid progenitor cells. This may partially explain the mechanism by which glucan also enhances survival in otherwise lethally irradiated mice.

Key words. Mice; glucan treatment; Co^{60}-irradiation; stem cells, pluripotent; granulocytes; macrophages; erythroid progenitor cells; hemopoietic stomal cells; hemopoiesis.

Introduction

Glucan, a β-1,3 polyglucose isolated from the inner cell wall of the yeast *Saccharomyces cerevisiae*[1, 2] is a potent stimulator of the reticuloendothelial system[3, 4] and a dose-dependent modulator of the cellular[5, 6] and humoral[7] immune systems and hemopoietic system[8–12]. Specifically, in terms of effects on hemopoiesis, the administration of glucan to normal mice results in an overall increase in the production of pluripotent stem cells and also granulocyte-macrophage, pure macrophage, and erythroid progenitor cells. The enhanced granulocyte and macrophage genesis observed in glucan-treated animals has been associated with glucan's ability to induced the production and/or release of granulocyte-macrophage colony-stimulating activity (CSA)[8–11]. At this time, the mechanisms of glucan's enhancement of other aspects of hemopoiesis are not fully understood.

Because of glucan's profound stimulatory effects on hemopoiesis at the stem cell and progenitor cell levels, its use as a therapeutic agent in cases of hemopoietic depletion induced by drugs and/or radiation has been suggested[10–12]. Recently, it has been reported that glucan induced increased numbers of endogenous pluripotent spleen colony-forming units (E-CFU)[9] and also increased numbers of peripheral blood granulocytes[11] when administered either before or after hemopoietically damaging doses (550–650 rads) of gamma radiation. The purpose of this study was to examine in detail the effects of pre- and post-irradiation glucan treatment on the recovery of hemopoietic stromal cells (HSC), transplantable pluripotent hemopoietic stem cells (CFU-s), granulocyte-macrophage progenitor cells (GM-CFC), macrophage progenitor cells (M-CFC), and erythroid burst and colony-forming cells (BFU-e, CFU-e).

Materials and methods

10- to 12-week-old female B6D2F_1 mice were used in all experiments. All mice were quarantined and acclimated to laboratory conditions for 2 weeks before experimentation. Particulate, endotoxin-free glucan was obtained from Accurate Chemical and Scientific Corporation (Westbury, N.Y.) and was prepared according to DiLuzio's modification[1] of Hassid's original procedure[2]. Glucan was diluted in sterile 5% dextrose, and 1.5 mg (approximately 75 mg/kg) was intravenously injected into experimental mice either 1 h before or 1 h after exposure to 650 rads of total-body cobalt-60 radiation.

Normal control (not irradiated and not glucan-treated) and radiation control (irradiated, but not glucan-treated) mice were injected with an equivalent volume (0.5 ml) of sterile 5%-dextrose. At 1, 3, 6, 8, 10, 14, and 21 days after irradiation, 2 mice from each group were killed by cervical dislocation, and the bones (2 femurs per mouse) and spleens were removed to be assayed for total nucleated cellularity (TNC), HSC, CFU-s, GM-CFC, M-CFC, BFU-e, and CFU-e.

Cell suspensions. Each cell suspension represented the pool of tissues from 2 mice. Cells were flushed from bones with 3 ml of Hank's Balanced Salt Solution (HBSS) containing 5% heat-inactivated fetal bovine serum (HIFBS). Spleens were pressed through a stainless steel mesh screen, and the cells were washed from the screen with 6 ml of HBSS plus 5% HIFBS. The total number of nucleated cells in each suspension was determined by counting the cells on a hemocytometer.

Hemopoietic cell assays. The hemopoietic assays used have been described in detail elsewhere[11,12]. Bone marrow and splenic hemopoietic stromal cells were cultured according to the method of Wathen et al.[16]. On days 7 and 14, respectively, bone marrow and splenic cultures were fixed in methanol, stained with Mallory's Azure II Methylene Blue, and the number of HSC colonies (> 50 cells) counted. CFU-s were evaluated by the spleen colony assay[17] as previously described[11]. 8 days after transplantation, the recipients were sacrificed and their spleens removed. The spleens were fixed in Bouin's solution, and the number of grossly visible colonies were counted. Committed granulocyte-macrophage hemopoietic progenitor cells (GM-CFC) were assayed by MacVittie's modification[18] of the semi-solid agar technique originally described by Bradley and Metcalf[19] and Pluznik and Sachs[20]. Colonies (> 50 cells) were counted after 10 days of incubation in a 37°C humidified environment containing 7.5% CO_2. Committed pure macrophage hemopoietic progenitor cells (M-CFC) were assayed by the technique described by MacVittie et al.[21]. Cultures were incubated for 28 days at 37°C in a humidified atmosphere containing 7.5% CO_2, before scoring colony formation. Bone marrow and splenic CFU-e and BFU-e were assayed by a modification[22] of the original plasma clot technique described by Stephenson et al.[23]. Clotted CFU-e and BFU-e cultures were incubated at 37°C in a humidified atmosphere containing 5% CO_2 in air for 2 days and 7 days, respectively. Plasma clots were then harvested, fixed with 5% glutaraldehyde, and stained with benzidine and giemsa[24]. A CFU-e was defined as an individual aggregate of 8 or more benzidine-positive cells. A BFU-e was defined as a group of many large contiguous clusters of benzidine-positive cells.

Statistical analysis. In each experiment, the normal control values were used to convert radiation control and glucan values into percentages (i.e., percent of normal control). Percent values presented in tables 1–4 represent the means of percent values obtained from at least 3 replicate experiments. Student's 2-tailed t-test was used to determine the statistical difference between mean values obtained from radiation control and glucan-treated mice.

Results

Bone marrow hemopoietic recovery in mice administered glucan 1 h before irradiation is shown in table 1. It can be seen that recovery of the hemopoietic parameters commenced earlier in glucan-treated animals than in animals receiving radiation alone (radiation controls). By 21 days post-irradiation, femoral TNC, HSC, and CFU-e in radiation controls had reached levels comparable to those in glucan-treated mice, while CFU-s, GM-CFC, M-CFC, and BFU-e in glucan-treated mice remained significantly elevated above radiation control levels. Like in the bone marrow, all aspects of splenic hemopoietic recovery commenced earlier in pre-irradiation glucan-treated mice than in radiation controls (table 2). Again, splenic HSC and CFU-e values in the 2 groups of mice were comparable by 21 days post-irradiation, while splenic TNC, CFU-s, GM-CFC, M-CFC, and BFU-e levels in glucan-treated mice remained elevated above radiation control levels. This was true even when splenic CFU-s, GM-CFC and BFU-e numbers in radiation controls exceeded those of normal control mice (i.e., were greater than 100%). Specifically, although an overshoot in CFU-s, GM-CFC, and BFU-e splenic values was observed in radiation controls by day 21 post-irradiation, the overshoot in glucan-treated mice first became apparent as early as 10 days post-irradiation and remained above radiation control levels through day 21 post-irradiation.

The results of experiments assaying the effects of post-irradiation glucan treatment on bone marrow and splenic hemopoietic recovery are shown in tables 3 and 4, respectively. In all instances except that of bone marrow HSC, hemopoietic recovery again commenced earlier in glucan-treated than in radiation control mice.

Table 1. Bone marrow hemopoietic recovery in B6D2F$_1$ mice given 1.5 mg of glucan at 1 h before 650 rads of whole-body cobalt-60 radiation (% normal control)

Day post irradiation	TNC Radiation control	TNC + Glucan	HSC Radiation control	HSC + Glucan	CFU-s Radiation control	CFU-s + Glucan	GM-CFC Radiation control	GM-CFC + Glucan	M-CFC Radiation control	M-CFC + Glucan	BFU-e Radiation control	BFU-e + Glucan	CFU-e Radiation control	CFU-e + Glucan
1	8	18	12	12	0	0	0	0	0	0	0	0	0	0
3	4	4	11	11	0	0	0	2	0	1	0	0	0	0
6	8	8	11	10	0	5	1	5	0	3	0	3	9	13
8	19	28*	18	18	1	12*	3	16*	2	4	1	16*	28	51*
10	21	58*	19	35*	3	30*	5	35*	3	18*	4	28*	35	83*
14	27	69*	23	44*	5	41*	29	50*	13	42*	14	32*	76	86*
21	82	81	60	56	22	68*	41	92*	22	70*	57	68*	88	96

* $p \leq 0.01$ with respect to the respective time matched radiation control values

Table 2. Splenic hemopoietic recovery in B6D2F$_1$ mice given 1.5 mg of glucan at 1 h before 650 rads of total-body cobalt-60 radiation (% of normal control)

Day post irradiation	TNC Radiation control	+ Glucan	HSC Radiation control	+ Glucan	CFU-s Radiation control	+ Glucan	GM-CFC Radiation control	+ Glucan	M-CFC Radiation control	+ Glucan	BFU-e Radiation control	+ Glucan	CFU-e Radiation control	+ Glucan
1	9	9	2	0	0	0	0	0	0	0	0	0	0	0
3	9	8	2	2	0	0	0	0	0	0	0	0	0	0
6	7	10	4	3	0	2	0	21[a]	0	6[a]	0	0	0	1
8	9	15	10	13	0	4	0	34[a]	0	7[a]	0	2	1	19[a]
10	10	50[a]	13	88[a]	0	60[a]	1	250[a]	1	96[a]	0	180[a]	2	343[a]
14	65	84[a]	41	122[a]	32	190[a]	94	1207[a]	8	316[a]	40	326[a]	410	684[a]
21	76	88[a]	54	50	191	300[a]	744	2503[a]	60	360[a]	121	451[a]	920	918

[a] $p > 0.01$ with respect to the respective time matched radiation control value.

Table 3. Bone marrow hemopoietic recovery in B6D2F$_1$ mice given 1.5 mg of glucan at 1 h before 650 rads of total-body cobalt-60 radiation (% normal control)

Day post irradiation	TNC Radiation control	+ Glucan	HSC Radiation control	+ Glucan	CFU-s Radiation control	+ Glucan	GM-CFC Radiation control	+ Glucan	M-CFC Radiation control	+ Glucan	BFU-e Radiation control	+ Glucan	CFU-e Radiation control	+ Glucan
1	8	8	12	6	0	0	0	0	0	0	0	0	0	0
3	4	4	11	9	0	0	0	1	0	1	0	0	0	0
6	8	11	11	10	0	0	1	3	0	1	0	0	9	3
8	19	23	18	13	1	0	3	4	2	2	1	1	28	25
10	23	34[a]	19	14	3	17[a]	5	24[a]	3	12[a]	4	9	35	69[a]
14	27	43[a]	23	19	5	22[a]	29	41[a]	13	26[a]	14	45[a]	76	67
21	82	65[a]	60	45[a]	22	37[a]	41	71[a]	22	52[a]	57	94[a]	88	50[a]

[a] $p > 0.01$ with respect to the respective time matched radiation control value.

CFU-s, GM-CFC, M-CFC, and BFU-e bone marrow contents and splenic TNC, GM-CFC, M-CFC, BFU-e, and CFU-e contents in glucan-treated mice were all significantly elevated over those of radiation controls from days 10 to 21 post-irradiation. However, several other hemopoietic parameters in glucan-treated mice neither remained above nor even equaled those of radiation controls. For example, in glucan-treated mice at 21 days after irradiation, the femoral TNC, HSC, and CFU-e contents and the splenic HSC and CFU-s contents were actually less than those of radiation control mice.

The splenic 'overshoot' phenomenon observed in pre-irradiation glucan-treated mice was again observed in the CFU-s, GM-CFC, M-CFC, BFU-e, and CFU-e post-irradiation glucan-treated mice. Interestingly, the overshoot in CFU-s, GM-CFC, and M-CFC in post-irradiation glucan-treated mice was less dramatic than in pre-irradiation glucan-treated mice, whereas the overshoot in BFU-e and CFU-e in post-irradiation glucan-treated mice was more dramatic than in pre-irradiation glucan-treated mice.

Discussion

Injection of particulate glucan into normal mice has previously been shown to result in increased numbers of bone marrow and/or splenic CFU-s, GM-CFC, M-CFC, BFU-e, and CFU-e [1]. The studies presented here demonstrate the ability of glucan to speed bone marrow and/or splenic HSC, CFU-s, GM-CFC, M-CFC, BFU-e, and CFU-e recovery in hemopoietically compromised animals. Specifically, glucan was shown to enhance the recovery of these hemopoietic progenitors when administered either before or after a hemopoietically damaging 650-rad dose of total-body gamma radiation. For example, the most severe depletion of all hemopoietic elements in both radiation control and glucan-treated mice was observed 1–3 days after radiation exposure. However, most hemopoietic elements in glucan-treated mice exhibited a major rebound within 6–14 days after irradiation, while the major rebound in radiation control mice was not observed until 14–21 days after irradiation. It should be pointed out that although both pre-irradiation and post-irradiation glucan treatments significantly enhanced hemopoietic repopulation in comparison to that in radiation controls, the pre-irradiation glucan treatment appeared to be more effective than post-irradiation glucan treatment. These results correlate well with our previous observations that although equal numbers of endogenously arising spleen colonies (E-CFU) were observed in both 1-h pre- and 1-h post-irradiation glucan-treated mice[14], the size of the E-CFU appeared to be larger in mice receiving glucan before irradiation.

In addition it should be noted that the hemopoietic effects of glucan primarily occurred within the first 2 weeks after irradiation, since by 3 weeks post-irradiation hemopoietic values in radiation control and glucan-treated mice in many instances were similar. This was true even in instances when recovery had not yet progressed to normal control values (i.e., 100%), and no explanation for this apparent latent slow down in glucan-induced hemopoiesis is proposed at this time.

It is interesting to note that additional particulate substances (e.g., Zymosan, *C. parvum*, glass beads, Portland cement) have also been shown to enhance hemopoiesis when administered before and in some cases after sublethal irradiation. However, we do not that feel the enchanced hemopoietic recovery observed in our

Table 4. Splenic hemopoietic recovery in B6D2F$_1$ mice given 1.5 mg of glucan at 1 h before 650 rads of total-body cobalt-60 radiation (% normal control)

Day post irradiation	TNC Radiation control	+ Glucan	HSC Radiation control	+ Glucan	CFU-s Radiation control	+ Glucan	GM-CFC Radiation control	+ Glucan	M-CFC Radiation control	+ Glucan	BFU-e Radiation control	+ Glucan	CFU-e Radiation control	+ Glucan
1	9	14	2	0	0	0	0	0	0	0	0	0	0	0
3	9	7	2	1	0	0	0	0	0	0	0	0	0	0
6	7	9	4	5	0	0	0	2	0	1	0	0	0	0
8	9	11	10	13	0	1	0	5[a]	0	3	0	2	1	1
10	10	21[a]	13	66[a]	0	9[a]	1	68[a]	1	20[a]	0	23[a]	2	103[a]
14	65	100[a]	41	149[a]	32	129[a]	94	1338[a]	8	126[a]	40	468[a]	410	776[a]
21	76	122[a]	54	44[b]	191	159[a]	744	1706[a]	60	198[a]	121	564[a]	920	1515[a]

[a] $p > 0.01$ with respect to the respective time-matched radiation control value; [b] $p > 0.05$ with respect to the respective time-matched radiation control value.

studies is due merely to the particulate nature of glucan, sinced we can easily reproduce these results using a soluble glucan preparation (manuscript in preparation). In addition, previous studies evaluating the hemopoietic radioprotective properties of various other substances have primarily used enhancement of endogenous colony-forming unit (E-CFU) numbers to indicate an agent's radioprotective capacity. Although E-CFU recovery does correlate well with CFU-s recovery, neither the E-CFU nor the CFU-s assays can reveal information about the recovery of the various committed hemopoietic progenitors cells (e.g., GM-CFC, M-CFC, CFU-e, BFU-e). Thus, our study has also demonstrated the radioprotective effects of glucan on these specific progenitor cells as well as on the pluripotent stem cells measured by the E-CFU and CFU-s assays.

Recently we have also shown that the administration of glucan before exposure to lethal whole-body gamma radiation (e.g., 900 rads) is capable of enhancing survival[25]. The exact correlation between glucan's hemopoietic enhancing capabilities and glucan's effects on post-irradiation survival remains to be determined. Since death after irradiation often results from the surgence of opportunistic infections, glucan treatment may provide a critical advantage by early-on stimulating the repopulation of hemopoietic precursors (i.e., CFU-s, GM-CFC, M-CFC) capable of replenishing the granulocytes and macrophages necessary for resisting bacterial invasion. This may indeed be possible since in non-irradiated animals glucan has been shown to profoundly enhance the resistance of animals to a variety of experimental infections[2, 26-28]. Additionally, recent experiments in our laboratory have indicated that glucan-treated irradiated animals present fewer opportunistic infections than do radiation controls (Patchen, Brook, Walker, unpublished observations).

Although much remains to be understood concerning the ability of glucan to enhance the recovery from radiation-induced hemopoietic aplasia, the implications and possible applications of glucan treatment are intriguing.

1 Hassid, W.Z., Joslyn, M.A., and McCready, M., The molecular constitution of an insoluble polysaccharide from yeast *Saccharomyces cerevisiae*. J. Am. chem. Soc. *63* (1941) 295–298.

2 DiLuzio, N.R., Williams, D.L., McNamee, R.B., Edwards, B.F., and Kitahama, A., Comparative tumor-inhibitory and antibacterial activity of soluble and particulate glucan. Int. J. Cancer *24* (1979) 773–779.

3 DiLuzio, N.R., Pisano, J.C., and Saba, T.M., Evaluation of the mechanism of glucan induced stimulation of the reticuloendothelial system. J. reticuloendoth. Soc. *7* (1970) 731–742.

4 DiLuzio, N.R., in: Pharmacology of the reticuloendothelial system-accent on glucan; in The reticuloendothelial system in health and disease. Functions and characteristics, pp. 412–421. Eds S.M. Reichard, M.E. Escobar and H. Friedman. Plenum Press, New York 1976.

5 Cook, J.A., Taylor, D., Cohen, C., Rodrigue, J., Malshet, V., and DiLuzio, N.R., Comparative evaluation of the role of macrophages and lymphocytes in mediating the antitumor action of glucan, in: Immune modulation and control of neoplasma by adjuvant therapy, pp. 183–194. Ed. M.A. Chirigos. Raven Press, New York 1978.

6 DiLuzio, N.R., Evaluation of the graft-vs-host reaction of the immune competence of lymphoid cells of mice with altered reticuloendothelial function. J. reticuloendoth. Soc. *4* (1967) 459–475.

7 Woodes, W.R., and DiLuzio, N.R., Reticuloendothelial function and immune response. Science *142* (1961) 1078–1080.

8 Burgalet, C., and Goldie, D.W., Effect of glucan on granulopoiesis and macrophage genesis in mice. Cancer Res. *38* (1978) 1739–174.

9 Niskanen, E.O., Burgaleta, C., Chne, M.J., and Goldie, D.W., Effect of glucan, a macrophage activator, on murine hemopoietic cell proliferation in diffusion chambers in mice. Cancer Res. *38* (1978) 1406–1409.

10 Patchen, M.L., and Lotzova, E., Modulation of murine hemopoiesis by glucan. Exp. Hemat. *8* (1980) 409–422.

11 Patchen, M.L., and MacVittie, T.J., Dose-dependent responses of murine pluripotent stem cells and myeloid and erythroid progenitor cells following administration of the immunomodulating agent glucan. Immunopharmacology *5* (1983) 303–313.

12 Patchen, M.L., and MacVittie, T.J., Temporal response of murine pluripotent stem cells and myeloid and erythroid progenitor cells to low-dose glucan treatment. Acta hemat. *70* (1983) 281–288.

13 Patchen, M.L., and Lotzova, E., The role of macrophages and T-lymphocytes in glucan mediated alteration of murine hemopoiesis. Biomedicine *34* (1981) 71–77.

14 Patchen, M.L., and MacVittie, T.J., Use of glucan to enhance hemopoietic recovery after exposure to cobalt-60 irradiation, in: Macrophages and natural killer cells, pp. 267–272. Eds S.J. Norman and E. Sorkin. Plenum Press, New York 1982.

15 Pospisil, M., Jaty, J., Netukova, J., and Marek, M., Glucan-induced enhancement of hemopoietic recovery in gamma-irradiated mice. Experientia *38* (1982) 1232–1234.

16 Wathen, L.K., Knapp, S.A., and DeGowin, R.L., Suppression of marrow stromal cells and microenvironmental damage following sequential radiation and cyclophosphamide. Int. J. Radiat. Oncol. biol. Phys. *7* (1981) 935–941.

17 Till, J.E., and McCulloch, E.A., A direct measurement of radiation sensitivity of normal bone marrow cells. Radiat. Res. *14* (1961) 213–222.

18 MacVittie, T.J., Alterations induced in macrophage and granulocyte-macrophage colony-forming cells by a single injection of mice with *Corynebacterium parvum*. J. reticuloendoth. Soc. *26* (1979) 479-490.
19 Bradley, T.R., and Metcalf, D., The growth of mouse bone marrow cells in vitro. Aust. J. exp. Biol. med. Sci. *44* (1966) 287-300.
20 Pluznik, D.H., and Sachs, L., The cloning of normal 'mast' cells in tissue culture. J. Cell Physiol. *66* (1965) 319-324.
21 MacVittie, T.J., and Weatherly, T.L., Characteristics of the *in vitro* monocyte macrophage colony forming cells detected in mouse thymus and lymph nodes, in: Experimental Hematology Today, pp. 147-156. Eds S.J. Baum and G.D. Ledney. Springer-Verlag, New York 1977.
22 Weinberg, S.R., McCarthy, E.G., MacVittie, T.J., and Baum, S.J., Effect of low-dose irradiation on pregnant mouse hemopoiesis. Br. J. Haemat. *48* (1981) 127-135.
23 Stephenson, J.R., Axelrad, A.A., McLeod, D.L., and Shreeve, M.M., Induction of colonies of hemoglobin-synthesizing cells by erythropoietin in vitro. Proc. natl Acad. Sci. USA *68* (1971) 1542-1546.
24 McLeod, D.L., Shreeve, M.M., and Axelrad, A.A., Culture system in vitro for the assay of erythropoietic and megakaryocytic progenitors; in: In vitro aspects of erythropoiesis, pp. 31-36. Ed. M.J. Murphy. Springer, New York 1978.
25 Patchen, M.L., Immunomodulation and Hemopoiesis. Surv. Immun. Res. *2* (1983) 237-242.
26 Kokosis, P.L., Williams, D.L., Cook, J.A., and DiLuzio, N.R., Increased resistance to *Staphylococcus aureus* infection and enhancement in serum lysozyme activity by glucan. Science *199* (1978) 1340-1342.
27 Reynolds, J.A., Kastello, M.D., Harrington, D.G., Crobbs, C.L., Peters, C.J., Jemski, J.V., Scott, G.H., and DiLuzio, N.R., Glucan-induced enhancement of host resistance to selected infectious disease. Infect. Immun. *30* (1980) 51-57.
28 DiLuzio, N.R., Williams, D.L., and Browder, W., Immunopharmacology of glucan: The modification of infectious disease, in press.

0014-4754/84/111240-05$1.50 + 0.20/0

Alterations in Gastric Mucus Secretion in Rhesus Monkeys After Exposure to Ionizing Radiation

T. SHEA-DONOHUE, E. DANQUECHIN-DORVAL, E. MONTCALM, H. EL-BAYAR, A. DURAKOVIC, J. J. CONKLIN, and A. DUBOIS
Department of Medicine, Uniformed Services University of the Health Sciences, and Radiation Sciences Department, Armed Forces Radiobiology Research Institute, Bethesda, Maryland

The aim of the present study was to evaluate the effect of γ-irradiation on soluble gastric mucus. Six conscious chair-adapted rhesus monkeys were studied once before and twice after exposure to ionizing irradiation (800 rads). Using a marker (^{99m}Tc-DTPA) dilution technique, acidic glycoprotein (AG), neutral glycoprotein (NG), ion, and fluid output were determined during a basal period and after the administration of an 80-ml water load. Irradiation significantly increased the outputs of both AG and NG during the basal period. After the water load, NG output remained elevated but irradiation abolished postload AG output thus inhibiting the normal rise in AG output stimulated by the load. Two days after irradiation NG output had returned to control levels whereas AG output was still suppressed. Sodium and potassium ion outputs were unaltered by irradiation. Chloride and fluid outputs were significantly inhibited on the day of irradiation but had returned to control levels within 3 days. These results indicate that irradiation produces significant changes in both the quantity and nature of the soluble mucus glycoproteins secreted into the gastric juice. It is suggested that these changes may compromise the protective ability of gastric mucus.

Exposure to high doses of radiation (>600 rads) produces diarrhea, infection, and fluid loss within 1 wk as a result of damage to epithelial cells. Moreover, a recent study has demonstrated that gastric mucosal biopsy specimens obtained on the day of radiation exposure (800 rads) produce superficial ulceration which fail to heal within 7–9 days (1). This observation could be related to many factors including the secretion of mucus, the presence of a mucosal gel layer, the intragastric hydrogen ion concentration, as well as the integrity and rate of renewal of epithelial cells. In the present study, the effect of irradiation on changes in gastric soluble mucus and ion secretion were evaluated in primates. Gastric secretion of glycoproteins was used as an index of both soluble and insoluble mucus production (2).

Methods

Six male unanesthetized monkeys (*Macaca mulatta*) weighing 3–4 kg were adapted to primate restraining chairs and housed in closed, ventilated, lighted booths between 9 AM and 12 PM. The monkeys were trained to accept a 12F double-lumen nasogastric ventrol Levin tube (National Catheter, Mallencrodt, Argyle, N.Y.; bore, 4 mm; wall thickness, 1 mm). The experiments were conducted after an overnight fast and were started 45 min after the tube had been placed. Proper positioning of the tube in the most dependent part of the stomach was verified by demonstrating that, after injecting 15 ml of water into a

Received April 2, 1984. Accepted September 28, 1984.

Address requests for reprints to: Terez Shea-Donohue, Ph.D., Department of Medicine, Uniformed Services University, 4301 Jones Bridge Road, Bethesda, Maryland, 20814-4799.

This work was supported in part by the Uniformed Services University of the Health Sciences Protocol No. C08343.

The opinions and assertions contained herein are the private ones of the authors and are not to be construed as official or reflecting the views of the Department of Defense or the Uniformed Services University of the Health Sciences.

The experiments reported herein were conducted according to the principles set forth in the "Guide for the Care and Use of Laboratory Animals," Institute of Animal Resources, National Research Council, DHEW Publication No. (NIH) 78-23.

The authors thank M. Flynn, J. Stewart, J. Warrenfeltz, and N. L. Fleming for their valuable support in animal handling and radiopharmaceutical preparation and administration. They also thank Linda Iwanyck and Joy Barchers for their expert editorial assistance.

Abbreviations used in this paper: AB, Alcian blue; AG, acidic glycoprotein; NG, neutral glycoprotein.

previously emptied stomach, the total volume could be recovered.

A marker (^{99m}Tc-DTPA) dilution technique previously described and validated in monkeys and humans (3–6) was used to determine gastric ion and mucus output. The animals were studied during a 40-min basal period and for 60 min after the intragastric administration of an 80-ml water load (pH 7.4, 37°C). Samples of gastric juice were centrifuged and samples of the clear supernatant were counted in a auto-γ-counter (Ultragamma, LKB Instruments Inc., Gaithersburg, Md.). Intragastric volumes of fluid (V_1, V_2, . . .) and amounts of ^{99m}Tc-DTPA were determined using the marker dilution principle (4,7,8). Net rate of fluid output was determined for each 10-min interval (t) between two dilutions assuming that it remained constant over the given interval and using the equation

$$R_v = [V_2 - V_1 \times \exp(-gt)] \times g/[1 - \exp(-gt)],$$

where g is the fractional emptying rate.

The concentration of soluble mucus in each sample was estimated using two methods; the Alcian blue (AB) dye binding and the periodic acid–Schiff reaction. Alcian blue is a cationic dye that forms an irreversible complex with acidic glycoproteins and other negatively charged macromolecules. A modification of the method of Piper et al. (9) was used for the determination of AB binding to acidic glycoproteins. Briefly 0.1 ml of gastric juice was mixed with 4.2 ml of McIlvaine's citrate phosphate buffer (pH 5.8, 0.12 M $NaHPO_4$ and 0.4 M citric acid) and 0.2 ml of AB (10 mg/ml). The volume was then increased to 5 ml by adding distilled water. The concentration of AB in the reaction mixture was 0.4 mg/ml and the pH was 5.8. The reaction mixture was incubated at 22°C for 24 h and centrifuged at 2500 rpm for 10 min. The concentrations of AB in the supernatant fraction were estimated spectrophotometrically at 615 mm (Gilford Microsample, Oberlin, Ohio) and compared with a standard curve constructed using porcine gastric mucin (Sigma Chemical Co., St. Louis, Mo.).

The periodic acid–Schiff method described by Mantle and Allen (10) was used to estimate neutral glycoproteins. The reaction mixture consisted of 0.2 ml of gastric juice and 1.8 ml of isotonic saline to make a volume of 2 ml. Then, 0.2 ml of fresh periodic acid solution (10 μl of 50% periodic acid in 10 ml of 7% acetic acid) was added to the reaction mixture and was incubated at 37°C for 2 h. Subsequently, 0.2 ml of active Schiff solution was added and all tubes were vortexed immediately. The specimens stood for 30 min at room temperature after which the optical density was determined spectrophotometrically at 555 nm using porcine gastric mucin as a standard.

The intragastric concentration of soluble mucus at the start of the interval (M_1) and at the end of the interval (M_2) are expressed as milligrams of mucin per milliliter. The net rate of soluble mucus output (R_M) expressed in milligrams of mucin equivalents was then calculated using the equation

$$R_M = [M_2 - M_1 \times \exp(-gt)] \times g/[1 - \exp(-gt)].$$

The concentration and output of neutral glycoprotein (NG) and acidic glycoprotein (AG) were determined separately. Sodium (Na^+) and potassium (K^+) ion concentrations were measured using a flame photometer (Instrumentation Laboratory, Inc., Model 443, Lexington, Mass.) and chloride (Cl^-) ion concentration was determined using an amperometric titration method (Corning 920 M, Medfield, Mass.). The intragastric mass of each ion (I_1, I_2, . . .) was determined by multiplying the intragastric ion concentration by the corresponding intragastric volume. The net rate of each ion output (R_I) was then calculated using the equation

$$R_I = [I_2 - I_1 \times \exp(-gt)] \times g/[1 - \exp(-gt)].$$

The calculations were performed using a locally developed program and PDP-10 computer (Division of Computer Research Technology, National Institutes of Health, Bethesda, Md.). The assumptions involved have been described and discussed elsewhere (3–6) and are based on the original contribution of Hildes and Dunlop (8).

In this study each monkey was studied on three separate days: once before (preirradiation), on the day of (irradiation), and 2 days after (2 days postirradiation) irradiation; 800 rads were delivered bilaterally to the whole body using a large 10^5 Ci ^{60}Co irradiation at 500 rads/min. Values for gastric secretory parameters obtained during the first two 10-min intervals of each study were discarded in order to allow for the establishment of a steady state. Those obtained during the third and fourth 10-min fasting intervals were averaged for each study to obtain one fasting (basal) value per animal, and the mean (±SE) was calculated for each day of the study. Values obtained during seven 5- or 10-min intervals after the 80-ml water load (postload) were also averaged for each study to determine one postload value per animal. The mean (±SE) postload value was then calculated for each type of study. The statistical significance of differences observed for each measurement of gastric function (e.g., Na^+ output, mucus output) was evaluated using a three-factor (treatment, time, and monkey) analysis of variance with repeated measures on the last two factors (11), the program LDU-040 (K.L. Dorn), and an IBM 370 computer (Division of Computer Research and Technology, National Institutes of Health).

Results

Before irradiation, the basal output and concentration of AGs is approximately twice that of NGs (Figures 1 and 2). In addition, the output and concentration of AG are significantly ($p < 0.05$) increased by 270% and 88%, respectively, in response to the water load (Figures 3 and 4 vs. Figures 1 and 2). In contrast, NG output and concentration are relatively unchanged by the administration of the water load. As a result of this difference, postload AG output is ~7 times postload NG output and postload AG concentration is 5–6 times that of postload NG concentration.

Exposure to irradiation significantly stimulated both the basal (Figure 1) and postload (Figure 2) output of NG by 150%. In addition, NG concentra-

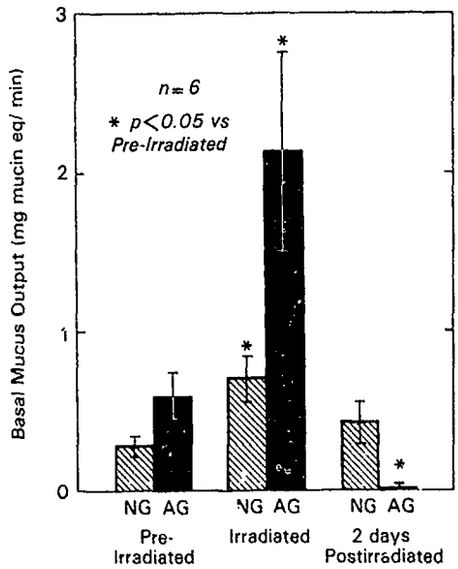

Figure 1. Basal soluble mucin output before, on the day of, and 2 days after exposure to irradiation. Each bar represents the mean ± SE of values obtained in 6 monkeys.

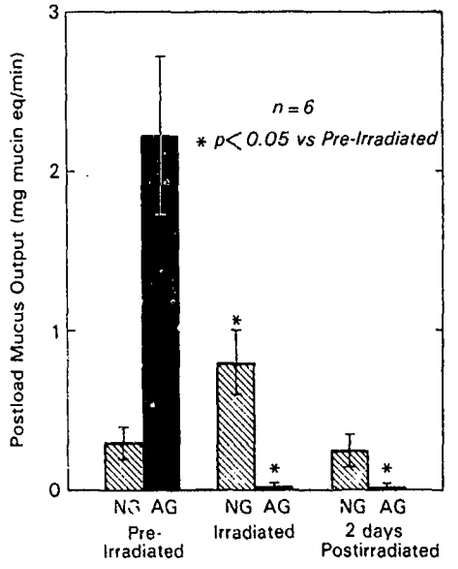

Figure 3. Postload soluble mucin output before, on the day of, and 2 days after exposure to irradiation. Each bar represents the mean ± SE of values obtained in 6 monkeys.

tion in the gastric juice was increased by 61% basally (Figure 3) and was significantly enhanced by 270% after the water load (Figure 4). However, both basal and postload NG output and concentration had returned to preirradiation levels within 2 days after irradiation. Like NG output, the basal secretion of AG was increased significantly by 250% after exposure to radiation (Figure 1). In addition, basal AG concentration was elevated by 137% (Figure 2). However, in contrast to NG, postload AG output (Figure 3) and concentration in the gastric juice (Figure 4) were significantly suppressed by irradiation and remained suppressed after 2 days. Thus, the increase in AG output and concentration stimulated by the water load in the control state was abolished after irradiation.

Na^+ and K^+ output and concentration were unaltered by irradiation (Table 1) but Cl^- concentration was significantly reduced after irradiation during the basal period. Fluid and Cl^- secretion were signifi-

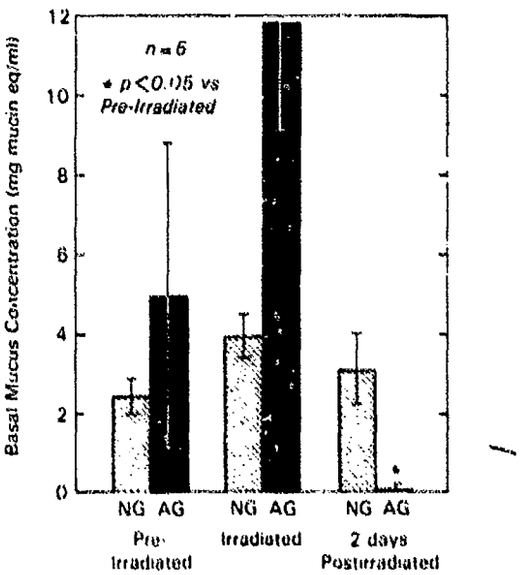

Figure 2. Basal soluble mucin concentration in the secreted juice before, on the day of, and 2 days after exposure to irradiation. Each bar represents the mean ± SE of values obtained in 6 monkeys.

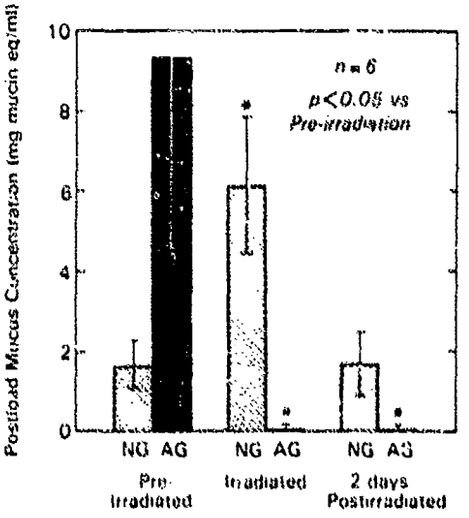

Figure 4. Postload soluble mucin concentration in the secreted juice before, on the day of, and 2 days after exposure to irradiation. Each bar represents the mean ± SE of values obtained in 6 monkeys.

Table 1. Effect of Irradiation on Basal and Postload Fluid and Ions

Treatment	Fluid output (ml/min)	Na^+ output (μEq/min)	Na^+ conc (μEq/ml)	K^+ output (μEq/min)	K^+ conc (μEq/min)	Cl output (μEq/min)	Cl conc (μEq/ml)
Basal							
Preirradiation	0.12 ± 0.04	12.2 ± 3.1	122 ± 33	2.8 ± 0.6	27 ± 5	18.3 ± 3.5	195 ± 40
Irradiation	0.18 ± 0.04	18.6 ± 3.6	110 ± 10	4.3 ± 1.3	20 ± 3	16.9 ± 3.2	119 ± 31[a]
2 days postirradiation	0.14 ± 0.02	13.4 ± 4.2	93 ± 18	2.9 ± 0.8	20 ± 4	25.5 ± 5.0	221 ± 44
Postload							
Preirradiation	0.19 ± 0.03	10.2 ± 1.9	85 ± 24	3.3 ± 0.6	24 ± 7	24.6 ± 6.6	174 ± 58
Irradiation	0.12 ± 0.02[b]	10.8 ± 2.2	153 ± 35	2.3 ± 0.6	19 ± 6	11.0 ± 1.5[a]	228 ± 89
2 days postirradiation	0.15 ± 0.03	9.1 ± 1.4	111 ± 36	2.7 ± 0.7	25 ± 6	26.4 ± 6.3	311 ± 143

Values are mean ± SE of measurements in 6 monkeys. [a] $p < 0.05$ and [b] $p < 0.01$ when compared with preirradiation using a three-factor (treatment, time, and monkey) analysis of variance with repeated measures on the last two factors.

cantly inhibited by irradiation only after the water load. However, 2 days after irradiation, fluid and ion output and ion concentration were not significantly different from preirradiation levels.

Discussion

The human gastric mucosa has several histologically distinct cell types which secrete various mucins. These cells include the mucus neck cells in the fundus, the mucus cells of the cardiac and pyloric glands, and the surface epithelia. The normal gastric mucosa is covered with a continuous thin layer of adherent mucus. This film is not only a product of the surface epithelial cells and mucus neck cells of the adjacent area but also of the mucosa higher in the stomach. Decreases in the quantity and quality of mucus glycoproteins have been associated with gastric mucosal injury and may reflect alterations in the integrity of the surface epithelial cells which produce the mucosal gel layer as well as the cellular ability to synthesize glycoproteins and secrete mucus. Studies correlating changes in soluble and insoluble mucus are inconsistent (2,12). However, Lamont et al. (2) recently found that increases in the AG concentrations of soluble mucus were associated with increases in the AG concentration of the adherent mucus gel. In addition, AG in both soluble and insoluble mucus was inversely correlated with gastric mucosal damage.

The present study demonstrates that, immediately after irradiation, both basal and postload NG output are significantly increased. This, however, is a transient effect as 2 days after irradiation, NG output is not significantly different from control output. In contrast, AG output follows a biphasic time course after irradiation. Immediately after total body exposure, AG output, like NG output, is significantly stimulated; this early elevation of glycoprotein output does not appear to result from an increased acid-pepsin digestion of the mucus layer, as it coincides with an inhibition of gastric acid secretion (13). After the water load, however, AG output is completely abolished. This absence of the normal rise in postload AG output can be attributed to either a prolonged effect of irradiation at that time or to a complete radiation-induced depletion of available AG material during the preceding basal period. Unlike NG output, AG output remains suppressed 2 days after irradiation. As AG output returns to normal within 2 days in the absence of radiation, this much longer lasting effect on both basal and postload AG output can be attributed directly to the effects of irradiation on the gastric mucosa.

The radiation-induced response in soluble mucus output may represent the secretory counterpart of morphologic changes described in the same model (1). In this study, using different monkeys, no gross mucosal damage (endoscopic view) was apparent 3 h after irradiation. Furthermore, light microscopic evaluation of biopsy specimens taken at this same time revealed no disruption of the lining epithelial cells or mucus-containing cells for up to 3 days after irradiation (1). However, SEM showed a marked hypertrophy of the microvilli of some surface epithelial cells. This is similar to the appearance of surface cells before the apical expulsion of mucus. Although earlier biopsy specimens were not obtained, this hypertrophy may represent the final stages of an initial extrusion of mucus from cells, which is reflected in the initial increase in NG and AG output observed immediately after irradiation in the present study. Interestingly, release of mucus by apical expulsion is often followed by cell degeneration and may be characteristic of a response to injury (14).

Alcian blue binds not only to acidic glycoproteins but to other negatively charged macromolecules as well. Thus, an increase in AG output could be due to an increase in cell shedding immediately after irradiation. Scanning electron microscopy and light microscopy, however, do not reveal significant increases in cell shedding at the approximate time of the rise in AG output observed after irradiation in the present study. Moreover, if significant cell shed-

ding occurred later on, one would expect an increase in AG output rather than the observed decrease.

The differences between AG and NG output observed 2 days after irradiation may be related to a differential effect of irradiation on mucus cells producing biochemically distinct mucins. Zalewsky and Moody (14) reported that in dogs, mucus cells located on the surface and in gastric pits contain a highly sulfated mucin, as well as neutral glycoproteins, whereas neck cells in gastric glands contain predominantly neutral glycoproteins. Although the presence or function of sulfated mucin in normal gastric mucosa of humans has been questioned (15), increased levels of sulfated glycoproteins have been found in humans following stress (16). The results of the present study support the distribution of AG and NG proposed by Zalewsky and Moody (14). The surface epithelial cells extend into the gastric pits and are renewed approximately every 3 days. The mucus neck cells which lie deeper in the mucosa near the parietal cells are renewed in about 1 wk. Cells with a high turnover rate are particularly susceptible to radiation injury (17). Thus, the AG-containing suface epithelial cells in this model exhibit a markedly greater vulnerability to radiation damage than do the NG-containing mucus neck cells. This is further supported by the fact that both NG output and acid secretion, but not AG output, have returned to normal within 3 days of radiation exposure. The significance of this observation is illustrated by SEM studies of gastric biopsy specimens. At 2 days postirradiation, there is damage or absence of numerous surface cells, the presence of exposed lamina propria in some areas, and a persistence of ulceration at the site where biopsy specimens were obtained on the day of irradiation (1).

The increase in soluble mucus output in the present study may be part of a response to stress. An increase in the release of β-endorphin from the pituitary has been shown to accompany other types of experimental stress (18,19). That irradiation is a stress is supported by the fact that total body irradiation has been shown to significantly enhance plasma β-endorphin (20). The initial rise in soluble mucus output observed immediately after irradiation in the present study is not reported in earlier studies of experimental stress. This may be attributed to differences in methodology. In previous studies, the stress was applied for a longer period of time and gastric samples were usually not obtained until several hours after the stress was initiated. In the current study, the monkeys were exposed to irradiation for <2 min and samples of gastric juice were obtained within 10 min. Thus, this initial rise in soluble mucus glycoprotein secretion may not have been observed previously. In contrast, the significant inhibition of AG output observed after the water load is similar to the previous findings of a reduction in glycoprotein content of the gastric juice within the first 24 h (16,21,22). Earlier studies have shown that AGs are the major type of glycoproteins secreted in the rat (2). Although purified monkey mucin was not used as a standard in the present study, AGs also appear to be the major type of glycoproteins in the present model. Thus, even in the presence of an elevated postload NG output, the potent suppression of postload AG output results in a net reduction of the mucus glycoprotein content of the gastric juice.

After the first 24 h, radiation-induced changes in soluble mucus do not parallel those reported after other types of stress. Much of this difference can be attributed to the more disruptive or permanent changes in the gastric mucosal barrier that arise from radiation exposure. Studies of experimental stress show a gradual increase in soluble mucus glycoproteins and acid secretion during the 5–6 days post-trauma (16). After irradiation, acid output was also found to return to control levels within 3 days (13). In the present study, however, although NG output returns to normal, AG output is still deficient at this time.

Irradiation produces significant changes in mucus secretion, but does not appear to be accompanied by a "break" of the gastric mucosal barrier. Such a breakdown has been associated with the appearance of Na^+ in the lumen and a back diffusion of H^+ ions. In the present study, however irradiation did not significantly alter Na^+ or K^+ output or concentration, suggesting a lack of significant mucosal damage for 3 days after irradiation. The significant decrease in fasting Cl^- concentration and in postload Cl^- and fluid output on the day of irradiation reflect the reported suppression of acid secretion (13). Two days after irradiation the observed return of Cl^- and fluid output to control values accompanies the previously reported restoration of acid secretion to normal (13).

These studies demonstrate that irradiation produces significant alterations in the amount and type of mucus glycoprotein secreted into the gastric juice. It is not likely that these changes are a response to gastric injury because the gastric mucosal barrier remains intact. However, they may seriously affect the protective ability of gastric mucus.

References

1 Dubois A, Danquechin-Dorval E, Wood L, et al. Effect of γ irradiation on the healing of gastric biopsy sites in monkeys. An experimental model for peptic ulcer disease and gastric protection. Gastroenterology 1983;84:12–18

2 Lamont JT, Ventola AS, Maull EA, Szabo S. Gastrotoxic and

prostaglandin $F_{2\beta}$ stimulate rat gastric mucin release. Gastroenterology 1983;84:306–13.
3. Dubois A, Natelson B, Van Eerdewegh P, Gardner J. Gastric emptying and secretion in the rhesus monkey. Am J Physiol 1977; 232:E186–92.
4. Dubois A, Van Eerdewegh P, Gardner J. Gastric emptying and secretion in Zollinger-Ellison syndrome. J Clin Invest 1977;59:255–63.
5. Shea-Donohue PT, Myers L, Castell DO, Dubois A. Effect of prostacyclin on gastric emptying and secretion in rhesus monkeys. Gastroenterology 1980;78:1476–9.
6. Shea-Donohue PT, Adams N, Arnold J, Dubois A. Effects of met-enkephalin and naloxone on gastric emptying and secretion in rhesus monkeys. Am J Physiol 1983;245:G196–200.
7. George JD. New clinical method for measuring the rate of gastric emptying: the double sampling test meal. Gut 1968;9:237–42.
8. Hildes HA, Dunlop KL. A method for estimating the ratio of gastric secretion and emptying. Can J Med Sci 1951;29:83–9.
9. Piper DW, Whitecross D, Leonard P, Clarke A. Alcian blue dye binding properties of gastric juice. Gastroenterology 1970;59:534–8.
10. Mantle M, Allen A. A colorimetric assay for glycoproteins based on the periodic acid Schiff stain. Biochem Soc Trans 1978;6:607–9.
11. Kirk RE. In: Experimental design: procedures for the behavioral sciences. Monterey, California: Brooks Cole, 1968:110–2.
12. McQueen S, Hutton D, Allen A, Garner A. Gastric and duodenal surface mucus gel thickness in rat: effects of prostaglandins and damaging agents. Am J Physiol 1983;8:G388–93.
13. Danquechin-Dorval E, Eng R, Columbaro P, Durakovic A, Conklin J, Dubois A. Radiation-induced vomiting and altered gastric emptying and secretion. Gastroenterology 1983; 84:1183.
14. Zalewsky CA, Moody EF. Mechanisms of mucus release in exposed canine gastric mucosa. Gastroenterology 1979; 77:719–29.
15. Lambert R, Andre C, Bernard A. Origin of sulphated glycoproteins in human gastric secretions. Digestion 1971;4:234–9.
16. Stremple JF, Mori H, Lev R, Glass GBJ. In: Ravitch M, ed. Current problems in surgery. Chicago: Yearbook Medical Publishers, Inc., 1973:1–64.
17. Lipkin M, Shenock P, Bell B. Cell proliferation kinetics in the gastrointestinal tract of man. II. Cell renewal in the stomach, ileum, colon, and rectum. Gastroenterology 1963;45:721–9.
18. Guillemin R, Vargo T, Rossier J, et al. β-Endorphin and adrenocorticotropin are secreted concomitantly by the pituitary gland. Science 1977;197:1367–9.
19. Rossier J, French E, Rivier C, Ling N, Guillemin R, Bloom F. Foot-shock induced stress increases β-endorphin in rat blood but not brain. Nature 1977;270:618–20.
20. Danquechin-Dorval E, Mueller GP, Eng R, Durakovic A, Conklin J, Dubois A. Involvement of endogenous opiates in radiation-induced suppression of gastric emptying. Gastroenterol Clin Biol 1983;7:712.
21. Dekanski JB, MacDonald M, Sucra P. Effects of fasting, stress and drugs on gastric glycoprotein synthesis in the rat. Br J Pharmacol 1975;55:385–92.
22. Ludwig W, Lipnin M. Biochemical and cytological alterations in gastric mucosa of guinea pigs under restraint stress. Gastroenterology 1969;56:895–902.

AFRRI CONTRACT REPORT

A practical guide to ionization chamber dosimetry at the AFRRI reactor

AFRRI CR85-1

DEFENSE NUCLEAR AGENCY
ARMED FORCES RADIOBIOLOGY RESEARCH INSTITUTE
BETHESDA, MARYLAND 20814-5145

REVIEWED AND APPROVED

VINCENT L. McMANAMAN
CDR, MSC, USN
Chairman
Radiation Sciences Department

LAWRENCE S. MYERS, Ph.D.
Scientific Director

BOBBY R. ADCOCK
COL, MS, USA
Director

AFRRI CR 85-1
March 1985

A PRACTICAL GUIDE TO IONIZATION CHAMBER DOSIMETRY AT THE AFRRI REACTOR

This manual was prepared by
Leon J. Goodman, Physical Scientist
National Bureau of Standards
Center for Radiation Research
Nuclear Radiation Division
Under Contract No. DNA IACRO 83-847

ARMED FORCES RADIOBIOLOGY RESEARCH INSTITUTE
Defense Nuclear Agency
Bethesda, Maryland

Contents

1.0. Introduction

1.1. Purpose of Dosimetry Guide

This report was written to provide the dosimetrists at the Armed Forces Radiobiology Research Institute (AFRRI) with practical guidance on the use of ionization chambers in performing mixed-field dosimetry at the TRIGA reactor operated in a steady-state mode. A large part of the material presented is also applicable to dosimetry measurements made at other ionizing radiation facilities.

This dosimetry guide discusses the essential information needed to carry out ionization chamber measurements in the mixed neutron and gamma-ray fields produced at the reactor, and describes the practical aspects that are often neglected in formal treatises on dosimetry. Thus, the essential formulas needed to reduce the measured quantities to the required kermas or absorbed doses are presented without derivations, but the formulas and their various parameters are fully explained. Similarly, definitions of standard terminology, such as kerma or absorbed dose, are not given. However, the less familiar correction factors are discussed so that the reader will know not only what they are but also how to measure them and what magnitude of values to expect.

The thrust of this guide is to illuminate the practice rather than the theory of ionization chamber dosimetry. This approach has been adopted with the aim of providing consistency and long-term continuity to the reactor dosimetry program at AFRRI, particularly in consideration of the relatively frequent turnover of the scientific and technical staff.

1.2. Review of Contents

Following this Introduction, Section 2 discusses the general principles of mixed-field dosimetry, including where and how ion zation chambers are calibrated and checked for proper operation. The calibration formulas are discussed in Section 3. Section 4 describes how measurements of neutron and gamma-ray kerma or absorbed dose are performed. The required formulas are presented and explained, but details on the required physical parameters and correction factors are deferred to Sections 5 and 6, respectively. Section 5 describes the needed physical parameters and gives their values for some of the routine irradiation configurations used at the reactor. The correction factors that need to be considered and possibly evaluated are discussed in Section 6. This section describes the methods used to measure these factors, and offers suggestions on which factors may be neglected or avoided by suitable measurement procedures. Finally, Section 7 offers advice on establishing and maintaining a reliable gas-flow system for the ionization chambers. The reference list is given in Section 9.

1.3. Supplementary Information

As mentioned above, this report does not give formula derivations or definitions of standard terminology used in radiation dosimetry. The author has assumed that the reader has at least some familiarity with the physical principles, quantities, and units used in ionization chamber dosimetry. For some readers this may be a poor assumption. To augment the information in this dosimetry guide, it is

recommended that the scientists and technical personnel making practical use of this guide acquire and become familiar with the following supplementary information (references 1-8) (Section 9 gives reference details):

Neutron Dosimetry for Biology and Medicine. This is Report 26 of the International Commission on Radiation Units and Measurements (ICRU), containing a wealth of information on neutron dosimetry. It is recommended as a primer for those who are new to this field.

Clinical Dosimetry for Neutrons. This ICRU Report is in preparation, and may become available in the latter part of 1985. It includes much information on the theory and practice of neutron dosimetry as applied to the therapeutic application of neutron beams of high energy in the clinical situation. Nevertheless, it is a useful reference for reactor dosimetry since it contains derivations and explanations of the formulas used in the present report.

Radiation Quantities and Units. This is Report 33 of the ICRU, and contains a concise exposition of the terminology, quantities, and units used in radiation dosimetry. It is a valuable reference giving both verbal and mathematical definitions.

"European protocol for neutron dosimetry for external beam therapy," by Broerse et al. This journal paper presents detailed derivations and rationale for the formulas applied to the clinical use of fast neutron beams, and provides helpful information to supplement the present report. It was written for use by clinical neutron dosimetrists in the European community.

Protocol for Neutron Beam Dosimetry. This report is similar to the European protocol but was written by a task group of the American Association of Physicists in Medicine (AAPM) for use by clinical neutron dosimetrists in the United States. It is presently available as AAPM Report 7, but it is undergoing revision and should be reissued in modified form in the near future.

"Determination of absorbed dose and kerma in a neutron field from measurements with a tissue-equivalent ionization chamber," by Mijnheer and Williams. This journal paper also presents the derivations and rationale for the formulas used in the present report. It is recommended for its clear and concise presentation of neutron dosimetry information.

"Calibration procedures of tissue-equivalent ionization chambers used in neutron dosimetry," by Mijnheer and Williams. This paper, in a report of the International Atomic Energy Agency, also gives many formulas and derivations applicable to neutron dosimetry, and presents an analysis of the uncertainties involved in different calibration methods.

Ion Chambers for Neutron Dosimetry. This monograph is based on reports presented at a 1979 workshop of the Commission of the European Communities. It reviews the status of ionization chambers used for neutron dosimetry. In addition to discussions of the characteristics of a variety of ionization chambers (including those available from two commercial vendors), the report also has discussions on calibrations, corrections, cavity chamber theory, physical constants, and experimental techniques. It is recommended as a source for detailed, practical chamber data.

2.0. General Principles of Mixed-Field Ionization Chamber Dosimetry

2.1. Instrument Selection and Use

In principle, any of several instruments or combinations of instruments can be used for neutron dosimetry, including ionization chambers, calorimeters, proportional counters, and instruments for the measurement of fluence and spectral data. This report discusses only the use of a pair of ionization chambers for determining neutron and gamma-ray kermas and absorbed doses. Reference 1 should be consulted for information on other suitable instruments and methods.

Neutron dosimetry is more complex than gamma-ray dosimetry, mainly because neutron fields always contain gamma rays produced by the source and by field-defining structures, by the irradiation environment, and by the irradiated object itself. Because neutrons can have a different biological effect compared to an equal absorbed dose of gamma rays, it is necessary to report the separate values of these two components. With ionization chambers this requires the use of the two-dosimeter method. One of the chambers is constructed of A-150 tissue-equivalent (TE) plastic, and it uses a steady flow of methane-based TE gas through the cavity. This instrument, referred to as the TE-TE chamber, has approximately the same response to neutrons and to gamma rays. Details of the wall and gas compositions are given in Appendix B of reference 1.

The second chamber is constructed with magnesium walls, and uses a steady flow of argon gas. This instrument will be referred to as the Mg-Ar chamber, and its response to neutrons is much less than its response to gamma rays. The use of a graphite chamber with carbon

dioxide gas is deprecated because of the higher relative neutron response (see Section 5.9) of this wall and gas combination, and because the porosity of graphite makes it difficult to maintain gas purity without excessively high flow rates. A photon energy-compensated Geiger-Müller (GM) dosimeter is often used as the second dosimeter. However, experience has shown that in the exposure rooms of the AFRRI reactor the ambient gamma-ray background is usually excessive relative to the high gamma-ray response of the GM dosimeter.

Two or more ionization chambers may be arranged laterally to the radiation direction for simultaneous measurements. A few centimeters of separation between chambers having volumes of a few cubic centimeters or less should suffice to make interchamber radiation scatter negligible. The chambers should be oriented so that their axes are perpendicular to the radiation direction since this will best define the location of the center of the cavity volume with respect to the radiation source. After the chambers have been mounted, the gas flow adjusted, and the collecting potential applied, sufficient time should be allowed for transient phenomena to subside before beginning measurements. This practice should be followed whenever a chamber is disturbed by repositioning, adding or removing a chamber cap, or changing the applied voltage. The chamber may be considered to be stable when the electrometer response in the absence of radiation is fairly constant and does not exceed a few percent of the anticipated radiation response. Charge integration during irradiation should be performed long enough to obtain an electrometer reading that is large with respect to system instabilities. It is good practice to make several measurements in succession to evaluate the response variance. Charges measured before

and after the chamber is irradiated should be integrated for the same time as used during irradiation so as to provide an assessment of the compensation required to compute the net charge accumulated during irradiation.

2.2. Ionization Chamber Calibration

This section discusses the general procedure for maintaining ionization chamber calibrations that are traceable to a national standard, and the procedures for routine verification of proper chamber operation. The formulas needed to apply the chamber calibrations to neutron dosimetry are presented in Section 3.

2.2.1. Calibration at NBS or ADCL. It is recommended that a chamber be designated as the AFRRI transfer standard chamber and that this instrument be used only for transferring the calibration from the standards laboratory to the ^{60}Co calibration source at AFRRI. The procedure for using such a transfer standard chamber is as follows. The chamber is flushed with air and then left open to the ambient atmosphere. It is irradiated at AFRRI in a fixed and reproducible arrangement and its response is recorded along with the ambient temperature and pressure. The irradiation source may be either a specially designed check source or the ^{60}Co gamma-ray machine that will be later used for calibrations of other dosimeters.

The chamber is then transported to the National Bureau of Standards (NBS) or to an AAPM Accredited Dosimetry Calibration Laboratory (ADCL) for calibration in a standard ^{60}Co beam. This measurement will be performed with the chamber open to atmospheric air, and will be in terms of the exposure or air kerma required to produce unit response

from the chamber, i.e., roentgen per coulomb of charge collected (exposure) or grays per coulomb of charge collected (air kerma). When the chamber is returned to AFRRI, it should first be irradiated in the fixed check-source field to verify that the trip to and from the standards laboratory has not changed the chamber's response. Assuming that the result of this second check-source measurement is satisfactory, the transfer instrument is then used to determine the exposure rate or air kerma rate of the AFRRI ^{60}Co machine. The transfer instrument is then stored for future use to verify the ^{60}Co beam calibration periodically or when a problem is suspected.

2.2.2. Calibration at AFRRI. The procedure outlined in the previous subsection calibrates the gamma-ray beam from the ^{60}Co machine in terms of the exposure rate or air kerma rate at one or more well-defined positions in the beam. This calibrated beam is then used to calibrate other AFRRI chambers (with their usual cavity gases) used routinely for reactor dosimetry. These ^{60}Co chamber calibrations will be in terms of the exposure or air kerma required to produce unit response from the chamber, i.e., the same as for the transfer instrument. Such calibrations should also be preceded by and followed by a measurement with the check source. Section 3 discusses the conversion of these calibrations to the tissue absorbed dose calibration factor.

2.3. Calibration Verification

It is good practice to verify the proper operation of an ionization chamber prior to its use for making mixed-field measurements. Two methods are described for making such checks.

2.3.1. Verification With Check Sources. Using check sources to verify the calibration of an ionization chamber is a comprehensive test since this method not only checks the integrity of the chamber, its cables, and the electrometer but also verifies the proper neutron and gamma-ray response if a neutron and a gamma-ray source are used. Even though the neutron source will also be a gamma-ray emitter, the response of a TE-TE or a Mg-Ar chamber in the mixed field will serve to verify that the gas in the TE chamber is TE gas and that the gas in the Mg chamber is Ar (provided, of course, that the earlier check source data used for comparison were obtained under appropriate conditions). The check sources should be used in an arrangement that allows response measurements to be made with a random uncertainty of 1% or less. It is essential that a log sheet be maintained for each chamber, detailing its history of calibrations and check source tests. Such records are necessary for documenting a long-term drift or deterioration of chamber response.

2.3.2. Verification by Capacitance Measurement. A simple and quick method of verifying the integrity of a three-terminal chamber (i.e., a guarded chamber), its cables, collecting potential supply, and electrometer is by measuring the distributed capacitance between the outer chamber wall (to which the collecting potential is applied) and the inner collecting electrode. This is done as follows. With the chamber connected to the electrometer system and a moderate collecting potential applied, several measurements of drift charge are made using a fixed time interval. The second step is to make several measurements of

the charge accumulated in the fixed time while applying a change in collecting potential, ΔV, during the charge accumulation time. This is done by ungrounding the electrometer input and then slowly changing the collecting potential at a rate so that ΔV has been applied before the fixed time has elapsed. When the fixed time is reached, the charge, ΔQ, induced into the collecting electrode by ΔV acting through the distributed capacitance C, is recorded. The collecting potential should be returned to the same initial value and the system allowed to stabilize before each repeat measurement is made.

The final step is to make several more measurements of drift charge in the fixed time interval. The drift charges measured before and after the ΔV charge measurements are then averaged and subtracted from the charges induced by the ΔV changes. The capacitance is then computed as $C = \Delta Q/\Delta V$, where ΔQ is the net drift-compensated change in charge corresponding to the voltage change ΔV. The magnitude of ΔV should be one that will produce a ΔQ with a small random uncertainty, and the fixed time over which each of the measurements is made should be chosen such as to allow the voltage to be changed at a moderate rate. For example, for a 0.5-cm^3 thimble chamber having $C \approx 0.7$ pF, the initial potential can be set at 400 V with $\Delta V = 100$ V, the fixed time being 30 s.

These capacitance check measurements should be repeatable on the order of 1% between different measurement sessions. It is recommended that a log sheet of capacitance measurements be maintained for each chamber. This may help in identifying a chamber that is undergoing long-term dimensional changes.

3.0. Calibration Formulas

3.1. Volume Calibration

It is possible to derive the radiation calibration of an ionization chamber from detailed knowledge of the cavity volume, chamber materials, and various physical parameters. The difficulty arises in knowing accurately the effective cavity volume in which ion production and collection take place. Even for the relatively simple geometry of a parallel-plate chamber, the field distortion present in the region of the guard electrode complicates a straightforward computation of the effective cavity volume. The usual resolution to this problem is to calibrate the chamber in a gamma-ray field of known exposure rate and to use these data to derive the mass of cavity gas and hence its volume. Details and formulas for such computations are given in references 4 through 7.

3.2. Radiation Sensitivity Calibration

Dosimetrists generally ignore the computation of chamber cavity volume and instead focus their attention on deriving the tissue-absorbed-dose calibration factor, α_c, which is the quotient of the absorbed dose in tissue adjacent to the cavity of the chamber by the corrected chamber response. It is defined as

$$\alpha_c = \frac{X_c}{R_c} (f_t)_c \frac{(\pi k_A)_c}{(\pi k_R)_c} \qquad (1)$$

where the ratio X_c/R_c is the exposure calibration in which X_c is the exposure at the geometric center of the chamber in the absence of the chamber, and R_c is the chamber response. The subscript c denotes the calibration radiation field. The conversion factor, which converts exposure to tissue-equivalent absorbed dose, $(f_t)_c$, is discussed in Section 5.2.

During 1985 NBS and the ADCL's will begin to supply air kerma calibrations in addition to exposure calibrations, which later will be discontinued. This change to $(K_{air})_c/R_c$ for the air kerma calibration will require that $(f_t)_c$ in equation 1 be changed to an air kerma-to-tissue absorbed dose factor, $(f'_t)_c$, as discussed in Section 5.2.

The product of several correction factors Πk_A compensates for small distortions of the radiation field when measurements are made with the chamber in free air, and is given by

$$\Pi k_A = k_w k_{st} k_{rn} k_{an} \qquad (2)$$

where k_w is the chamber wall attenuation and scatter correction factor (Section 6.2),

k_{st} is the stem-scatter correction factor (Section 6.4),

k_{rn} is the radial nonuniformity correction factor (Section 6.5), and

k_{an} is the axial nonuniformity correction factor (Section 6.6).

The product of several correction factors Πk_R converts the reading, R, taken from the electrometer, to the electric charge produced within an ideal cavity at a reference temperature and pressure, and is given by

$$\Pi k_R = k_{t,p} k_s k_e k_l k_p k_f k_h \qquad (3)$$

where $k_{t,p}$ is the temperature and pressure correction factor (Section 6.1),

k_s is the saturation correction factor (Section 6.3),

k_e is the electrometer correction factor (Section 6.7),

k_l is the leakage correction factor (Section 6.8),

k_p is the polarity correction factor (Section 6.9),

k_f is the gas flow-rate correction factor (Section 6.10), and

k_h is the humidity correction factor (Section 6.11).

This may appear to be a formidable list of correction factors, but (as discussed in Section 6) many of these factors can be either neglected or included in the method of making the measurements. Note that in equation 1 the two correction factor products have the subscript c, indicating that these factors are to be evaluated for the calibration radiation field.

4.0. Mixed-Field Measurements

4.1. Neutron and Gamma-Ray Kerma and Absorbed Dose

At a point in a mixed field where the neutron and gamma-ray tissue absorbed doses or kermas are D_n and D_γ, respectively, the relative responses of the two chambers are given by

$$R'_T = k_T D_n + h_T D_\gamma \tag{4}$$

$$R'_U = k_U D_n + h_U D_\gamma \tag{5}$$

where the subscript T refers to the TE-TE chamber and the subscript U refers to the Mg-Ar chamber. The coefficients k_T and k_U are the responses of each chamber to the neutrons in the mixed field relative to its response to the gamma rays used for the calibration, and h_T and h_U are the responses of each chamber to the gamma rays in the mixed field relative to its response to the gamma rays used for the calibration. Consequently, R'_T and R'_U are the readings of the two chambers in the mixed field relative to their responses to the gamma rays used for the calibration.

The separate absorbed doses are obtained by simultaneous solution of equations 4 and 5 to give

$$D_n = \frac{h_U R'_T - h_T R'_U}{h_U k_T - h_T k_U} \tag{6}$$

$$D_\gamma = \frac{k_T R'_U - k_U R'_T}{h_U k_T - h_T k_U} \tag{7}$$

The relative gamma-ray responses h_T and h_U can be computed from

$$h = \frac{W_c}{W_\gamma} \frac{(s_{m,g})_c}{(s_{m,g})_\gamma} \frac{[(\mu_{en}/\rho)_t/(\mu_{en}/\rho)_m]_c}{[(\mu_{en}/\rho)_t/(\mu_{en}/\rho)_m]_\gamma} \tag{8}$$

where c denotes the calibration gamma rays,

γ denotes the mixed-field gamma rays,

t denotes tissue,

m denotes wall material,

W is the average energy required to produce an ion pair in the cavity gas (Section 5.3),

$s_{m,g}$ is the wall-to-gas restricted collision mass stopping power ratio, commonly referred to as the gas-to-wall absorbed-dose conversion factor (Section 5.4), and

μ_{en}/ρ is the mass energy absorption coefficient (Section 5.6).

The values of h_T and h_U are close to unity, and the simplifying assumption $h_T = h_U = 1$ is usually made. This is equivalent to assuming that the effective quality of the gamma rays in the mixed field is equivalent to the quality of the gamma rays used for the calibration with respect to the values of W, $s_{m,g}$ and μ_{en}/ρ. Equations 6 and 7 may then be simplified to

$$D_n = \frac{R'_T - R'_U}{k_T - k_U} \tag{9}$$

$$D_\gamma = \frac{k_T R'_U - k_U R'_T}{k_T - k_U} \tag{10}$$

The relative neutron response k_T of the TE-TE chamber is computed in a manner similar to that used for h_T. Thus

$$k_T = \frac{W_c}{W_n} \frac{(s_{m,g})_c}{(r_{m,g})_n} \frac{[(\mu_{en}/\rho)_t/(\mu_{en}/\rho)_m]_c}{(K_t/K_m)_n} \tag{11}$$

where the subscript n denotes the mixed field, $r_{m,g}$ is the gas-to-wall absorbed-dose conversion factor for the non-Bragg-Gray cavity conditions generally produced by neutrons (Section 5.5), and $(K_t/K_m)_n$ is the ratio of neutron kerma in tissue to the neutron kerma in the chamber materials (Section 5.7).

Due to the lack of data for the wall and gas materials of the Mg-Ar chamber, the value of k_U cannot be readily computed, so it is usually evaluated by experimental methods (Section 5.9).

The relative chamber responses R'_T and R'_U are computed from the reading, R, obtained for each chamber in the mixed field.

$$R' = R\alpha_c \frac{(\Pi k_R)_n}{(\Pi k_A)_n} (k_d)_n \tag{12}$$

The two products of correction factors Πk_R and Πk_A are defined the same as in equations 2 and 3 except that the subscript n in equation 12 indicates that the factors are to be evaluated for the mixed field. When equations 9 and 10 are solved for the tissue kermas in free air, then $(\Pi k_A)_n$ should be evaluated. When these equations are used to obtain the absorbed doses in a phantom, then $(\Pi k_A)_n$ is set to unity.

The displacement factor $(k_d)_n$ corrects for the perturbation produced by the chamber gas cavity when measurements of absorbed dose are made in a phantom. If we set $(k_d)_n = 1$, then the computed absorbed doses will be at the effective center of the chamber rather than at its geometric center. Section 5.8 discusses suitable values of this factor for phantom measurements. For tissue kerma determinations in free air, the displacement factor is unity.

Equation 10 sometimes will yield a negative value for D_γ, particularly when the gamma-ray kerma or absorbed dose is small relative to D_n, say a few percent. This is, of course, a physical impossibility. Assuming that the chamber responses have been measured accurately, a negative value of D_γ usually indicates that the value of k_U used is too large. Values of k_U are determined only approximately by experiment, and even then they apply only to the specific chamber configuration and radiation field used.

More puzzling is the rare occasion when equation 9 yields a computed value of D_n that is negative. This can occur in a radiation field containing only a small neutron kerma or absorbed dose relative to D_γ. Equation 6, which gives the relationship for D_n before the simplifying assumption $h_T = h_U = 1$ was made, shows that D_n depends on h_T and h_U; and it can be concluded that the simplifying assumption used to derive equation 9 is invalid if $D_n < 0$. It would be necessary to have spectral data for the gamma-ray component of the mixed field in order to evaluate the relative gamma-ray responses h_T and h_U of the two chambers using equation 8.

4.2 Total Kerma or Absorbed Dose

The total tissue kerma or absorbed dose, D_T, can be obtained simply by summing the two components computed from equations 9 and 10, i.e.,

$$D_T = D_n + D_\gamma \tag{13}$$

An alternative is the simple expression

$$D_T = \frac{R'_T}{k_T} \frac{1}{1+\delta} \tag{14}$$

where

$$\delta = \frac{D_\gamma}{D_T} \frac{h_T - k_T}{k_T} \tag{15}$$

Now, since $k_T \approx 0.95$ and h_T is close to 1, if $D_\gamma/D_T < 0.4$ tnen we will have $\delta < 0.021$. Thus, in equation 14 if we set $\delta = 0$, then an error of less than about 2% will be made in computing D_T, i.e.,

$$D_T \approx \frac{R'_T}{k_T} \quad \text{for} \quad \frac{D_\gamma}{D_T} < 0.4 \tag{16}$$

Table 1 lists the errors produced in computing D_T from equation 14 when it is assumed that $\delta = 0$. Even for $D_\gamma/D_T = 1$, the error does not exceed 5% as a consequence of setting $k_T = 0.95$. A potentially more serious error in this case might be the failure to realize that D_T does not contain a component of absorbed dose due to neutrons.

Table 1. Errors produced in computing D_T from equation 14 by assuming $\delta = 0$*

D_γ / D_T	D_n / D_γ	% error in D_T
0.02	49	0.1
0.05	19	0.3
0.1	9	0.5
0.2	4	1.0
0.3	2.3	1.6
0.4	1.5	2.1
0.6	0.67	3.1
0.8	0.25	4.0
1.0	0	5.0

*For this table, $k_T = 0.95$ and $h_T = 1.00$ were used.

When $D_\gamma/D_T = 1$, i.e., $D_n = 0$, equation 14 reduces to

$$D_\gamma = R'_T/h_T \tag{17}$$

which is the same result as given by equation 4 with $D_n = 0$.

D_γ in a mixed field can be evaluated from equation 5, with the assumption $h_U = 1$, as

$$D_\gamma = R'_U - k_U D_n \tag{18}$$

If the low values of k_U for a small Mg-Ar ionization chamber are considered (as shown in Table 2, page 23), then it is possible to make the following approximation with an error of less than 2%:

$$D_\gamma \approx R'_U \quad \text{for} \quad \begin{cases} D_n / D_\gamma < 2, \text{ 6 inches of Pb-shielded reactor;} \\ D_n / D_\gamma < 1, \text{ bare reactor;} \\ D_n / D_\gamma < 0.8, \text{ 12 inches of water-shielded reactor.} \end{cases} \tag{19}$$

It may be useful to note that (see also Table 1)

$$\frac{D_n}{D_\gamma} = \frac{D_T}{D_\gamma} - 1 \tag{20}$$

Equation 16 can be used to approximate D_T from measurements made with only a TE-TE chamber, and equation 19 can be used to approximate D_γ from measurements made with only a Mg-Ar chamber. These approximations are useful for making quick dosimetry evaluations or when more complete data are not available. However, the errors in these approximations are not random, and they result in errors that make D_T or D_γ systematically too high. It is recommended that the final dosimetry evaluations be made without these errors by using equations 9 and 10.

Table 2. Values of physical parameters for three shielding configurations used in Exposure Room 1 of the AFRRI reactor (reference 19)

Parameter	Shielding Configuration 6" Pb*	Bare†	12" H_2O■
$\bar{E}_n$§	0.45	0.8	1.55
W_n,‖ MTE¶ gas	32.2	32.0	31.7
W_n/W_c**	1.099	1.092	1.082
K,†† ICRU muscle	1.52	1.96	2.76
K, A-150 plastic	1.54	2.02	2.83
K, MTE gas	1.54	2.00	2.80
k_U, Mg-Ar	0.01	0.02	0.025
k_U, GM	0.002	0.0016	0.0027

*Reactor core shielded with 6 inches of Pb

†Bare reactor room, i.e., no added shielding

■Reactor core shielded with 12 inches of water

§Tissue-kerma-weighted mean neutron energy in MeV

‖W_n is in units of eV.

¶MTE denotes methane-based TE gas.

**W_c = 29.3 eV.

††Kerma factors are in units of 10^{-11} Gy cm^2.

5.0. Physical Parameters

5.1. Spectral Information

The items discussed in the following subsections as physical parameters are quantities whose values are usually obtained either directly or by computation from previously published or otherwise available data. The evaluation of these physical parameters generally requires knowledge of the radiation spectrum for which the parameter is to be computed. In some cases only rough radiation quality information is needed, whereas other cases require use of a reliable and detailed spectrum. Table 2 gives the tissue-kerma-weighted mean neutron energies for three reactor configurations. The data presented in Table 2 were computed using neutron and gamma-ray spectral data from reference 9.

5.2. Exposure- and Air Kerma-to-Tissue Absorbed Dose Conversion Factors, $(f_t)_c$ and $(f_t')_c$

The factor $(f_t)_c$ required to convert exposure to tissue-absorbed dose for computing the calibration factor, a_c, is defined as

$$(f_t)_c = \frac{(W_{air})_c}{e} \left[\frac{(\mu_{en}/\rho)_t}{(\mu_{en}/\rho)_{air}}\right]_c \qquad (21)$$

where subscript c denotes the calibration radiation quality, subscript t denotes tissue, and e is the electronic charge. For dry air and ICRU muscle or soft tissue, $(f_t)_c$ = 37.3 J/C or $(f_t)_c = 9.62 \times 10^{-3}$ Gy/R for either ^{60}Co or ^{137}Cs in air (reference 10).

The factor $(f_t')_c$ required to convert air kerma to tissue absorbed dose for computing the calibration factor, α_c, is defined as

$$(f_t')_c = \left[\frac{(\mu_{en}/\rho)_t}{(\mu_{en}/\rho)_{air}}\right]_c [1 - g]_c \qquad (22)$$

where g is the fraction of charged-particle kinetic energy lost to bremsstrahlung in the material. For ^{60}Co and ^{137}Cs gamma rays, the ratio of the mass energy-absorption coefficients is 1.102 for either ICRU striated muscle or ICRU soft tissue (reference 11). For ^{60}Co and ^{137}Cs gamma rays, the fraction g is 0.003 and 0.001, respectively (reference 12). With these values, equation 22 yields $(f_t')_c = 1.099$ for ^{60}Co in air, and $(f_t')_c = 1.101$ for ^{137}Cs in air.

5.3. Average Energy Required to Produce an Ion Pair, W

The basic quantity measured with an ionization chamber is the electric charge or current produced in the gas cavity. To obtain the kerma or absorbed dose, this quantity is converted to energy by the use of W, the average energy required to produce an ion pair in the gas. For the electrons produced by the energetic gamma rays used for calibration, i.e., ^{60}Co, a value of $W_c = 29.3$ eV is appropriate for methane-based TE gas (reference 13).

Values of W_n for the secondary particles produced in methane-based TE gas by neutrons are given in reference 13, which also describes the method of calculating W_n for a known neutron spectrum. Table 2 lists computed values of W_n and W_n/W_c for three reactor configurations.

5.4. Wall-to-Gas Stopping-Power Ratio, $s_{m,g}$

The wall-to-gas stopping-power ratio, $s_{m,g}$, applies when the ionization chamber can be considered to have a Bragg-Gray cavity. For ^{60}Co gamma rays and for the gamma rays present in the mixed field, $s_{m,g} = 1.00$ is a good assumption for the TE-TE chamber.

5.5. Gas-to-Wall Absorbed-Dose Conversion Factor, $r_{m,g}$

The gas-to-wall absorbed-dose conversion factor, $r_{m,g}$, applies to ionization chamber measurements of neutron fields for which the gas cavity contributes significantly to the secondary particle spectrum. Attempts to compute $r_{m,g}$ have yielded values that differ from unity by 1% or 2% and have uncertainties of about 2%. It is recommended that $r_{m,g} = 1.00$ be used for neutron measurements with the TE-TE chamber.

5.6. Mass Energy-Absorption Coefficient Ratio, $(\mu_{en}/\rho)_t/(\mu_{en}/\rho)_m$

Because of the good simulation of ICRU muscle or soft tissue by the TE-TE chamber for ^{60}Co gamma rays and for the gamma rays present in the mixed field, it is recommended that $(\mu_{en}/\rho)_t/(\mu_{en}/\rho)_m = 1.00$ be used for the mass energy-absorption coefficient ratio.

5.7. Neutron Kerma-Factor Ratio, $(K_t/K_m)_n$

Neutron kerma factors, i.e., the quotients of kerma by fluence, are given for a variety of elements, compounds, and mixtures in reference 14. These values can be used to derive suitably weighted mean kerma factors using data on the neutron spectrum at the measurement position. For the relatively low energy neutrons present in reactor spectra, the chamber kerma is due to both the wall and gas materials.

Since the wall and gas compositions of the TE-TE chamber are very similar, it is satisfactory to use the average of the wall and gas kermas for the kerma in the chamber material, K_m. Kerma factors for ICRU muscle tissue, A-150 plastic, and methane-based TE gas are listed in Table 2 for three reactor configurations. Spectrum changes as a neutron beam passes into a tissue phantom will probably have little effect on the kerma-factor ratio.

5.8. Displacement Factor, $(k_d)_n$

The displacement factor, $(k_d)_n$, corrects the measured ionization charge or current to compensate for the differences in attenuation and scattering of the primary radiation caused by the displacement of phantom material by the ionization chamber cavity. Thus the charge or current is obtained that would have been measured by a hypothetical chamber of zero volume centered at the same location. For high-energy neutrons, $(k_d)_n$ can be 1% or 2% less than unity. However, for the low-energy neutrons produced by the reactor, experiment has shown that $(K_d)_n = 1.00$ is a good approximation (reference 15).

5.9 Relative Neutron Response, k_U

In principle, the relative neutron response, k_U, for the Mg-Ar chamber can be calculated using an equation similar to equation 11. However, calculations of k_U have large uncertainties due to the uncertainties of the parameters needed for computation. Thus, values of k_U are usually obtained by a variety of experimental methods. Reference 16 gives values of k_U for a Mg-Ar chamber, and reference 17 gives k_U values for a GM dosimeter. Since k_U is a function of neutron energy, these data must be appropriately weighted to derive values of k_U applicable to neutron fields with known spectra. Table 2 gives k_U values for a Mg-Ar chamber and a GM dosimeter for three reactor configurations.

6.0. Correction Factors

The correction factors discussed in the following subsections are quantities whose values are usually determined by making measurements in specific arrangements of radiation source and instrumentation system.

6.1. Temperature and Pressure Correction Factor, $k_{t,p}$

All chamber readings have to be converted to a reference temperature and pressure, which are usually chosen to be those used by the standardizing laboratory at which the exposure chamber is calibrated. In the U.S. the reference values used by NBS and the ADCL's are 295.16 K (22°C) and one standard atmosphere (760 mm of Hg or 101.3 kPa). When the chamber cavity temperature and pressure for a measurement are T_m(°C) and P_m (mm of Hg), respectively, the correction factor is given by

$$k_{t,p} = \frac{273.16 + T_m}{295.16} \times \frac{760}{P_m} \qquad (23)$$

To keep uncertainties less than 0.1%, the thermometer should be capable of being read with an overall uncertainty of 0.3°C or less, and the barometer should be capable of being read with an overall uncertainty of 0.8 mm Hg or less. It is important to assure that the chamber, gas supply, and phantom temperatures are in equilibrium with the ambient temperature, and that the gas-flow rate is not so large as to cause the cavity pressure to be significantly greater than the atmospheric pressure (see Section 6.10).

6.2. Chamber Wall Attenuation and Scatter Correction Factor, k_w

When a TE-TE chamber is used to make absorbed dose measurements in a phantom, the chamber wall attenuation and scatter correction factor is $k_w = 1.00$. This factor also applies for measurements in a phantom with the Mg-Ar chamber, but in this case the magnesium wall should be thick enough to stop the most energetic recoil protons generated in the hydrogenous phantom material. This factor, however, must be evaluated when chamber measurements are used to derive tissue kerma in free air since such a determination implies that the radiation is neither attenuated by the chamber wall nor augmented by scatter from the chamber wall. First, it is important to establish that the chamber wall, plus a buildup cap if needed, is of adequate thickness to assure that transient secondary-particle equilibrium is attained in the chamber for the kerma measurement. Measurements must then be made by adding caps to the chamber to assess the effect of further increases in wall thickness.

In general, attenuation is dominant over scatter, and increasing wall thickness decreases chamber response. A graph of response versus wall thicknesses beyond that required to produce secondary particle equilibrium is extrapolated to zero wall thickness, and k_w is computed as the ratio of the response obtained with the wall thickness usually used to the response obtained by the extrapolation to zero wall thickness. Strictly, the extrapolation should be made to the mean center of charged-particle production; however, for the low-energy neutrons at the reactor, this center is very close to the inner wall of the chamber so that extrapolation to zero wall thickness is an acceptable procedure. The factor k_w is usually on the order of a few percent less than unity, depending on the actual wall thickness used for the measurement of tissue kerma in free air and on the radiation quality.

6.3. Saturation Correction Factor, k_s

The electric charge measured with an ionization chamber is less than the charge liberated in the chamber cavity by the directly ionizing particles due to initial (intratrack) and general (intertrack) ion recombination. Tests to determine the ionization saturation correction factor, k_s, should be made using an absorbed dose rate and radiation field the same as or similar to that for which dosimetry is required. The tests consist of making response measurements with several values of collecting potential. One voltage polarity may be used for all the measurements, but use of both polarities for each voltage will increase the precision and reliability of the data. Using reciprocal response and voltage quantities, these data are extrapolated to infinite voltage (reference 18). For neutrons, initial ion recombination usually dominates, and a plot of R^{-1} against V^{-1} will enable k_s to be evaluated as the ratio of R at $V^{-1} = 0$ to R at the potential used to make the kerma or absorbed dose measurements. Typically, $1 < k_s < 1.01$.

At high absorbed dose rates, general recombination may dominate and then a plot of R^{-1} against V^{-2} is appropriate for performing the extrapolation. For some intermediate cases it may be necessary to fit the data to a function of both V^{-1} and V^{-2} to make a reliable extrapolation.

Although this dosimetry guide is not intended to cover dosimetry for reactor pulses, it is appropriate to remark that the main problem in performing such measurements with ionization chambers is the difficulty of accurately accounting for the large amount of general ion recombination that occurs in this mode of reactor operation. Calorimetric

dosimetry is recommended for this situation, and could be used to assess the saturation correction factors for ionization chambers. However, this approach must be used with caution since these factors will depend on the pulse intensity, duration, and shape. Large factors, say greater than 5%, are acceptable, provided that the pulse characteristics do not vary significantly.

6.4. Stem-Scatter Correction Factor, k_{st}

For measurements in a phantom, the stem-scatter correction is $k_{st} = 1.00$. When measurements are made to determine tissue kerma in free air, the effect of stem scatter is to augment slightly the chamber response. The stem-scatter correction factor can be assessed by placing a dummy stem on the chamber end opposite to the functional stem, and measuring the charge produced relative to the charge produced without the dummy stem. The value of k_{st} is then the ratio of the response with the dummy stem to that without the dummy stem. Typically $1 < k_{st} < 1.01$, and it is often difficult to attain the precision required for its determination. Since k_{st} is close to unity and has about the same value for the calibration and mixed radiation fields, an acceptable procedure is to neglect stem scatter for both measurements, i.e., assume $k_{st} = 1.00$.

6.5. Radial Nonuniformity Correction Factor, k_{rn}

If the radiation field in the plane perpendicular to the axis of the beam is not uniform, it may be necessary to apply a correction factor k_{rn} for this radial nonuniformity. In most calibration and measurement situations, $k_{rn} = 1.00$.

6.6. Axial Nonuniformity Correction Factor, k_{an}

Most measurements are made with the ionization chamber at a large enough distance from the radiation source so that there is no appreciable variation in kerma averaged over the axial extent of the chamber relative to the kerma at the center of the chamber. If the distance from the source to the chamber center is ten or more times the chamber radius, the use of $k_{an} = 1.00$ will be in error by less than 0.3% (reference 19).

6.7. Electrometer Correction Factor, k_e

The electrometer correction factor, k_e, relates the reading of the electrometer to the actual charge generated. If the same electrometer is used for the calibration and for the measurements in the mixed field, then the absolute accuracy of the electrometer is of no consequence, and $k_e = 1.00$. When different electrometers are used, either they should be adjusted to measure charge accurately or their relative calibrations should be measured to assess k_e.

6.8. Leakage Current Correction Factor, k_l

Electrometers, cables, and ionization chambers should not have significant leakage current relative to the charges or currents to be measured. Electrometer drifts due to system instabilities or to ambient background radiation have the same effect as a leakage current; i.e., they increase or decrease the chamber response. An efficient method of taking such drifts into account is to make several drift

measurements before and after the measurements of the radiation field are made, and then to add or subtract the average drift to the measured charge produced by the radiation so as to compute a net charge. When this is done, $k_1 = 1.00$.

6.9. Polarity Correction Factor, k_p

A change in the polarity of the collecting potential can cause a change in the absolute value of the measured charge. Experience has demonstrated that measurements in Exposure Room 1 of the AFRRI reactor produce polarity effects that can be as much as 20% to 30% at large distances (> 3 m) from the reactor core. These differences are probably due to extra-cameral currents, and their effect can be essentially eliminated by making several measurements at both polarities and using the average response. If this procedure is followed, $k_p = 1.00$.

6.10. Gas Flow-Rate Correction Factor, k_f

It is possible to assess experimentally the variation in chamber response with gas flow rate. Diffusion of air into the chamber cavity is significant at low flow rates, and pressure buildup in the cavity is significant at high flow rates. Between these extremes there usually exists a broad plateau of uniform response not significantly dependent on flow rate. Operation of the chamber in this range of flow rates allows us to set $k_f = 1.00$. For the 0.5 cm^3 Exradin ionization chamber, this range of flow rates is from about 10 to 100 $cm^3\ min^{-1}$. A good approach is to always use the same flow rate, say 30 $cm^3\ min^{-1}$.

6.11. Humidity Correction Factor, k_h

For a chamber flushed with TE gas or argon, the humidity correction factor is $k_h = 1.00$. A humidity correction may be made for an air-filled chamber open to the atmosphere when the standardizing laboratory provides a calibration factor for the exposure standard chamber for dry air. Reference 20 gives a curve of k_h^{-1} as function of relative humidity which shows that k_h differs from unity by 0.3%, at most. In the United States, standardizing laboratories provide calibration factors for ambient air, so that $k_h = 1.00$.

6.12. Summary of Correction Factors

The foregoing subsections have discussed 11 correction factors; however, only $k_{t,p}$ and k_w are usually large enough to require careful evaluation. The other factors can be either neglected, determined approximately, or set equal to 1.00 by suitable measurement procedures. Thus, the evaluations of ΠK_A and ΠK_R are rendered much less formidable. It is recommended that records be kept of these correction factors as they are evaluated for specific chambers and radiation fields, so that they will be available for future use.

As examples and for future reference, Table 3 lists correction factors for two commercially available models of ionization chambers* irradiated in ^{60}Co beams and in AFRRI reactor fields. These factors were derived from measurements performed at NBS and at AFRRI.

---

*In the interests of accuracy and clarity in describing various items of instrumentation, mention is made of commercial sources. This in no way implies endorsement of such products by the U.S. Government.

7.0. Gas Flow Systems

7.1. Static Gas Filling Versus Gas-Flow Systems

Sealed ionization chambers containing a static gas filling are sometimes used. For example, proportional counters can often be used over moderate time periods with a static gas filling. The ionization chambers routinely used at the AFRRI reactor have too low a ratio of cavity volume to surface area for reliable operation as sealed instruments.

7.2. Gas Composition and Verification

It is prudent when procuring TE gas to request an analysis to ensure that the cylinder of gas obtained has a composition close to that desired, and that the components of the gas mixture have been thoroughly mixed. Commercial gas vendors mix the gas before a sample is taken for analysis. Once mixed, thermal diffusion will prevent the gas components from separating.

The acceptability of a TE gas mixture can be evaluated by computing the kerma factor for the analyzed composition using the data of reference 14. A deviation of a few percent from the kerma factors shown in Table 2 for methane-based TE gas is acceptable, and the small difference may be taken into account in the evaluation of the neutron kerma factor ratio as discussed in Section 5.7.

If the composition of gas on hand and in use becomes suspect, a sample of the gas can be drawn and analyzed. A gas sample may be obtained by connecting a suitable clean sample container to a gas manifold to which a vacuum pump, pressure gauge, and the gas supply cylinder

Table 3. Correction factors for two commercially available ionization chambers (Exradin model T2 with TE cavity gas and Exradin model MG2 with argon cavity gas) irradiated in ^{60}Co beams and in AFRRI ER1 reactor fields

Chamber and Radiation	Correction Factors		
	k_w	k_s [§]	k_{st}
Model T2			
^{60}Co	0.992[‖]	1.001	1.008
6" Pb[*]	0.984	1.002	-
Bare[†]	0.976[¶]	1.002	-
12" H_2O[▦]	0.995[**]	1.002	-
Model MG2			
^{60}Co	0.992[‖]	1.009	1.009
6" Pb[*]	0.988	1.006	-
Bare[†]	0.986[¶]	1.006	-
12" H_2O[▦]	0.964[**]	1.006	-

[*] At 1 m from nominal center of reactor core with 6 inches of Pb shielding

[†] At 1 m from nominal center of reactor core with no added shielding

[▦] At 1 m from nominal center of reactor core but with core displaced so as to provide 12 inches of water shielding

[§] Factors with 400 V collecting potential

[‖] Factor with 1-mm-thick cap of same material as chamber wall

[¶] Factor with 2-mm-thick cap of same material as chamber wall

[**] Factor with 5-mm-thick cap of same material as chamber wall

have been connected. All connections to the manifold should be made via shutoff valves, except for the gauge. The sample container, gauge, and manifold are evacuated and then filled with the gas several times to flush the air out of the system. Finally, the sample container is filled with the gas to an appropriate pressure and then isolated via its shutoff valve. In some cases it may be possible to transport the gas supply cylinder to the analysis laboratory, which will then have the responsibility of drawing the sample for analysis.

A quicker check of gas composition can often be made by using a neutron source, such as ^{252}Cf, to check the response of the chamber. This technique can reveal significant departures from the optimum hydrogen content of TE gas or the presence of hydrogenous contamination in argon.

7.3. Flow System Hardware

The valves, flow meter, tubing, and connectors that comprise the gas flow system should be chosen with care to achieve a reliable system that can be readily assembled and modified as needed. All joints should seal tightly to avoid leakage and waste of gas. Two systems of gas fittings that have been found to be versatile and reliable for use with ionization chambers are:

Gra-Tec, Inc., 156 North Plymouth Avenue, Rochester, New York 14608, telephone (716) 232-1180. Brass modular fittings are available in a large variety of adaptors and interconnections using rubber O-ring seals. Manifolds, valves, and starter kits are available for use with various sizes of tubing.

Alltech Associates, Incorporated, Applied Science Labs, 2051 Waukegan Road, Deerfield, Illinois 60015, telephone (312) 948-8600. Teflon modular fittings designed for use in liquid chromatography are available for use with small-diameter (1/16- and 1/8-inch) teflon tubing.

The components available from the latter supplier are particularly suitable for use at and close to the chamber. Teflon tubing is recommended for lengthy connections rather than tubing of soft plastic or rubber.

7.4. Establishing and Checking Gas Flow

Section 6.10 discusses the rationale for choosing an appropriate gas-flow rate. Since low flow rates are required, only low gauge pressures above atmospheric pressure are needed from the pressure-reducing regulating valve at the gas cylinder. Gas flow should be started at a high flow rate to flush all tubing and the chamber cavity with the desired gas. After flushing for a time long enough to assure that only clean cylinder gas flows through the chamber, the flow rate should be reduced to the desired low rate as indicated by a gas-flow meter having adequate resolution to permit repeatable settings. Gas flow through the cavity can be verified by temporarily connecting one end of a short length of tubing to the gas exhaust port and observing the gas bubbles produced when the opposite end of the tube is placed in water. Care should be exercised to prevent any water or its vapor from being introduced into an argon gas system, since the response of a Hg-Ar chamber can be adversely affected by even small amounts of hydrogenous material.

Acknowledgment

The author thanks Charles M. Eisenhauer, Physicist, National Bureau of Standards, for calculating the values given in Table 2.

References

1. Neutron Dosimetry for Biology and Medicine. ICRU Report 26. International Commission on Radiation Units and Measurements, Washington, DC, 1977.

2. Clinical Dosimetry for Neutrons. International Commission on Radiation Units and Measurements, Washington, DC, in preparation.

3. Radiation Quantities and Units. ICRU Report 33. International Commission on Radiation Units and Measurements, Washington, DC, 1980.

4. Broerse, J. J., Mijnheer, B. J. and Williams, J. R. European protocol for neutron dosimetry for external beam therapy. Brit. J. Radiol. 54: 882-898, 1981.

5. American Association of Physicists in Medicine. Protocol for Neutron Beam Dosimetry. AAPM Report No. 7 of Task Group 18, Fast Neutron Beam Physics, Radiation Therapy Committee, 1980.

6. Mijnheer, B. J. and Williams, J. R. Determination of absorbed dose and kerma in a neutron field from measurements with a tissue-equivalent ionization chamber. Phys. Med. Biol. 26: 57-69, 1981.

7. Mijnheer, B. J. and Williams, J. R. Calibration procedures of tissue-equivalent ionization chambers used in neutron dosimetry. In: Advances in Dosimetry for Fast Neutrons and Heavy Charged Particles for Therapy Applications. International Atomic Energy Agency, Vienna, 1984, pp. 127-139.

8. Commission of the European Communities. Ion Chambers for Neutron Dosimetry. CEC Report EUR 6782 EN. Broerse, J. J., ed. Harwood Academic Publishers, New York, 1980.

9. Verbinski, V. V. and Cassapakis, C. G. Calculation of the Neutron and Gamma-Ray Environment In and Around the AFRRI TRIGA Reactor. Defense Nuclear Agency Report DNA 5792F-2, Washington, DC, 1981.

10. Wyckoff, H. O. Reply to corrected f factors for photons from 10 keV to 2 MeV. Med. Phys. 10: 715-716, 1983.

11. Hubbell, J. H. Photon mass attenuation and energy-absorption coefficients from 1 keV to 20 MeV. Int. J. Appl. Radiat. Isot. 33: 1269-1290, 1982.

12. Loevinger, R. National Bureau of Standards. Private communication, 1985.

13. Goodman, L. J. and Coyne, J. J. W_n and neutron kerma for methane-based tissue-equivalent gas. Radiat. Res. 82: 13-26, 1980.

14. Caswell, R.S., Coyne, J. J. and Randolph, M. L. Kerma factors of elements and compounds for neutron energies below 30 MeV. Int. J. Appl. Radiat. Isot. 33: 1227-1262, 1982.

15. Zoetelief, J., Engles, A. C., and Broerse, J. J. Displacement correction factors for spherical ion chambers in phantoms irradiated with neutrons of different energies. Phys. Med. Biol. 26: 513-514, 1981.

16. Waterman, F. M., Kuchnir, F. T., Skaggs, L. S., Kouzes, R. T., and Moore, W. H. Energy dependence of the neutron sensitivity of C-Co_2, Mg-Ar, and TE-TE ionization chambers. Phys. Med. Biol. 24: 721-733, 1979.

17. Guldbakke, S., Jahr, R., Lesiecki, H., and Scholermann, H. Neutron response of Geiger-Müller photon dosimeters for neutron energies between 100 keV and 19 MeV. Health Physics 39: 963-969, 1980.

18. Boag, J. W. Ionization chambers. In: Radiation Dosimetry, Vol. II. Attix, F. H., Roesch, W. C., and Tochilin, E., eds. Academic Press, New York, 1966, pp. 1-72.

19. Kondo, S. and Randolph, M. L. Effect of finite size of ionization chambers on measurements of small photon sources. Rad. Res. 13: 37-60, 1960.

20. Average Energy Required to Produce an Ion Pair. Report 31. International Commission on Radiation Units and Measurements, Washington, DC, 1977.

21. Eisenhauer, C. M. National Bureau of Standards. Private communication, 1984.